

UNIVERSITY OF CALIFORNIA,
IRVINE

Chemical Composition and Photochemical Evolution of Limonene Secondary Organic Aerosol
Studied Using High Resolution Electrospray Ionization Mass Spectrometry

DISSERTATION

submitted in partial satisfaction of the requirements
for the degree of

DOCTOR OF PHILOSOPHY

in Chemistry

by

Adam Patrick Bateman

Dissertation Committee:
Professor Sergey A. Nizkorodov, Chair
Professor Barbara J. Finlayson-Pitts
Professor Eric O. Potma
Dr. Alexander Laskin

2011

Chapter 3 & portions of Chapter 2 © 2008 American Chemical Society
Chapter 4 & portions of Chapter 2 © 2009 the Owners Societies
Chapter 5 © 2010 American Chemical Society
Chapter 6 © 2011 the Owners Societies
All other materials © 2011 Adam Patrick Bateman

DEDICATION

To

my mentors

who always encouraged me

my family

who were always there for me

my friends

who always believed in me.

TABLE OF CONTENTS

	Page
LIST OF FIGURES	v
LIST OF TABLES	vii
ACKNOWLEDGEMENTS	ix
CURRICULUM VITAE	x
ABSTRACT OF THE DISSERTATION	xi
CHAPTER 1: Introduction and Literature Review	1
Aerosols in the Atmosphere	
Monoterpenes in the Atmosphere	
Limonene in the Atmosphere	
Limonene Oxidation – SOA Formation	
Objectives	
CHAPTER 2: Experimental Methods	19
Introduction	
Aerosol Generation	
Aerosol Particle Collection	
HR ESI-MS	
CHAPTER 3: Solvent Effects	36
Introduction	
Experimental	
Results	
Discussion	
Conclusion	
CHAPTER 4: Particle Size and Reaction Time	53
Introduction	
Experimental	
Results	
Discussion	
Conclusion	
CHAPTER 5: Water Soluble Organic Aerosols	78
Introduction	

	Experimental Results Discussion Conclusion	
CHAPTER 6:	Aqueous Photolysis Introduction Experimental Results Discussion Atmospheric Implications	93
CHAPTER 7:	Condensed Phase Photolysis Introduction Experimental Results Discussion	124
CHAPTER 8:	ESI Sensitivity Introduction Experimental Results and Discussion	141
REFERENCES:		152

LIST OF FIGURES

		Page
Figure 1.1	SOA Absorption and Actinic Flux vs. Wavelength	3
Figure 1.2	Yields of Limonene SOA as a Function of Mass Loading	14
Figure 1.3	Photochemical Aging of SOA	17
Figure 2.1	SOA Generation in a Large Chamber	23
Figure 3.1	Model Compounds used to Investigate Solvent-Analyte Reactions	38
Figure 3.2	Solvent Effect on ESI Mass Spectra of Limonene SOA	40
Figure 3.3	Occurrence Frequency of Solvent-Analyte Reactions in Limonene SOA	42
Figure 3.4	Mass Spectra of SOA Compounds Capable of Forming Hemiacetals	44
Figure 3.5	Time Dependent Data from Model Compounds	45
Figure 4.1	Limonene SOA Yield from SMPS Data	54
Figure 4.2	Positive Mode ESI Mass Spectra of Limonene SOA as a Function of Particle Size	56
Figure 4.3	VK and DBE 3-Dimensional Plot for Limonene SOA	57
Figure 4.4	DBE vs. Compound Molecular Weight for Limonene SOA	58
Figure 4.5	SEM Images and Size Distribution of Limonene SOA Particles Collected with MOUDI	60
Figure 4.6	Effect of Reaction Time on O/C and H/C	61
Figure 4.7	Average Properties of Limonene SOA vs. Reaction Time	63
Figure 4.8	Dependence of O/C and H/C on Conditions of SOA Generation	64

Figure 4.9	Structure of the First Generation Oxidation Products of Limonene	66
Figure 4.10	Effect of Possible Oligomerization Reactions on DBE	68
Figure 4.11	Abundance of Select Limonene Oxidation Products vs. Time	73
Figure 4.12	Effect of RH on abundance of $C_{10}H_{18}O_4Na^+$	75
Figure 5.1	Mass Spectra Generated from Limonene SOA and BBOA Collected using PILS and Filter/ACN Extraction Methods	83
Figure 5.2	SOA ESI Abundance vs. Extraction Method	85
Figure 5.3	BBOA ESI Abundance vs. Extraction Method	88
Figure 6.1	Limonene SOA Mass Spectra vs. Precursor Concentration	99
Figure 6.2	Limonene SOA Average O/C and DBE vs. Precursor Concentration	100
Figure 6.3	Limonene SOA Mass Spectra - Photolysis	105
Figure 6.4	Limonene SOA Average O/C and DBE - Photolysis	106
Figure 6.5	Limonene SOA Photolysis – UV/vis	113
Figure 6.6	Limonene SOA Photolysis – pH and Peroxide	116
Figure 7.1	Sample Absorption Spectrum of CO Recorded with IR-CRDS	127
Figure 7.2	Example of an IR-CRDS Calibration	129
Figure 7.3	FTIR of 2-nitrobenzaldehyde Before and After Photolysis	132
Figure 7.4	Calibration of Photon Flux in PMMA Experiments	134
Figure 7.5	Action Spectra and CO Quantum Yields from Photolysis of Undecanal	138
Figure 8.1	Comparison of Measured O/C Values for Calibration Mixtures from ESI-MS and AMS	147
Figure 8.2	Compound Sensitivity vs. Log P	150
Figure 8.3	Compound Sensitivity vs. O/C	151

LIST OF TABLES

		Page
Table 1.1	Biogenic Emissions of VOCs by their source	5
Table 1.2	Observed Emissions and Concentrations of Limonene	7
Table 1.3	Rate Constants for Oxidation of Limonene	8
Table 1.4	Major Products from Oxidation of Limonene	10
Table 3.1	Abundance of Solvent-Analyte Reaction Peaks after 24 hours of Storage in Methanol	46
Table 3.2	Observed Solvent-Analyte Reactivity of SOA Compounds	49
Table 3.3	Functional Group Classification for 5 Largest Peaks in Limonene SOA Mass Spectrum	50
Table 5.1	SOA and BBOA Average Values from PILS and Filter/CAN Extraction Methods	84
Table 5.2	Number of Peaks Detected From BBOA Mass Spectra vs. Extraction Method	86
Table 5.3	Percentage of Ion Current from SOA and BBOA Mass Spectra Binned according to the Compound O/C	90
Table 6.1	Limonene SOA Precursor Concentrations, Mass Loadings and PILS Collection Settings	98
Table 6.2	Limonene SOA Average Values vs. Precursor Concentration and Photolysis Time	101
Table 6.3	Dilution Effects on Limonene SOA Average Values	102
Table 6.4	Functional Groups in Limonene SOA Constituents vs. Precursor Concentration	104
Table 6.5	Average Values for Limonene SOA Compounds Grouped According to Response of Corresponding Peaks to Photolysis	108
Table 6.6	Functional Groups in Limonene SOA Constituents vs. Photolysis Time	110

Table 6.7	Limonene SOA Average Values from Aqueous and Dry Photolysis	111
Table 8.1	Standard Compounds and Mixtures Used for ESI Sensitivity Tests	144
Table 8.2	Measured ESI Sensitivity Factors for Different Compounds	148

ACKNOWLEDGEMENTS

I would first and foremost like to thank my thesis advisor, Professor Sergey Nizkorodov, for his motivation, support, and guidance during my graduate career at UCI. He has both encouraged and motivated me to reach my maximum potential. I would also like to thank all members of the Nizkorodov Aerosol Photochemistry group both past and present, for both their help and patience. A special thanks goes to Dr. Chris Harmon for many fruitful science discussions and many more distractions as well as to Dr. Steve Mang for all his help and patience in training and teaching.

I have been fortunate enough to have an additional set of mentors, Dr. Alex Laskin and Dr. Julia Laskin, from the Pacific Northwest National Laboratory. The time and support I received from these two talented scientists was invaluable to my success in graduate school. I am most grateful for all the opportunities they have provided for me and I would like to thank them for all they have done for me.

Finally, I would like to thank my friends and family. Most importantly, I could not have achieved my goals without the daily love and support from my significant other, Alexis. My parents, Phil and Pam, my sister Elizabeth and her family (Kyle, Hailey, & Sydney), have all been inspirations for my achievements and I thank them for “always being on my side”. Finally, to my best friends Tim and John, I thank you for all the golfing and surfing distractions.

Permissions have been granted for the reproduction of all copyright material. I would like to thank the American Chemical Society for permission to reproduce Chapter 3 and Chapter 5. The text of Chapter 3 is a reprint of the material as it appears in *Environmental Science & Technology*. I would like to thank the co authors, Maggie Walser, Yury Desyaterik, Julia Laskin, Alexander Laskin, and Sergey Nizkorodov. The text of Chapter 5 is a reprint of the material as it appears in *Analytical Chemistry*. I would also like to thank the Owners Societies for permission to reproduce Chapter 4 and Chapter 6. The text of Chapter 4 and Chapter 6 are reprints of the material as it appears in *Physical Chemistry Chemical Physics*. I would like to thank the co-authors listed on all publications, Alex Laskin, Julia Laskin, and Sergey Nizkorodov.

This work was supported by the National Science Foundation, through grant ATM-0831518 and through the Environmental Molecular Science Institute program; grant CHE-0909227 (formerly CHE-0431312). In addition, I was supported by the Department of Energy Global Change Education Program, with a Graduate Research Environmental Fellowship. The work presented in Chapter 3, Chapter 4, Chapter 5, and Chapter 6 was performed at the Environmental Molecular Sciences Laboratory located in Pacific Northwest National Laboratory. Additional support came from 2007, 2008, and 2009, Summer Research Institute organized at Pacific Northwest National Laboratory.

CURRICULUM VITAE

Adam Patrick Bateman

EDUCATION

- B.S. in Chemistry 2006
University of California, Santa Barbara
- Ph.D. in Chemistry 2011
University of California, Irvine

PUBLICATIONS

- Photochemical processing of secondary organic aerosols dissolved in cloud droplets, A.P. Bateman, J. Laskin, A. Laskin, S.A. Nizkorodov, *Phys. Chem. Chem. Phys.*, 2011, Accepted, DOI:10.1039/C1CP20526A.
- High-Resolution Electrospray Ionization Mass Spectrometry Analysis of Organic Aerosol Samples Collected with a Particle into Liquid Sampler (PILS), A.P. Bateman, J. Laskin, A. Laskin, S.A. Nizkorodov, *Anal. Chem.*, 2010, 82, 8010.
- High-resolution mass spectrometry analysis of secondary organic aerosol generated by ozonolysis of isoprene, T.B. Nguyen, A.P. Bateman, D.L. Bones, S.A. Nizkorodov, J. Laskin, and A. Laskin, *Atm. Env.*, 2010, 44, 1032.
- Appearance of strong absorbers and fluorophores in limonene-O₃ secondary organic aerosol due to NH₄⁺-mediated chemical aging over long time scales, D.L. Bones, D.K. Henricksen, S.A. Mang, M. Gonsior, A.P. Bateman, T.B. Nguyen, W.J. Cooper, and S.A. Nizkorodov, *J. Geophys. Res. D*, 2010, 115, D05203.
- Time-resolved molecular characterization of limonene/ozone aerosol using high-resolution electrospray ionization mass spectrometry, A.P. Bateman, J. Laskin, A. Laskin, S.A. Nizkorodov, *Phys. Chem. Chem. Phys.*, 2009, 11, 7931.
- The effect of solvent on the analysis of secondary organic aerosol using electrospray ionization mass spectrometry, A. P. Bateman, M. L. Walser, Y. Desyaterik, J. Laskin, A. Laskin, S. A. Nizkorodov, *Env. Sci. & Tech.*, 2008, 42, 7341.
- Contribution of carbonyl functional photochemistry to aging of atmospheric secondary organic aerosol, S.A. Mang, A.P. Bateman, M. Anderson, D. Blake, S.A. Nizkorodov, *J. Phys. Chem. A.*, 2008, 112, 8337.
- Photochemistry of secondary organic aerosol formed from oxidation of monoterpenes, S.A. Mang, M.L. Walser, X. Pan, J.H. Xing, A.P. Bateman, J.S. Underwood, A.L. Gomez, J. Park, and S.A. Nizkorodov, *Atmospheric Aerosols: Characterization, Chemistry, and Modeling (ACS Symposium Series)* Valsaraj, K. T., Kommalapati, R. R., Eds., 2009, 216 pages. ISBN13: 9780841269736; ISBN10: 0841269734

ABSTRACT OF THE DISSERTATION

Chemical Composition and Photochemical Evolution of Limonene Secondary Organic Aerosol Studied Using High Resolution Electrospray Ionization Mass Spectrometry

By

Adam Patrick Bateman

Doctor of Philosophy in Chemistry

University of California, Irvine, 2011

Professor Sergey A. Nizkorodov, Chair

Organic aerosols comprise hundreds, if not thousands, of distinct chemical compounds. Traditional analytical techniques for analysis of chemical composition lack the ability to completely characterize complex mixtures such as organic aerosol. Until recently, the best available methods could only provide information on selected aerosol compounds, on selected groups of compounds, or on sample-averaged elemental ratios. Such experimental limitations posed significant barriers to understanding the detailed chemical composition of organic aerosols and its atmospheric evolution.

The unique HR ESI-MS methods developed in this research are able to not only characterize the organic aerosols average elemental ratios, but also simultaneously obtain information about hundreds or even thousands of individual compounds in organic aerosols. One of the key achievements of this work was the development of new methods for classification of individual compounds in organic aerosols by their functional groups using reactive HR ESI-MS. This contribution made it possible to track organic aerosols throughout their atmospheric evolution via functional group composition and average elemental ratios while still retaining the chemical composition of each individual compound.

Other important scientific advances described in this thesis include: complete characterization of the chemical composition of limonene SOA as a function of particle size and reaction time; adaptation of PILS (particle-into-liquid sampler) to the HR ESI-MS platform; chemical characterization of the water soluble component of several types of organic aerosols; the effects of photochemical aging on the water soluble component of limonene SOA through characterization of the optical properties coupled with chemical composition; and investigation of photochemistry of carbonyls in model SOA matrices.

The research included in this dissertation reviews the development of unique aerosol characterization tools utilizing the facilities at UCI and the Environmental Molecular Sciences Laboratory at the Pacific Northwest National Laboratory. The research project answered important questions regarding organic aerosol formation, evolution, and chemical composition that impact the direct and indirect influences of aerosols on Earth's climate.

Chapter 1

Introduction and Literature Review

1.1 Aerosols in the Atmosphere

An aerosol is defined as a stable suspension of liquid or solid material in a gas. Strictly speaking, the term aerosol includes both the particles and the surrounding gas molecules, however, this term is often colloquially used to describe just the particles. Particulate matter (PM) is the preferred terminology for air pollution regulations and refers to the suspended liquid/solid material only. Particulate matter in the atmosphere is classified by mass, size, shape, number concentration, chemical composition, and optical properties.¹ Typical particle sizes range from ~ 0.001 to ~ 10 μm . Particles larger than 10 μm occur in the atmosphere in the form of rain drops, hail, and fine/coarse sand particles, however, the majority of these particles settle out fast enough to not be included as atmospheric particles. Molecular clusters with sizes below ~ 0.001 μm are not typically viewed as particles, however, the distinction between nanoparticles and clusters is vague. Particulate matter is further refined into: coarse particles (PM_{10}) with diameters <10 μm ; fine particles ($\text{PM}_{2.5}$) with diameters <2.5 μm ; and ultrafine particles ($\text{PM}_{0.1}$) with diameters <0.1 μm . Typical atmospheric particle mass concentrations are $1 - 80$ $\mu\text{g m}^{-3}$, with the highest concentrations originating from areas of high population and industrialization.² The chemical composition of organic aerosols varies by region, but is generally dominated by sulfate ($0.2 - \sim 20$ $\mu\text{g m}^{-3}$) and organic carbon ($0.2 - >10$ $\mu\text{g m}^{-3}$).² Other contributors to particulate matter are ammonium, nitrate, elemental carbon, sea salt, soil dust, and trace metals from combustion sources.^{1,2}

Multiple field observations found that a substantial fraction (>50%) of atmospheric particulate matter can be classified as organic.^{3,4} Even particles that have traditionally been regarded as inorganic (sea-salt aerosol, soot, sulfuric acid aerosol) are now shown to carry an organic coating on their surfaces.⁵⁻⁷ Organic particulate matter is loosely classified into two groups, primary organic aerosol (POA) and secondary organic aerosol (SOA). POA is emitted directly into the atmosphere by natural and anthropogenic sources; examples include coal combustion, waste incineration, diesel exhaust, meat cooking, plant debris, and microbial particles. SOA is formed from reactions between volatile organic compounds (VOC) and atmospheric oxidants. VOCs can be emitted from anthropogenic sources, such-as car exhaust or biogenic sources such as monoterpene emissions (isoprene, α -pinene, d-limonene, etc.) from trees/forests.

Atmospheric PM impacts the Earth radiative balance both directly and indirectly.^{3,8,9} Direct effects include both absorption and scattering of incoming solar radiation by particles. Indirect effects of aerosols¹⁰ include several complex phenomena dealing with aerosol-cloud interactions. Any particle that it is sufficiently large and hygroscopic can act as a cloud condensation nucleus (CCN) for a cloud droplet. As a result, aerosol increases reflectivity of the clouds by several mechanisms.⁸ Organic coatings affect the CCN activity of particles in poorly understood ways, therefore the impact of organic particles on climate is difficult to assess. IPCC 2001 and 2007 reports^{8,9} identified organic aerosols (OA) as the least understood contributors to radiative forcing.

A major challenge for reliable predictions of radiative forcing by biogenic SOA comes from our poor understanding of its formation and evolution in the atmosphere. The relationship between the composition and CCN properties of SOA particles is uncertain.⁴ In addition, SOA

is highly dynamic:¹¹ its chemical composition continuously evolves because of exposure to gas-phase oxidants,^{12, 13} reactions with nitrogen containing compounds,¹⁴⁻¹⁶ processing in cloud droplets,¹⁷ and photolysis due to solar radiation.¹⁸⁻²¹ Polymerization reactions occurring in the organic particle-phase could also be important.²²⁻²⁶ Thus “aging” processes play an important role in determining the physical and optical properties of organic particulate matter.^{3, 4, 12, 27}

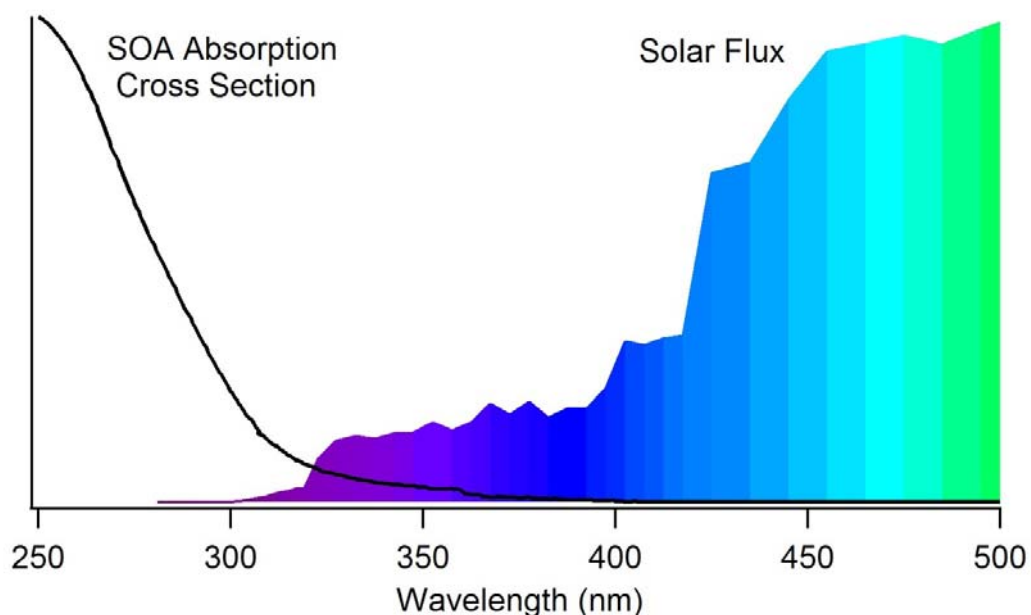


Figure 1.1. Normalized SOA absorption cross section plotted over the observed flux of photons for solar radiation < 500 nm. Both plots have been normalized to display the overlap responsible for SOA photochemistry.

The optical properties of fresh SOA indicate that there is some overlap between the actinic radiation that reaches the earth surface/troposphere and SOA absorption, seen in Figure 1.1. Radiation with wavelengths less than 290 nm is not available for tropospheric photochemistry, with higher-energy radiation being screened by stratospheric ozone. The small overlap between the solar flux and SOA absorption spectrum gives rise to photochemistry through photolysis of SOA compounds. Significant aging of SOA compounds produces “brown carbon” i.e. compounds that absorb visible light ~ (400 – 700 nm). Such compounds have been

identified from both limonene SOA¹⁴ and isoprene SOA.¹⁵ Therefore photochemistry excited in the visible range of the solar spectrum may also be possible in aged SOA, in addition to the UV photochemistry. Evidence of brown carbon in the atmosphere has been observed across the globe from Southern US,²⁸ and Mexico City,²⁹ to large portions of Asia.³⁰ An important aspect of current climate models is the assumption that all aerosols have a negative radiative forcing component.^{3, 8} Recent findings indicate that organic aerosols could have a positive radiative forcing component that would have a profound impact on climate.^{30, 31}

In addition to climate effects, a number of studies have shown the organic fraction of PM to be deleterious to human health.^{3, 32-34} Particles have been associated with an increased risk of asthma,^{35, 36} cardiovascular problems,^{37, 38} and an increased incidence of lung cancer.^{39, 40} In addition, studies have correlated increased concentrations of particulate matter with increased mortality.^{32, 41-43} While regulations have been passed by the environmental protection agency (EPA) on coarse (PM₁₀) and fine (PM_{2.5}) particles, no regulations have been established for ultrafine particles (PM_{0.1}) despite evidence of their ability to directly enter the blood stream.⁴⁴

1.2 Monoterpenes in the Atmosphere

On a global scale, biogenic VOC emissions are an order of magnitude greater than anthropogenic VOC emissions.⁴⁵ Isoprene (C₅H₈) and monoterpenes (C₁₀H₁₆) often comprise a significant portion of biogenic VOC, as can be seen in Table 1.1 adopted from Guenther et al, 1995.^{45, 46} The most commonly occurring monoterpenes are α - pinene, β - pinene, Δ^3 -carene, d-limonene, camphene and myrcene.⁴⁷ Monoterpenes are emitted mainly from forested/woodland

regions containing coniferous and deciduous trees. The ratio of individual monoterpene emissions is a function of each plant/tree species.^{45, 47}

Table 1.1. Emission estimations of VOC's are categorized by their natural source. Chemical species include: isoprene, monoterpenes, other reactive VOC (ORVOC), and other VOC (OVOC). Table adopted from Guenther et al., 1995.⁴⁵

Source	Isoprene	Monoterpenes	ORVOC	OVOC	Total VOC
Woods	372	65	177	177	821
Crops	24	6	45	45	120
Shrub	103	25	33	33	194
Ocean	0	0	2.5	2.5	5
Other	4	1	2	2	9
All	503	127	260	260	1150

Estimates in Tg C yr⁻¹

The most common method of quantifying individual monoterpene mixing ratios is by pumping a known volume of air through a carbon filter (Tenax TA) that adsorbs the monoterpene hydrocarbons. The compounds on the filter are then thermally desorbed/cold trapped and injected into Gas Chromatographic (GC) column for separation. This is followed by detection with either flame ionization detector (FID) or a quadrupole mass spectrometer (MS).^{48, 49} More recent measurements of VOC mixing ratios, including monoterpenes,⁵⁰ have been conducted by proton transfer mass spectrometry (PTR-MS). VOCs are ionized by H₃O⁺ and the masses of the ions are detected. A major drawback of this method is that the masses are not unique indicators for the VOCs present (for example, all monoterpenes have the same mass). While, PTR-MS has a high sensitivity and a fast response time, the technique is only useful for quantifying the total concentrations of monoterpenes.⁵¹

Techniques used to estimate the flux of monoterpenes from the measured atmospheric concentrations are described in the following section. Relaxed eddy accumulation⁵²⁻⁵⁴ and eddy covariance^{55, 56} techniques use data from an anemometer to observe the mean vertical velocity.

This information is then used to direct the flow of air into either an up-draft channel or a down-draft channel, each containing a Tenax TA filter, for monoterpene collection. Eddy covariance measurements are typically conducted with an on-line detection system while relaxed eddy accumulation concentrations measurements are made offline. Another technique, gradient flux measurement,^{57, 58} measures monoterpene concentrations at different heights along with the meteorological conditions, to estimate the emissions to the atmosphere. Finally, direct emission measurements from plants are made by enclosing tree branches / leaves in a chamber and measuring the concentrations of monoterpenes.^{46, 54, 59-65} This final technique allows the analysis of emissions from individual tree species, while the other techniques measure emissions from all species present. In general, monoterpene emissions are highest in forested regions and quite low in desert regions.⁴⁷ There is a strong positive correlation between monoterpene emissions and temperature. Therefore monoterpene emissions are typically the highest in summer,^{46, 56, 60, 65} and follow a diurnal pattern with the highest emissions during the day.^{46, 48, 61}

Typical monoterpene concentrations above forested regions range from 10 – 5000 pptv, (pptv = part per trillion by volume) while limonene mixing ratios range from 2 – 500 pptv (Table 1.2). The measured concentrations of monoterpenes are 2-3 times higher inside the canopy, attributed to emissions from the forest floor (litter) and less turbulent mixing inside the forest canopy.^{48, 56} Average atmospheric mixing ratios of monoterpenes follow the seasonal emissions of monoterpenes, with the highest concentrations measured during the summer.⁶⁰ However, monoterpene mixing ratios follow a diurnal pattern opposite of the emission patterns, with highest concentrations measured at night.^{46, 48, 56, 61, 66} This inverse relationship is due to both meteorological effects, i.e. night-time temperature inversions, and the increased concentrations of atmospheric oxidants (O₃ and OH radical) during the daytime.¹

Table 1.2. Observed concentrations of limonene above forested regions and emissions from various tree species measured throughout the world.

Tree species	Location	Total Monoterpene Concentration pptv (<i>Limonene Concentration</i>)	Percent of Total Monoterpene Measurement	Emission Rate Technique	Total Monoterpene Measured/Estimated Emission Rate	Study
Pine	Sweden	500 – 8000 (100 – 500)	18%	---	---	Jansen et al., 1992
Pine (resin)	Portugal	---	1.4%	Chamber	15-6700 μg	Pio et al., 1998
Boreal Pine	Finland	50 – 400 (10-80)	1 - 10%	---	---	Hakola et al., 2000
Boreal Pine	Finland	---	5 %	Gradient	120 $\text{ng m}^{-2} \text{s}^{-1}$	Rinne et al., 2000
Pine	Japan	100 - 500 (7 - 140)	50 %	Eddy Covariance	0.6 $\text{nmol m}^{-2} \text{s}^{-1}$	Tani et al., 2002
Boreal Pine	Finland	100 - 400 (13)	5 %	Chamber	---	Hakola et al., 2003
Pine Needles	Finland	---	2 – 5%	Chamber	---	Kainulainen et al., 2003
Boreal Pine	Finland	10 - 100 (2 – 25)	20%	Gradient	49 $\mu\text{g m}^{-2} \text{h}^{-1}$	Spirig et al., 2004
Pine	California	700 – 2100 (76 – 223)	10%	---	---	Bouvier-Brown et al., 2009
Orange	Spain	---	10 – 20 %	REA	50 $\text{ng m}^{-2} \text{s}^{-1}$	Ciccioli et al., 1999
Orange	Spain	140 – 900 (80 – 400)	50%	REA	160 $\text{ng m}^{-2} \text{s}^{-1}$	Christensen et al., 2000
Apple	Italy	---	2- 30 %	Chamber	366 $\text{ng g}^{-1}(\text{dw}) \text{h}^{-1}$	Rapparini et al., 2001
Cherry	Italy	---	6 – 21 %	Chamber	1213 $\text{ng g}^{-1}(\text{dw}) \text{h}^{-1}$	Rapparini et al., 2001
Spruce	Denmark	---	6 %	REA	6.8 $\text{ng m}^{-2} \text{s}^{-1}$	Christensen et al., 2000
Spruce (Soil)	United Kingdom	---	30 -40%	Chamber	5-70 $\mu\text{g m}^{-2} \text{h}^{-1}$	Hayward et al., 2001
Fir	Greece	---	30 %	Chamber	0.76 $\mu\text{g g}^{-1}(\text{dw}) \text{h}^{-1}$	Harrison et al., 2001
Oak	France	---	20 -35 %	Chamber	0.5 -15 $\text{nmol m}^{-2} \text{s}^{-1}$	Staudt et al., 2004
Beeches	Argentina	---	61- 67 %	Chamber	1.6 – 5.3 $\text{nmol m}^{-2} \text{s}^{-1}$	Centritto et al., 2008
Pine / Spruce / Cedar	United States	---	11 %	---	0.6 – 118 $\mu\text{g C m}^{-2} \text{h}^{-1}$	Geron et al., 2000

1.3 Limonene in the Atmosphere

Limonene has been chosen as our model monoterpene due to its prevalence in emission and concentration measurements of forests worldwide, as shown in Table 1.2. The table outlines

speciated monoterpene emission studies including, tree species, location, percent of total monoterpene emissions, and emission rate or atmospheric concentration. Species that emit limonene as the most abundant monoterpene include Orange trees and southern Beech trees. Strong limonene emissions have also been found from certain Pine species, Oak trees, and forest soil samples.^{53, 59, 62} In general, limonene makes up about 10 - 20% of the monoterpene emissions from pines, spruce, cedar, and fir which constitute most of the world's forests.⁴⁷

The primary removal mechanism for limonene in the atmosphere is reaction with atmospheric oxidants. Limonene has poor water solubility and cannot be readily removed by wet deposition. Table 1.3 lists the rate constants and lifetimes for reaction of limonene with the four primary atmospheric oxidants. The primary daytime oxidants are OH radical and O₃ (ozone), while the primary nighttime oxidant is NO₃ radical. Cl radical is a strong oxidant present in the atmosphere. However, low mixing ratios prevent it from being a major contributor towards terpene oxidation. The experimental rate constants determined include contributions from both double bonds of limonene. The internal double bond is much more reactive, with relative estimated rate constants for reaction with ozone of $3 \times 10^{-16} \text{ cm}^3 \text{ molecules}^{-1} \text{ s}^{-1}$ and $7 \times 10^{-18} \text{ cm}^3 \text{ molecules}^{-1} \text{ s}^{-1}$ for the endocyclic (internal) and exocyclic (external) double bonds, respectively.⁶⁷

Table 1.3. Rate constants for reactions of limonene with atmospheric oxidants.

Oxidant	Rate Constant $k \text{ (cm}^3 \text{ molec}^{-1} \text{ s}^{-1}\text{)}$	Concentration $\text{(molecule cm}^{-3}\text{)}$	Lifetime $\tau \text{ (min)}$
OH	1.7×10^{-10} (a)	5×10^6 (0.25 ppt)	18
O ₃	2.0×10^{-16} (a)	1×10^{12} (55 ppb)	71
NO ₃	1.3×10^{-11} (a)	1×10^7 (1 ppt)	107
Cl	6.4×10^{-10} (b)	1×10^5 (c)	200

(a) Atkinson et al., 2003 (b) Finlayson-Pitts et al., 1999 (c) Spicer et al., 1998

1.4 Limonene Oxidation – SOA formation

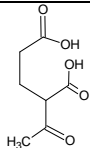
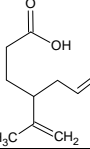
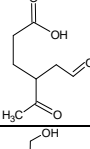
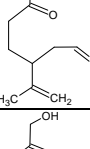
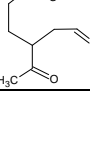
Laboratory Studies

The involvement of monoterpenes in the formation of atmospheric aerosol was recognized in 1960 by Went, who observed a blue haze formed by pine needles in the presence of ozone.⁶⁸ As a result of extensive laboratory and field research, it is now well established that oxidation of monoterpenes is a major source of SOA. The yields of SOA from reaction of monoterpenes with atmospheric oxidants will be discussed in the following section. First, the products formed from the reaction of limonene with atmospheric are of low volatility and contain hydroxyl, carbonyl, carboxyl, nitro, peroxy, and other functionalities.⁶⁹⁻⁷⁸ The high degree of chemical complexity of atmospheric organics has inspired a number of sophisticated methods that are capable of separating and detecting a variety of different analytes in PM samples.⁷⁹ As the majority of the above compounds contain polar functional groups, derivitization is required for identification through gas chromatography techniques.⁸⁰⁻⁸²

Through derivitization and GC techniques, limononaldehyde, keto-limonene, keto-limononaldehyde, limononic acid, and keto-limononic acid, have been identified as major products and account for ~60% of the observed aerosol mass from reaction of limonene with ozone.⁸³ The major products observed in the aerosol phase from reaction of limonene with OH radical are keto-limonene and limononaldehyde.⁸⁴ The photooxidation of limonene in the presence of NO_x results in formation of limononic acid, keto-limononic acid and keto-limononaldehyde as major products.⁸⁵ Table 1.4 lists the observed particle phase compounds from limonene oxidation.

Table 1.4. Observed major products identified in the aerosol phase from oxidation of limonene using various oxidants. Compounds are named according to conventions of Larsen et al., 1998.⁸⁶

Compound Name	Chemical Formula	Molecular Structure	Oxidant	Reference
limononaldehyde	C ₁₀ H ₁₆ O ₂		Ozone OH+NO _x	Leungsakul et al., 2005 ⁸³ Glasius et al., 2000 ⁸⁷ Hakola et al., 1994 ⁸⁴ Jaoui et al., 2006 ⁸⁵
keto-limonene (limonaketone)	C ₉ H ₁₄ O		Ozone OH+NO _x	Leungsakul et al., 2005 ⁸³ Glasius et al., 2000 ⁸⁷ Hakola et al., 1994 ⁸⁴ Jaoui et al., 2006 ⁸⁵
keto-limononaldehyde	C ₉ H ₁₄ O ₃		Ozone OH+NO _x	Leungsakul et al., 2005 ⁸³ Glasius et al., 2000 ⁸⁷ Jaoui et al., 2006 ⁸⁵
limonic acid	C ₁₀ H ₁₆ O ₃		Ozone OH+NO _x	Leungsakul et al., 2005 ⁸³ Warscheid et al., 2001 ⁸⁸ Glasius et al., 2000 ⁸⁷ Jaoui et al., 2006 ⁸⁵
keto-limonic acid	C ₉ H ₁₄ O ₄		Ozone OH+NO _x	Leungsakul et al., 2005 ⁸³ Warscheid et al., 2001 ⁸⁸ Glasius et al., 2000 ⁸⁷ Jaoui et al., 2006 ⁸⁵
limonic acid	C ₉ H ₁₄ O ₄		Ozone	Warscheid et al., 2001 ⁸⁸ Glasius et al., 2000 ⁸⁷
norlimonic acid	C ₉ H ₁₄ O ₃		Ozone	Warscheid et al., 2001 ⁸⁸ Glasius et al., 2000 ⁸⁷
7-hydroxy-limononic acid	C ₁₀ H ₁₆ O ₄		Ozone	Warscheid et al., 2001 ⁸⁸ Glasius et al., 2000 ⁸⁷
7-hydroxy-keto-limononic acid	C ₉ H ₁₄ O ₅		Ozone	Warscheid et al., 2001 ⁸⁸ Glasius et al., 2000 ⁸⁷
keto-limonic acid	C ₈ H ₁₂ O ₅		Ozone	Glasius et al., 2000 ⁸⁷

norlimonic acid	$C_7H_{10}O_5$		Ozone	Glasius et al., 2000 ⁸⁷
limonic acid	$C_9H_{14}O_3$		Ozone	Glasius et al., 2000 ⁸⁷
keto-limonic acid	$C_8H_{12}O_4$		Ozone	Glasius et al., 2000 ⁸⁷
7-hydroxy-limononaldehyde	$C_{10}H_{16}O_3$		Ozone	Glasius et al., 2000 ⁸⁷
7-hydroxy-keto-limononaldehyde	$C_9H_{14}O_4$		Ozone	Glasius et al., 2000 ⁸⁷

Electrospray ionization mass spectrometry (ESI-MS) offers a number of advantages for the analysis of SOA samples.^{26, 72, 74, 80, 82, 89-91} The highly oxidized nature of the SOA chemical constituents makes them easily amenable to ionization in both positive and negative ion modes of ESI-MS. Lack of significant ion fragmentation during soft ionization in the ESI source greatly simplifies the analysis of complex mixtures of organics in SOA samples. Finally, the high sensitivity of ESI-MS makes it possible to analyze small quantities of SOA material, minimizing the sample collection time and more importantly the concentrations. For example, using an on-line ESI detection technique Warscheid et al. identified limonic acid, keto-limonic acid, limonic acid, norlimonic acid, 7-hydroxy-limononic acid, and 7-hydroxy-keto-limononic acid as immediate products of ozonolysis of limonene.^{88, 92}

Coupling ESI with state-of-the-art high resolution MS methods makes it possible to unambiguously identify multiple components in complex SOA extracts based on the accurate mass measurements of individual peaks and their MS/MS fragmentation patterns.^{88, 89, 93-97} For

example, Walser et al identified hundreds of compounds in limonene SOA using a high resolution mass spectrometer.⁹⁰ The high accuracy mass measurements (± 0.001 m/z) are essential for unambiguous identification of the elemental composition of the hundreds of individual compounds found in SOA extracts. The prevalent ionization mechanisms were deprotonation in the negative ion mode leading to (M-H)⁻ ions and complexation with Na⁺ in the positive ion mode leading to (M+Na)⁺ ions. A chemical mechanism predicted a large number of isobaric products, including oligomers, containing -OH, -COOH, -CHO, -OO-, and -C(O)- functional groups.⁹⁰

Predicting the distribution of products from oxidation of limonene with ozone⁸³ and with OH radical in the presence of NO_x⁹⁸ has been the subject of several kinetic models, established from gas-phase literature rate constants. The model predictions for total aerosol mass were reasonable (~ 30% error) but the model could not correctly predict the gas and particle phase concentrations of products.⁸³ This was attributed to particle phase reactions “driving” gas-phase species into the particle phase through oligomerization reactions, resulting in an almost two orders of magnitude difference in the experimental partition coefficient and the predicted partition coefficient.⁸³

Many studies have examined the formation of oligomers and the role of potential heterogeneous reactions.²² Oligomer formation through heterogeneous reaction has been demonstrated from the presence of sulfate esters during ozonolysis of limonene using sulfate and sulfuric acid seed particles.⁷⁴ The formation of oligomers has also been demonstrated to start immediately upon limonene oxidation.⁹⁹ Recent work in our group identified possible oligomer formation reactions as reactions between Criegee intermediates and stable oxidation

products, or hemiacetal formation from alcohol and aldehyde oxidation products as likely candidate reactions for SOA formation.¹⁰⁰

The role of heterogeneous oxidation reactions in the formation of limonene secondary organic aerosol has also been studied. As previously mentioned, the endocyclic double bond reacts almost 30 times faster with gas-phase ozone than the exocyclic double bond. However, only under very high NO_x conditions is this two stage oxidation observed.⁶⁷ In addition, experiments probing oxidation of keto-limonene (no exocyclic double bond) resulted in significantly less aerosol formation than limonene, indicating the exocyclic bond has some role in total SOA formation.¹⁰¹ It is now established that the initial ozone attack on limonene is the rate-limiting step for SOA formation while the exocyclic double bond remains intact after the initial oxidation, however, it is quickly oxidized via heterogeneous ozone uptake.^{102, 103} This has been confirmed by our research, which found an oxygen to carbon ratio of ~ 0.4 for limonene SOA particles within ~ 4 minutes of the reaction and a much slower (~ 1 hr) increase in oxidation to ~ 0.45 due to reactions of ozone with stable products (aldehydes etc.).¹⁰⁰

The fractional yield of SOA (Y) is defined according to the following equation:

$$Y = \frac{M_0}{\Delta ROG} \quad (1.1)$$

where M₀ is the measured aerosol mass concentration (μg m⁻³) and ΔROG is the reacted quantity of organic gas (μg m⁻³).¹⁰⁴ The measured SOA yields from limonene are 4 -5 times higher than from other monoterpenes such as α-pinene,⁶⁷ due to the presence of two double bonds in limonene.¹⁰⁵ SOA yields from photo oxidation of limonene with OH radical in the presence of NO_x are ~ 40% by mass and increase with increasing initial hydrocarbon concentration.¹⁰⁴ SOA yields from oxidation of limonene with ozone, also increase with increasing initial hydrocarbon concentration and range from 30% - 180% (yields in excess of

100% are possible because oxygenated products of limonene have higher molecular weights than limonene itself).¹⁰⁶ This behavior has also been observed from our own measurements as in Figure 1. 2. The increasing yields from increasing initial hydrocarbon can be explained by gas/particle partitioning. As the gas-phase concentrations increase, more volatile products are able to partition into the aerosol phase, thus increasing the measured yield.¹⁰⁷⁻¹⁰⁹ At concentrations similar to the atmosphere, SOA yields from limonene range from 20 - 40% by mass.⁶⁷

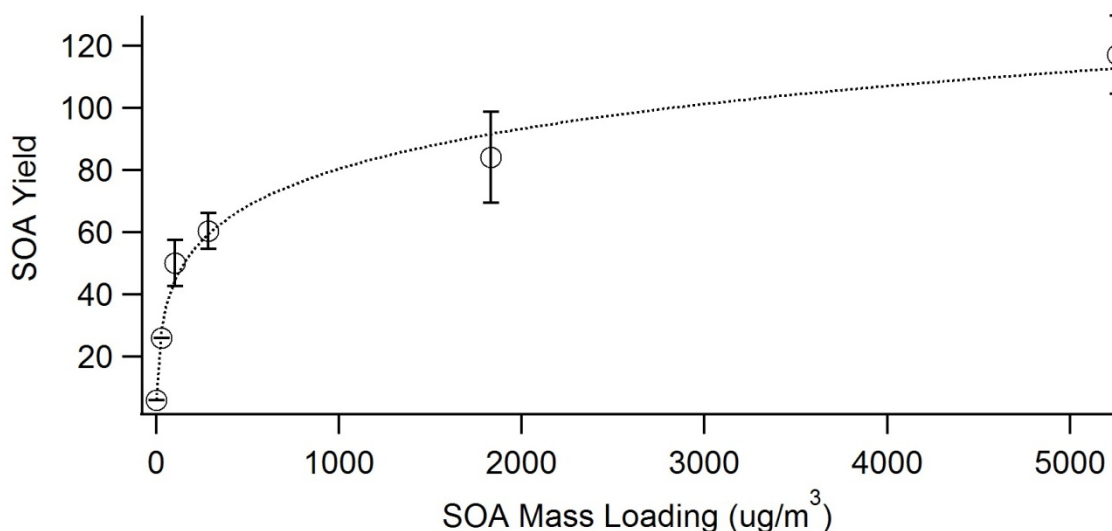


Figure 1.2. Experimental observations of SOA mass yield as a function of SOA mass loading. The error bars represent one standard deviation. Multiple experiments at the two lowest concentrations have not been conducted. The data was fit to a log normal function.

UV radiation has a small effect on yields likely due to photolysis of a reactive intermediate in formation of SOA.⁶⁷ The presence of NO_x during ozonolysis has little effect on the total limonene SOA yields, although individual product yields vary.¹¹⁰ The effect of humidity on limonene ozonolysis was a ~ 4-8 fold increase in SOA mass due to formation of lower volatility products.^{18, 105} The SOA yield from limonene ozonolysis decreases with

addition of OH scavenger.¹¹¹ The effect of temperature on the SOA yield from ozonolysis of limonene has been studied and found to decrease by a factor of ~ 2.5 from 313 K to 253 K. Aerosol yield from particle-phase heterogeneous reactions has been studied using acidic seed particles and found to increase the aerosol mass.¹¹²

The effects of the initial limonene to ozone ratio on SOA yield and the distribution of oxidation products has been studied.^{103, 113} High ratios of ozone to limonene (limonene limited) create products containing secondary ozonide functional groups, likely from condensed phase oligomer formation. Low ratios of ozone to limonene (ozone limited) create products which still contain the terminal double bond due to incomplete ozonolysis.¹⁰³ These changes only represent a small perturbation of the bulk functionality.¹⁰³ The maximum yields of SOA were obtained from ozone to limonene ratios of 1 – 2, likely due to increased mass from heterogeneous oxidation of first generation products.¹¹³

Field Studies

There have been few observations of limonene oxidation products from atmospheric field studies. As the emission of limonene is often only a fraction of the isoprene emissions, many field studies focus on isoprene oxidation products, as they are observed in much larger quantities. In addition, most new studies use PTR-MS to detect and quantify VOCs in the atmosphere. As oxidation products from α -pinene and limonene are often of the same mass, but α -pinene emissions are greater than limonene, compounds could be incorrectly attributed to α -pinene oxidation.⁸⁵ Separation using LC-MS or GC-MS allow for proper characterization and detection of limonene oxidation products. Limona ketone (keto-limonene) has been identified and observed over boreal forests in Finland at concentration of 5 ng m^{-3} .¹¹⁴ Jaoui et al. identified

~ 21 limonene oxidation products from ambient samples including: ketolimononaldehyde, limonic acid, and ketolimonic acid.⁸⁵ Only two compounds were identified that could be used as unique tracer compounds for limonene oxidation in the ambient atmosphere. These compounds were 3-carboxyheptanedioic acid and another compound with an unidentified structure.⁸⁵ The limonene SOA tracer compound 3-carboxyheptanedioic acid has also been observed near a rural forested region in Hungary.¹¹⁵ Observed concentrations ranged from 0 – 21 ng m⁻³ from diurnal variations, with the highest concentrations at night.¹¹⁵

The global yields of SOA production from limonene has been estimated as ~ 5% of the total SOA yield from all monoterpenes using the OSLO CTM2 global chemical transport model.¹¹⁶ We note, however, that many models of SOA formation vastly under predict the concentration of SOA as compared to atmospheric measurements. Using a community atmosphere model (CAM3) OA formation has been studied from biogenic and anthropogenic emissions, and found that the global SOA burden in 2100 was predicted to increase by 36% compared to year 2000 values.¹¹⁷

Indoor Limonene SOA and Health Effects

Indoor environments are also susceptible to the formation of SOA. Monoterpenes, such as d-limonene, are common ingredients in many cleaning solutions and air fresheners. The potential for harmful SOA formation in indoor environments is therefore a significant issue.^{118,}
¹¹⁹ Formation of indoor SOA from reactions of ozone and limonene or limonene containing products has been extensively studied.^{106, 118-122} The specific health effects of limonene SOA constituents has been investigated and is found to have adverse effects including lung and eye

irritation.¹²³⁻¹²⁵ Whether the size, mass or the chemical composition of the particles makes them toxic, is still open to debate.¹²⁶

1.5 Objectives

The main objective of this work was the development of novel methods for chemical composition analysis of organic aerosols based on high resolution electrospray ionization mass spectrometry (HR ESI-MS). The methods were developed using limonene secondary organic aerosol (SOA) as a model system while investigating issues central to the chemistry of organic aerosols. The HR ESI-MS work identified a new avenue of research in aerosol science and provided an opportunity to obtain exciting results for research associated with the chemical composition of complex environmental samples.

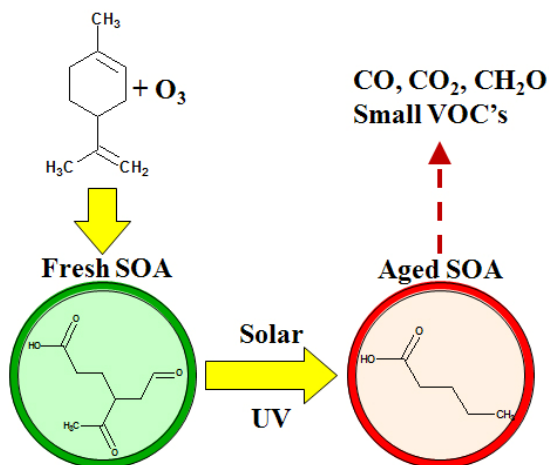


Figure 1.3. SOA is produced from the dark reaction of ozone and d-limonene. The fresh SOA is then exposed to simulated solar radiation. Changes to the chemical composition of SOA and the release of smaller volatile organic products due to photodegradation are monitored.

Another goal of my graduate research was to understand the *photochemical evolution* of SOA derived from oxidation of monoterpenes, as depicted in Figure 1.3. The powerful toolset developed for HR ESI-MS was combined with UV/vis absorption spectroscopy to study the effect of simulated solar radiation of limonene SOA dissolved in aqueous solution. In addition, the photochemical stability of SOA was investigated in a rigid matrix thin film utilizing recently developed methods of photo-dissociation action spectroscopy.^{18, 20, 21} Infrared cavity ring-down spectroscopy (IR-CRDS) was used for analysis of gas-phase products formed during photolysis. Absolute quantum yields were calculated from both aqueous and solid/thin film photolysis techniques. The results indicate that photolysis leads to significant chemical composition changes of organic aerosols on atmospherically relevant timescales. Important questions regarding the role of photolysis in the photochemical evolution of SOA in the atmosphere were answered.

Chapter 2

Experimental Methods

Reproduced in part with permission from Environ. Sci. Technol., 2008, 42, 7341-7346.

Copyright ©2008 American Chemical Society

Reproduced in part with permission from Phys. Chem. Chem. Phys., 2009, 11, 7931-7942.

Copyright © 2009 the Owner Societies

2.1 Introduction

This chapter describes the experimental techniques and methods that are common to the projects described in this thesis. Topics include aerosol generation, aerosol collection, instrumentation, and data analysis used for analysis of organic aerosols via high resolution electrospray ionization mass spectrometry (HR ESI-MS). Experimental information pertinent to each research project will be discussed in the appropriate chapters.

2.2 Aerosol Generation

A chamber made of non-reactive material is required to contain the reactive gas mixtures necessary for aerosol generation. Solid materials such as glass or stainless steel create rigid chambers of constant volume. Inflatable/expandable materials such as Teflon are also common. Both fixed-volume and inflatable reaction chambers can operate in a flow mode, where reactants are added continuously, or in a static mode, where the mixture sits undisturbed

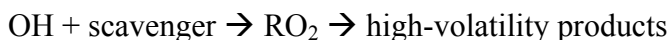
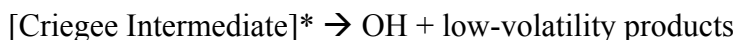
for a certain period of time. The general scheme for static operation with an inflatable chamber is as follows. Dry, purified air is injected into the chamber until the desired volume is reached. A VOC is then injected into the chamber and thoroughly mixed, for example with a fan installed inside the chamber. Following this, an oxidant is added and mixing is generally stopped to reduce the loss of particles to the walls. The mixture is allowed to react in the chamber and then pumped out to collect the particles. In this work, aerosol has been generated using a number of Teflon chambers with volumes ranging from 0.3 to 5 m³, operated in the “static” mode, and using a variety of initial conditions as will be described in more details in the following paragraphs.

As mentioned in chapter 1, important atmospheric oxidants include OH radical, ozone, and the NO₃ radical. Generation of OH radical in reaction chambers is accomplished through the photolysis of precursor compounds, commonly hydrogen peroxide (H₂O₂), nitrous acid (HONO), or isobutyl nitrite. Chambers are either irradiated with natural sunlight or UV lamps which are capable of photolyzing H₂O₂ and/or HONO. NO_x is typically present in the chamber to simulate the urban atmospheric environment. The nitrate radical (NO₃) can be introduced into chambers by flowing air over solid N₂O₅ in a trap, which thermally decomposes into NO₂ and NO₃ as the air flow enters the chamber. Ozone is typically produced through photolysis of oxygen (O₂) using 254 nm UV light, either through a mercury lamp inserted into the air flow, or a commercial ozone generator. Alternatively, ozone can be produced with a discharge generator of the type used to make ozone for water cleaning applications. This work focuses on oxidation of limonene through ozone.

The initial steps for oxidation of limonene by ozone leading to SOA are relatively well known.¹²⁷ However, aging reactions occurring after the SOA formation, including reactive

uptake of gas-phase species and reactions of SOA constituents with themselves, with water vapor, and possible effects of ultraviolet radiation are not well understood. The atmospheric oxidation of terpenes by ozone proceeds via the well known Criegee mechanism.¹²⁸ A primary ozonide (POZ) is formed when ozone adds across a carbon-carbon double bond, forming a 5-membered ring. The POZ decomposes quickly, forming one of two possible stable carbonyl species and reactive Criegee intermediate (CI) pairs. The highly reactive CI is stabilized via isomerization, decomposition or recombination, yielding a variety of products.¹²⁹ Reaction of unsaturated hydrocarbons with ozone leads to formation of lower volatility species, and is an important pathway for aerosol formation.¹⁰⁴

During ozonolysis of terpenes/alkenes, OH radical is also produced. The dominant mechanism for production of OH is isomerization of a Criegee intermediate to a vinylhydroperoxide followed by decomposition.¹²⁹ The OH radical is highly reactive and will react with both the original VOC and the stable ozonolysis products, further complicating the chemical composition.¹³⁰ For this reason it is quite common to include an OH scavenger, a molecule that is unreactive towards ozone and is added in large excess to effectively quench unwanted reactions with OH radical as described in the reactions below:



However, it has been shown that the presence of an OH scavenger affects SOA formation, arising from independent production of HO₂ and RO₂ radicals, which can influence SOA formation chemistry.^{131, 132} The influence of OH scavenger has a marked effect on SOA yields,

however, not on the product distribution as measured using ESI mass spectrometry.⁹⁰ This can be justified from the similar products observed from the reaction of limonene with ozone and OH radical (Table 1.4).

SOA was generated throughout these studies in several small volume chambers made by sealing Teflon film to form a closed volume. After final sealing, chambers were purged with high levels of ozone (~ 10 ppm). The chambers were purged several times and filled with zero air (99.998%) to 0.3 – 0.4 m³ (300 - 400 L). Ozone was introduced by adding pure oxygen through a commercial ozone generator (Pacific Ozone, Model L11/R-LAB111) and turning the generator on for several seconds. The concentration of ozone was adjusted to approximately 1 ppm, as measured with a commercial ozone monitor (Thermo Electron UV photometric O₃ analyzer). After the ozone concentration stabilized, a 10 μL mixture containing 25 v% D-Limonene (98 % purity, Acros Organics) and 75 v% cyclohexane (HPLC grade) was injected with a gas-tight syringe through a septum to achieve an initial limonene mixing ratio on the order of 1 ppm. Following the injection, limonene and cyclohexane quickly evaporated and the resulting gas-phase mixture reacted, producing particles. The mixing ratios of limonene and cyclohexane were of the same magnitude, while the rate constant for reaction of limonene with OH radical is ~ 10 times larger than that of cyclohexane. Therefore mixing ratios for OH scavenger should be ~ 100 times larger to efficiently scavenge the OH radical generated during oxidation. As this was not the case in these experiments, SOA generated from the reaction of limonene and ozone will be referred to as “limonene SOA”, as reactions with OH radical will play a role in the formation of SOA.

Most small volume chamber experiments were conducted in dry (RH < 2%), dark conditions. Experiments were also conducted in humidified air generated by the bubbling of

zero air through two bubblers filled with nanopure water. Another set of experiments was conducted in the presence of UV radiation produced by 8 UV-A lamps (Sylvania, Inc., model F20T12/350BL) and 6 UV-B lamps (Light Sources, Inc., model FS20T12/UVB-BP - emission centered at 310 nm). The lamps were mounted on both sides of the Teflon reaction chamber, approximately 10 cm away from the chamber walls. Operation of these lamps resulted in a 3-5°C temperature increase in the chamber relative to room temperature. The UV radiation from the lamps did not decompose ozone in the chamber to any measurable extent but it could potentially photolyze peroxides and aldehydes in SOA particles. The lamps were therefore used to simulate ozone and limonene reaction under sunlight (daytime) conditions.

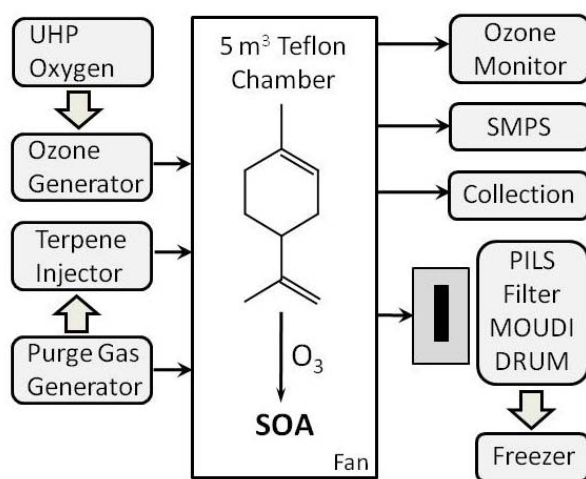


Figure 2.1. Schematic diagram of a 5 m³ teflon chamber used for the generation of limonene SOA including attached instrumentation and collection methods.

To achieve smaller reaction concentrations and still collect adequate material for SOA analysis, a new larger chamber was created at UC Irvine containing a 5 m³ inflatable Teflon chamber as depicted in Figure 2.1.¹³³ The contribution of reactions on the chamber walls is reduced in a larger chamber as the surface to volume ratio is reduced. The chamber was operated in a static mode as follows. The chamber was filled with dry filtered air generated from

a purge-gas generator (Parker Balston, Model 75-62). Ozone was added by passing ultra-high purity oxygen (99.994%) through a Teflon tube with inserted Hg pen-ray UV lamp (Jelight Company, Inc.), until the mixing ratio stabilized at a desired level (0.05 – 1 ppm). The ozone concentration was measured with a photometric ozone analyzer (Thermo Scientific, Inc., Model 49i). Liquid d-limonene was injected into a small glass bulb with a microsyringe through a gas-tight septum and quantitatively transferred into the chamber with a flow of dry purified air. The amount of d-limonene was selected such that its mixing ratio in the chamber was approximately equal to that of ozone (1:1 stoichiometry). Multiple sets of experiments were performed with the initial mixing ratios of limonene and ozone equal to 1, 0.5, 0.1, 0.05 ppm. The chamber air was mixed with a fan for ~ 5 minutes after the injection of limonene. The fan was then turned off to minimize particle losses on the chamber walls. The SOA mixture remained inside the chamber, in the dark, for one hour prior to particle collection. Relative humidity in the chamber was less than 2%.

The particle concentration in the chamber was monitored with a scanning mobility particle sizer (SMPS), which consisted of a differential mobility analyzer (DMA) platform (TSI Model 3080), DMA column (TSI Model 3081) and condensation particle counter (TSI Model 3775). In most experiments, particles appeared within ~ 5 minutes after the limonene injection.

2.3 Aerosol Particle Collection

The collection of particles involves the separation of the surrounding gas molecules from the suspended material. There are two general techniques used to separate the particles from the gas, 1) filter separation and 2) inertial impaction.

Filter Separation

This technique involves pumping aerosol through a filter which impedes the particles and allows the surrounding gas to pass through. This technique is susceptible to a number of collection artifacts, such as evaporation of semi-volatile SOA compounds from the filter, physisorption of VOCs onto the filter, and reaction of SOA compounds with residual ozone/oxidants. Some of these artifacts can be avoided by using a denuder to remove potential reactive gases. A denuder uses the difference in the diffusion of gases and particles to effectively remove gas-phase species from a flow of air while retaining the particles. Denuder walls are often coated with a material to remove a particular gas or class of gases, i.e. acids/bases/ozone.¹ A second method to test artifacts during filter collection is to apply a second or third filter in-line, to monitor collection efficiencies and evaporation / physisorption of VOC's.^{1, 134} After collection, filters are typically stored frozen.

In general, limonene SOA particles were collected by pumping the reaction mixture through a glass fiber filter at 15 -30 LPM for 10 – 40 minutes. Filters were then cut into smaller segments, and extracted in 1 - 10 mL of a solvent, assisted by sonication, for ~20 minutes. The solvents included water (MilliQ), methanol (HPLC grade, Fisher Scientific, Inc.), d₃-methanol (99.8 atom% D, Sigma-Aldrich, Inc.), d₄-methanol (99.8 atom% D, Sigma-Aldrich, Inc.), acetonitrile (HPLC grade, Fisher Scientific, Inc.), and d₃-acetonitrile (99.8 atom% D, Sigma-Aldrich, Inc.). The solvent of choice for SOA analysis is acetonitrile, due to its unreactivity and polar nature, as will be discussed in Chapter 3.¹³⁵ The resulting extracts were filtered through 0.45 μm Nuclepore™ filters. ESI mass spectra of SOA samples were typically taken minutes to hours after the extraction.

Inertial Impaction

Inertial impaction relies on the large differences in masses of suspended particles and gas molecules. As gas molecules are inherently lighter than particles, they are able to flow around the quasi-stationary air cushion formed around the impactor surface. The larger inertia of the particles allows them to penetrate the air cushion around the impactor and collide with the surface. Therefore, particles above a certain size, specific to the impactor design, can be efficiently separated from the gas molecules and smaller particles. As the flow velocity increases, the lower size limit of the particles impacted decreases. An impactor is not limited to a single stage; more complex multi-stage impactors have been used in this work, as will be described in the following sections.

A modified 3-Stage Davis Rotating Uniform-size-cut Monitoring (DRUM) impactor (UC Davis, CA) was used to collect particles as a function of the reaction time.¹³⁶ This instrument collected particles by impaction on three rotating drums. Each drum contained a strip of collecting substrate, either Teflon or Aluminum foil, attached around the circumference of the drum. The drums were controlled by a stepper motor, which advanced the strip by 5 mm every 4 min. The SOA material was collected into ~2 mm spots, each spot corresponding to a specific 4-min reaction time interval. The aerodynamic size ranges were 1.2 – 2.5 μm (drum A), 0.34 – 1.2 μm (drum B), and 0.07 – 0.34 μm (drum C). The vast majority of particles were collected on drum C, therefore, only samples from drum C were used for later ESI-MS analysis. Typically, 16-20 samples were collected in one experiment with 4 min time resolution. After the experiment, the relevant segments were cut out from the strip substrate, placed into labeled vials, and sonicated for twenty minutes in 1 mL of acetonitrile. The samples collected on Teflon strips did not need additional filtration, as there was no significant substrate degradation during

sonication. Aluminum foil substrates partly disintegrated during sonication, requiring filtration with a syringe filter.

A micro-orifice uniform-deposit impactor (MOUDI, MSP Corp., model 110-R) was used to collect size-fractionated samples of SOA. The MOUDI consists of ten stages of impaction. At each subsequent stage the velocity of the particles increases allowing impaction of smaller particles. Aluminum foil substrates were used to collect the samples on the lowest five stages: 6 through 10 (cut-off sizes of $D_{50} = 0.56, 0.32, 0.18, 0.10,$ and $0.056 \mu\text{m}$, respectively). Filmed microscopy grids (Carbon Type-B, 400 mesh copper grids, Ted Pella Inc.) were mounted on the aluminum foils to collect particle samples for computer controlled scanning electron microscopy (CC-SEM) analysis. CCSEM analysis of SOA particles morphology and sizes was performed using a FEG XL30 digital scanning electron microscope (FEI, Inc); specific details of the analysis are provided elsewhere.¹³⁷ The SOA samples were collected at a flow rate of 30 LPM. The collection time varied depending on the intended analysis: 30 s - 2 min for CC-SEM; 2-4 min for HR ESI-MS. Two sets of samples at different times were collected in most experiments: 10 min and 90 min after adding limonene to the chamber. As the chamber volume was ~ 400 L, collecting more than two sets of samples per experiment was not feasible. A significant amount of particles was reproducibly collected on stages 7-10 ($0.32 - 0.056 \mu\text{m}$). Stage 6 ($1.0 - 0.56 \mu\text{m}$) collected almost an order of magnitude less material than stages 7-10 resulting in inferior signal-to-noise ratio in mass spectra of stage 6 samples. Stages 0-5 ($>1.0 \mu\text{m}$) collected no visible amount of particles, and were not used for the ESI-MS analysis. After the aluminum foils were removed from the MOUDI, the microscopy grid substrates were detached and used for SEM imaging. The remaining foils were then cut into small pieces, sonicated for twenty minutes in 1 mL of acetonitrile, and filtered with syringe

filters (glass microfiber filter, 0.7 μm pore size – Whatman, Inc.) for the ESI-MS analysis.

Blank samples were also prepared and analyzed following all of the steps above except for the SOA collection.

A particle-into-liquid-sampler (PILS) was developed in 2001 for the purpose of collection and real-time analysis of water soluble compounds in aerosols.¹³⁸ The PILS approach relies on rapid growth of particles to the size of microdroplets in the presence of supersaturated water vapor, followed by impaction onto a surface covered with a flow of water that washes out the impacted particles. A syringe pump directs the “wash”, either into small glass vials for off-line analysis, or into an instrument for real-time measurements, and thus eliminates many of the common artifacts attributed to particle collection on filters.¹³⁸ Some of the advantages of the PILS collection method compared to the filter-based method include: improvement in time resolution through automation of sampling; reduction in contamination associated with the filter extraction process; and especially useful for the analysis of WSOC, PILS selectivity for water-soluble compounds, (filter methods collect both water-soluble and water-insoluble compounds).

We used a PILS instrument developed by Brechtel Manufacturing Inc. (BMI). During collection the PILS inlet flow was fixed at 14 LPM, while the collection time and the flow of flush water varied depending on initial precursor concentration and final sample volume. The PILS sample vials were standard 2 mL brown glass vials, of the type used for GC/MS autosamplers. Collection times ranged from 10 – 45 minutes and flow of flush water ranged from 33 – 100 $\mu\text{L}/\text{min}$. Typically samples collected were 1 mL, however, 1.5 mL samples were collected when necessary. PILS samples require no separate solvent extraction step, significantly reducing the time requirements for SOA sample work-up. Collected PILS samples were stored frozen until ESI-MS analysis. Immediately prior to the ESI-MS analysis 0.5 mL of

each PILS sample was mixed with 0.5 mL of acetonitrile, in order to decrease the surface tension and facilitate a more stable electrospray.¹³⁹

2.4 HR ESI-MS

All samples were analyzed using a Finnigan LTQ (linear ion trap)-OrbitrapTM hybrid mass spectrometer (Thermo Electron Corporation, Inc.) with a modified ESI source (Prosolia, Inc.). The general operation of the mass spectrometer is as follows: ions are generated using the ESI source and admitted into the linear ion trap where they are analyzed then transferred into a RF-only quadrupole with a curved central axis, known as a C-trap.¹⁴⁰ The C-trap is filled with bath gas to collisionally cool the ions, avoiding any fragmentation and is also used to store the ions before injection into the Orbitrap.¹⁴⁰ The ions are then passed through ion optics and three stages of differential pumping before entering the ultra-high vacuum compartment of the Orbitrap.¹⁴¹ The Orbitrap employs a unique geometry containing a barrel-shaped outer electrode and spindle-shaped inner electrode as developed by Alexander Makarov.¹⁴² The electrostatic field created is the sum of a quadrupole field of the ion trap and a logarithmic field of a cylindrical capacitor, known as a quadro-logarithmic field. The characteristic distinction from other mass analyzers is that the mass-to-charge (m/z) ratio is related to the frequency of harmonic oscillations along the axis of the field, not the frequency of orbital motion.¹⁴² Thus ions rotate about the inner electrode and oscillate harmonically along its axis.^{142, 143} The oscillations on axis are detected from the outer electrode using current imaging techniques and then converted to a frequency spectrum using Fourier transforms.^{142, 143} This frequency

spectrum is then converted into a mass spectrum using ThermoFinnigan's Xcalibur software and a two-point calibration.^{140, 141}

Overall, performance of the LTQ-Orbitrap hybrid mass spectrometer is unparalleled. A 5 ppm mass accuracy was achieved with a dynamic range of ~ 5000 .¹⁴¹ This allows accurate mass detection for compounds with signal to noise (S/N) ratios down to 2 or 3.¹⁴¹ The instrument can operate with a maximum resolving power of 100,000 (fwhm), although most operations are conducted at resolving power of 60,000 allowing for 1 spectrum s^{-1} .¹⁴⁰ In addition, the use of multiple ion traps allows for high-mass resolution MS-MS and MSⁿ experiments.¹⁴⁰

Experimental conditions employed in this work were as follows. Samples were injected through a pulled fused silica capillary tip (50 μm i.d.) at a flow rate of 0.5-1.0 $\mu\text{L}/\text{min}$. The instrument was operated in positive (+) and negative (-) ionization modes with resolving power of $m/\Delta m \sim 60,000$ at m/z 400. Calibration was frequently verified using a standard solution of caffeine, MRFA, and Ultramark 1621(calibration mix MSCAL 5, Sigma-Aldrich, Inc.).

Data Analysis

To facilitate processing the large number of mass spectra recorded during this work, a number of batch processing and data analysis tools were developed. The centroid data generated by the mass spectrometer was first deconvoluted into a list of peak positions and intensities using Decon2LS, a program developed in the Pacific Northwest National Laboratory (<http://ncrr.pnl.gov/software/>); only peaks with a signal-to-noise (S/N) of 3 and higher were included. A LabView 7.0 program developed by our group at UCI was used to sort the peak lists from all the files in the same experimental batch, including blank samples, and generate a

master table of all observed peaks along a common m/z axis. Another LabView 7.0 program developed at UCI calculated the molecular formulae based on accurate mass measurements. All SOA constituents examined in this work are closed-shell molecules, $C_cO_oH_h$, containing c carbon atoms, h hydrogen atoms, o oxygen atoms, and no other elements. The following restrictions were imposed on the atom valence states and atomic ratios (typical values are given in parenthesis): the maximum number of atoms, ($c < 50$; $h < 100$; $o < 60$; number of sodium atoms, $Na = 0$ or 1); range of possible DBE values (-0.5 to 12.5, see Equation 2.1 for the definition of DBE below); O:C values (0.05-1.3); H:C values (0.7-2.2); and m/z tolerance (< 0.001). The DBE values of the neutral molecules are integers. Half-integer values of DBE correspond to protonated, sodiated, or deprotonated ions, as the observed ionization mechanisms were Na^+ addition or protonation in the (+) mode ($C_cH_hO_oNa^+ / C_cH_hO_oH^+$), and deprotonation in the (-) mode ($C_cH_{h-1}O_o^-$). For limonene SOA, the vast majority of the assigned peaks in the (+) ionization mode corresponded to sodiated molecules ($C_cH_hO_oNa^+$). Protonated molecules ($C_cH_hO_oH^+$) in the limonene SOA case typically accounted for less than 10 % of the peaks, and were always accompanied by the corresponding sodiated counterparts. This is not that case for all SOA types.

The initial set of assigned peaks was used to verify the accuracy of the calibration of the m/z axis; deviations between the exact m/z values and experimentally measured values were typically within ± 0.0005 m/z units over the 100-1000 m/z range. Systematic deviations in excess of this value were adjusted by re-calibrating the m/z axis with respect to peaks assigned with certainty. The following peaks were excluded from assignments and further analysis, the typical percent fractions of the total ion current are given for each group in parenthesis: i) peaks that were observed in blank samples (~ 10 %); ii) peaks with even nominal masses corresponding to

molecules containing one ^{13}C atom and/or impurities ($\sim 20\%$); iii) peaks that appeared in only a small fraction of SOA samples within a given batch ($\sim 2\%$); iv) assigned peaks that produced unrealistic values in their mass defect, DBE, O:C ratio, and/or H:C ratio ($\sim 2\%$); v) peaks that could not be assigned to either $\text{C}_c\text{H}_h\text{O}_o\text{Na}^+ / \text{C}_c\text{H}_h\text{O}_o\text{H}^+$ or $\text{C}_c\text{H}_{h-1}\text{O}_o^-$ ions within the expected m/z tolerance ($\sim 5\%$). Therefore, $\sim 60\%$ of the total signal was assigned a molecular formula. After the peak assignment for a given batch of SOA samples was complete, the molecular weights of the SOA compounds were then calculated from the m/z of the corresponding molecular ions (Na^+ and H^+ were subtracted from $\text{C}_c\text{H}_h\text{O}_o\text{Na}^+$ and $\text{C}_c\text{H}_h\text{O}_o\text{H}^+$ ions, respectively, and H^+ was added to $\text{C}_c\text{H}_{h-1}\text{O}_o^-$). All data discussed in this study correspond to the neutral SOA constituents in order to facilitate comparison between (+) and (-) mass spectra.

Analysis of the HR-MS data benefit from a number of advanced data processing and visualization tools, such-as Kendrick plots,⁹⁴ van Krevelen (VK) diagrams,^{95,97} double bond equivalency index (DBE),^{144, 145} aromaticity index (AI),¹⁴⁵ elemental ratios (O/C and H/C), and organic mass to organic carbon ratio (OM:OC). Kendrick plots make it possible to easily recognize related (homologous) families of molecules built by repeated addition of structural units (e.g., CH_2 or O), greatly aiding in calibration and peaks assignments. The most common variation of VK diagrams plots the O/C ratios on the x-axis and the H/C ratios on the y-axis, thus classifying each molecule by its individual O/C and H/C ratios. DBE is a convenient measure of the number of rings and unsaturated bonds in a molecule, while AI is a metric for measuring extent of aromaticity.

The DBE values are calculated as follows:

$$DBE = 1 - \frac{h}{2} + c \quad (2.1)$$

and are equal to the total number of double bonds ($\text{C}=\text{C}$, $\text{C}=\text{O}$) and rings in a molecule.

The aromaticity index is a useful metric of the extent of aromaticity in molecules. For a molecule that contains only carbon, oxygen, and hydrogen atoms, AI is calculated as

$$AI = \frac{1 + c - o - \frac{h}{2}}{c - o} \quad (= 0 \text{ if negative}) \quad (2.2)$$

Positive values of AI can result from the presence of multiple C=C (but not C=O) double bonds or aromatic rings in such molecules. For example, benzoic acid (C₇H₆O₂) has an AI value of 0.6, which is smaller than that of benzene (AI = 0.67) despite having a C=O bond in its structure. In general, the AI values in excess of 0.5 indicate the presence of isolated aromatic rings in the molecule, while values in excess of 0.67 are characteristic of polyaromatic compounds with fused rings.¹⁴⁵ One has to keep in mind that the value of AI > 0.5 does not necessarily provide a proof of aromaticity as highly conjugated aliphatic systems also have reasonably large AI values. For example, the AI of butadiene (C₄H₆), which is not an aromatic molecule, is 0.5.

The OM:OC is a strong function of the organic oxygen content of aerosol constituents, which is difficult to quantify using traditional analytical techniques. High-resolution mass-spectrometry could provide a valuable complementary method for measurements of the OM:OC ratio.¹⁴⁶ To illustrate the approach used in this work, consider a limonene SOA sample that has *i* different chemical species with molar fractions x_i and individual molecular formulas $C_{c_i}O_{o_i}H_{h_i}$. The ratio of the total number of organic oxygen atoms to that of organic carbon atoms is then:

$$\frac{N_o}{N_c} = \frac{\sum_i x_i o_i}{\sum_i x_i c_i} \quad (2.3)$$

The ratio of the organic oxygen mass (*OO*) to the organic carbon mass in the sample can be obtained by scaling Equation 2.4 by the corresponding atomic weights.

$$\frac{OO}{OC} = \frac{16}{12} \sum_i x_i o_i / \sum_i x_i c_i \quad (2.4)$$

The OM:OC ratio can be calculated in a similar way

$$\frac{OM}{OC} = 1 + \frac{16}{12} \sum_i x_i o_i / \sum_i x_i c_i + \frac{1}{12} \sum_i x_i h_i / \sum_i x_i c_i \quad (2.5)$$

The average O:C ratio can alternatively be calculated in a molecule-by-molecule fashion:

$$\langle O / C \rangle = \sum_i x_i \frac{o_i}{c_i} \quad (2.6)$$

Note that the quantity obtained Equation 2.6 is not the same as the one in Equation 2.3, and it cannot be easily related to the *OO:OC* mass ratio. The main advantage of Equation 2.6 is that it is more closely related to the van Krevelen representation of mass spectra as discussed above. It should be noted that for limonene SOA, the values calculated from Equation 2.6 are not strongly dependent on the specific choice of x_i ; setting all of the x_i to 1 produces almost the same results as using relative peak intensities as weights.¹⁰⁰ For all limonene SOA samples discussed here, Equation 2.3 and Equation 2.6, gave nearly identical results

For the ESI-MS analysis, the SOA sample is dissolved in an appropriate solvent. The ESI-MS instrument measures ion counts, which, for a sufficiently dilute solution, should be directly proportional to the molar fractions of respective organic molecules.

$$Intensity_i = Sensitivity_i \times x_i \quad (2.7)$$

If all sensitivity factors are the same the molar fractions in Equations 2.3 - 2.6 can be replaced with the corresponding normalized peak intensities in the mass spectrum. For example, the average O:C ratio is obtained as follows:

$$\langle O / C \rangle = \sum_i Intensity_i \frac{o_i}{c_i} / \sum_i Intensity_i \quad (2.8)$$

Similar equations can be written for the average H:C ratio, and the average DBE value:

$$\langle H / C \rangle = \frac{\sum_i Intensity_i \frac{h_i}{c_i}}{\sum_i Intensity_i} \quad (2.9)$$

$$\langle DBE \rangle = \frac{\sum_i Intensity_i (DBE)_i}{\sum_i Intensity_i} \quad (2.10)$$

$$\langle OM / OC \rangle = 1 + \frac{16}{12} \langle O / C \rangle + \frac{1}{12} \langle H / C \rangle \quad (2.11)$$

Several recent studies estimated the OM:OC ratio in complex mixtures of organics assuming equal ionization efficiencies for various compounds without systematically testing the validity of this assumption.^{147, 148} ESI response is a complex function of the solution composition, concentration of analytes and instrumental factors.^{139, 149} It is well-known that ESI is sensitive towards polar organic molecules containing basic or acidic groups and nonpolar molecules that can readily form adducts with electrolyte ions in solution. Other nonpolar molecules such as aliphatic hydrocarbons, polycyclic aromatic hydrocarbons or cholesterol are usually not observed in ESI mass spectra. It has been demonstrated that surface active molecules are most responsive to ESI analysis suggesting that ESI is most sensitive to molecules that have significant nonpolar regions and contain ionizable functional groups, while highly oxygenated soluble organic molecules may be not well represented in ESI mass spectra.^{139, 150} Because all first-generation products of limonene ozonolysis contain at least one functional group that is capable of ionization in an ESI source and retain the surface active hydrocarbon backbone of the precursor molecule, it is reasonable to assume similar sensitivity of ESI-MS experiments from limonene ozonolysis products. In summary, one should treat the quantities calculated from Equations 2.8 – 2.11 as approximate but nonetheless useful measures of the overall degree of oxidation of SOA constituents.

Chapter 3

Solvent Effects

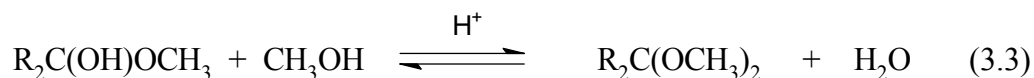
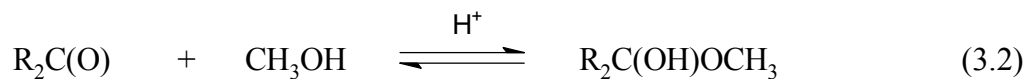
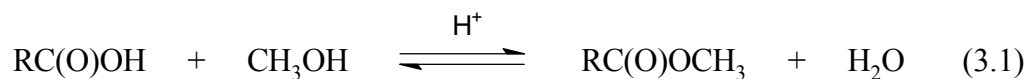
Reproduced in part with permission from Environ. Sci. Technol., 2008, 42, 7341-7346.

Copyright ©2008 American Chemical Society

3.1 Introduction

The high degree of chemical complexity of atmospheric organics has inspired a number of sophisticated methods that are capable of separating and detecting a variety of different analytes in PM samples.⁷⁹ A common approach involves collection of a sufficient quantity of PM on filters or impactors, extraction of the collected material into suitable solvents, and chromatographic / mass-spectrometric analysis.^{80-82, 89, 90} Electrospray ionization mass spectrometry (ESI-MS) offers a number of advantages for the analysis of OA samples.^{26, 72, 74, 80, 82, 89-91} Coupling ESI to state-of-the-art high resolution MS technologies makes it possible to unambiguously identify multiple components in complex OA extracts based on the accurate mass measurements of individual peaks and their MS/MS fragmentation patterns.^{88, 89, 94, 95, 97}

Both liquid chromatographic separation and ESI require OA samples to be dissolved in an appropriate solvent. Methanol/water and acetonitrile/water mixtures are the most commonly used solvents in ESI.¹³⁹ However, one has to keep in mind that polyfunctional compounds found in OA can be reactive with methanol. Specifically, carboxylic acids reacting with methanol may yield esters (Equation 3.1); carbonyls reacting with methanol may yield hemiacetals (Equation 3.2) and acetals (Equation 3.2 - 3.3).¹⁵¹



According to the currently accepted organic nomenclature, ketals are regarded as a subset of acetals; the term “acetal” will be used in reference to both acetals and ketals in the subsequent discussion.

Substantial formation of esterification products was reported in humic acid samples stored in alcohol solvents.¹⁵² Because the complexity of OA samples is comparable to that of humic substances,¹⁵³ we expect similar solvent-analyte reactions to be significant in OA-alcohol extracts as well. Analogous solvent-analyte reactivity has also been reported in the analysis of amoxicillin using ESI-MS in methanol.¹⁵⁴ This chapter examines solvent-analyte reactions of SOA material generated by ozonolysis of monoterpenes and extracted in methanol and acetonitrile for the purposes of direct ESI-MS analysis. In addition, the possibility of using these solvent reactions for qualitative detection of functional groups in OA is explored.

3.2 Experimental

Laboratory generated SOA particles were prepared by the ozone-initiated oxidation of *d*-limonene vapor in an inflatable 300 L Teflon reaction chamber as described in Ref. 90. The particles were collected by pumping the reaction mixture through a glass fiber filter at 30 slpm

for ~6 minutes. The filters were cut into 2-4 equal segments, and each filter segment was separately extracted in 10 mL of a solvent, assisted by sonication, for ~20 minutes. The solvents included methanol, d₃-methanol, d₄-methanol, acetonitrile, and d₃-acetonitrile. The resulting extracts were filtered through 0.45 μm filters. ESI mass spectra of SOA samples were typically taken minutes to hours after the extraction.

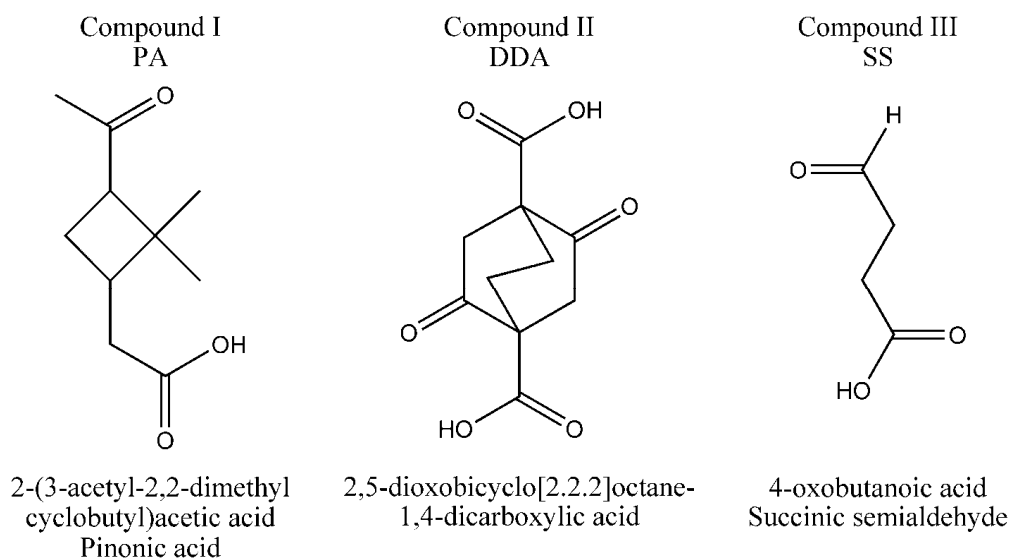


Figure 3.1. Structures, acronyms (used throughout this paper), IUPAC names, and common names of test organic compounds used to investigate the rate and extent of solvent-analyte reactions.

In addition to the SOA samples, ESI mass spectra of three test compounds were investigated, Figure 3.1. They are referenced by their acronyms throughout this paper. PA refers to *cis*-pinonic acid, a carboxylic acid with an additional ketone group and a major constituent of SOA formed from the oxidation of α -pinene.⁸¹ SS stands for succinic semialdehyde, a carboxylic acid with an additional aldehyde group. DDA refers to 2,5-dioxobicyclo[2.2.2]octane-1,4-dicarboxylic acid, a dicarboxylic acid with two additional ketone groups. Glacial acetic acid was used to acidify the solutions of these test compounds.

Commercial sources and purity grades of all chemicals and solvents used in this work are as follows: *d*-limonene (98%, Acros Organics, Inc.), methanol (HPLC grade, Fisher Scientific, Inc.), d_3 -methanol (99.8 atom% D, Sigma-Aldrich, Inc.), d_4 -methanol (99.8 atom% D, Sigma-Aldrich, Inc.), acetonitrile (HPLC grade, Fisher Scientific, Inc.), d_3 -acetonitrile (99.8 atom% D, Sigma-Aldrich, Inc.), *cis*-pinonic acid (98 %, Sigma-Aldrich, Inc.), succinic semialdehyde (4-oxobutanoic acid, 15% solution in water, Thermo-Fisher, Inc.), and 2,5-dioxobicyclo[2.2.2]octane-1,4-dicarboxylic acid (>90 %, Maybridge Scientific, Inc.).

ESI mass spectra of the test compounds were recorded as a function of time since dissolution. Solution concentrations were $43.5 \pm 5.0 \mu\text{M}$ DDA, $53.5 \pm 5.0 \mu\text{M}$ PA and $186 \pm 10 \mu\text{M}$ SS. The solutions were promptly acidified to achieve acetic acid concentrations of $16 \pm 2 \mu\text{M}$, $1.6 \pm 0.2 \text{ mM}$, or $16 \pm 2 \text{ mM}$. As all test compounds contain carboxyl groups, the solutions were slightly acidic even without the acetic acid addition. Solutions were stored in 1.5 mL clear glass vials at room temperature (25°C) in the dark. At certain time intervals, $\sim 100 \mu\text{L}$ aliquot was transferred in a syringe for ESI-MS analysis in both positive and negative modes.

3.3 Results

Figure 3.2 shows characteristic positive ion mode mass spectra for *d*-limonene SOA extracted into methanol, d_3 -methanol, acetonitrile, and d_3 -acetonitrile. For discussion purposes, only a small portion of each spectrum around m/z 190-230 is displayed. Full spectra recorded in acetonitrile are reported in *Walser et al.*⁹⁰ The mass spectra recorded in acetonitrile and d_3 -acetonitrile are nearly identical. On the contrary, substantial differences exist between mass spectra of the same SOA sample extracted into methanol and acetonitrile, with a number of

additional peaks appearing in the methanol-based mass spectra. Furthermore, methanol and d₃-methanol mass spectra differ from each other in terms of peak positions and relative intensities.

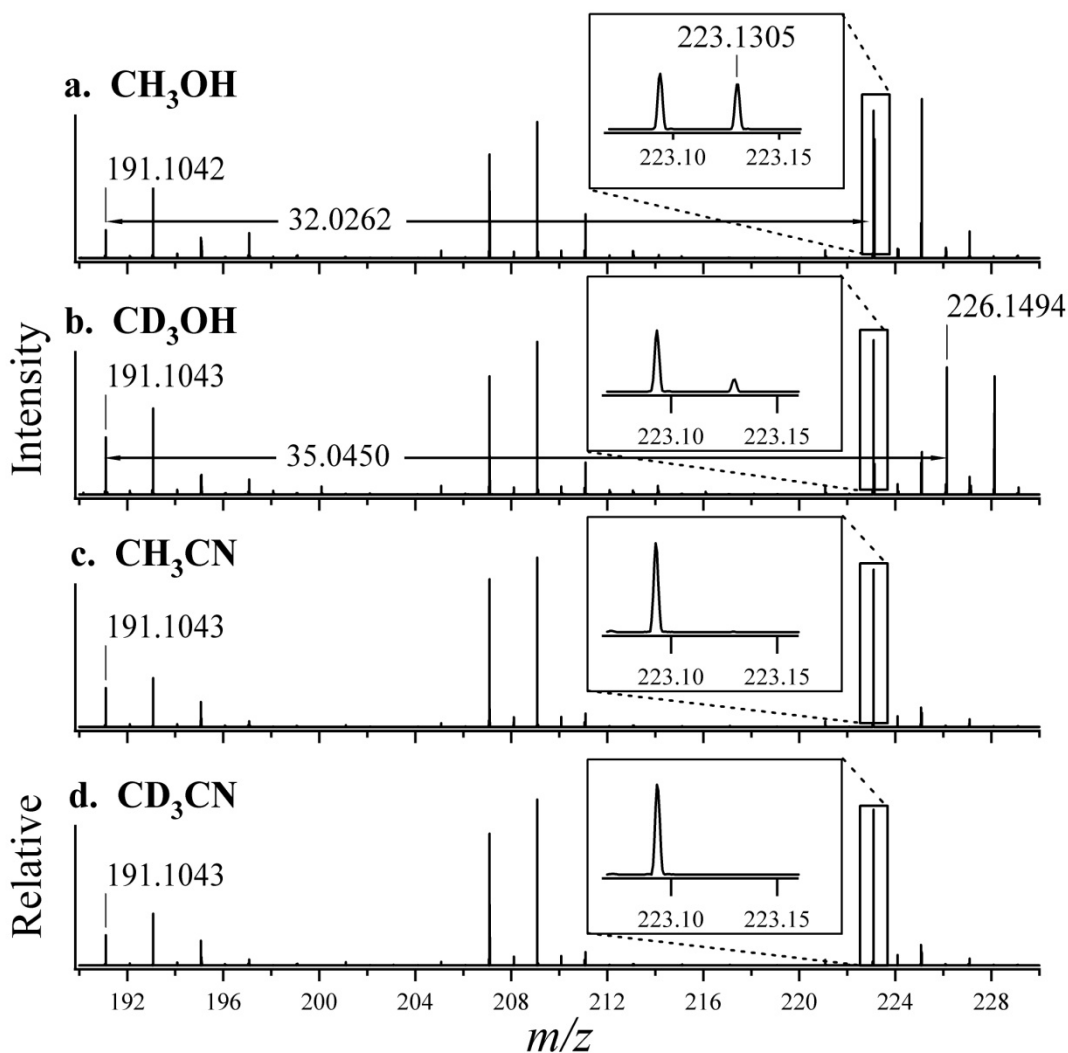


Figure 3.2. Sections of ESI positive ion mode mass spectra of the same *d*-limonene SOA sample extracted into four different solvents: a) methanol; b) d₃-methanol; c) acetonitrile; and d) d₃-acetonitrile. Peaks appearing at m/z 223.1305 in methanol and at m/z 226.1494 in d₃-methanol correspond to hemiacetals of the precursor peak at m/z 191.1043.

Similar observations were made for the negative ion mode spectra of *d*-limonene SOA; additional peaks appeared in the methanol-based mass spectra, and their isotopic shifts were

consistent with reactions of analytes with one or more methanol molecules. The negative ion mode spectrum of *d*-limonene SOA contained fewer peaks, most of which were also detected in the positive ion mode.⁹⁰ Because the positive ion mode data set is larger, the following discussion will deal primarily with the positive ion mode mass spectra.

Careful examination of the differences in peak positions reveals that the majority of extra peaks correspond to an addition of one methanol molecule to an existing ion. For example, there is a progression of peaks with a general formula $C_{10}H_{16}O_nNa^+$, with *n* ranging from 2 to 7, observed in the positive ion mode mass spectra of all solvents.⁹⁰ Figure 3.2 includes three members of this progression: *m/z* 191.1043 (*n*=2) arising predominantly from limononaldehyde, *m/z* 207.0992 (*n*=3), and *m/z* 223.0942 (*n*=4). In mass spectra of SOA extracted into methanol, an additional peak is observed at *m/z* 223.1305, which corresponds to the $C_{11}H_{20}O_3Na^+$ ion and differs from the limononaldehyde peak by the exact mass of one CH_3OH molecule. A similar peak is observed at *m/z* 226.1494 in mass spectra of SOA extracted into d_3 -methanol, which corresponds to the $C_{11}H_{17}D_3O_3Na^+$ ion and differs from the limononaldehyde peak by one CD_3OH molecule. A weak peak at *m/z* 223.1305 also appears in d_3 -methanol based mass spectra, presumably resulting from CH_3OH residue in d_3 -methanol.

In order to assess the extent of reactions between methanol and various SOA constituents, we compared positive ion mode ESI mass spectra of *d*-limonene SOA samples in d_3 -methanol, methanol, and acetonitrile. Only peaks in the range of *m/z* 100-500, corresponding to monomeric and dimeric oxidation products,⁹⁰ above the 0.5% abundance threshold, were selected for analysis. We focused our attention on reactions (Equations 3.1 - 3.3) resulting in the following *m/z* shifts: 14.0156 (+ $CH_3OH - H_2O$) and 17.0345 (+ $CD_3OH - H_2O$) for ester formation (Eqn. 3.1); 32.0262 (+ CH_3OH) and 35.0450 (+ CD_3OH) for hemiacetal formation

(Eqn. 3.2); and 46.0419 (+2 CH₃OH – H₂O) and 52.0794 (+ 2 CD₃OH – H₂O), for acetal formation (Eqns. 3.2+3.3). It is important to note that interference between different solvent-analyte reactions can introduce ambiguities to the assignment of functional groups, especially for polyfunctional SOA constituents. For example, esterification of a carboxyl group (+CH₃OH – H₂O) produces the same mass shift as hemiacetal formation followed by dehydration of an aldehyde. Similarly, acetal formation from a carbonyl (+2 CH₃OH – H₂O) results in the same mass shift as a concurrent hemiacetal formation and esterification of a molecule that has both carbonyl and carboxyl functional groups. In addition, $\Delta(m/z)$ values for the CH₃OH reactions can naturally occur in all solvents because ozonolysis of *d*-limonene generates many homologous families of products.⁹⁰

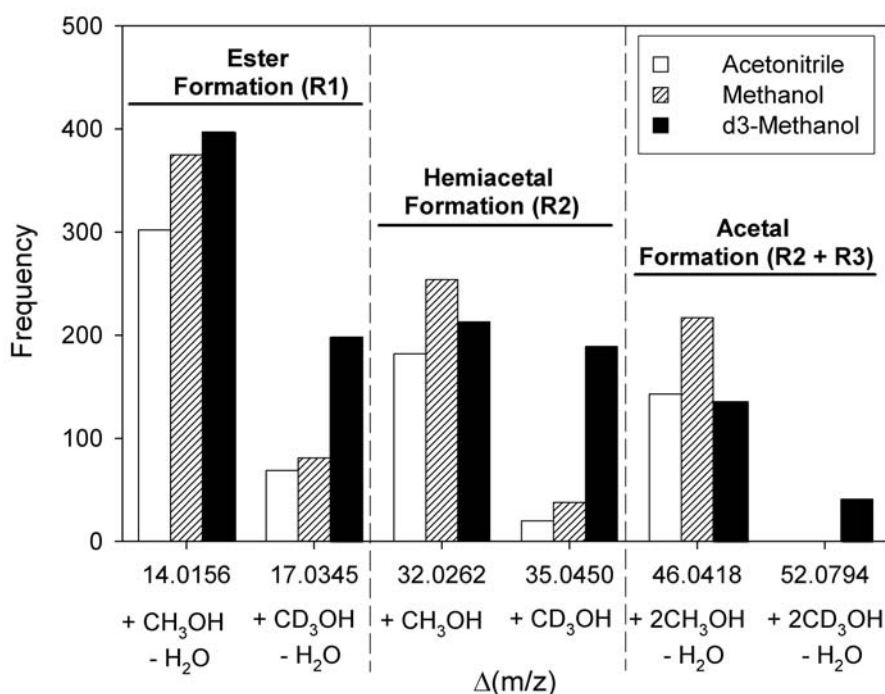


Figure 3.3. Frequency of occurrence of selected $\Delta(m/z)$ differences between peak positions in *d*-limonene SOA positive ion mode mass spectra recorded in acetonitrile, methanol and d₃-methanol in *m/z* range of 150-500.

The results of this comparison, Figure 3.3, clearly demonstrate that mass spectra recorded in CD₃OH provide the most information about the extent of solvent-analyte reactions. Positive ion mode d₃-methanol-based spectra contained over 200 peaks at even m/z values attributable to the solvent-analyte reaction products. In most cases, these peaks could be clearly distinguished from the isobaric ¹³C containing ions, based on the relative abundance and exact m/z values. Specifically, 189 pairs of peaks were separated by the exact mass of d₃-methanol, representing hemiacetal formation. In addition, there were 198 pairs of peaks corresponding to the formation of esters, and 41 pairs corresponding to the formation of acetals. In more than 100 instances, the same products were formed by more than one reaction (Eqns. 3.1 - 3.3) because of the simultaneous presence of both carbonyl and carboxyl functional groups in many SOA constituents.

Figure 3.4 is a graphical representation of the extent of solvent-analyte reactions in SOA extracts. It compares the positive ion mode mass spectrum of *d*-limonene SOA recorded in acetonitrile with mass spectra of the same SOA sample recorded in methanol and d₃-methanol. The acetonitrile-based mass spectra (top) contains all peaks with >0.5% relative intensity, including those from ¹³C containing ions. In contrast, the methanol- and d₃-methanol-based spectra (bottom) include only peaks corresponding to compounds capable of forming hemiacetals. Approximately 39% of *d*-limonene oxidation products in the monomeric range and 47% in the dimeric range are capable of adding one methanol molecule to form a hemiacetal. We stress that it is not just the smallest peaks that are affected by the methanol-analyte reactions. For example, if we limit the discussion only to peaks with relative abundance greater than 2% of the base peak (instead of 0.5%), the fraction of compounds capable of forming hemiacetals increases to 55% in the monomeric range and to 63% in the dimeric range.

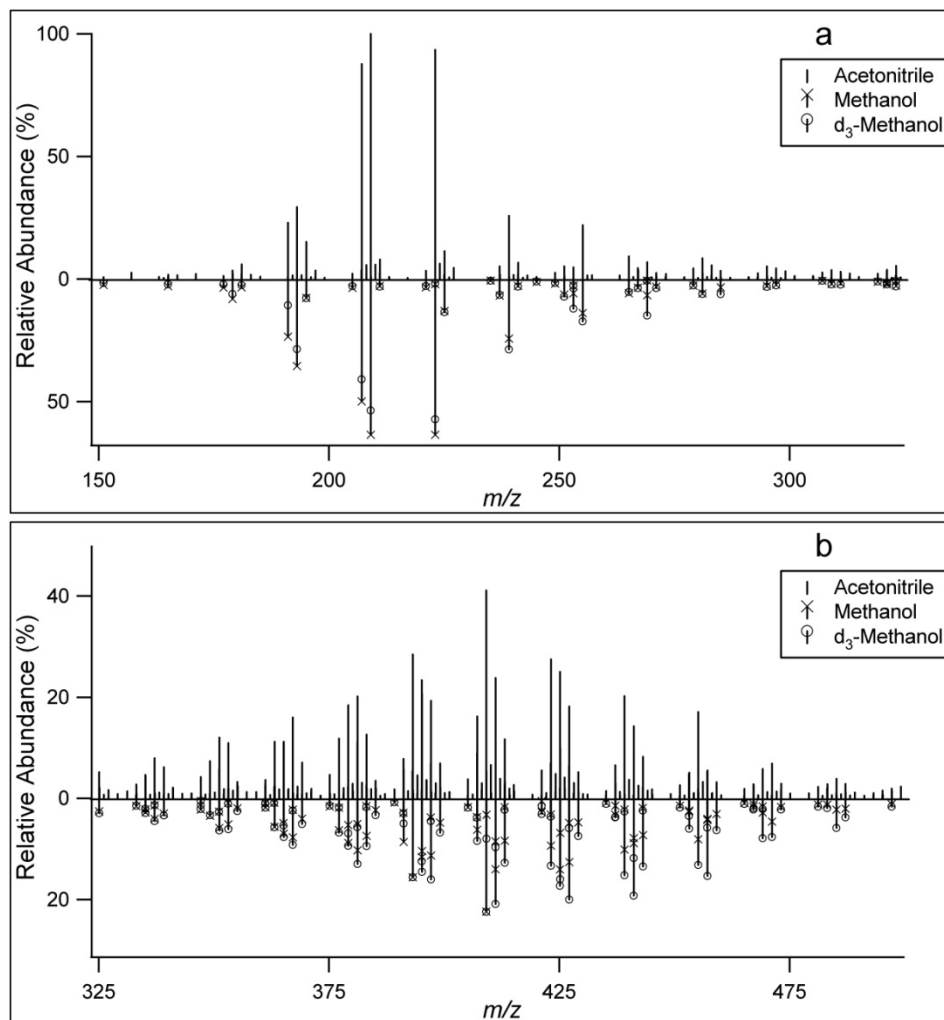


Figure 3.4. Graphical representation of the fraction of SOA compounds capable of forming hemiacetal products. The monomer range (a) and dimer range (b) are displayed separately for clarity. The full *d*-limonene SOA positive ion mode mass spectrum recorded in acetonitrile is given in the positive portions of the graphs. The negative portions display mass spectra recorded in methanol and d_3 -methanol, and include only peaks corresponding to compounds capable of forming hemiacetals.

To examine reactions occurring in methanol under more controlled conditions, we compared ESI mass spectra of the test compounds shown in Figure 3.1 using d_3 -methanol, methanol, and acetonitrile as electrospray solvents. All test chemicals contain a carboxylic acid group, and their mass spectra in acetonitrile are dominated by the $[M+Na]^+$ and $[M-H]^-$ peaks in

the positive and negative ion modes, respectively. In addition, these test compounds have one or two carbonyl groups, leading to the appearance of the corresponding ester and acetal peaks in the d_3 -methanol and methanol spectra.

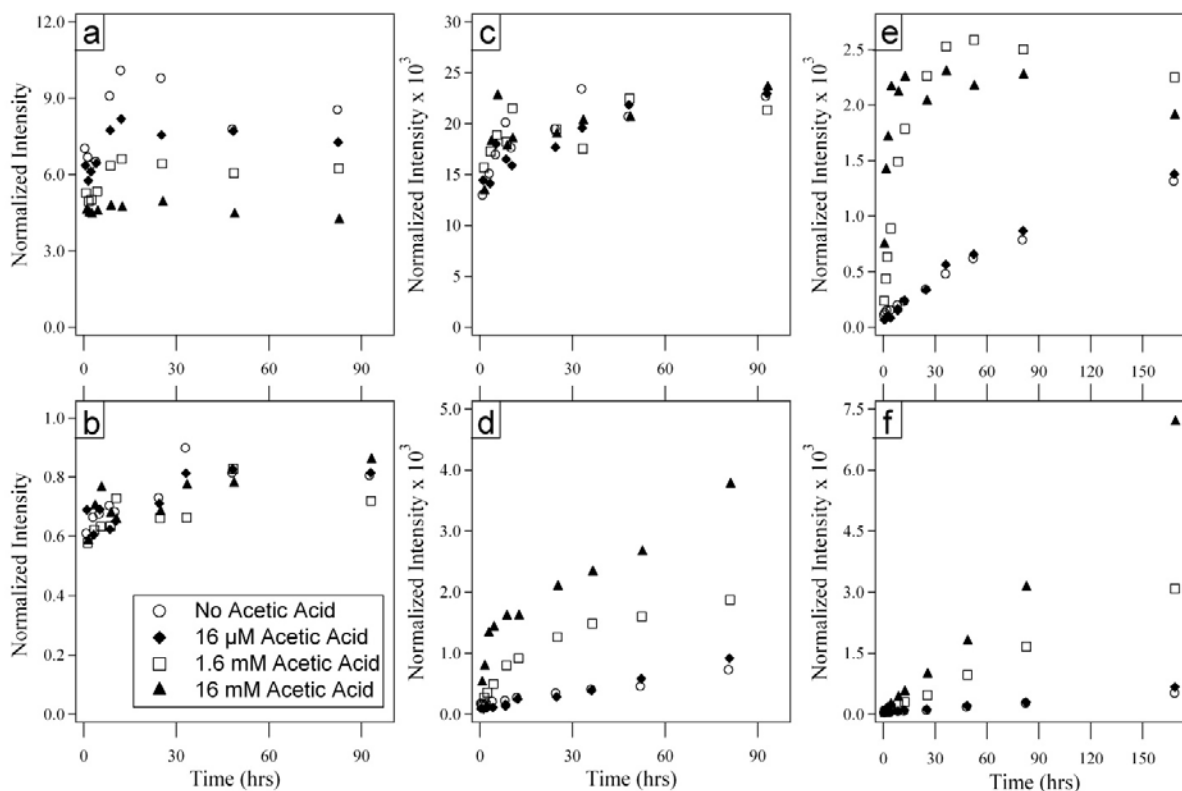


Figure 3.5. Representative data for time-dependent growth of products in reactions of test compounds with methanol: a) hemiacetal of SS; b) hemiacetal of DDA; c) ester of DDA; d) ester of PA; e) acetal of PA; and f) acetal of SS. All product intensities are measured in the positive ion mode and normalized to the corresponding precursor ion.

Sample measurements of product peak intensities as a function of the storage time are presented in Figure 3.5, wherein all intensities are normalized to the corresponding precursor peaks. The hemiacetal product peaks had a comparatively weak dependence on storage time and solution acidity. For example, Figure 3.5a and Figure 3.5b show the abundances of hemiacetals of SS and DDA, respectively. In both cases, the relative abundance of the hemiacetal started at a

high initial value of ~5 and ~0.6 for SS and DDA, respectively, and remained constant with time within the experimental uncertainty. These hemiacetals presumably attained an equilibrium with their precursor carbonyls *before* the first mass spectrum was taken (in less than ~5 min), and this equilibrium was then slowly shifted by the much slower acetal formation. We conclude that solvent-analyte reactions can result in large peaks appearing in the ESI mass spectra immediately after the sample preparation.

The intensity of the ester product peaks grew considerably more slowly with time. For example, all DDA solutions reached the ester \leftrightarrow DDA equilibrium in less than 24 hours with no apparent dependence on the acetic acid concentration (Figure 3.5c). On the contrary, the PA solutions did not attain the ester \leftrightarrow PA equilibrium even after 90 hours of storage, although the extent of the reaction noticeably increased with acidity (Figure 3.5d). The normalized abundance was larger for the DDA ester compared to that for the PA ester, presumably due to the presence of two carboxylic groups in DDA.

The acetal product peaks slowly increased in their relative abundance as a function of both time and solution acidity. For example, the relative abundance of the PA acetal (Figure 3.5e) started at a very low initial value, and reached a steady state corresponding to the acetal \leftrightarrow PA equilibrium after about one day of storage in solutions acidified with 16 mM and 1.6 mM acetic acid. Solutions containing 16 μ M or no acetic acid did not reach equilibrium even after one week of storage. The relative abundance of the SS acetal (Figure 3.5f) similarly increased with time and with solution acidity. However, the system was far from the acetal \leftrightarrow SS equilibrium even after one week of storage in the presence of 16 mM acetic acid.

3.4 Discussion

Drastic changes in the SOA mass spectrum resulting from isotopic substitution in the solvent molecules (methanol \rightarrow d_3 -methanol) clearly demonstrate that many SOA constituents undergo chemical reactions with methanol during extraction, storage, and possibly during the electrospray process. The reaction equilibria (Eqns. 3.1 - 3.3) generally favor the initial reactants but can be pushed toward the products with excess methanol, i.e., under typical conditions of extraction of a small quantity of organic material by a large volume of solvent. In addition, excess methanol can replace all $-OR$ groups in various esters present in SOA sample with $-OCH_3$ groups introducing additional artifacts to the mass spectra.

As opposed to the methanol case, isotopic substitution of acetonitrile for d_3 -acetonitrile has nearly no effect on the appearance of ESI mass spectra of SOA samples. Acetonitrile can undergo addition reactions with certain alcohols in the presence of concentrated acids.¹⁵⁵ In the presence of strong bases, acetonitrile can be deprotonated to form the cyanomethide ion, which is reactive towards carbonyls¹⁵⁶ and alcohols.¹⁵⁷ The laboratory generated OA extracts as well as extracts of field PM samples are expected to be neutral or weakly acidic.¹⁵⁸ Reactions of carbonyls and alcohols with acetonitrile are very unlikely under such mild conditions.

Formation of esters, hemiacetals, and acetals is well known to be acid-catalyzed.¹⁵¹ Therefore the effect of increasing acidity should lead to the faster appearance of reaction products in the mass spectra. This prediction is consistent with the observed time dependence of solvent reactions with test species SS, PA, and DDA (Figure 3.5). As expected, the acidity affects the rate but not the extent of the reaction: given enough time the same final equilibrium state is attained. The observed reduction of the hemiacetal peaks with the solution acidity (e.g.,

Figure 3.5a) can be explained by assuming fast hemiacetal/carbonyl equilibrium, followed by much slower hemiacetal/acetal equilibrium. As the solution acidity increases, the latter equilibrium is attained faster, leading to the relative increase in the acetal peak at the expense of the hemiacetal and analyte peaks.

Table 3.1. Relative abundance of ESI MS peaks after 24 hours of storage in methanol in the presence of variable amounts of acetic acid (AA) normalized to the corresponding precursor peaks (e.g., $[M+Na]^+$ and $[M-H]^-$ the positive and negative ion modes, respectively).

	Acetal Positive Mode	Acetal Negative Mode	Hemiacetal Positive Mode	Hemiacetal Negative Mode	Ester Positive Mode
PA / No AA added	1.27×10^{-4}	3.40×10^{-4}	1.03×10^{-4}	5.65×10^{-5}	3.45×10^{-4}
PA / 16 μ M AA	5.54×10^{-5}	3.38×10^{-4}	5.51×10^{-5}	1.57×10^{-5}	2.84×10^{-4}
PA / 1.6 mM AA	1.53×10^{-4}	2.26×10^{-3}	1.72×10^{-5}	2.31×10^{-5}	1.27×10^{-3}
PA / 16 mM AA	1.37×10^{-4}	2.03×10^{-3}	5.82×10^{-5}	3.66×10^{-5}	2.08×10^{-3}
DDA / No AA added	2.55×10^{-3}	6.89×10^{-5}	7.31×10^{-1}	1.24×10^{-3}	1.95×10^{-2}
DDA / 16 μ M AA	3.00×10^{-3}	6.47×10^{-5}	7.12×10^{-1}	1.11×10^{-3}	1.77×10^{-2}
DDA / 1.6 mM AA	2.71×10^{-3}	6.32×10^{-5}	6.62×10^{-1}	1.19×10^{-3}	1.94×10^{-2}
DDA / 16 mM AA	2.65×10^{-3}	5.54×10^{-5}	6.81×10^{-1}	6.71×10^{-4}	1.89×10^{-2}
SS / No AA added	2.70×10^{-2}	9.80×10^{-5}	9.79	1.34×10^{-2}	5.55
SS / 16 μ M AA	2.41×10^{-2}	1.31×10^{-4}	7.55	1.38×10^{-2}	5.71
SS / 1.6 mM AA	4.01×10^{-2}	4.68×10^{-4}	6.43	1.26×10^{-2}	5.51
SS / 16 mM AA	7.45×10^{-2}	9.76×10^{-4}	4.89	6.27×10^{-3}	4.94

Table 3.1 lists the relative abundance of the methanol-analyte reaction peaks from each test solution after 24 hours of storage. The methanol-analyte reaction peak abundances are normalized to the abundances of the $[M+Na]^+$ and $[M-H]^-$ precursor ions in the positive and negative ion mode, respectively. The relative abundance of product peaks is generally quite small, often smaller than a fraction of a percent. For example, all product peaks for PA are <0.3% of the precursor acid peak. However, relative abundances of the SS product peaks are

quite significant. The SS hemiacetal and ester peaks are in fact both larger than the SS peak in the positive ion mode. The hemiacetal and ester of DDA are also fairly abundant. The observed trend in reactivity towards methanol, SS > DDA > PA, is consistent with the higher reactivity of aldehydes versus ketones towards methanol due to both steric and electronic factors.¹⁵¹ In addition, large substituent groups in carbonyls tend to shift the equilibria (Eqns. 3.1 – 3.3) toward the initial reactants, i.e. away from ester, hemiacetal, and acetal formation.¹⁵⁹

Table 3.2: Observed reactivity of OA components with d₃-methanol. The last column provides approximate lower limits for the percentages of carbonyls and carboxyls in *d*-limonene SOA.

New peak at $\Delta m/z$ in d ₃ -methanol	Product	Functional group	Observed fraction in <i>d</i> -limonene SOA (%)
+35.0450	Hemiacetal	Carbonyl	~42
+17.0345	Ester*	Carboxylic acid	~55
+52.0794	Acetal**	Carbonyl	~13

* Can also result from hemiacetal formation followed by dehydration

** Can also result from hemiacetal formation followed by esterification

Table 3.2 shows how a direct comparison of mass spectra of the same sample dissolved in acetonitrile and d₃-methanol can be used to detect carbonyl and carboxyl groups in SOA constituents. Isotopically labeled methanol should be used for such a comparison because of the natural occurrence of CH₂- and H₂O- homologous series in SOA samples.^{89,90} Direct counting of peaks in *d*-limonene SOA positive ion mode mass spectrum between m/z 150-500 and above the 2% abundance threshold suggest that at least 42% and 55% of detectable SOA constituents contain carbonyl and carboxylic acid groups, respectively. This may appear unrealistically low given the extent of *d*-limonene oxidation reported in Ref. 90, with the O:C ratio approaching

~0.5. However, this peak-counting approach is expected to provide only a lower limit for the fraction of carbonyls and carboxyls in the sample because not every OA constituent is sufficiently reactive with methanol to produce significant product peaks in the ESI mass spectrum. Furthermore, the polyfunctional nature of SOA constituents could result in the simultaneous derivatization of multiple functional groups within the same molecule, which cannot be assigned using this simple peak counting procedure. The remaining oxygen required to achieve the high O:C ratio observed in Ref. 90 most likely resides in hydroxyl, ether and peroxy functional groups in SOA constituents, which do not readily react with methanol.

Table 3.3. The most abundant peaks observed in the positive ion mode ESI mass spectrum of d-limonene SOA in acetonitrile, methanol, and d₃-methanol. Relative abundance is given in parentheses next to m/z values, with “(100)” being the most abundant peak in a given mass spectrum. The table includes hemiacetal peaks resulting from addition of one methanol or d₃-methanol molecule to the precursor molecule. The corresponding neutrals are classified as aldehydes or ketones based on the relative abundance of the hemiacetal peak.

m/z (abundance) acetonitrile	m/z (abundance) methanol	m/z (abundance) d ₃ -methanol	Non-ionized composition	Likely classification
209.0785 (100)	209.0785 (54)	209.0784 (63)	C ₉ H ₁₄ O ₄	Ketone
-	241.1047 (30)	-		
-	-	244.1236 (16)		
207.0992 (88)	207.0992 (41)	207.0992 (50)	C ₁₀ H ₁₆ O ₃	Aldehyde
-	239.1255 (100)	-		
-	-	242.1444 (100)		
223.0942 (94)	223.0942 (57)	223.0942 (64)	C ₁₀ H ₁₆ O ₄	Ketone
-	255.1203 (10)	-		
-	-	258.1391 (8)		
193.0835 (30)	193.0835 (29)	193.0835 (35)	C ₉ H ₁₄ O ₃	Aldehyde
-	225.1098 (62)	-		
-	-	228.1286 (49)		
191.1043 (23)	191.1042 (11)	191.1043 (23)	C ₁₀ H ₁₆ O ₂	Aldehyde
-	223.1305 (47)	-		
-	-	226.1494 (52)		

The potential utility of solvent-analyte reactivity as a tool for interpretation of ESI mass spectra of SOA samples is further illustrated in Table 3.3. Table 3.3 lists the intensities of the five largest peaks in the *d*-limonene SOA positive ion mass spectrum in acetonitrile and classifies them as either aldehydes or ketones, based on the peak intensity of the hemiacetal compared to that of the precursor carbonyl. Table 3.3 clearly demonstrates all major SOA constituents listed in the table contain a carbonyl group. This is consistent with the known mechanism of gas-phase ozonolysis of alkenes, which generates carbonyls in high yields by splitting unstable primary ozonides, and carboxylic acids by isomerization of carbonyl oxides.⁹⁰ Table 3.3 also demonstrates that the peaks corresponding to the reactions between SOA constituents and methanol have appreciable intensities. Indeed, the most abundant peaks observed in the positive ion mode ESI mass spectra of *d*-limonene in methanol and d_3 -methanol correspond to hemiacetals. We conclude that solvent-analyte reactions occur to a significant extent in methanol extracts and should be taken into serious consideration in the analysis of organic aerosol samples by ESI-MS.

3.5 Conclusion

This study examined the effect of solvent on the analysis of organic aerosol extracts using electrospray ionization mass spectrometry (ESI-MS). Secondary organic aerosol (SOA) produced by ozonation of *d*-limonene, as well as several organic molecules with functional groups typical for OA constituents, were extracted in methanol, d_3 -methanol, acetonitrile, and d_3 -acetonitrile to investigate the extent and relative rates of reactions between analyte and solvent. High resolution ESI-MS showed that reactions of carbonyls with methanol produce significant amounts of hemiacetals and acetals on time scales ranging from several minutes to

several days, with the reaction rates increasing in acidified solutions. Carboxylic acid groups were observed to react with methanol resulting in the formation of esters. In contrast, acetonitrile extracts showed no evidence of reactions with analyte molecules, suggesting that acetonitrile is the preferred solvent for SOA extraction. The use of solvent-analyte reactivity as a tool for the improved characterization of functional groups in complex organic mixtures was demonstrated. Direct comparison between mass spectra of the same SOA samples extracted in methanol versus acetonitrile was used to estimate the lower limits for the relative fractions of carbonyls ($\geq 42\%$) and carboxylic acids ($\geq 55\%$) in *d*-limonene SOA.

Chapter 4

Size and Time-Resolved Molecular Characterization

Reproduced in part with permission from Phys. Chem. Chem. Phys., **2009**, 11, 7931-7942.

Copyright © the Owner Societies 2009

4.1 Introduction

The main objective of this chapter is to examine the variance of SOA chemical composition with particle size, reaction time, humidity, and presence of actinic radiation in the reaction chamber using HR ESI-MS methods of analysis. This work builds on our previous study,⁹⁰ which probed limonene aerosol under a single set of reaction conditions, by examining the evolution of SOA chemical composition as a function of particle size and reaction time.

Another objective of this chapter is to investigate the use of the HR ESI-MS technique towards quantifying oxygen content. Many field and laboratory studies rely on measuring the organic carbon mass (*OC*) of collected particulate matter. The total organic mass (*OM*) is then estimated by multiplying by a constant conversion factor, *OM:OC* ratio, which was historically set at 1.4, current literature values for urban aerosol and non-urban aerosol are, 1.6 ± 0.2 and 2.1 ± 0.2 , respectively.^{160, 161} This conversion factor is a strong function of the organic oxygen content of the aerosol, which is difficult to quantify using traditional analytical techniques. High-resolution mass-spectrometry could provide a valuable alternative method for measurements of the *OM:OC* ratio.¹⁴⁶

4.2 Experimental

Briefly, limonene SOA was generated from the reaction of d-limonene vapor and O_3 in an inflatable $\sim 400L$ Teflon FEP reaction chamber. The particles were collected with both a drum impactor and MOUDI as described in Chapter 2. Representative particle size and number concentration data obtained from the SMPS system are included in Figure 4.1. The geometric mean particle diameter typically reached $\sim 0.3 \mu m$ after thirty minutes of reaction and continued to increase slowly after that.

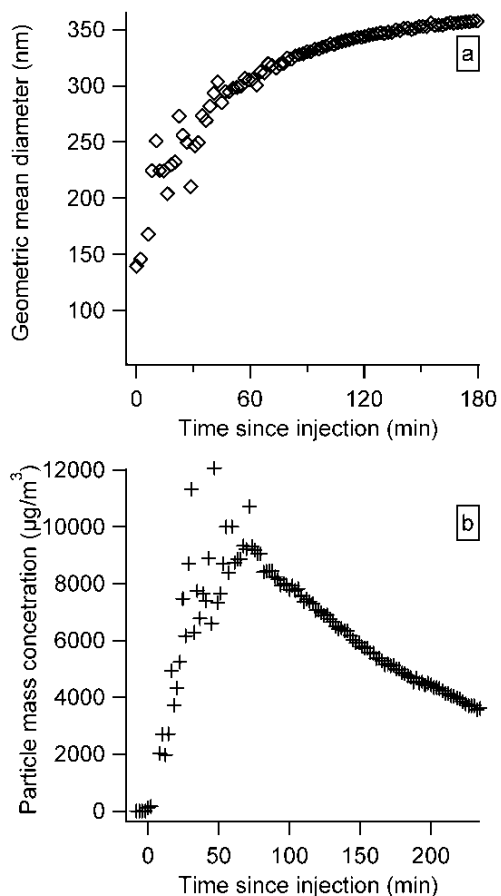


Figure 4.1. Representative data from SPMS measurements during reaction of limonene and ozone in the dark. The particle geometric mean diameter (a) and total particle mass concentration (b) are plotted versus time from injection of limonene into reaction chamber. The noise in the data is due to the lack of active mixing in the chamber.

4.3 Results

Our previous work presented positive and negative ion mode mass spectra of limonene SOA generated under dry conditions, in dark, in pure oxygen, and with comparable (ppm level) initial concentrations of reagents.¹³⁵ Mass spectra and, as expected, the generated VK diagrams obtained in this work look very similar to those published in Ref. 90. An example of a positive ion mode mass spectrum is provided in Figure 4.2. We were able to observe and assign more peaks compared to our previous work.⁹⁰ However, the general features of the mass spectrum and VK diagrams are the same. The most recognizable feature of the mass spectrum is clustering of peaks into the monomeric range ($< 300 m/z$), dimeric range (300-500 m/z), trimeric range (500-700 m/z), and tetrameric range (700-1000 m/z) corresponding to products containing one, two, three, and four oxygenated limonene units, respectively. Similar clustering of peaks in mass-spectra has been observed in previous publications on monoterpene/ O_3 SOA.^{25, 72, 77, 89, 99,}

162

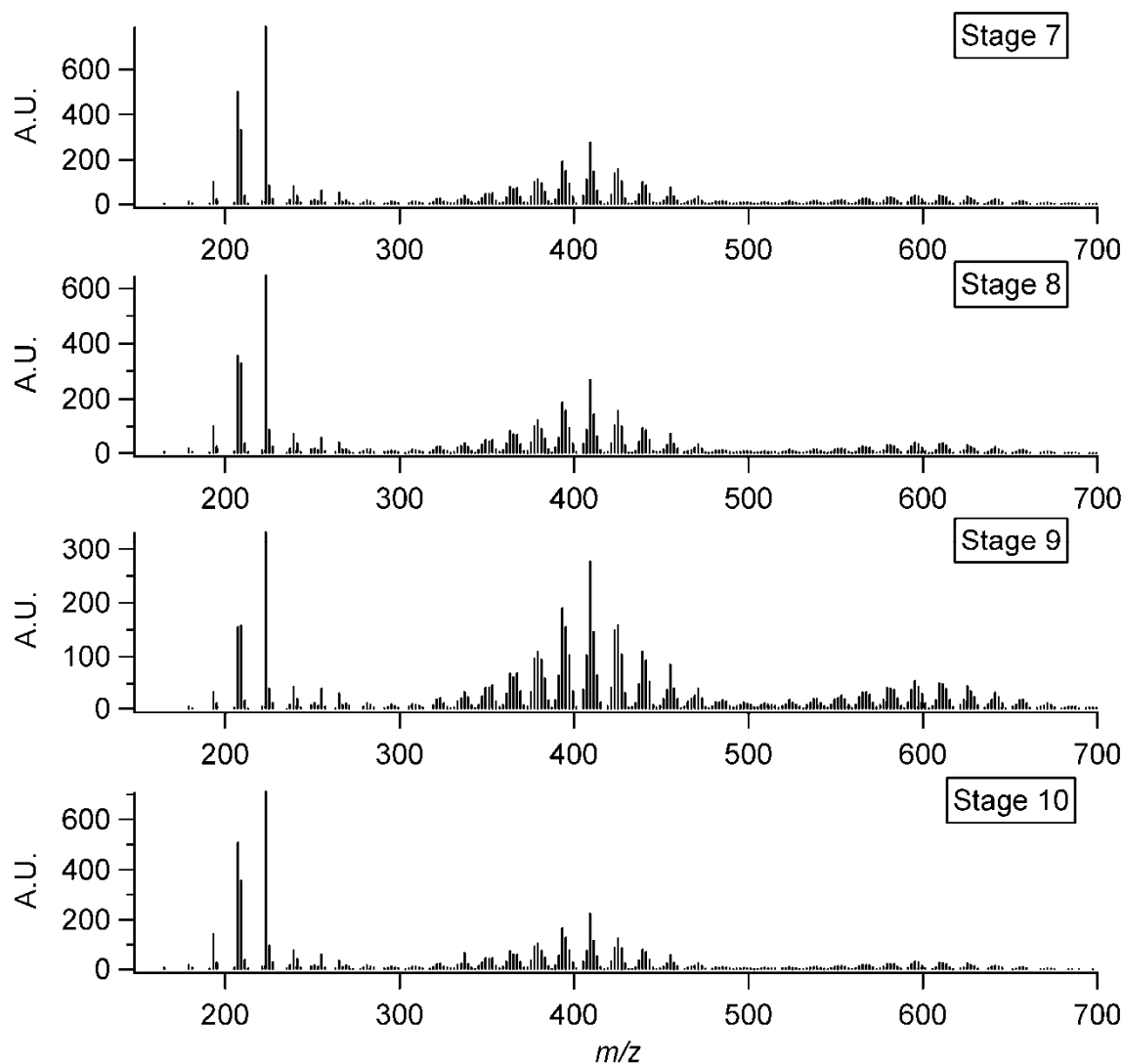


Figure 4.2. Representative positive ion mode ESI mass spectra from the dark reaction of limonene and ozone 10 min after injection of limonene as collected using MOUDI and extracted into acetonitrile. The average sizes of the particles decrease from stage 7 to stage 10 but the shapes of the mass spectra remain approximately the same.

The limonene SOA constituents have H:C ratios ranging from 1.1 to 1.8 and O:C ratios ranging from 0.2 to 0.7 for most compounds. Due to the chemical complexity of SOA, several different molecules often end up having the same H:C and O:C values in the VK diagram. It is therefore useful to use either DBE or molecular weight as an additional dimension for visualization of the HR-MS data. Figure 4.3 shows the result of stretching the VK plot along the

DBE dimension. Examination of this plot shows that the H:C ratios are anti-correlated with DBE values, i.e. molecules with higher DBE tend to have lower average H:C ratios. The group of apparent outliers with very low H:C values (1.1-1.3) and high DBE values (9 – 10) is especially striking. No obvious trends with respect to DBE are observed for the O:C ratios.

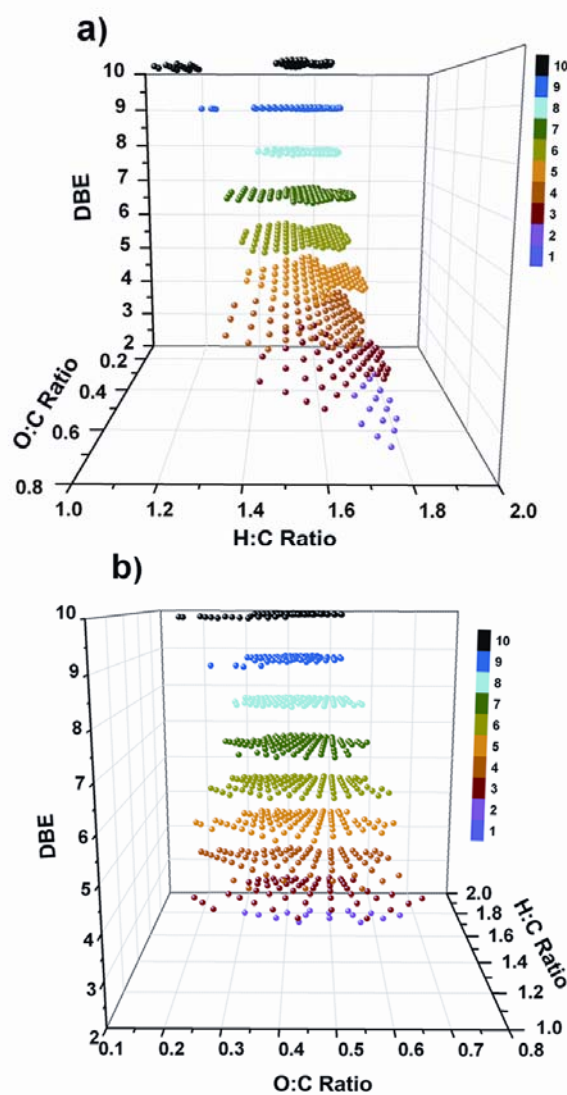


Figure 4.3. An expansion of the Van Krevelen plot along the DBE dimension for SOA sample from the dark reaction of limonene and ozone. The particles were collected using a DRUM impactor, extracted into acetonitrile, and immediately analyzed via ESI-MS. This sample corresponds to the first 4 minutes of reaction between ozone and limonene.

The observed DBE values range from 2 to values exceeding 10, and appear to be positively correlated with the molecular weights of the SOA constituents (Figure 4.4). For the majority of the molecules, DBE scales roughly linearly with molecular weight (one DBE unit per 100 g/mol). The outliers in this plot are the same ones that stand out in Figure 4.3. They likely correspond to molecules formed by unique chemical processes; perhaps cyclization of the first generation SOA products leading to conjugated systems or even aromatic rings.

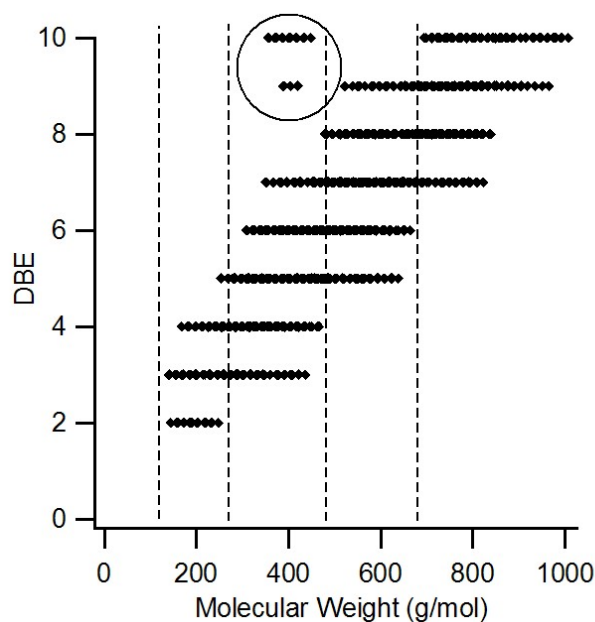


Figure 4.4. DBE values plotted against molecular weights of SOA compounds for the sample in Figure 4.2. Dashed lines separate different regions in the mass spectrum (monomers, dimers, trimers, tetramers). The circled group of points corresponds to molecules with positive values of aromaticity index.

Figure 4.5 shows an SEM image of typical SOA particles collected on stage 7 of MOUDI and particles size distributions measured by CC-SEM based on the equivalent circle diameters of two-dimensional projection areas. Close examination of the SEM image (Figure 4.5a) reveals two interesting observations: i) the distribution of the apparent particle sizes was

quite broad; ii) the apparent sizes of many collected particles significantly exceeded the expected size range for that MOUDI stage (0.56-0.32 μm for stage 7). Similar observations were made for particles collected on other MOUDI stages. Figure 4.5b demonstrates that the normalized distributions of apparent particle sizes for all stages overlapped quite significantly. In contrast, collection of crystalline NaCl particles¹⁶³ and CaCO₃ particles¹⁶⁴ with the same MOUDI setup reproducibly resulted in much narrower size distributions. We believe that some of the amorphous, presumably jelly-like, SOA particles were flattened by the impaction onto the substrate, resulting in their two-dimensional projection areas larger than their original airborne size. An alternative possibility that SOA particles coagulated on the substrate after the impaction, similar to the coagulation of mercury droplets on a surface, is unlikely given that the size distribution of samples with much reduced total number of particles was also broad. As the particle impact velocity increases for smaller particles, the degree of particle flattening is larger for higher MOUDI stages (Figure 4.5c). Despite the large width of the apparent size distribution, the average collected particle size did increase by a factor of four from stage 10 to stage 6 making it possible to investigate the effects of the average particle size on the SOA composition.

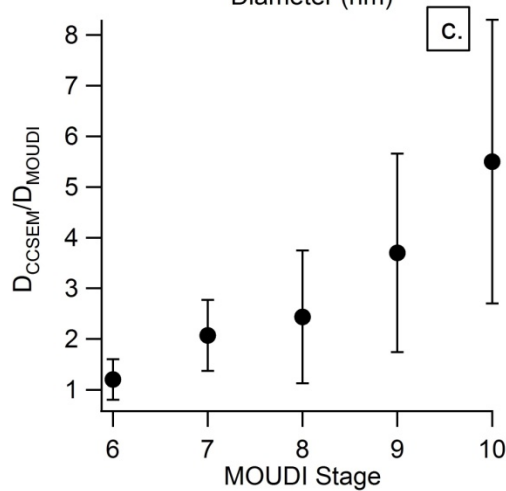
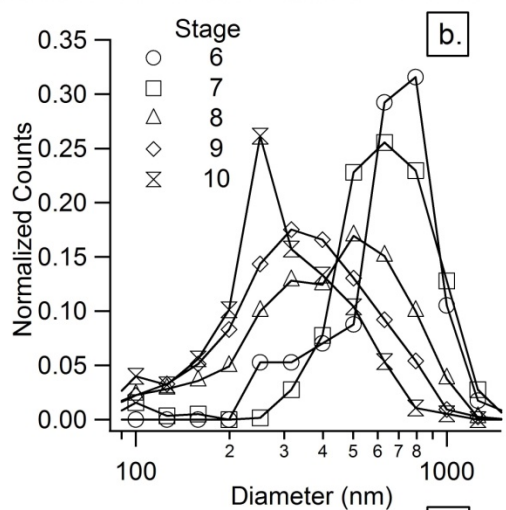
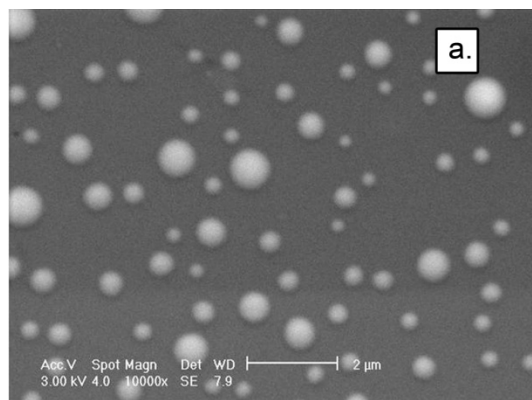


Figure 4.5. (a) Representative CC-SEM image of particles collected on Stage 7 of MOUDI from the dark reaction of d-limonene and ozone. (b) Distribution of the apparent particle sizes for stages 6-10 as measured by CC-SEM. (c) Ratio of the average apparent size to the MOUDI cut-off diameter plotted against the MOUDI stage. Error bars correspond to one standard deviation.

We compared the mass spectra of extracts from different MOUDI stages and collected at different times after mixing limonene and ozone. The mass spectra were fairly similar for all examined MOUDI stages. However, there was a small but reproducible difference between samples collected after 10 min and 90 min of reaction. Specifically, the oxidation state of molecules appeared to increase slightly with time. To better illustrate this point, Figure 4.6 shows the average O:C and H:C ratios for stages 7 through 10. After 90 min of reaction, the H:C ratio did not change within experimental uncertainties, whereas the O:C increased from 0.42 to 0.45.

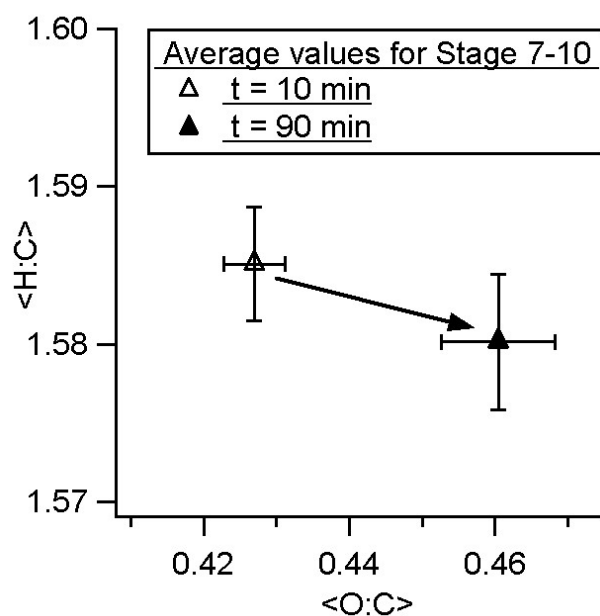


Figure 4.6. Average H:C and O:C values calculated for stages 7 through 10. Data for two MOUDI samples, 10 min and 90 min after the injection of limonene are plotted. Error bars correspond to one standard deviation for the corresponding ratios.

To examine the observed evolution of the average chemical composition with better time resolution, we analyzed several batches of the DRUM impactor data. Weighted average O:C ratios, H:C ratios and DBE values were computed for each spectrum. Figure 4.7 shows a representative result, with these values plotted as a function of the reaction time for four

separate subsets of the SOA constituents corresponding to the monomeric (150-300 m/z), dimeric (300-500 m/z), trimeric (500-700 m/z) and tetrameric (700-1000 m/z) regions in the mass spectra. The average DBE values increase in this order, as can be expected from Figure 4.4. However, within a given subset of products, they do not significantly change with time. The average O:C ratios systematically increase with the reaction time and tend to level off after ~1 hr, with the typical final values of ~0.44 for the monomer and dimer regions and ~0.46 for the trimer and tetramer region. In all the other data sets we examined, products with larger molecular weights similarly appeared to have slightly higher average O:C ratios. The average H:C ratio has a much smaller spread than the O:C ratio and shows no significant time dependence.

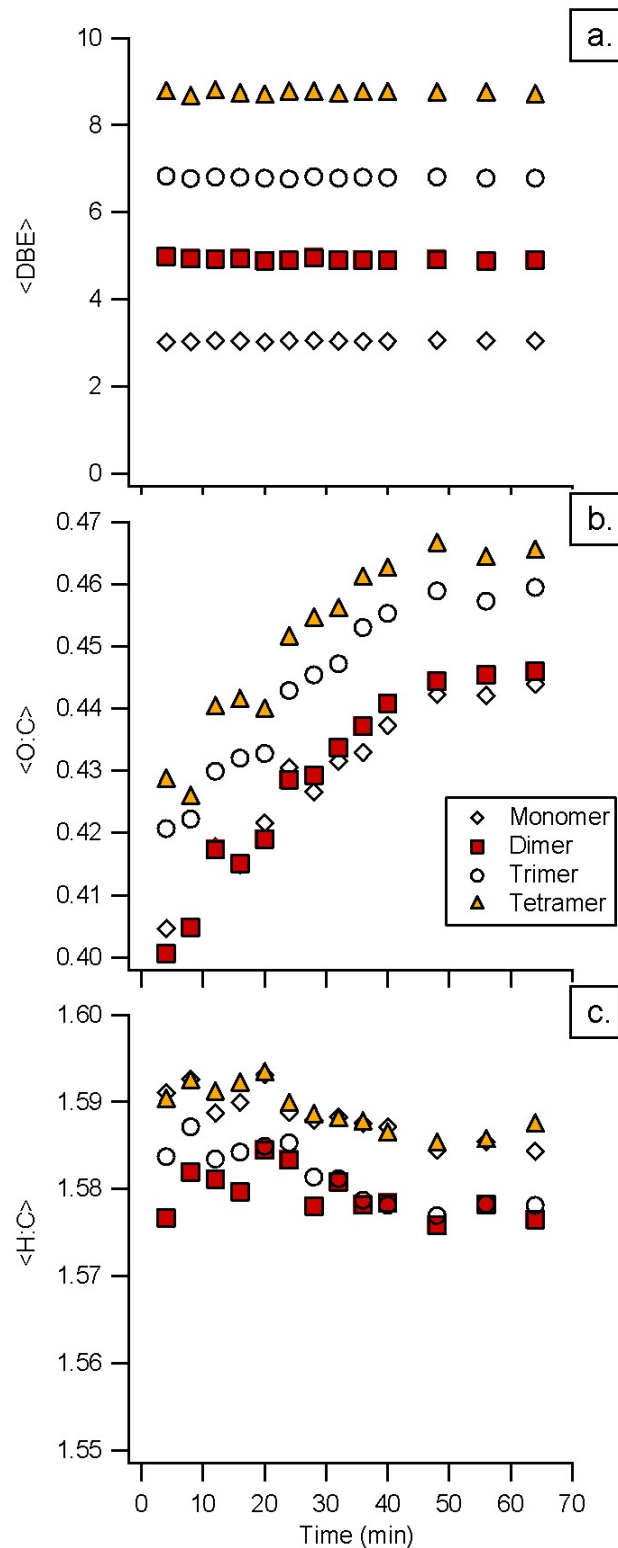


Figure 4.7. Averaged properties of SOA collected during dark reaction of d-limonene and ozone using a drum impactor vs. reaction time and region of the mass spectra: (a) average DBE; (b) average O:C; (c) average H:C.

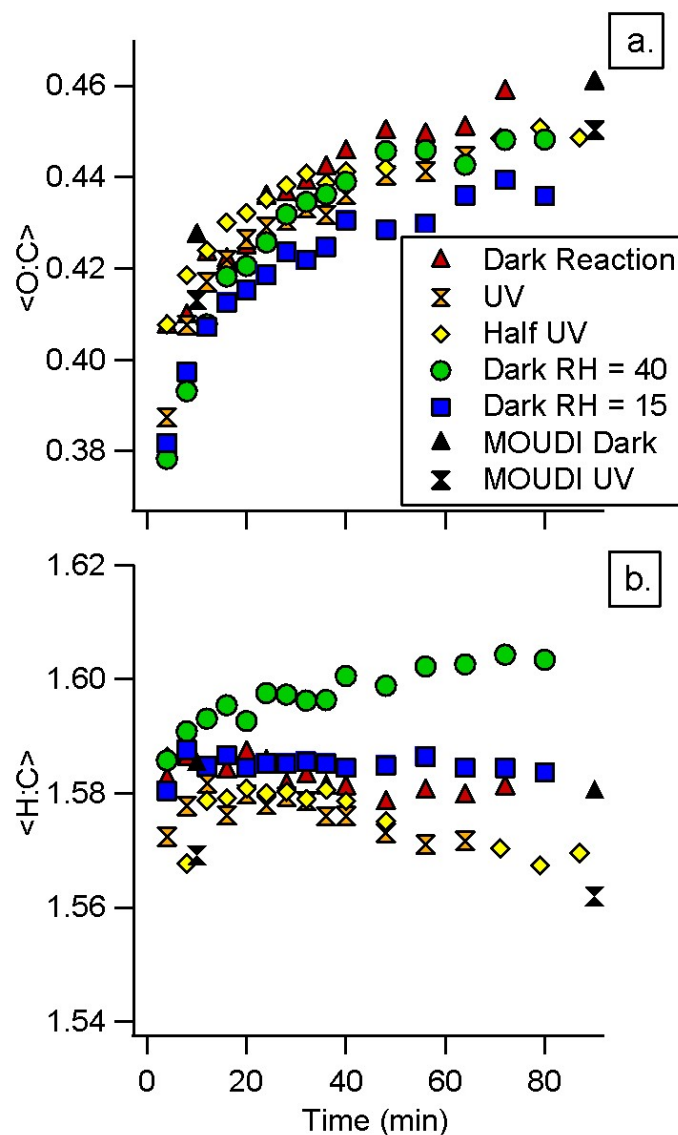


Figure 4.8. Time dependence for (a) average O:C and (b) average H:C ratios under different conditions in the reaction chamber. Black symbols result from MOUDI samples and colored symbols result from rotating strip impactor samples. Reaction conditions include: Dark – no radiation, dry air; UV – radiation is on during entire reaction, dry air; Half UV – radiation turned on after 30 min of reaction time, dry air; RH = Relative Humidity, no UV radiation.

Similar plots were constructed for SOA samples prepared under different relative humidity and UV radiation levels (Figure 4.8). The reaction conditions include: i) dark reaction in dry air; ii) reaction in dry air in the presence of UV radiation; iii) reaction in dry air with the

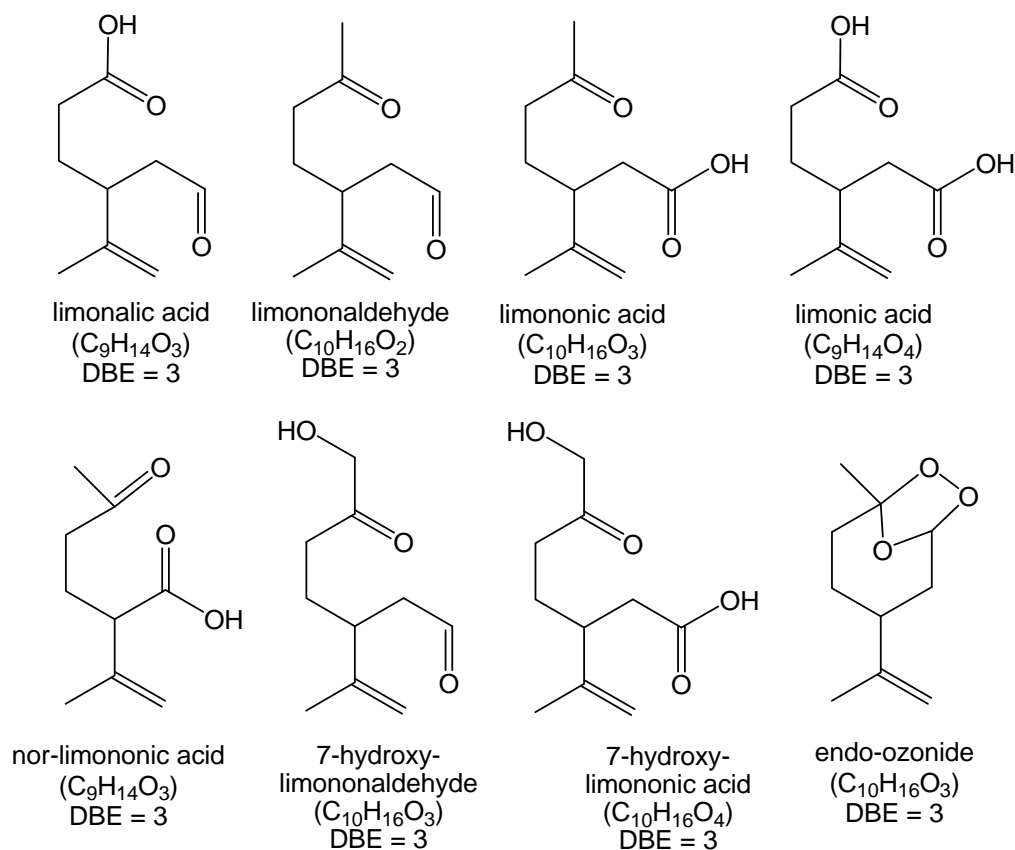
UV lamps turned on 30 min after mixing the reagents; iv) dark reaction at ~ 15 %RH; iv) dark reaction at ~ 40 %RH. Additionally, the O:C and H:C ratios calculated from the MOUDI samples (stages 7-10 combined) are included for comparison. For simplicity, the H:C and O:C ratios are not differentiated by the region of the mass spectra as in Figure 4.7, but are computed for the entire set of assigned SOA constituents. The average DBE values for all reaction conditions are nearly identical to those for the dark reaction, and have no significant time dependence; they are not shown in Figure 4.8. The slow increase in the O:C ratio was observed for all reaction conditions, with an excellent agreement between the MOUDI samples and rotating strip impactor samples. Within the experimental uncertainties, the H:C ratios were constant under different reaction conditions. Only the high RH experiments showed measurable increase in the H:C ratio.

4.4 Discussion

Molecular Composition of Limonene SOA

The observed DBE values for all monomeric SOA products fall between 2 and 4. Limonene itself has a DBE of 3, corresponding to its two C=C double bonds and one ring. The most prominent first generation products of limonene ozonolysis, such as endo-ozonide, limonic acid, limononic acid, limonic acid, limonic acid, 7-hydroxy-limononaldehyde, 7-hydroxy-limononic acid, and limononaldehyde also have a DBE of 3, structures of these products are shown in Figure 4.9.

Selected examples of the first generation products resulting from reaction of ozone and the endocyclic double bond of limonene. Most of these products have DBE = 3.



Selected examples of monomeric products with DBE ≠ 3. Such products can arise from chemistry involving isomerizations and/or decompositions of RO radicals formed the decomposition of Criegee intermediates.

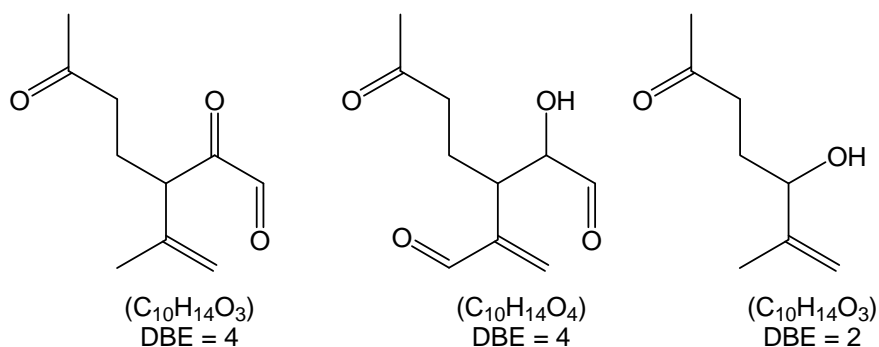


Figure 4.9. Selected first generation products from limonene ozonolysis along with their molecular formulas, names, and DBE values.

Although ozone destroys the limonene's endocyclic double bond and opens up its six-membered ring, reducing DBE by 2, this is compensated by the formation of two new C=O bonds (e.g., carbonyl and carboxyl) or two new rings in the case of the endo-ozonide. Subsequent oxidation of the exocyclic double bond into a carbonyl maintains the DBE value at 3 in products like keto-limononaldehyde or keto-limononic acid. Formation of monomeric products with DBE of 2 and 4 requires more complicated chemistry involving multiple isomerization and/or decomposition processes in alkoxy radicals formed from the decomposition of the Criegee intermediates.⁹⁰ Selected examples of the first generation products with DBE of 2 and 4 are also included in Figure 4.9.

There is a clear tendency for the DBE value to increase with the molecular weight of the SOA compounds (Figure 4.4). The most common DBE values for the monomeric, dimeric, trimeric, and tetrameric products are 3, 5, 7, and 9, respectively (Figure 4.7). This increase by two DBE units is consistent with oligomer formation occurring by reactions between one of the first generation products (typical DBE = 3) and a Criegee intermediate formed in the initial attack of ozone on limonene. Both Criegee intermediates resulting from an attack on the endocyclic double bond have an effective DBE of 3, which corresponds to one remaining C=C double bond, one carbonyl group, and one carbonyl oxide group. Figure 4.10 shows the formation of a DBE = 5 organic peroxide in reaction between limononic acid and one of the Criegee intermediates. This mechanism of oligomerization becomes operative already at the very early stages of ozonolysis.⁹⁹ As evidenced by the data in Figures. 4.3, 4.4 and 4.7, oligomers were found in samples collected only four minutes into the reaction and throughout the subsequent reaction, regardless of the particle size.

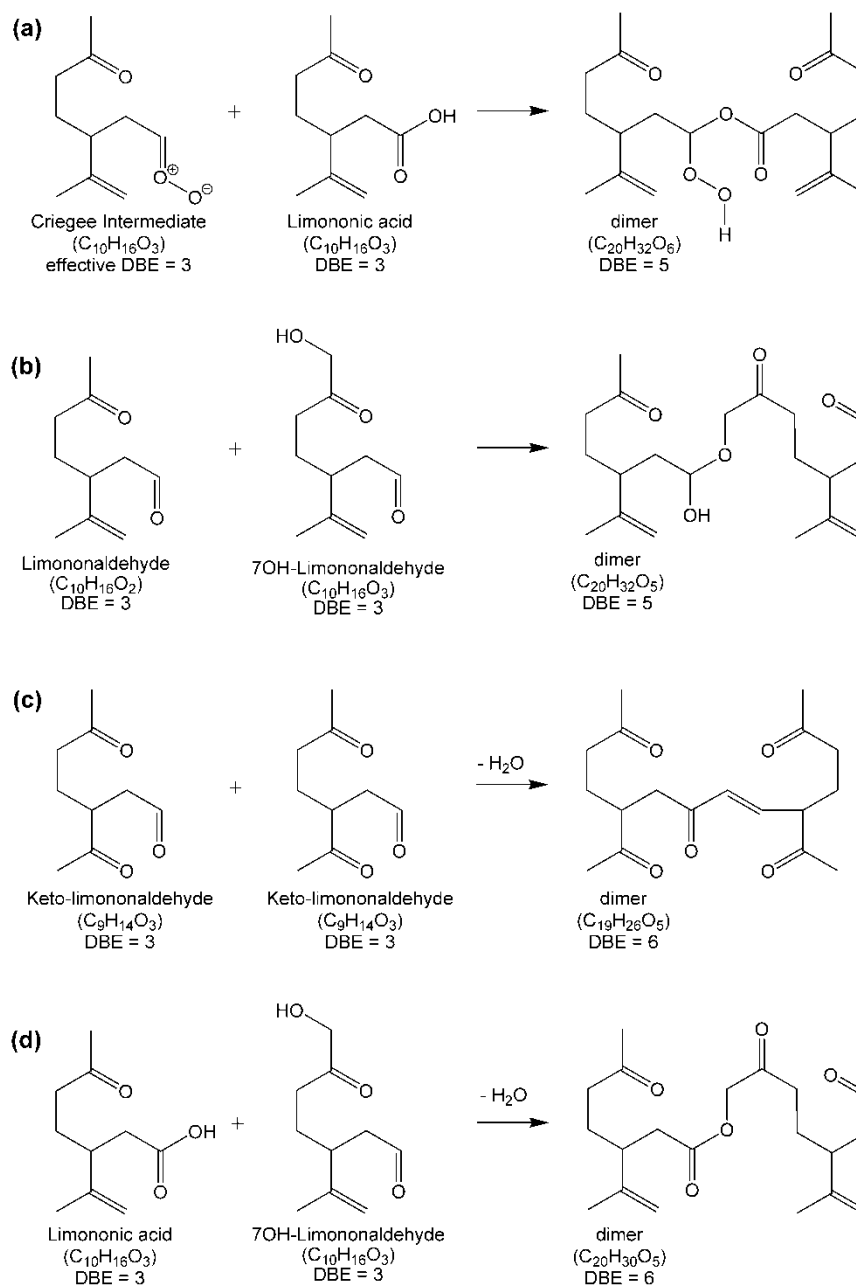


Figure 4.10. Growth of DBE in different oligomerization reactions. (a) reaction between a Criegee intermediate and an acid or alcohol; (b) hemiacetal formation from an aldehyde and an alcohol; (c) aldol condensation involving two aldehydes; (d) esterification reaction between a carboxylic acid and an alcohol. Mechanisms (a) and (b), which increase DBE by 2 per oligomerization step, are more consistent with the trend shown in Figures 4.4, and 4.7.

Another mechanism that increases DBE by 2 in each oligomerization step involves formation of hemiacetals through reactions of alcohols with aldehydes and ketones. Figure

4.10b shows an example involving a reaction between two common limonene ozonolysis products, limononaldehyde (DBE = 3) and 7-hydroxy-limononaldehyde (DBE=3). Because the aldehyde group is destroyed during this reaction, DBE of the resulting dimer is 5. Formation of hemiacetals in reactions of SOA constituents with methanol is quite efficient when methanol is used as the SOA extraction solvent.¹³⁵ Presumably, intramolecular hemiacetal formation reactions can also occur in the SOA matrix or/and in SOA extracted in acetonitrile, contributing to the appearance of oligomeric species.

Condensation reactions such as aldol condensation and esterification have also been proposed as possible oligomerization mechanisms in SOA.^{72, 165} Unlike the Criegee intermediate reaction and hemiacetal formation considered above, DBE is additive in condensation reactions. For example, the product of an aldol condensation of keto-limononaldehyde (DBE = 3) with itself has a DBE of 6 (Figure 4.10c). The esterification product produced from limonic acid (DBE = 3) and 7-hydroxy-limononaldehyde (DBE = 3) also has a DBE of 6 (Figure 4.10d). If condensation reactions were the major oligomerization pathway, we would expect the DBE to increase by 3 on every step from monomers to dimers, trimers, etc. Therefore, the observed increase in DBE by 2 units (Figure 4.2) suggests that oligomer formation via condensation reactions does not play an important role under the experimental conditions used in this study.

The majority of the observed SOA constituents appear to represent oxygen-rich aliphatic compounds. The aromaticity index (*AI*) values calculated for the compounds forming the main cluster of points in the VK plot in Figure 4.3 are all negative, which is consistent with the lack of aromatic rings in the molecules. However, there is a small group of compounds with considerably lower H:C values and positive *AI* values. They appear as “outliers” in the VK

plots, and are especially easy to see in Figures 4.3 and 4.4 as an isolated group of points with high DBE values. The calculated *AI* values for these compounds start to approach the *AI* = 0.5 threshold for the existence of aromatic structures. These compounds were found in nearly every mass spectrum, regardless of reaction time or particle size. They may arise from a cyclization of certain polyketide-like SOA constituents, which create aromatic rings separated by aliphatic carbons. To the best of the authors knowledge and with the exception of reactions carried out under unrealistically acidic conditions,^{166, 167} this was the first report of aromatic species formed as products of ozonolysis of limonene or other monoterpenes. The findings have since been confirmed using α -pinene ozonolysis, yields and a mechanism were proposed.¹⁶⁸ This chemical pathway certainly warrants further investigation as the presence of aromatic structures is likely to have a major effect on the optical (light absorbing) and chemical properties of SOA.

Particle Size Dependence of SOA Composition

The general appearance of the mass spectra from different MOUDI stages, see Figure 4.2, is similar for all size fractions suggesting that the chemical composition of SOA generated from the reaction of limonene and ozone is not especially sensitive to the particle size. Subtle changes in the relative peak intensities of monomer, dimer, trimer, and tetramer regions possibly originate from matrix effects in the ESI ionization. At low concentrations (below $\sim 10^{-6}$ M), the ion current is proportional to the concentrations of analytes, whereas at high concentrations (above $\sim 10^{-4}$ M) the ion current saturates.¹⁵⁰ At these high concentrations, surface-active analytes are expected to out-compete polar analytes for the limited excess charge.¹³⁹ With the amount of SOA material collected on each MOUDI stage ($\sim 30 \mu\text{g}$), the effective overall concentration of SOA constituents was $\sim 10^{-4}$ M (assuming an effective

molecular weight of 300 g/mol). Under these conditions, the higher molecular weight species in SOA can be artificially enhanced in intensity. This enhancement is clearly visible in the mass spectrum for MOUDI stage 9, Figure 4.2, which typically collected the largest amount of SOA material.

The average values of O:C and H:C ratios and the general appearance of the VK plots were nearly identical for all size fractions. We attribute this to a prompt consumption of limonene and particle growth early in the reaction, before the first MOUDI sample was collected. The experiments described here were carried out with ~1 ppm level of the initial ozone and limonene mixing ratios, with ozone being in a slight excess. The reaction rate constant between limonene and ozone of $2 \times 10^{-16} \text{ cm}^3 \text{ molec}^{-1} \text{ s}^{-1}$ translates into a reaction half-time of ~3 min. The nonvolatile fraction of the first generation products should therefore all condense into SOA within minutes after the limonene addition. Indeed, in all the experiments the particle mass-concentration and particle size, as measured by the SMPS, Figure 4.1, increased the fastest during the first ten minutes after mixing the reagents. After that, the particle size grew slowly due to coagulation processes and particle mass concentration decreased slowly due to the wall loss. Therefore, both large particles that grew by coagulation and small particles that have not yet coagulated should contain more or less the same set of condensable organics.

Time Dependence of SOA Composition

Once particles are formed, the SOA constituents can participate in the following types of aging processes: i) further oxidation of the initial products by the residual ozone, both in the gas and particle phase; ii) photolysis by UV radiation; iii) various reactions between the condensed

SOA constituents; iv) uptake of and reactions with H₂O vapor; v) reactive uptake of gas-phase organic species, such as small aldehydes. Because there was a delay between collecting samples and taking their mass spectra, we cannot expect to be equally sensitive to all of these aging processes. MOUDI samples were collected twice during the reaction; the samples were promptly processed after that. The oxidation by ozone, UV photolysis, and reactive uptake of VOCs by the SOA particles ceased more or less immediately after the collection. However, the particles could still react with the H₂O vapor in the laboratory air (~20 %RH), and any conceivable condensed-phase reactions between the SOA constituents (cross-esterification, acetal formation, etc.) likely continued on the MOUDI substrate with the same rate they were occurring in the chamber. The DRUM impactor collected the particles continuously throughout the reaction. The particles deposited on the strip remained exposed to some levels of the residual ozone, humidity and VOCs carried with the sampling flow. All these factors could potentially suppress the time dependence of chamber processes. For example, if the only aging process taking place were slow oligomerization inside the particles, and all collected samples were then extracted and analyzed simultaneously, we would not expect to see significant changes in the mass spectra because the overall age of the particles, in the chamber and on the substrate, were the same.

Despite these limitations, several interesting trends emerged in the time-dependent mass spectra (Figures 4.6 - 4.8). The particles collected in the first few minutes of reaction already had relatively high oxidation levels as measured by the average O:C ratio in the products (Figures 4.7 and 4.8). The O:C ratio reached ~95 % of its final level by the first 4 minutes and the remaining ~5 % of O:C increase took almost an hour. At the same time there were no significant changes in the average DBE values and H:C ratios (Figure 4.7). We suspect that

these changes were due to a slow oxidation of the remaining exocyclic C=C double bonds by the residual ozone. Slow conversion of aldehydes into carboxylic acids by the residual ozone¹⁶⁹ or by organic peroxides present in the SOA could also contribute to the observed growth in the O:C ratio.

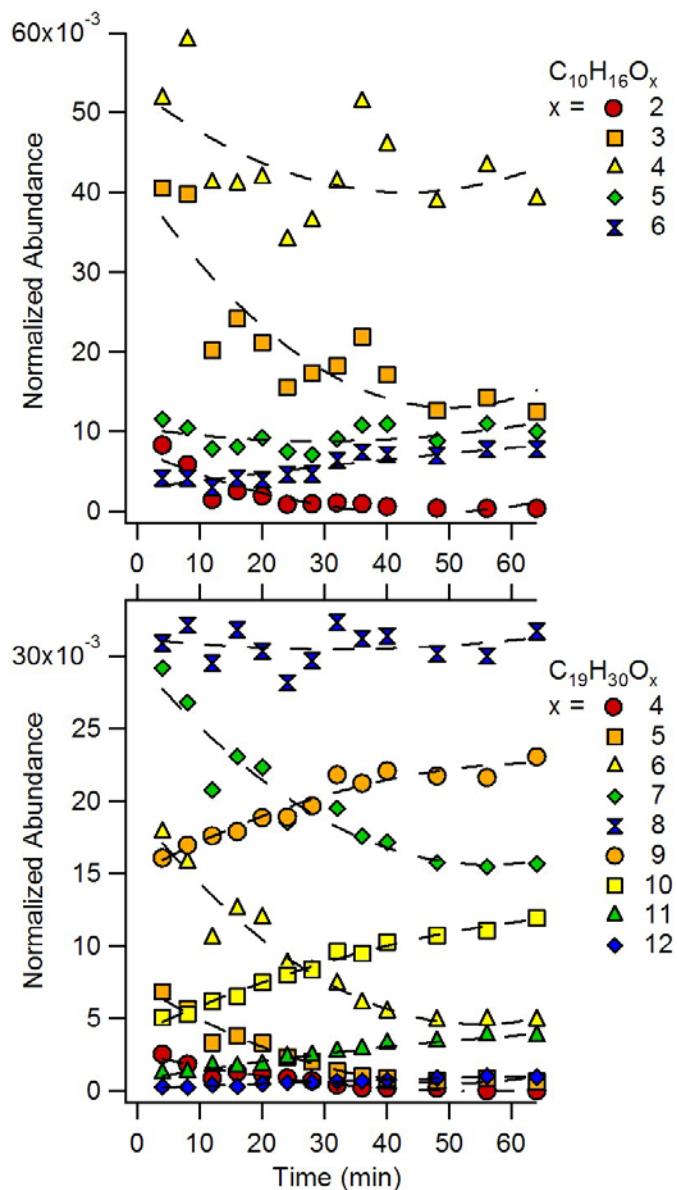


Figure 4.11. Normalized peak intensities for the $C_{10}H_{16}O_x$ and $C_{19}H_{30}O_x$ families of products as a function of time during a dark reaction of limonene and ozone. Dashed lines represent polynomial fits to data as guides.

More information about the mechanism can be inferred from the time dependence of the relative abundances from homologous families of products with the same number of carbon and hydrogen atoms, but differing in the number of oxygen atoms. Figure 4.11 shows the time evolution for two representative monomeric and dimeric families of products, $C_{10}H_{16}O_{x=2-6}$ and $C_{19}H_{30}O_{x=4-12}$. The dashed lines have been included to guide the eye, by following the general trend of each peak. It can be seen that the compounds with the lower oxygen content (smaller x) decrease with time, compounds with the larger oxygen content (larger x) increase with time, while the ones in the middle stay relatively constant. When averaged over the large number of such families of compounds present in limonene SOA, the net result is the slow increase in the O:C ratio. The characteristic reaction time in Figure 4.11 appears to be on the order of ~ 30 min. If we assume ~ 1 ppm residual O_3 , and adopt an Ostwald coefficient of ~ 2 for solubility of ozone in the limonene SOA material (typical value for polar organic solvents)¹⁷⁰ we obtain $k \sim 10^3$ - 10^4 $L\ mol^{-1}\ s^{-1}$ for the effective rate constant between the dissolved ozone and SOA constituents. This value is similar to ozone-alkene rate constants in liquid phase.¹⁷¹ It is two to three orders of magnitude larger than typical ozone-aldehyde rate constants. We therefore conclude that the major mechanism of the O:C increase was ozonolysis of the exocyclic C=C double bonds in the first generation SOA products.

Effects of Relative Humidity and UV Radiation

Presence of the UV radiation in the reaction chamber had rather insignificant effect on the molecular composition of limonene SOA, as evidenced by the remarkable insensitivity of the average O:C and H:C ratios to UV (Figure 4.8). Under the present experimental conditions, the changes in the observed mass spectra were relatively subtle. The UV radiation caused a

slight redistribution in the relative peak intensities; it also generated some additional small peaks in the mass spectrum. Photodegradation of the SOA material by actinic UV radiation is likely to take place on a time scales of hours or even days.^{18, 20} This is much slower than the time scales of the competing processes: minutes for the formation of the first generation products; an hour or so for the secondary oxidation chemistry.

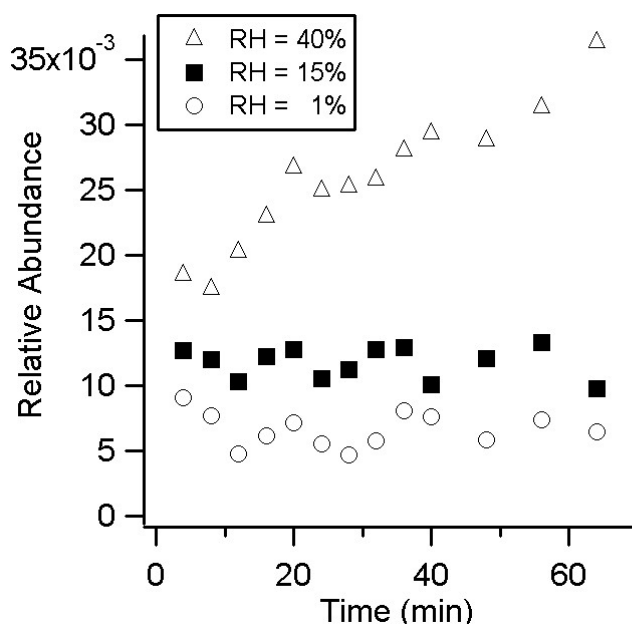


Figure 4.12. Time dependence of the normalized abundance for $m/z = 225.1096$, $C_{10}H_{18}O_4Na^+$. The experiment was conducted in the dark with different initial %RH. The relative intensities are calculated by dividing the peak intensity by the sum of all peak intensities in the mass spectra.

The effect of the relative humidity was more pronounced. There was a clear shift of the relative peak intensities towards higher m/z values. Several peaks responded particularly strongly, with intensity changes taking place on a time scale of the order of one hour. For example, the peak at $m/z 225.1096$, $C_{10}H_{18}O_4Na^+$, increased significantly under humidified conditions (Figure 4.12). Furthermore, this peak kept growing with time at 40 %RH, possibly due to a slow hydration of the $C_{10}H_{16}O_3$ carbonyl compound resulting in its gem-diol form. The

peak corresponding to $C_{10}H_{16}O_3$ decreased at higher %RH. Such hydration reactions are consistent with the small but reproducible H:C increase and with the faster growth in the O:C ratio with time (Figure 4.8).

OM:OC Ratios from HR-ESI-MS Measurements

We calculated an average OM:OC ratio (organic mass to organic carbon mass) of ~ 1.7 and OO:OC ratio (organic oxygen mass to organic carbon mass) of ~ 0.6 for our limonene SOA samples. The OM:OC value is close to the suggested value for the OM:OC ratio for the nonurban (2.1 ± 0.2) organic aerosols.¹⁶⁰ The OO:OC ratio is within the range of OO:OC ratios for water soluble species ($0.4-2.0$).¹⁶¹ Both ratios provide a good match for the oligomeric organic compounds (OM:OC = $1.5-2.1$; OO:OC = $0.4-1.0$).^{22, 161} These observations suggest that the HR-ESI-MS techniques can provide reasonable estimates for the OM:OC and OO:OC ratios for the solvent extractable fraction of SOA. The HR-ESI-MS method obviously needs further validation and refinement. For example, our calculations assume equal detection sensitivities for all SOA constituents; the applicability of this approximation to SOA samples is yet to be tested. However, the small sample requirements of this method offer a significant advantage compared to more traditional techniques. In combination with an appropriate aerosol collector such as the DRUM impactor used in this work or with a particle-into-liquid sampler (PILS), the HR-ESI-MS can potentially provide the OM:OC and OO:OC ratios with time resolution of several minutes.

4.5 Conclusion

We have applied the HR-ESI-MS methods to the molecular characterization of limonene SOA samples as a function of the reaction time and conditions. The following conclusions can be drawn from this chapter.

1) The HR-ESI-MS technique can be used to estimate the OM:OC ratio for the soluble fraction of SOA with a time resolution on the order of minutes. This method results in OM:OC~1.7 in the limonene SOA.

2) Molecules in limonene SOA are highly oxidized. The average chemical formula for the SOA constituents is $\text{CO}_{0.45}\text{H}_{1.6}$. The average O:C ratio increases slowly as the aerosol ages, whereas H:C ratio stays roughly constant.

3) An analysis of the distribution of double bond equivalency (DBE) factors and aromaticity index (AI) values suggest that limonene SOA contains aromatic species. These species are produced early in the ozone + limonene reaction by unknown chemical mechanisms.

4) In agreement with previous research on SOA formation in ozonolysis of monoterpenes,^{99, 172, 173} the limonene SOA formation can be divided in two steps. The first generation products, including the oligomeric species, appear early in the reaction. The mechanism of oligomerization is consistent with fast reactions of Criegee intermediates with other products of ozonolysis. Further oxidation leading to the second generation products occurs in condensed phase on a much slower time scale.

5) In the presence of humidity, additional aging processes take place as a result of hydration reactions on a time scale of hours. The presence of UV radiation can lead to additional aging reactions that happen on even longer time scales.

Chapter 5

Water Soluble Organic Aerosols

Reproduced in part with permission from Anal. Chem, 2010, 82, 8010-8016.

Copyright ©2010 American Chemical Society

5.1 Introduction

SOA produced via oxidation of biogenic VOC represents a large fraction of the global aerosol budget and is a major source of water-soluble organic carbon (WSOC) in the atmosphere.³ Biomass-burning organic aerosol (BBOA), although less water soluble, also makes a significant contribution to WSOC.^{3, 174} On the whole, organic aerosol (OA) compounds associated with particulate matter have been found to be 10-70% water-soluble.¹⁷⁵⁻¹⁷⁷ An estimated 47 TgC/yr of WSOC is being washed out of the atmosphere through wet deposition.¹⁷⁸ Characterization of the water soluble components of OA at the molecular level should improve our understanding of this important component of the global carbon cycle.

A particle-into-liquid-sampler (PILS) was developed in 2001 exactly for the purpose of collection and real-time analysis of water soluble compounds in aerosols.¹³⁸ Traditionally, PILS has been coupled with ion chromatography, allowing for quantitative measurements of common atmospheric water soluble inorganic ions and several small carboxylic acids in ambient and lab generated aerosols.¹⁷⁹⁻²⁰³ More recent applications include: PILS coupled to an on-line total organic carbon analyzer for measurements of the total WSOC content,^{110, 177, 204-209} PILS coupled to a liquid waveguide capillary cell and absorption spectrometer for detection of water

soluble iron in atmospheric aerosols,²¹⁰ and PILS coupled to offline ESI-MS,GC-MS, or LC-MS measurements.^{211, 212}

PILS coupled to online LC-MS was successfully deployed for collection and analysis of organic acids in ambient atmospheric aerosol.²¹² No field instruments involving PILS coupled to ESI-MS have been reported yet. While such an online PILS/ESI-MS approach would have been ideal, the size and weight of modern high-resolution ESI-MS instruments have so far precluded their use in field sampling. However, PILS collection into vials followed by offline ESI-MS analysis can be just as useful provided that molecules in the sample do not undergo extensive hydrolysis between collection and analysis. As both collection and offline analysis can be automated, the labor requirements of the offline PILS/ESI-MS method are not significantly higher compared to the real-time analysis.

The objective of this chapter is to examine the utility of PILS for detailed molecular characterization of water-soluble organics in aerosols in conjunction with the HR-ESI-MS approach. In the present study, laboratory generated SOA, from the ozone initiated oxidation of d-limonene, and BBOA, collected from burning pine needles and sticks, are used as model systems. During each SOA or BBOA experiment, particles are simultaneously collected using two methods: 1) filter collection with extraction into either acetonitrile or water; and 2) PILS collection with direct extraction into water. The resulting extracts are subsequently analyzed using HR ESI-MS. Chemical characterization (molecular formulas, O:C, H:C, Organic Mass: Organic Carbon (OM:OC) and double bond equivalency) of the detected compounds are used to determine the types of water soluble compounds present in organic aerosol. The comparison of mass spectra shows that PILS-HR-ESI-MS is a suitable method for the molecular analysis of water soluble compounds in both biogenic SOA and BBOA.

5.2 Experimental

Limonene SOA was generated by the reaction of d-limonene (Acros Organics, 98% purity) vapor and ozone in a 5 m³ inflatable Teflon chamber.¹³³ The initial reactant concentrations of both limonene and ozone were 0.5 ppm, resulting in particle mass concentrations of approximately 2000 µg/m³ (assuming an effective density of 1.2 g/cm³). The collection time lasted 40 minutes. Particles were collected simultaneously with a PILS instrument²⁰⁰ (Brechtel Manufacturing, Inc) and with a Teflon-coated filter (Millipore, 0.2 µm pore) at 15 LPM flow rate for both collection methods. To compensate for the 30 LPM withdrawn from the chamber by the collection, an equivalent amount of dry purified make-up air was added to the chamber. The PILS wash flow was set at 100 µL/min and four 1 mL samples were collected during the 40 min particle collection time. Only one filter sample was collected during the particle collection time, via the filter technique.

BBOA samples were collected from the burning/smoldering of approximately 10 g of dried pine needles and sticks, which were placed in a small charcoal grill, ignited, and covered with the grill lid. Smoke was collected about 10 cm above a vent in the cover with a copper collection tube. Particles produced from the biomass burning were first passed through a diffusion dryer filled with DriRite desiccant to reduce the amount of water vapor and then collected simultaneously using a PILS and a filter sampler. The filter and PILS collection flows were 15 LPM each. The collection time for BBOA particles was 5 minutes for both the filter samples and PILS samples. Even though the smoke was barely visible the particle concentration was high enough to significantly contaminate the PILS impaction plate with insoluble deposits after collecting several samples, and the filter contained visible amounts of BBOA. The PILS

vials and collected filters from all experiments were promptly placed on dry ice and kept frozen until later HR-ESI-MS analysis.

Immediately prior to the ESI-MS analysis the PILS vials from both SOA and BBOA were thawed and 0.5 mL of each sample was mixed with 0.5 mL of acetonitrile, in order to decrease the surface tension and facilitate a more stable electrospray.¹³⁹ The limonene SOA filters were cut in half and each half was sonicated in 2 mL acetonitrile for 30 minutes. A 0.5 mL aliquot of the resulting organic extract was diluted with 0.5 mL of MilliQ H₂O, prior to ESI-MS analysis. The BBOA filters were cut in half with one half sonicated in 0.5 mL acetonitrile and the other half sonicated in 0.5 mL MilliQ H₂O, each for 30 minutes. These extracts were then diluted with 0.5 mL of the opposite solvent to achieve the desired 1:1 volume ratio of acetonitrile and MilliQ H₂O. This ensured equal dilutions and equal solvent compositions for the electrosprayed solutions between all filter and PILS samples analyzed in this study. Therefore, differences in the mass spectra could be attributed to the collection/solvent extraction efficiency, and not solvent or analyte concentration effects on the ESI mass spectra. In the following discussion, organic aerosol will be distinguished as either SOA or BBOA, and samples will be referred to as “PILS samples”, “filter/ACN samples”, and “filter/H₂O samples” depending on the collection/extraction method (where ACN = acetonitrile).

5.3 Results

Limonene SOA: Aqueous vs. organic extraction

We recorded SOA mass spectra in both positive and negative ion modes. The comparison between the PILS and filter based spectra results in the same conclusions regardless

of the ion mode, therefore, only positive ion mode data will be presented in this paper. The limonene SOA mass spectra recorded here, Figure 5.1 (a), are similar in appearance to the spectra of limonene SOA that we previously reported for higher (10 ppm) mixing ratios of limonene and ozone.⁹⁰ The spectrum can be clearly divided into regions corresponding to monomeric (100 – 300 g/mol), dimeric (300 – 500 g/mol), trimeric (500 – 700 g/mol), and tetrameric (700 – 900 g/mol) products, where the numbers in parentheses are the neutral compounds' molecular weights. The compounds detected in mass spectra obtained from PILS and filter/ACN samples are nearly identical, furthermore, all major peaks were observed in *both* PILS and filter/ACN mass spectra (Figure 5.1 (a)). To emphasize the extent of similarity, Figure 5.1 (b) shows peaks that were detected in mass spectra solely from either the PILS or filter/ACN extraction methods. Most peaks that are unique to PILS or filter/ACN samples are less than 1% in relative abundance. In fact, the calculated percentage of total ion signal is dominated (96%) by compounds detected from both extraction methods, while compounds unique to only one extraction method, either filter/ACN or PILS, represent only 4% of the total ion signal. However, these compounds are not distributed equally across the entire mass spectrum, there is a somewhat greater density of peaks above 500 g/mol in the filter/ACN samples, as can be seen in Figure 5.1 (b).

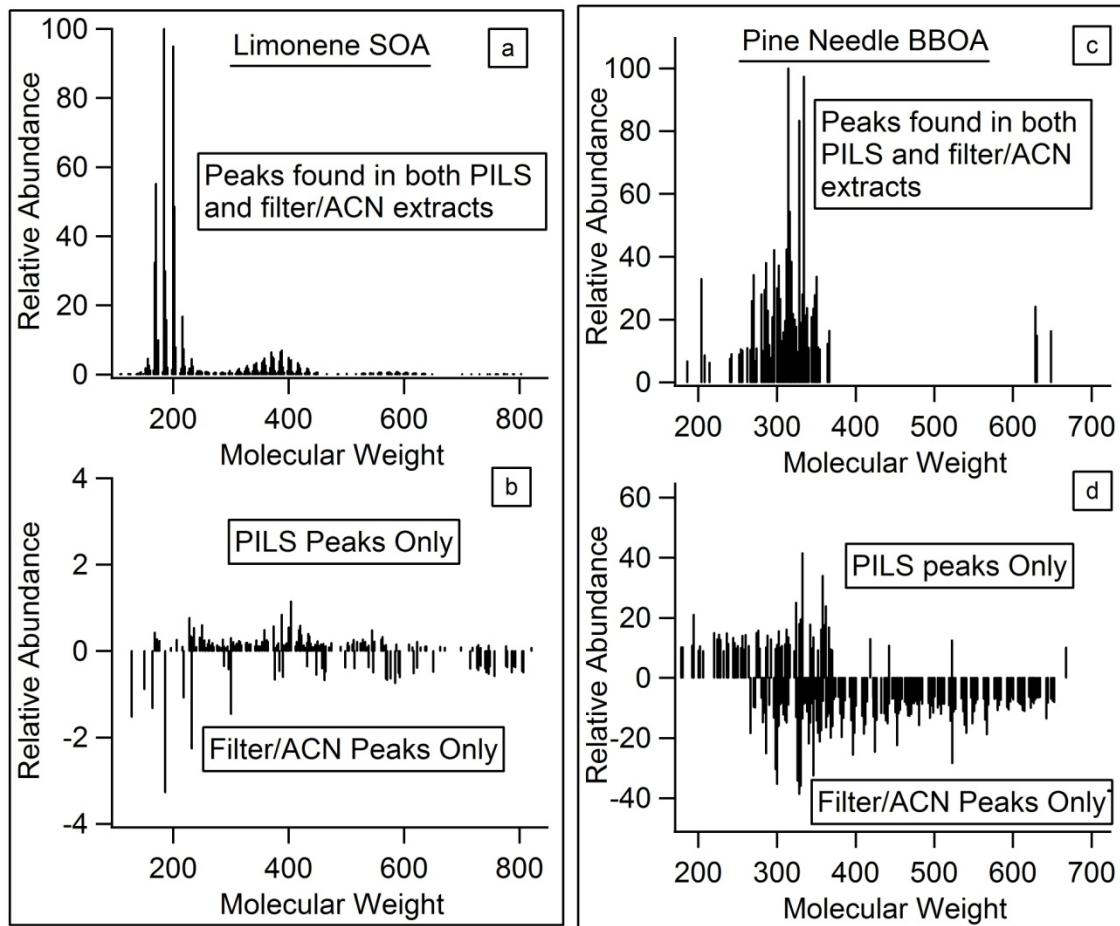


Figure 5.1. Positive ion mode ESI mass spectra of SOA (left panels) and pine needle BBOA (right panels). Panels (a) and (c) display peaks due to SOA/BBOA compounds detected from both PILS and filter/ACN extraction. Panels (b) and (d) display compounds detected only from the PILS extraction (positive peak abundances) and compounds detected only from the filter/ACN extraction (negative peak abundances). The peak abundances are normalized by setting the abundance of the largest peak in each spectrum to 100.

Additional analysis of the limonene SOA chemical composition is provided in Table 5.1.

The average atomic ratios, O:C and H:C, are essentially identical in PILS and filter/ACN samples. DBE values appear to be more sensitive to the extraction method; as the filter sample resulted in slightly but a reproducibly larger average DBE value than the PILS sample. The DBE values in limonene SOA compounds varies approximately linearly with molecular weight

(~ one DBE unit per 100 g/mol).¹⁰⁰ Therefore, the oligomeric species present in SOA have larger DBE values than the monomers. An increase in the average DBE value can be attributed to an increase in the relative amount of oligomeric material. Additionally, the filter/ACN samples contain a somewhat higher percentage of the total ion signal above 500 g/mol than the PILS samples, 8% versus 6%, respectively. These two observations suggest that the filter/ACN samples contained slightly more extractable oligomeric material than the PILS samples, possibly due to better solubility of oligomers in acetonitrile relative to water.

Table 5.1. Intensity weighted average values of O:C, H:C, DBE and OM:OC for SOA and BBOA compounds collected from PILS and filter/ACN SOA extracts. The table is calculated from the list of assigned molecules observed in (+) ion mode mass spectra.

		⟨O:C⟩	⟨H:C⟩	⟨DBE⟩	OM:OC
SOA	PILS	0.39	1.59	3.69	1.64
	Filter/ACN	0.38	1.57	4.10	1.65
BBOA	PILS	0.29	1.51	5.39	1.51
	Filter/ACN	0.19	1.62	5.18	1.38

In addition to observing closely overlapping subsets of compounds, there is a remarkable correlation between relative peak abundances in the two extraction methods. To facilitate the comparison between various mass spectra, peaks detected in all mass spectra were sorted onto a single mass axis by the formulas of the neutral SOA compounds. The relative abundance of each compound was compared for both extraction methods. Figure 5.2 (a) demonstrates remarkable correlation between the filter/ACN and PILS peak abundances; most observed peaks fall close to the reference 1:1 line corresponding to equal abundances in mass spectra generated from both collection techniques. The correlation coefficients for the

abundance-vs.-abundance linear fits are close to 1. Clearly, most SOA compounds are collected/extracted with near equal efficiencies by both methods.

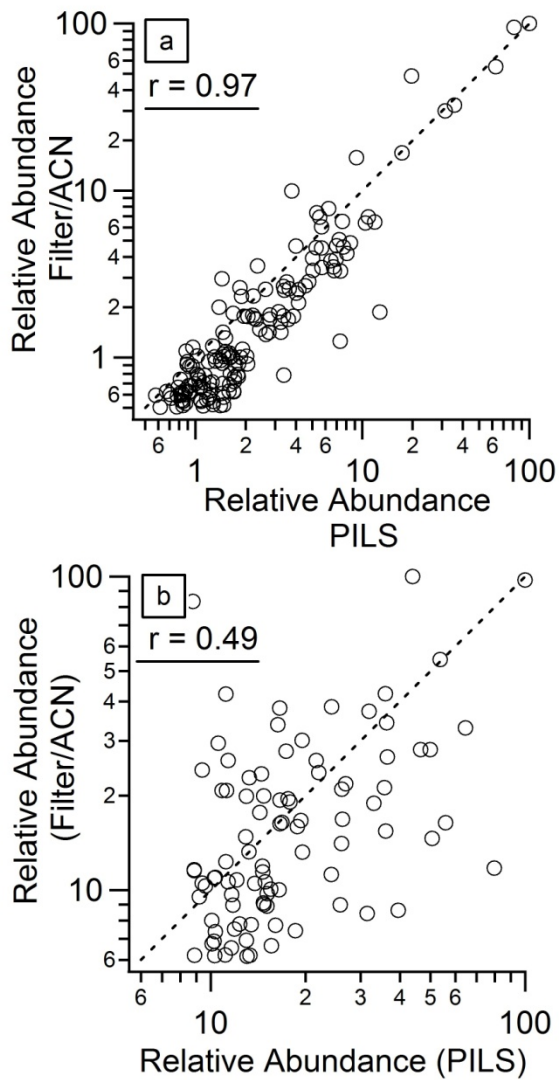


Figure 5.2. Log-log relative abundance plots generated from the mass spectra in Figure 5.1. Abundances in the positive ion mode PILS and filter/ACN ESI mass spectra are plotted against each other for (a) limonene SOA and (b) pine needle BBOA. As a reference, the dashed lines represent a 1:1 ratio. The r values are the correlation coefficients.

Pine needle BBOA: Aqueous vs. organic extraction

Sample BBOA mass spectra are shown in Figure 5.1 (c). A number of peaks that have been previously reported from BBOA ESI mass spectra are present, including levoglucosan, $m/z = 185.042$ ($C_6H_{10}O_5Na^+$), and compounds at m/z 293.209 ($C_{16}H_{30}O_3Na^+$), 315.193 ($C_{18}H_{28}O_3Na^+$), 325.177 ($C_{19}H_{26}O_3Na^+$), 335.125 ($C_{19}H_{20}O_4Na^+$), 335.219 ($C_{18}H_{32}O_4Na^+$, octadecenedioic acid), and 375.214 ($C_{20}H_{32}O_5Na^+$).²¹³ Unlike limonene SOA mass spectra, the PILS and filter/ACN mass spectra are quite different, and many major peaks are observed selectively in *only* PILS or filter/ACN mass spectra. These differences are apparent in Figure 5.1 (d), which shows peaks that were detected in mass spectra solely from either the PILS or filter/ACN methods. Many compounds unique to filter/ACN samples have molecular weights between 400 – 700 g/mol, indicating that acetonitrile extracts high molecular weight BBOA compounds more efficiently than water does. Unlike the SOA case, the fractional abundance of common peaks is considerably smaller than 100%. In fact, the majority of the total ion current for filter/ACN (61%) comes from peaks that are unique to this collection/extraction method.

Table 5.2. Number of peaks observed in PILS and filter extracted BBOA. In each mass spectrum, common compounds represent the peaks observed by all three collection methods and unique compounds represent the peaks observed by this collection method only (percentage of total peak number is in parentheses). The numbers do not add to 100% due to compounds that were detected by two out of three collection methods.

Method	Total # of peaks detected	# of peaks common to all 3 methods	# of peaks unique to this method
PILS	162	68 (42%)	65 (40%)
Filter/ACN	338	68 (20%)	234 (70%)
Filter/H ₂ O	91	68 (75%)	6 (7%)

Comparison of the PILS, filter/ACN, and filter/H₂O methods can help attribute the source of the differences discussed above to the collection method (PILS vs. filter) or extraction solvent (water vs. acetonitrile). Table 5.2 lists the total number (not total abundance) of assignable peaks (excluding ¹³C isotopes) found from each sample: PILS, filter/ACN, and filter/H₂O, number of peaks common to *all three samples*, as well as compounds found in *only one* of the methods. Sixty-eight common compounds were detected in BBOA from the three collection methods, representing a large portion of the total number of compounds found in the filter/H₂O mass spectrum (75%). In contrast, this fraction is much smaller for filter/ACN (20%) samples further confirming that more compounds are extracted by ACN than H₂O. Clearly, many BBOA compounds are extracted into organic solvent but not into aqueous solvent.

While the overlapping subset of compounds is not as extensive as in the SOA case, there is correlation between the relative peak abundances for BBOA compounds observed in all three spectra. Similar to the limonene SOA mass spectra, peaks detected in all mass spectra were sorted onto a single mass axis by the compounds' molecular weights. The relative abundance of each compound was compared for all extraction methods. Figure 5.2 (b) shows the results for PILS vs. filter/ACN comparison and Figure 5.3 (a) compares relative abundances for filter/H₂O and filter/ACN. In all cases the abundance correlation between the filter and PILS data sets is less defined ($r < 0.78$) than for the SOA samples ($r > 0.97$). In Figure 5.3 (b), which compares relative abundances for PILS and filter/H₂O, the majority of compounds falls below the reference 1:1 line, suggesting that PILS is the more efficient collection method for WSOC compared to the filter/H₂O extraction method.

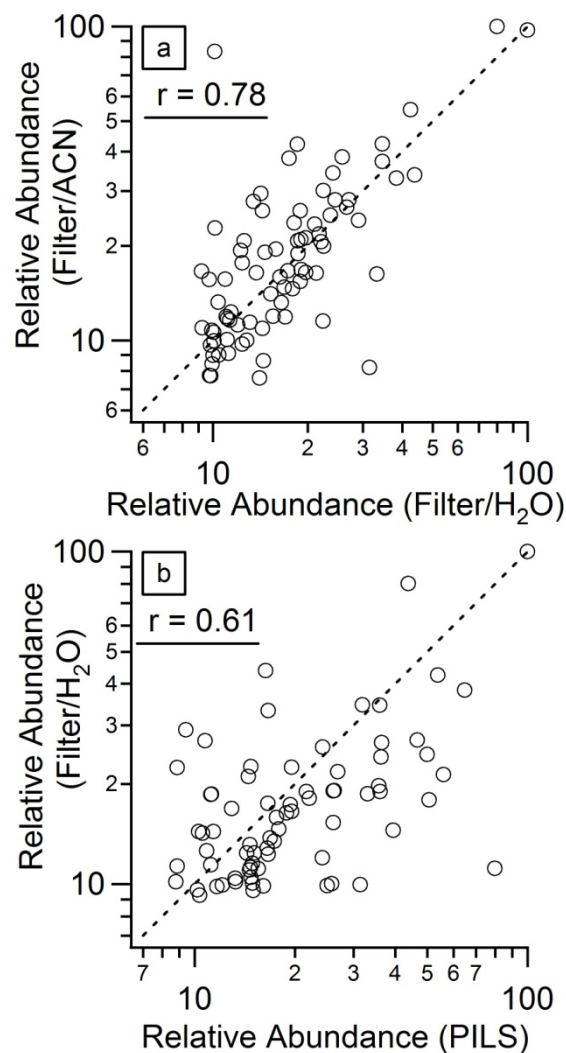


Figure 5.3. Log-log relative abundance plots generated from positive ESI mode BBOA mass spectra. (a) filter/H₂O vs. filter/ACN and (b) PILS vs. filter/H₂O. As a reference, the dashed lines represent a 1:1 ratio. The r -values are the fit correlation coefficients.

5.4 Discussion

Limonene SOA samples collected using an aqueous PILS extraction and more traditional filter collection followed by extraction into acetonitrile resulted in nearly identical ESI mass spectra. It was found that compounds extracted via both methods/solvents accounted for >95% of the total ion signal at very large aerosol loadings in excess of 1 mg m^{-3} and

corresponding extract mass concentrations approaching g/L levels. This similarity implies high solubility of limonene SOA in both water and acetonitrile, likely due to the polyfunctional nature of its components. Indeed, the OM:OC ratio of 1.65 obtained here for limonene SOA as measured via HR ESI-MS falls in the range of OM:OC values that are considered water-soluble, 1.5 to 3.8.¹⁶⁰ Additionally, less than 5% of the ionization current in limonene SOA is detected as compounds with an OM:OC ratio less than 1.5 (considered to be non-soluble on average).

Pine needle BBOA samples collected using the same techniques resulted in substantially different mass spectra. Mass spectra generated from PILS, filter/ACN, and filter/H₂O samples showed only marginal correlation. Specifically, we found that compounds extracted via all three methods/solvents only accounted for about a third of the total ion signal detected from acetonitrile extracts. These observations are consistent with high water solubility of limonene SOA (estimated WSOC fraction ~ 100%) and only partial water solubility of BBOA (estimated WSOC fraction ~ 40%). This conclusion is consistent with the type of compounds observed in the BBOA sample. Table 5.1 lists the OM:OC ratio obtained for pine needle BBOA extracted from PILS and filter/ACN. The BBOA compounds extracted with filter/ACN method have an average OM:OC ratio of 1.38, lower than the suggested value for water-soluble compounds.¹⁶⁰ This also indicates that the filter/ACN method is extracting more compounds with poor water solubility. In comparison, BBOA compounds extracted with PILS method have an average OM:OC ratio of 1.51, suggesting barely soluble compounds.

The average O:C ratio is sometimes used as an alternative to OM:OC for predicting the solubility in water. Previous research suggests that compounds with O:C ratios greater than 0.4 can generally be considered water soluble.^{161, 214} Taking advantage of the high mass resolution, assigned compounds in SOA and BBOA can be grouped according to their individual O:C

ratios, as illustrated in Table 5.3. The average OM:OC ratio increases with each successive O:C bin as expected from Eq. (5). For the SOA case, the majority of compounds have O:C ratios between 0.3 - 0.6, while the majority of BBOA compounds have O:C ratios between 0.0 – 0.3. Comparing PILS and filter/ACN extracted BBOA compounds indicates that acetonitrile extracts a higher percentage of low O:C material (0.0-0.3) while PILS extracts a higher percentage of higher O:C material (0.3-0.6). These observations are again consistent with the high water solubility of limonene SOA and low solubility of BBOA compounds and support the known correlation between elemental ratios and solubility in water.^{160, 161}

Table 5.3. Percentage of total ion signal calculated from detected compounds with O:C ratios of 0.0 - 0.3, 0.3 - 0.4, 0.4 – 0.5, 0.5 – 0.6, and 0.6 - 0.9 from both SOA and BBOA compounds collected using PILS and filter/ACN extracts. The table is calculated from the list of assigned molecules observed in positive ion mode mass spectra.

Compound O:C ratio	Average OM:OC	SOA		BBOA	
		PILS	Filter/ACN	PILS	Filter/ACN
0.0 – 0.3	1.39	10.0	12.2	75.9	96.3
0.3 – 0.4	1.56	35.3	35.5	12.1	2.1
0.4 – 0.5	1.69	40.6	37.9	1.4	0.1
0.5 – 0.6	1.82	11.7	12.3	1.0	0.1
0.6 – 0.9	2.08	2.0	2.0	10.0	1.0

Given the high solubility of limonene SOA in both water and ACN, any difference between the PILS and filter/ACN mass spectra should be attributed to artifacts generated from either filter or PILS collection methods. Analysis of blank samples from both methods

effectively removes ESI-MS impurity compounds that are unique to each collection method. Artifacts that would contribute to an increase (or decrease) of certain SOA constituents, for example, evaporation of SOA compounds from the filter, physisorption of VOCs onto the filter, reaction of SOA compounds with residual ozone, hydrolysis of compounds in PILS vials, etc., cannot be corrected for with blank samples. However, due to the similarity of mass spectra generated from both extraction methods, these effects appear to be insignificant for limonene SOA.

The differences in collection methods appear to be more significant for BBOA. If all WSOC in BBOA was accessible to the solvent in PILS vials or in filter extracts we would have obtained similar results for the PILS and filter/H₂O samples. The large difference between these two methods suggests that some BBOA compounds are buried inside the particles and cannot be extracted easily from the filtered samples. It is notable that the PILS method resulted in mass spectra containing more compounds and higher abundances than the filter/H₂O method, suggesting that the PILS method is more efficient for extracting WSOC from BBOA. PILS creates an internally mixed water/BBOA particle mixture favoring extraction of WSOC from particles,²⁰⁹ whereas particles on the filter may be sintered and resist penetration of water even under sonication conditions.

The discussion above has dealt with qualitative observation of various compounds by the PILS/ESI-MS and filter/ESI-MS methods. We also need to briefly comment on the possibility of quantitative measurements of specific OA compounds with these methods. The main limitation on quantitative measurements with either PILS or filter extraction coupled to an offline ESI mass spectrometer is non-linear ESI dependence on the solution concentration and on the “matrix” of ions competing for charge.¹³⁹ Therefore, absolute concentrations of the

unknown OA constituents cannot be recovered from PILS coupled with ESI-MS, without additional analytical techniques. We therefore expect that the PILS/ESI-MS method will be primarily used for identification of water soluble organic compounds in aerosols.

5.5 Conclusion

In conclusion, we have demonstrated that PILS can be used in combination with HR-ESI-MS methods to allow the simultaneous detection of hundreds of water-soluble organic species in a single measurement, and characterization of the distribution of their molecular formulas. This method works best for organic aerosol samples dominated by WSOC (OM:OC > 1.5) such as laboratory generated biogenic SOA examined in this work. No significant differences in the ESI-MS peak abundances of limonene SOA samples collected with PILS or more traditional filter extraction methods were observed. For aerosols dominated by water-insoluble organic species such as BBOA, PILS can still be used for the analysis of the molecular composition of the WSOC fraction, although one has to consider the issues associated with incomplete extraction of WSOC from particles and the difficulties associated with quantitative measurements of specific compounds. Despite these limitations, PILS-ESI-MS is a valuable method for the molecular analysis of WSOC in organic aerosols and for the determination of the average properties of WSOC such as effective OM:OC values.

Chapter 6

Aqueous Photolysis

Reproduced in part with permission from Phys. Chem. Chem. Phys., 2011

Copyright © the Owner Societies 2011

6.1 Introduction

Photolytic processing of dry (i.e., containing small amounts of absorbed water) biogenic SOA has been shown to involve direct photolysis of organic peroxides and carbonyl species.^{18, 20, 21} Recent, field observations also suggest significant photolytic processing of carbonyl compounds in aerosols during long range transport.¹⁹ Biogenic SOA is sufficiently soluble to undergo moderate hygroscopic growth (growth factor about 1.1 at RH =85%)²¹⁵ and nucleate clouds.²¹⁶⁻²¹⁹ Indeed, WSOC compounds are ubiquitous in atmospheric rainwater²²⁰⁻²²⁶ and cloud/fog droplets.²²⁷⁻²⁴⁰ There have been a number of studies on the UV irradiation, or photolytic processing, of field-collected SOA, DOM and model organic compounds in aqueous solution.²⁴¹⁻²⁵¹ Aqueous OH radical initiated oxidation of organics, referred to as photochemical processing in recent literature, has also been investigated.^{147, 148, 252-254} In photochemical processing experiments, hydrogen peroxide is intentionally added to the solution as an OH precursor. In photolytic processing, the solution is photolyzed directly without any additions. These two types of processing are closely related because hydrogen peroxide is itself a product of photolysis of aqueous solutions of organics.^{241, 249, 255, 256}

Here we present an examination of photolytic processing of aqueous solutions of SOA generated by oxidation of d-limonene, one of the six most common monoterpenes.⁴⁷ The chemical composition of d-limonene SOA has been extensively studied and a number of compound classes have been identified, making it an ideal model system for this work.^{80, 83, 87, 88, 90, 92, 99, 100, 135, 257-259} Although we have chosen a specific type of SOA for our experiments, we believe that our findings are not limited to d-limonene SOA but can be generalized to most types of biogenic SOA.

Previously a number of laboratory studies focused on aqueous photochemistry of individual organic compounds.^{242, 243, 250, 251} The photochemistry of aqueous solutions of biogenic SOA, however, has not been studied in detail. In this work, we investigate the photochemistry of a complex mixture of organics that more closely approximates biogenic aerosol in the atmosphere. This type of holistic approach reveals important new aspects of aqueous photolytic processing of SOA. The HR-MS results presented here demonstrate that the organic molecules associated with biogenic SOA undergo significant photolytic processing between the formation and removal of the particles in the atmosphere.

6.2 Experimental

Particle generation and collection

The dark reaction of d-limonene (Acros Organics, 98% purity) vapor and ozone was used to generate SOA (referred to as “limonene SOA” henceforth) in a 5 m³ inflatable Teflon chamber.¹³³ The amount of d-limonene was selected such that its mixing ratio in the chamber was approximately equal to that of ozone (1:1 stoichiometry). Multiple sets of experiments were

performed with the initial mixing ratios of limonene and ozone equal to 1, 0.5, 0.1 and 0.05 ppm.

A PILS²⁰⁰ (Brechtel Manufacturing, Inc.) was used to collect aqueous extracts of SOA. The vials with the collected samples were then frozen, pending later photolysis experiments or mass spectrometric analysis. In selected experiments, additional samples were collected on a Fluoropore PTFE 0.22 μm filter (Millipore) at the same sampling flow rate of 14 LPM.

Photolysis of aqueous and dry SOA samples

The PILS samples were thawed and transferred into a standard 1 cm quartz cuvette where they were irradiated for up to 24 hours in open air. The samples were exposed to lab air during photolysis and therefore contained dissolved oxygen. The radiation from a 100 W Xenon lamp placed in a Newport Photomax housing was reflected by a 90-degree 330 nm dichroic mirror, filtered with a 295 nm high-pass filter (Schott WG-295), and further filtered with a 2.5 cm cell containing water (to reduce sample heating by residual near-IR radiation), before entering the cuvette. The water temperature in the photolysis cell typically stabilized at 1-2 degrees C above room temperature. The total radiation power incident on the sample was ~ 1 W, as measured using a power meter (Coherent FieldMate, Model PS19Q). The wavelengths were confined to 300 – 400 nm as measured using a portable UV/Vis spectrometer (Ocean Optics, Model USB4000). UV/Vis spectra were obtained before and after photolysis using a dual-beam UV/Vis spectrometer (Shimadzu, Model UV-2450) with nanopure water as the reference. The samples were then transferred into clean 2 mL storage vials and frozen again for later ESI-MS analysis or pH and peroxide content tests.

Photolysis experiments for dry SOA were conducted directly on filters. The filters were cut in half, with one half saved as a reference and the other half irradiated in the same setup as used for the aqueous photolysis. The filters remained in open air during photolysis. After irradiation, the filters were stored frozen in sealed containers and in the dark, until analysis.

Peroxide concentration and pH measurements

The collection times for the PILS samples were increased to collect 1.5 mL (the full vial capacity) of SOA aqueous extracts. The vial content was then divided into two 0.75 mL aliquots. One sample was photolyzed using the system described above, while the other was kept in the dark. The photolyzed and reference samples were mixed with 0.75 mL of nanopure water and transferred into separate 5 mL conical vials. The pH was measured using a Mettler Toledo SevenEasy™ S20 pH meter with InLab^R surface electrode. The dilution with water was necessary to allow the solution to come into full contact with the electrode surface.

Following the pH measurements, a peroxide test was performed on each sample as described by Nguyen et al.¹³³ (a modified procedure of Docherty et al.²⁶⁰). The solutions were acidified with 0.75 mL glacial acetic acid (EMD, 99.7% purity). After ~5 min of purging with N₂ (g), 0.25 mL of a 0.7 M potassium iodide solution was added and allowed to react for 1 hour with constant mixing under a nitrogen atmosphere. The UV/Vis absorbance was measured at 470 nm in 1 cm quartz cells. The peroxide test was calibrated against diluted H₂O₂ (Fisher, ACS certified at 3.1%) measured under identical conditions.

In this work, we have relied on the methanol reactivity to separate the SOA compounds into four classes, where molecules in each class contain: 1) at least one carbonyl group, 2) at least one carboxyl group, 3) both a carbonyl and a carboxyl group, and 4) other compounds with

no carbonyl and carboxyl groups. These four classes of compounds were examined by HR-MS at different SOA precursor concentrations and photolysis times. We note that this classification was based on the compounds that were initially present in the 1 ppm SOA sample. Therefore, any new compounds appearing in mass spectra of photolyzed SOA and in mass spectra of samples with lower precursor concentration were placed in the “other functional group” category even though they could still contain carbonyl or carboxyl functional groups.

6.3 Results

Composition of limonene SOA prior to the photolysis

Chamber experiments on organic aerosols are typically done at elevated reactant concentrations in order to achieve sufficient sensitivity and avoid interference from impurities in the chamber. While the ozone concentrations used to prepare limonene SOA (0.05 to 1 ppm) overlap with the atmospherically relevant values, the limonene concentrations are 1-2 orders of magnitude higher than typical ambient values. The particle mass loading (calculated from the SMPS data) resulting from SOA precursor concentrations of 0.05 to 1 ppm were 100 to 5300 $\mu\text{g}/\text{m}^3$ (Table 6.1). The corresponding concentrations of dissolved SOA in the PILS samples ranged from 16 to 400 $\mu\text{g}/\text{mL}$, or from 80 μM to 2 mM, assuming an effective molecular weight of 200 g/mol for SOA compounds and a particle density of 1.2 g/cm^3 .²⁶¹ The concentrations used in this study are of the same order of magnitude as concentrations of organics observed in cloud water (micro – to millimolar).^{262, 263} Liquid water content of wetted aerosol particles is typically 3 - 5 orders of magnitude smaller than that of cloud/fog droplets, resulting in

concentrations of dissolved organics on the order of 0.1 – 10 M.²⁶⁴ Therefore the present experimental conditions are more appropriate for cloud/fog droplets than for wetted aerosols.

Table 6.1. Initial conditions and reaction parameters for the SOA preparation (measured and/or calculated from the SMPS data). The quoted uncertainties represent one standard deviation from averaging results of repeated experiments.

Initial Concentrations (Ozone = Limonene)	PILS vial Collection Time (min) ^{a,b}	PILS water flow rate ($\mu\text{L}/\text{min}$) ^b	SOA mass concentration at the start of collection ^c ($\mu\text{g}/\text{m}^3$)
1 ppm	10 or 15	100	5300 ± 1000
0.5 ppm	10 or 15	100	1800 ± 300
0.1 ppm	20 or 30	50	290 ± 60
0.05 ppm	30 or 45	33	100 ± 30

^a The particle collection started 1 hour after mixing ozone and limonene.

^b Each of the PILS vials contained 1 or 1.5 mL at the end of the collection

^c Mass concentration calculated from SMPS data assuming particle density⁸⁶ of $1.2 \text{ g}/\text{cm}^3$

The ESI mass spectra were similar in appearance to those published previously.^{90, 135} Figure 6.1 contains representative (+) mode mass spectra collected at all precursor concentrations prior to photolysis. The overall shape of the limonene SOA mass spectra did not change significantly when the precursor concentration was reduced. For example, the relative intensity of the dimer peaks (300-500 amu) with respect to the monomer peaks (100-300 amu) was approximately the same at all concentrations. The relative intensities of the trimer and tetramer decreased somewhat at the lower SOA loadings.

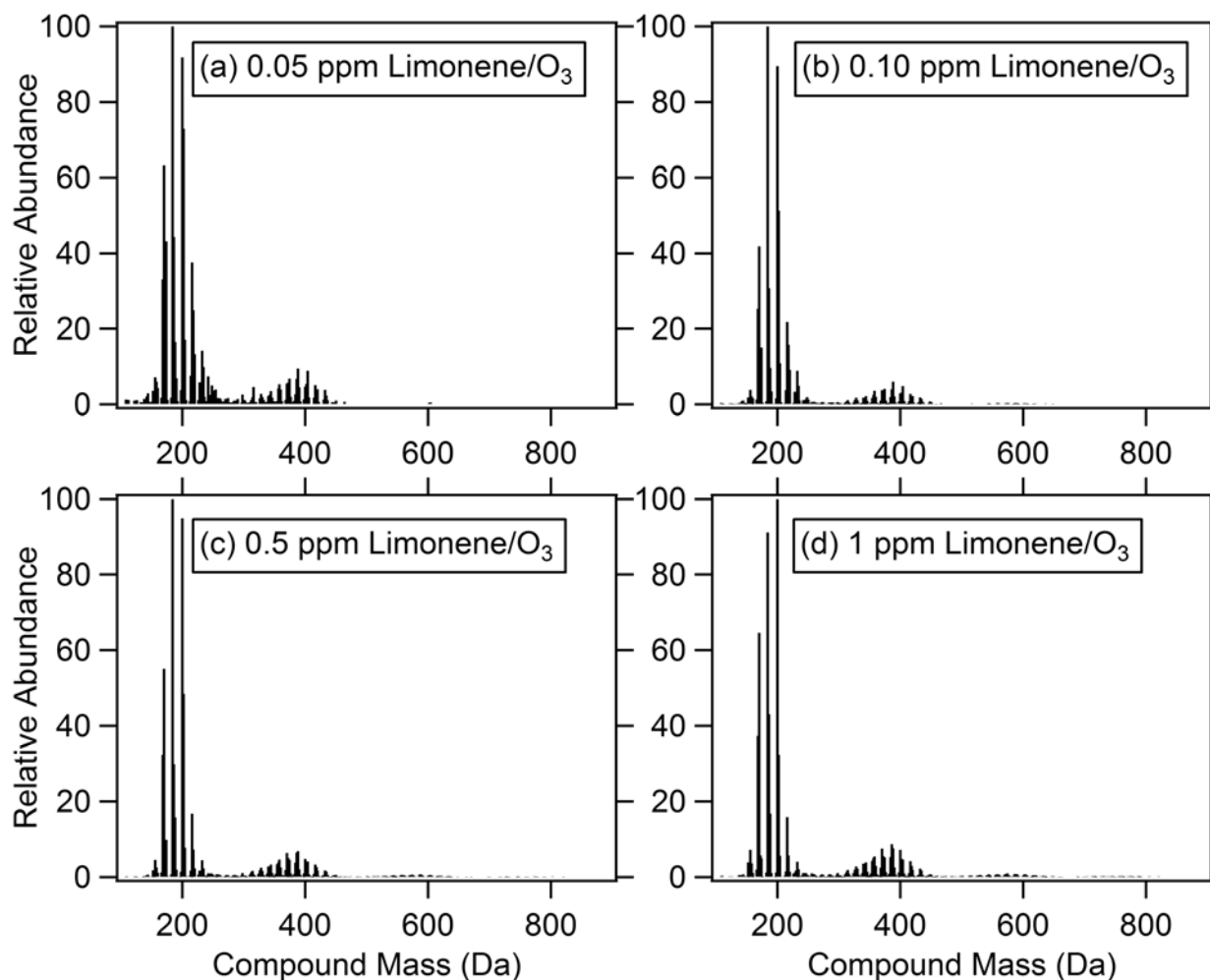


Figure 6.1. Representative ESI (+) mass spectra of SOA collected via PILS extraction for the four initial precursor concentrations studied: (a) 0.05 ppm; (b) 0.10 ppm; (c) 0.5 ppm; (d) 1.0 ppm of limonene and O₃. Trimer and tetramer species were not visible in the 0.05 ppm spectrum, and tetramer species were not visible in the 0.1 ppm spectrum because these peaks fell below the signal-to-noise threshold used in the analysis.

Useful information can be gained from various average quantities (elemental ratios, OM/OC values, DBE values, and number of carbons) calculated from the entire set of observed limonene SOA compounds.¹⁰⁰ These values are tabulated in Table 6.2. The average O/C and DBE values are also plotted versus the concentration of SOA precursors in Figure 6.2. The \langle O/C \rangle values calculated from the ESI (-) spectra are systematically larger. At 1 ppm ozone and

limonene, the calculated $\langle O/C \rangle$ are 0.40 and 0.50 in the (+) and (-) ionization modes, respectively, and agree well with previously published values of 0.43 and 0.50 for SOA generated at 10-times higher precursor concentration.⁹⁰ Systematically higher $\langle O/C \rangle$ values derived from the ESI (-) mass spectra are attributed to the preferential detection of more oxygenated compounds in the ESI (-) mode.

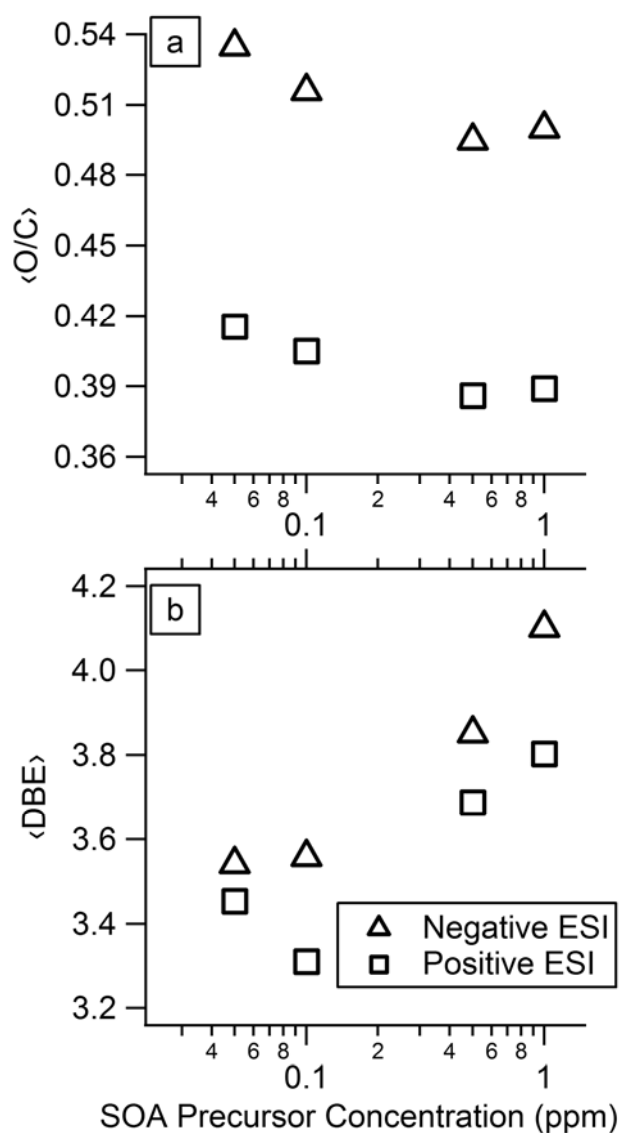


Figure 6.2. Average O/C and DBE values of SOA constituents before photolysis derived from ESI (+) and ESI (-) mass spectra of PILS samples and plotted against the initial d-limonene concentrations used for the SOA generation (Table 1).

Table 6.2. Intensity weighted average values of O/C, H/C, DBE, OM:OC, and number of carbons per molecule calculated from mass spectra generated for each initial concentration of limonene and O₃. The top and bottom sections of the table were calculated from ESI (-) and (+) mass spectra, respectively.

SOA Precursor Concentration (ppm)		0.05	0.10	0.50	1.00
Percent of Peaks Assigned		30	48	62	58
Negative ESI Mode	⟨O/C⟩ Before UV	0.53	0.52	0.49	0.50
	⟨O/C⟩ 2 hr UV	0.54	0.53	0.54	0.55
	⟨O/C⟩ 24 hr UV	-	-	0.57	0.57
	⟨H/C⟩ Before UV	1.55	1.54	1.55	1.55
	⟨H/C⟩ 2 hr UV	1.56	1.55	1.55	1.54
	⟨H/C⟩ 24 hr UV	-	-	1.53	1.53
	⟨DBE⟩ Before UV	3.54	3.56	3.85	4.10
	⟨DBE⟩ 2 hr UV	3.34	3.22	3.37	3.73
	⟨DBE⟩ 24 hr UV	-	-	3.23	3.27
	⟨OM:OC⟩ Before UV	1.83	1.80	1.78	1.79
	⟨OM:OC⟩ 2 hr UV	1.83	1.83	1.84	1.85
	⟨OM:OC⟩ 24 hr UV	-	-	1.88	1.88
	⟨#C⟩ Before UV	11.41	11.35	12.89	14.08
	⟨#C⟩ 2 hr UV	10.75	9.89	10.63	11.93
	⟨#C⟩ 24 hr UV	-	-	9.51	9.69
SOA Precursor Concentration (ppm)		0.05	0.10	0.50	1.00
Percent of Peaks Assigned		19	22	22	21
Positive ESI Mode	⟨O/C⟩ Before UV	0.42	0.41	0.39	0.39
	⟨O/C⟩ 2 hr UV	0.40	0.42	0.43	0.44
	⟨O/C⟩ 24 hr UV	-	-	0.43	0.45
	⟨H/C⟩ Before UV	1.58	1.60	1.59	1.59
	⟨H/C⟩ 2 hr UV	1.57	1.60	1.61	1.59
	⟨H/C⟩ 24 hr UV	-	-	1.55	1.54
	⟨DBE⟩ Before UV	3.45	3.31	3.69	3.80
	⟨DBE⟩ 2 hr UV	3.60	3.04	3.11	3.35
	⟨DBE⟩ 24 hr UV	-	-	3.26	3.15
	⟨OM:OC⟩ Before UV	1.67	1.66	1.64	1.64
	⟨OM:OC⟩ 2 hr UV	1.66	1.68	1.70	1.71
	⟨OM:OC⟩ 24 hr UV	-	-	1.69	1.73
	⟨#C⟩ Before UV	11.53	11.42	12.94	13.57
	⟨#C⟩ 2 hr UV	10.57	10.58	10.62	11.23
	⟨#C⟩ 24 hr UV	-	-	9.93	9.31

The increase in $\langle \text{DBE} \rangle$ with the SOA precursor concentrations reflects the increase in high-MW oligomeric compounds, which tend to have large DBE values (Figure 6.1).¹⁰⁰ The increase in detected high-MW oligomeric compounds with SOA precursor concentration can also be observed from the increase in the average number of carbons per compound ($\langle \#C \rangle$). In order to assess the effect of dilution, the same stock solution of limonene SOA was diluted a number of times, up to 1000:1 dilution factor, and an ESI-MS spectrum was recorded and analyzed for each dilution level. Average values were calculated for each mass spectrum generated and tabulated in Table 6.3. No significant changes to $\langle \text{O/C} \rangle$, $\langle \text{H/C} \rangle$, or $\langle \text{OM:OC} \rangle$ were observed from the dilution experiments. However, the $\langle \text{DBE} \rangle$ and $\langle \#C \rangle$ values decreased at lower concentrations. Unfortunately, it is difficult to completely decouple the effects of dilution from the effects of precursor concentrations on the ESI-MS spectra. However, for a given concentration, the photolysis induced changes in the average properties can be meaningfully compared.

Table 6.3. Effect of concentration on average values calculated from limonene SOA mass spectra. The data was obtained in a separate set of experiments. SOA was extracted into a stock solution and diluted to a different dilution level. The approximate concentration was estimated from SMPS data, assuming a molecular weight of 200 g mol^{-1} and a density of 1.2 g cm^{-3} . Data was collected only in the ESI (+) mode.

Positive ESI Mode	Dilution Factor (~ Concentration)	$\langle \text{O/C} \rangle$	$\langle \text{H/C} \rangle$	$\langle \text{DBE} \rangle$	$\langle \text{OM:OC} \rangle$	$\langle \#C \rangle$
		0.0001 ($1.2 * 10^{-5} \text{ M}$)	0.43	1.61	4.35	1.70
	0.001 ($1.2 * 10^{-4} \text{ M}$)	0.43	1.57	5.52	1.70	21.0
	0.1 ($1.2 * 10^{-3} \text{ M}$)	0.44	1.58	6.02	1.71	23.9
	1 ($1.2 * 10^{-2} \text{ M}$)	0.43	1.58	6.62	1.71	27.1

An interesting trend in Figure 6.2 is the small but reproducible increase in $\langle O/C \rangle$ as the precursor concentration and the resulting SOA mass loading decreases (this change in $\langle O/C \rangle$ is not observed in the dilution experiments). The $\langle O/C \rangle$ value increased from 0.40 to 0.43 and 0.50 to 0.53 in the ESI (+) and (-) modes, respectively, when the precursor concentrations decreased from 1 ppm to 0.05 ppm (the corresponding SOA mass loadings changed from $\sim 5300 \mu\text{g}/\text{m}^3$ to $100 \mu\text{g}/\text{m}^3$). An increasing degree of oxidation at lower mass loadings was also reported for α -pinene SOA.^{265, 266} This effect likely arises from a change in the gas-to-particle partitioning of semivolatiles. At high OM concentrations in the chamber, less oxygenated compounds with low O/C can partition effectively into the particle phase, whereas the same compounds partition predominantly into the gas-phase at lower OM concentrations.

The partitioning was further examined by tracking the subsets of carbonyl and carboxyl peaks determined using methanol reactivity.¹³⁵ Table 6.4 details the percent of total abundance from compounds with carbonyl functional groups, carboxyl functional groups, both carbonyl and carboxyl groups, and compounds with other functional groups, for all SOA precursor concentrations in both (+) and (-) ESI modes. The fraction of detected carboxylic acids increases with decreasing SOA mass loading, from ~ 8 to 13 % and from 14 to 21 % in the negative and positive ionization modes, respectively. This reflects the lower vapor pressures of carboxylic acids relative to carbonyls or alcohols of the same size.

Table 6.4. Effect of limonene/O₃ mixing ratios on estimated percent fractions of carbonyls and carboxyls in the limonene SOA extract. The ion current was subdivided by compounds known to contain carbonyl, carboxyl, both carbonyl and carboxyl, or neither group. Only compounds with MW < 500 g/mol were included in the analysis.

Negative ESI Mode		Carbonyl	Carboxyl	Both	Other	Total ion Signal
	0.05 ppm	4.31	13.41	65.44	16.84	11653
0.1 ppm	4.24	11.22	69.97	14.56	19407	
0.5 ppm	5.97	9.29	72.83	11.91	28154	
1 ppm	6.19	8.24	74.01	11.57	28928	
Positive ESI Mode		Carbonyl	Carboxyl	Both	Other	Total Ion Signal
	0.05 ppm	8.43	21.01	51.73	18.83	6125
0.1 ppm	5.86	22.06	64.56	7.51	18623	
0.5 ppm	7.35	16.67	66.55	9.44	29316	
1 ppm	8.09	13.88	69.31	8.73	32910	

Effect of photolysis on the HR-ESI-MS spectra of limonene SOA in water

Figure 6.3 displays ESI (-) mass spectra acquired from the samples of (a) 1 ppm limonene SOA before photolysis, (b) after 2 hrs, and (c) 24 hrs of photolysis (Fig. S3 of the supporting information contain the corresponding ESI (+) mass spectra). Photolysis results in significant changes to the relative abundances of SOA peaks. For example, the trimeric and tetrameric compounds present in the initial sample (Figure 6.3a) are almost fully degraded after 24 hours of photolysis (Figure 6.3c). Photodegradation of oligomeric species has also been observed during photochemical processing of dissolved organics with OH radical.²⁵⁴

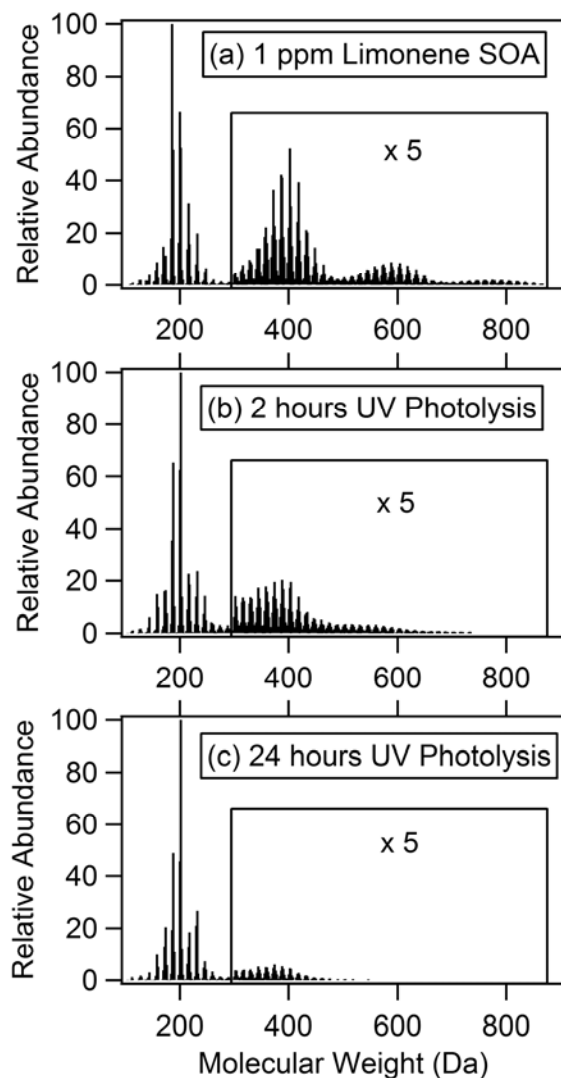


Figure 6.3. Representative ESI (-) mass spectra of 1 ppm limonene SOA collected with PILS: (a) before photolysis; (b) after 2 hours of photolysis, and (c) after 24 hours of photolysis. The corresponding ESI (+) spectra are included in the supporting information section in Fig. S3. All peaks are normalized to the most abundant peak in each mass spectrum. The observed m/z values have been converted to molecular weights of the neutral compounds.

The average elemental ratios and DBE values, before and after photolysis, are listed in Table 6.2, for all experimental conditions. UV photolysis has no significant effect on $\langle H/C \rangle$ but it tends to increase $\langle O/C \rangle$, decrease $\langle DBE \rangle$, increase $\langle OM/OC \rangle$, and decrease $\langle \#C \rangle$. Figure 6.4

shows the $\langle O/C \rangle$ and $\langle DBE \rangle$ values for all UV irradiation times plotted as a function of the SOA precursor concentrations. Although the UV irradiation increases $\langle O/C \rangle$ at all concentrations, the most significant change occurs at higher concentrations (Figure 6.4a). A possible explanation for this concentration effect is an increased fraction of photochemically active carbonyls in particles at higher mass loadings, and conversely an increased fraction of photochemically inactive carboxylic acids at lower mass loadings. This hypothesis is supported by the significant increase in the fraction of carbonyl and carbonyl/carboxyl containing compounds at high mass loading inferred from the methanol reactivity (Table 6.4).

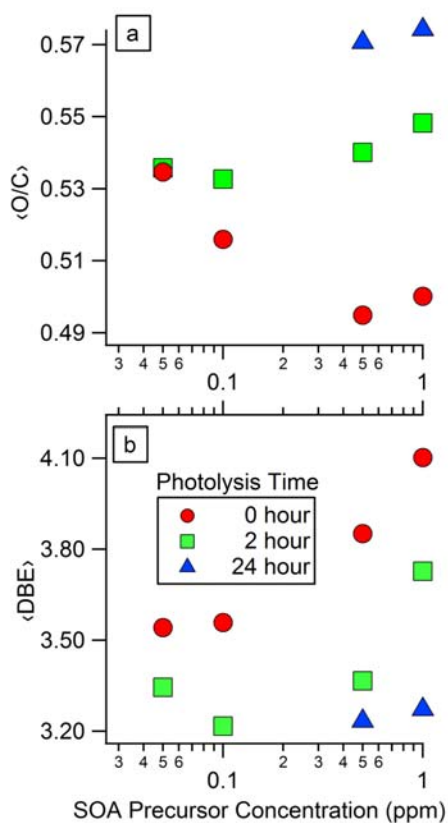


Figure 6.4. Average values of (a) O/C and (b) DBE calculated from ESI (-) mass spectra obtained at different precursor concentrations and aqueous SOA extract photolysis times. The 24 hr photolysis experiments were only conducted with the 0.5 ppm and 1 ppm data sets. The average O/C increases and DBE decreases with the photolysis time, especially at larger SOA loadings.

The decrease in $\langle \text{DBE} \rangle$ upon photolysis is observed at all precursor concentrations (Figure 6.4b). This decrease can be attributed to the preferential photolytic dissociation of high-MW oligomeric compounds, as seen in the mass spectra shown in Figure 6.3. As the average DBE values for monomers, dimers, trimers, and tetramers are $\sim 3, 5, 7,$ and $9,$ ¹⁰⁰ respectively, the preferential photodegradation of oligomers is expected to shift the $\langle \text{DBE} \rangle$ to lower values. As seen in Table 6.3, the dilution of SOA can also result in a decrease in $\langle \text{DBE} \rangle$. However, as photolysis is not expected to change the overall mass concentration in the solution, the dilution effects should not contribute to the observed $\langle \text{DBE} \rangle$ reduction.

Closer examination of the mass spectra reveals the appearance/disappearance of a number of peaks during photolysis as well as significant changes in peak abundances. Although peak intensities in the ESI-MS spectra of mixtures are not directly proportional to the concentrations,¹³⁹ the expectation is that peaks corresponding to photodegradable compounds should decrease in abundance or even disappear, whereas peaks corresponding to stable photolysis products should increase. It is therefore instructive to group SOA compounds based on the observed changes (α_i) to their abundance (x_i) in the mass spectrum:

$$\alpha_i = \frac{x_i^{\text{after photolysis}}}{x_i^{\text{before photolysis}}} \quad (6.1)$$

Values of α are then grouped into five categories: new compounds produced from photolysis ($\alpha = \text{“infinity”}$); increased relative abundance from photolysis ($\alpha > 2$); no significant change from photolysis ($2 > \alpha > 0.5$); decreased relative abundance from photolysis ($\alpha < 0.5$); and compounds obliterated by photolysis ($\alpha = 0$). The average O/C, H/C, DBE value and carbon number, were then calculated for each of these five categories, along with the percentage of the total abundance for each group.

Table 6.5. Average values of O/C, H/C, DBE, #C and percent ion current for limonene SOA compounds after 2 and 24 hours of photolysis. The SOA compounds have been grouped according to the response of the corresponding peaks in the mass spectra to photolysis. The top and bottom sections of the table were calculated from ESI (-) and (+) mass spectra, respectively. Compounds with low O/C and large DBE values are photolyzed preferentially giving rise to new compounds with lower DBE and increased O/C.

		2 hr Photolysis					24 hr Photolysis				
		⟨O/C⟩	⟨H/C⟩	⟨DBE⟩	⟨#C⟩	% Ion Current	⟨O/C⟩	⟨H/C⟩	⟨DBE⟩	⟨#C⟩	% Ion Current
Negative ESI Mode	New Compounds	0.68	1.44	5.11	14.0	1	0.72	1.47	4.09	10.7	1
	Increased Relative Abundance	0.59	1.54	3.58	11.0	23	0.65	1.45	3.46	8.9	20
	No Change	0.55	1.54	3.65	11.6	64	0.57	1.55	3.07	9.2	65
	Decreased Relative Abundance	0.45	1.56	4.38	15.7	11	0.47	1.54	3.92	12.8	14
	Destroyed Compounds*	0.46	1.59	7.43	31.5	5*	0.48	1.58	6.67	27.0	16*
Positive ESI Mode	New Compounds	0.50	1.55	3.94	11.6	1	0.54	1.54	3.21	8.4	1
	Increased Relative Abundance	0.48	1.56	3.03	9.0	27	0.48	1.52	2.98	8.1	53
	No Change	0.42	1.60	3.29	11.3	62	0.43	1.55	3.36	10.2	37
	Decreased Relative Abundance	0.38	1.59	4.40	16.8	10	0.39	1.66	3.27	12.7	10
	Destroyed Compounds*	0.41	1.57	7.00	28.8	5*	0.41	1.57	6.00	23.6	15*

* Percent ion current calculated from non-photolyzed mass spectra

Table 6.5 lists these values calculated from 2 hrs and 24 hrs of photolysis for 1 ppm limonene SOA in ESI (+) and (-) modes. The new photochemically formed compounds have *higher* ⟨O/C⟩ values compared to the other types of compounds but are of relatively low abundance. Compounds that increased in relative abundance ($\alpha > 2$) also have higher than average ⟨O/C⟩ and represent ~25 % of the total signal. Conversely, compounds that are detected

with decreased relative abundances ($0 < \alpha < 0.5$) have lower $\langle O/C \rangle$, and contribute to ~10 % of the total signal. Lastly, compounds that have been completely decomposed during photolysis (~10 % of the total signal) have relatively low $\langle O/C \rangle$ and the highest values of $\langle DBE \rangle$ compared to the other groups. The trends in the $\langle H/C \rangle$ values are anti-correlated with the trends in the $\langle O/C \rangle$ values, i.e., compounds with high $\langle H/C \rangle$ are more likely to be removed by photolysis, and low $\langle H/C \rangle$ compounds are more likely to be the products.

The average O/C value of the *monomeric* compounds that are decomposed by photolysis is low (ESI (+) ~ 0.34; ESI (-) ~ 0.45) compared to that of the entire monomeric region (ESI (+) ~ 0.45; ESI (-) ~ 0.57). Taken with the data from Table 6.5, the observed increase in the overall $\langle O/C \rangle$ (Figure 6.4a) and decrease in the overall $\langle DBE \rangle$ values (Figure 6.4b) can be attributed to “photodegradation of low O/C monomers and high DBE oligomers of SOA with production of high O/C compounds”. These results are consistent with previously reported data on aqueous photolysis of DOM samples.^{246, 247} HR-ESI-MS analysis of DOM before and after photolysis showed that chemical families with high DBE and low oxygen number are preferentially photolyzed, while compounds with low DBE and high oxygen content remained intact after photolysis.²⁴⁷ Another study found that hydrophilic moieties were preferentially degraded from photolysis, while more hydrophobic moieties remained unaffected, or were formed.²⁴⁶

The effect of photolysis on individual functional groups was further examined using methanol reactivity analysis.¹³⁵ The subset of peaks corresponding to aldehydes is significantly reduced by the UV photolysis, sometimes to the point of complete annihilation. For example, the compound $C_{10}H_{16}O_2$, previously identified as limononaldehyde,⁹⁰ decreases from 36% to 1% relative abundance after only 2 hours of photolysis, as measured in the ESI (+) mode. The peaks corresponding to compounds assigned as ketones are also reduced by UV photolysis. For

example, the compound C₉H₁₄O₄, previously assigned to keto-limononic acid, decreases from 100% to 35% relative abundance after 2 hours of photolysis, as measured in the ESI (-) mode.

Table 6.6. Effect of photolysis on the estimated percent fraction of carbonyls and carboxyls in the 1 ppm limonene SOA extract (the concentration dependence of these fractions is provided in Table S4 of the supporting information section). The fraction of HR-MS signal was calculated for each group, from the corresponding mass spectra taken before photolysis, after 2 hours, and after 24 hours of photolysis.

		Carbonyl	Carboxyl	Both	Other	Total ion Signal
Negative ESI Mode	No Photolysis	6.2	8.2	74.0	11.6	1.0
	2 hr Photolysis	5.7	12.5	62.2	19.6	1.0
	24 hr Photolysis	4.4	11.3	64.5	19.9	0.8
		Carbonyl	Carboxyl	Both	Other	
Positive ESI Mode	No Photolysis	8.1	13.9	69.3	8.7	1.0
	2 hr Photolysis	4.7	25.4	55.7	14.2	0.84
	24 hr Photolysis	3.2	19.1	58.0	19.7	0.47

Cumulative analysis of the complete set of compounds grouped by carbonyl, carboxyl, both carbonyl and carboxyl groups, or other functional group is tabulated in Table 6.6 (1 ppm data only). Compounds containing both carbonyl and carboxyl groups comprise the largest fraction (~ 70%) of the total HR-MS signal, emphasizing the multi-functional nature of the SOA constituents. Upon photolysis, this fraction decreases to ~ 60%, suggesting that these multi-functional compounds containing one or more carbonyl groups are dissociated. Carbonyl-only compounds (with no carboxyl group) account for a relatively small fraction (~ 6-8 %) of the total signal. This fraction is decreased by photolysis as well, all in agreement with the UV/Vis measurements described below. The signal corresponding to compounds containing only

carboxylic acid groups increased with photolysis relative to the starting solution. Finally, compounds classified in the other functional group category, increase in their relative abundance. However, part of this increase is due to the artificial attribution of all the new compounds generated by photolysis to the “other” category.

In order to investigate the role of aqueous solvation on the photochemistry of limonene SOA, we have also conducted photolysis experiments on dry limonene SOA. Surprisingly, the HR-ESI-MS results for the filter photolysis were not substantially different from the aqueous photolysis results. Table 6.7 compares the average elemental ratios and average DBE values as measured in the (+) and (-) modes for 0.5 ppm and 1 ppm precursor concentrations photolyzed for 2 hours in aqueous solution and directly on a filter. Similar general trends are observed from filter photolysis but photolysis in aqueous solution appears to be more efficient than photolysis on a filter. For example, both the increase in $\langle O/C \rangle$ and decrease in $\langle DBE \rangle$ are smaller in magnitude on the filter. It is likely that the more viscous environment in dry particles suppresses diffusion of free radical intermediates and increases the probability of geminate recombination making the photolysis less efficient. In addition, unlike the situation in the aqueous photolysis, volatile species formed during photolysis of dry samples are more likely to evaporate.

Table 6.7. Average values of O/C, H/C, DBE and number of carbons for SOA photolyzed in a **dry state directly on a filter** or in **aqueous solution**. The values were calculated from mass spectra taken before and after photolysis (in the filter case, the samples are extracted in H₂O and diluted with CH₃CN immediately before taking the mass spectra). The top and bottom sections of the table were calculated from ESI (-) and (+) mass spectra, respectively.

SOA Precursor Concentration (ppm)		0.50	0.50	1.00	1.00
		H₂O	Filter	H₂O	Filter
Negative ESI Mode	⟨O/C⟩ Before UV	0.49	0.50	0.50	0.50
	⟨O/C⟩ 2 hr UV	0.54	0.52	0.55	0.53
	⟨H/C⟩ Before UV	1.55	1.54	1.55	1.54
	⟨H/C⟩ 2 hr UV	1.55	1.54	1.54	1.53
	⟨DBE⟩ Before UV	3.85	3.93	4.10	3.88
	⟨DBE⟩ 2 hr UV	3.37	3.94	3.73	4.22
	⟨#C⟩ Before UV	12.89	12.87	14.08	12.61
	⟨#C⟩ 2 hr UV	10.63	12.76	11.93	13.73
Positive ESI Mode	⟨O/C⟩ Before UV	0.39	0.38	0.39	0.40
	⟨O/C⟩ 2 hr UV	0.43	0.43	0.44	0.43
	⟨H/C⟩ Before UV	1.59	1.57	1.59	1.58
	⟨H/C⟩ 2 hr UV	1.61	1.61	1.59	1.59
	⟨DBE⟩ Before UV	3.69	4.10	3.80	4.18
	⟨DBE⟩ 2 hr UV	3.11	3.60	3.35	3.89
	⟨#C⟩ Before UV	12.94	14.41	13.57	15.29
	⟨#C⟩ 2 hr UV	10.62	10.53	11.23	13.97

Effect of photolysis on the UV/vis spectra of limonene SOA in water

Characteristic UV/Vis spectra of 1 ppm limonene SOA aqueous solutions acquired during photolysis of PILS samples are shown in Figure 6.5. The response of the spectrum around 280 nm is especially interesting as it includes contributions from the $n \rightarrow \pi^*$ bands in carbonyls, with additional contributions from the $n \rightarrow \sigma^*$ bands in peroxides.²⁶⁷ Furthermore, 280 nm is close to the cut-off wavelength for tropospheric photochemistry, with higher-energy

radiation being effectively screened by stratospheric ozone. After only thirty minutes of photolysis the optical absorbance at 280 nm is visibly diminished, and after 24 hours, most of the initial absorbance at this wavelength has disappeared. The effective photolysis lifetime measured at 280 nm absorbance was ~ 105 min as estimated from an exponential fit to the measured absorbance (inset of Figure 6.5). At lower wavelengths, there was an initial gain in absorbance between 210 – 240 nm followed by a decrease after 24 hours of photolysis. In this wavelength range it is more difficult to attribute the change in absorbance to any particular functional group.

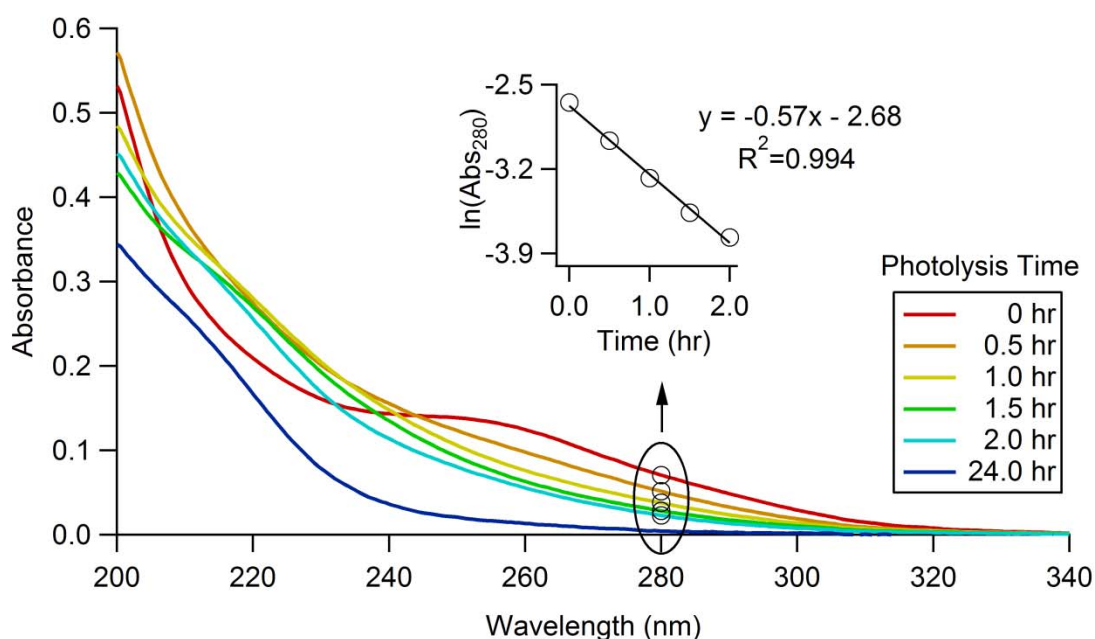


Figure 6.5. UV/Vis spectra taken during photolysis of 1 ppm limonene SOA sample collected using PILS. Spectra were obtained every thirty minutes during the first two hours of photolysis and again after 24 hours of photolysis. The inset shows the natural log of absorbance at 280 nm versus photolysis time. The lifetime with respect to photolysis is about 1.75 hours.

The efficiency of photolysis can be estimated by comparing the observed decay of the 280 nm absorbance with the excitation rate. The effective photolysis rate (J , in units of s^{-1}) of an SOA constituent is

$$J = \int_{\lambda} \sigma(\lambda) \phi(\lambda) F(\lambda) d\lambda \quad (6.2)$$

where $\sigma(\lambda)$ is the effective absorption cross section in $\text{cm}^2 \text{ molecule}^{-1}$, $\phi(\lambda)$ is the effective photolysis quantum yield, $F(\lambda)$ is the radiation flux density in photons $\text{cm}^2 \text{ nm}^{-1}$, and λ is the wavelength. The same expression with $\phi(\lambda)=1$ gives the excitation rate. The effective absorption cross section (base-e) can be obtained from the experimentally measured base-10 absorbance (A_{10}) as follows:

$$\sigma(\lambda) = \frac{A_{10}(\lambda) \cdot \ln(10)}{l \cdot C \cdot N_a \cdot 10^{-3}} \quad (6.3)$$

where l is the cuvette path length in cm, C is the concentration in mol L^{-1} , and N_a is Avogadro's number. The molar concentration of SOA compounds is estimated from the SMPS data (Table 1), assuming 100% PILS collection efficiency. We assume an effective molecular weight of 200 g/mol, as this is the average molecular weight of the monomer species observed in the ESI mass spectra. The integrated radiation flux can be related to the total power measured at the position of the photolysis cell.

$$\text{Measured Power} = S \int_{\lambda} F(\lambda) \frac{hc}{\lambda} d\lambda \quad (6.4)$$

where S is equal to the beam surface area, h is Planck's constant, and c is the speed of light. The shape of the wavelength dependence of $F(\lambda)$ is obtained from explicit measurements with an Ocean Optics spectrometer.

Using equations (6.2 – 6.4), we estimate an excitation rate of 0.0053 s^{-1} for the sample shown in Fig. 4. This rate is significantly larger than the observed rate of disappearance of the $n \rightarrow \pi^*$ carbonyl band (0.00016 s^{-1} from Figure 6.5). The wavelength-integrated photolysis quantum yield (ϕ) can be estimated as the ratio of these two rates. The resulting value of $\phi=0.03$, compares favorably with known quantum yields for carbonyl photolysis in liquid hydrocarbons (0.005-0.02).²⁶⁸ The low values are indicative of solution-phase carbonyl photolysis, with quantum yields reduced relative to the gas-phase.²⁶⁹

Although other compounds, such as peroxides, undergo direct photolysis in this wavelength range, both the shape of the absorption spectrum and the order of magnitude of the estimated photolysis quantum yield strongly suggest that carbonyl photochemistry plays a very important role in photolytic processing of SOA aqueous solutions. This conclusion is consistent with previous studies, where significant photochemical transformation of aqueous solutions of pyruvic acid and glycolaldehyde was observed upon exposure to actinic UV radiation.^{148, 242, 243, 250, 253}

Effect of photolysis on the pH and peroxide content of limonene SOA in water

To further confine the effects of photolysis on chemical composition, pH and peroxide measurements of the SOA extracts were performed before and after photolysis. The pH measurements provide indirect information about the total concentration of acidic species in SOA, and the peroxide test quantifies the total amount of water-soluble organic peroxides and hydrogen peroxide. As limonene SOA is water-soluble,²⁵⁹ the peroxide test should measure the total peroxide content in the solutions.

Figure 6.6 plots the observed pH (a) and peroxide concentration (b) vs. the SOA precursor concentrations: before, after 2, and 24 hours of photolysis. Before photolysis, the measured pH

decreases and peroxide concentration increases with the SOA precursor concentrations. These changes are expected because the mass of SOA extracted in water increases at higher precursor concentrations (Table 6.1). It is therefore more informative to compare the molar amounts of hydronium ion and peroxides normalized with respect to the mass of dissolved SOA (in the units of moles per mg of dissolved SOA) as done in Figure 6c. The normalized amounts ($\sim 10^{-7}$ mol mg^{-1}) remain constant within experimental uncertainties.

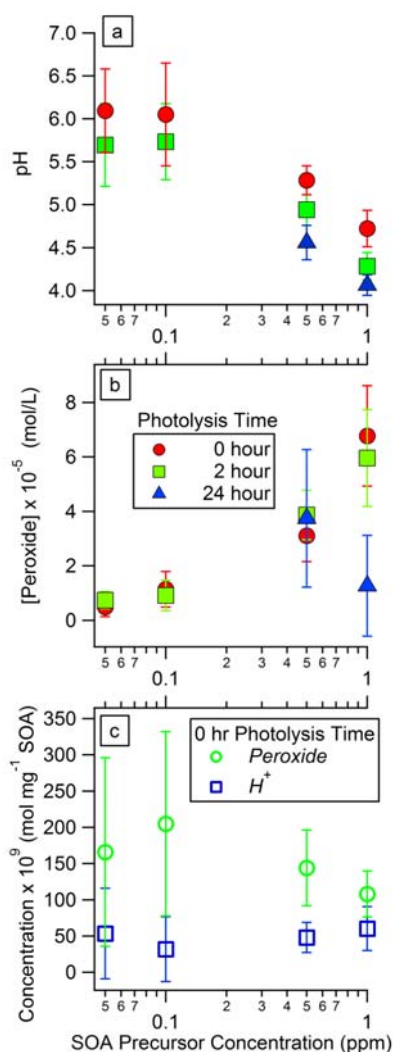


Figure 6.6. (a) Absolute pH values, and (b) peroxide concentrations measured in PILS samples of limonene SOA with varying precursor concentrations and photolysis times. (c) Normalized concentrations (in units of mol per mg of the dissolved SOA mass) of H⁺ ion and peroxides measured .

With the assumed average molecular weight of 200 g/mol for SOA compounds, our measurements suggest that there is one peroxide group per 50 SOA molecules (~ 2 %). This number is significantly lower compared to measurements by Docherty et al. for α -pinene (~47%) and β -pinene (~85%).²⁶⁰ The reasons for this discrepancy are not entirely clear but they may have to do with the differences in the experimental conditions. For example, our measurements were for the water-soluble fraction only, while Docherty et al. measured the organic-soluble fraction. The reactant concentrations were higher in the Docherty et al. study, and they used a scavenger that suppressed oxidation by OH. Our results are in much better agreement with the recent measurements of reactive oxygen species (ROS) in limonene SOA by Chen et.al., who reported ROS yields in fresh limonene SOA of the order of 1-2%.²⁷⁰

Estimating the fraction of carboxyl groups from the pH measurements is less straightforward, as we do not account for the effect of the dissolved atmospheric CO₂ (photolysis and pH measurements were done in room air). pKa values for the common acids found in biogenic SOA are in the 3-5 range (e.g., pKa = 4.6 for pinonic acid) and not all of these carboxylic acids are expected to ionize in solution at pH=4-6. In addition, compounds other than carboxylic acids can have pKa values in this range, for example, enols such as ascorbic acid, have a pKa value of ~ 4. Therefore, the proton concentration derived from pH measurements underestimates the concentration of acidic species, perhaps by as much as an order of magnitude. However, in photolysis experiments, pH can still be used as metric for the relative amounts of acidic species in SOA.

A reproducible reduction in pH was observed for all photolyzed SOA extracts (Figure 6.6). The carboxylic acid group by itself is not photochemically active at tropospherically relevant wavelengths.¹ However, it can participate in photochemistry if positioned next to a

photochemically active group. For example, pyruvic acid ($\text{CH}_3\text{C}(\text{O})\text{COOH}$) undergoes decarboxylation and photopolymerization quite readily when irradiated at 320 nm.²⁵⁰ Many carboxylic acids in limonene SOA are multifunctional compounds, and some of them may undergo similar photochemical processes. However, the decrease in pH suggests that production of carboxylic acids and other acidic compounds as end products of photolysis outweighs their decomposition. Photochemical production of carboxylic acids has been observed in aqueous solutions of DOM. For example, a study²⁴⁴ on soil derived humic substances observed an increase in acidic species due to photolysis in the presence of dissolved oxygen. Another study²⁴⁶ reported low-molecular weight acid (formic, acetic, pyruvic, oxalic, malonic and succinic acids) formation from photolysis of DOM. It appears that similar photochemical processes occur in SOA and DOM extracts with respect to the carboxylic acid production.

Based on the efficient photodegradation of carbonyls described in the previous section, we expected to find a similarly large reduction in the peroxide content in the photolyzed SOA extracts. While there is no experimental information on the photodissociation quantum yields of large organic peroxides in aqueous solutions, the yields are likely to be high based on comparison to the H_2O_2 and CH_3OOH aqueous photolysis.^{271, 272} Using absorption cross sections and photolysis quantum yields for H_2O_2 or CH_3OOH in equations (6.2-6.4), we estimated that peroxides should undergo photodegradation as fast if not faster than carbonyls. However, according to Figure 6.6, the peroxide concentrations did not change after 2 hours of photolysis within the measurement uncertainties. After 24 hours of photolysis, the 1 ppm samples experienced a reduction in the peroxide content, while the 0.5 ppm samples had no statistically significant change (24 hour photolysis experiments at the lower SOA loadings were not conducted). Based on these observations, we conclude that the secondary reactions of the

primary photolysis products must generate smaller peroxides such as H_2O_2 . Indeed, photochemical production of H_2O_2 has been observed from cloudwater^{241, 255, 256} and DOM²⁴⁹ in aqueous solution. As the peroxide test employed in our analysis does not distinguish between organic peroxides and H_2O_2 ,²⁶⁰ the combined result of photodissociation of organic peroxides and formation of H_2O_2 would result in no net change to the observed peroxide content.

6.4 Discussion

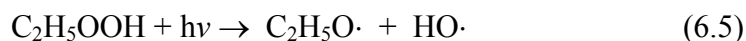
Possible mechanisms of photolysis

Because SOA represents a very complex mixture of organic compounds, it is difficult to determine a detailed mechanism of the photolytic processing of its aqueous extract. However, one can draw general conclusions about the behavior of different functional groups based on the examination of mass-spectrometric, spectroscopic, pH, and peroxide content results described in the previous sections. The goal of the following discussion is to rationalize the observed photodegradation of carbonyls (Figure 6.6 and Table 6.6), cycling of peroxides (Figure 6.6b), and photoproduction of acidic compounds (Figure 6.6a) during photolysis.

Broadly speaking, there are two mechanisms for the photolytic processing occurring in the SOA extracts: direct photodissociation and secondary reactions with free radicals formed by the direct processes. Examples of the direct processes are $n \rightarrow \pi^*$ Norrish type-I and -II splitting of carbonyls,²⁷³⁻²⁷⁵ and $n \rightarrow \sigma^*$ direct photolysis of peroxides. The observed reduction in carbonyl functional groups during photolysis is consistent with the direct photodissociation. However, the fact that the total amount of peroxides does not change significantly during

photolysis suggests that the secondary reactions must also be taking place, and that these reactions generate peroxides and carboxylic acids as products.

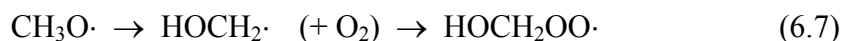
Photolysis of simple organic hydroperoxides CH_3OOH and $\text{C}_2\text{H}_5\text{OOH}$ in water has been studied extensively.²⁷² The primary photolysis of these peroxides results in formation of an alkoxy radical and hydroxyl radical, e.g.:



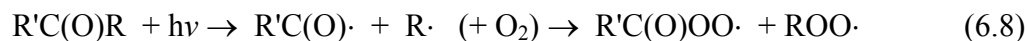
Photolysis of more complex organic peroxides has not been investigated in detail but most of them likely break in a similar way via fission of the O-O bond:



It has been suggested and confirmed that the alkoxy radicals isomerize in water into hydroxyalkyl radicals, which can then add oxygen to form hydroxyperoxy radicals.²⁷²



Additional peroxy radicals can also be produced by direct Norrish type-I photolysis of carbonyls in the presence of dissolved oxygen:



Norrish type-I splitting of carbonyls is the predominant path for small ($\text{C}_1\text{-C}_5$) carbonyls.²⁷³⁻²⁷⁵

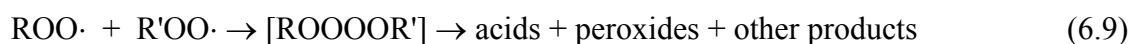
Norrish type-II splitting dominates in larger carbonyls with accessible hydrogen atoms in the γ -position relative to the carbonyl group. Photolysis products resulting from the Norrish type-II channel are olefins and smaller aldehydes or ketones,²⁶⁹ which can then be photolyzed further by the Norrish type-I mechanism.

Hydroxyl radicals generated from the photolysis of organic hydroperoxides (Equation 6.5) will react with *all* stable organic molecules present in the extract, including the hydrated

aldehydes. In fact, OH oxidation has been shown to be a primary loss mechanism for small aldehydes in aqueous solutions, with carboxylic acids formed as the end products.²⁷⁶⁻²⁷⁸

The peroxy radicals, including the hydroxy substituted ones formed in (Equation 6.7), are relatively stable in solution. Their primary fate is self-reaction or reaction with HO₂ radicals, which can form a number of products including, organic hydroperoxides, and aldehydes.²⁷⁹

Some of the peroxy radical self-reactions will go through tetroxide intermediates, which are highly unstable and break to form carboxylic acids and hydrogen peroxide in solution:^{272, 280}



As such processes involve two free radicals their rate should increase quadratically with the concentration of the primary absorbers. This may contribute to the faster photolytic processing of more concentrated SOA solutions.

6.5 Atmospheric implications

We have demonstrated that the molecular composition of limonene SOA undergoes extensive changes when exposed to radiation in the tropospherically relevant region of the solar actinic spectrum (300-400 nm). This photolytic processing can take place in dry SOA particles but it appears to be faster when SOA is dissolved in an aqueous solution. The main implication of these results is that the processed aerosol will have a different chemical composition from the one formed in the initial oxidation of VOC. More specifically, the processed aerosol will be depleted in carbonyl compounds, depleted in oligomeric compounds, and enriched in acidic compounds.

The photolytic processing of SOA increases the average O/C ratio for the aerosol constituents, and may help account for the discrepancy between lower $\langle O/C \rangle$ values measured in chamber studies and higher $\langle O/C \rangle$ values measured in the field.²⁸¹ For example, AMS measurements²⁸² reported $\langle O/C \rangle$ ratios of ~ 0.7 for low-volatility OA and ~ 0.4 for semi-volatile OA for a wide range of ambient aerosols.²⁸³ The SOA generated by oxidation of monoterpenes generally falls into the semi-volatile OA category with $\langle O/C \rangle$ of 0.3-0.5. Extensive photolytic processing, in cloud water and in the dry state, has the potential to enrich SOA with higher O/C compounds, and shift it the low volatility OA category.

The photolytic processing of POA has also been studied.¹³ Diesel exhaust was used as a surrogate for POA. Experiments were conducted in the gas/particle phase, and reached a similar conclusion that photolysis of oxygenated organics produces further oxidized products of lower volatility.¹³

The preferred photodegradation of the oligomeric compounds may contribute to the scarcity of their observations in field studies as opposed to the laboratory investigations in smog chambers.²⁸⁴ While actinic radiation is often present, the high level of humidity necessary to make aqueous dissolved SOA droplets is rarely achieved in smog chambers. Unlike the smog chambers, the oligomeric compounds formed in ambient aerosols have a higher probability of photodegradation through aqueous photolytic processing before the particles (or droplets) are collected.

The optical properties of the aerosol are also affected by the photolysis. Specifically, the near-UV absorbance of limonene SOA in the carbonyl $n \rightarrow \pi^*$ absorption band is reduced almost entirely. The reduction in the UV absorbance suggests that photobleached SOA absorb UV

radiation to a smaller extent than freshly formed SOA do. This may have implications for surface UV flux in areas characterized by significant organic air pollution.

From the perspectives of SOA aging, it is instructive to estimate the time scale of the photolytic processing and contrast it to other aging mechanisms, such as heterogeneous oxidation by OH. The photolytic lifetime of carbonyl compounds dissolved in cloud water can be calculated from Equation (6.2) using the experimentally measured absorption cross section of limonene SOA in water, the estimated quantum yield (~ 0.03), and the solar actinic flux measured between 290 and 500 nm.¹ At a solar zenith angle (SZA) of 10° , typical for Southern California in the summer, the resulting photolysis lifetime is ~ 5 hours. At SZA of 60° , typical of Chicago, Illinois in the winter, the lifetime increases to ~ 9.2 hours. We note that significant changes to ambient organic aerosol composition occur on comparable time scale but they are usually attributed to heterogeneous OH chemistry rather than direct photolysis.²⁸² Given that organic particles spend days in the air in a dry state and hours in a dissolved state, photolytic processing should be an important mechanism of aging. Whether heterogeneous oxidation by OH or photolytic processing of aerosol is more important will depend on specific atmospheric conditions (SZA, relative humidity, cloudiness, etc.).

Chapter 7

Condensed Phase Photolysis

7.1 Introduction

Carbonyl compounds are found ubiquitously in the environment due to both direct emission from anthropogenic sources and secondary formation from oxidation of biogenic and anthropogenic volatile emissions.^{285, 286} Carbonyl compounds are formed in the gas phase from the reaction of atmospheric oxidants with terpenes^{127, 287} and isoprene.²⁸⁸ Due to their lower volatility, the newly formed carbonyl containing compounds can partition to the particle phase, such as SOA formed from the oxidation of monoterpenes^{80, 83, 130} and isoprene.²⁸⁹ The initial chemical composition of SOA is quite complex and further evolves due to atmospheric aging, i.e. further oxidation from gas-phase oxidants, water vapor condensation and evaporation, heterogeneous reactions in the particle phase and photolysis from solar radiation.²⁸² Understanding the mechanisms that affect SOA aging is currently incomplete. Direct photolysis of carbonyl containing compounds inside SOA particles has been proposed as a possible mechanism of chemical aging of SOA.²⁰ Recent field observations also suggest significant photolytic processing of carbonyl compounds in aerosols during long range transport.¹⁹

The photochemistry of *gas-phase* carbonyls has been extensively studied, with well established mechanisms,²⁷³⁻²⁷⁵ quantum yields,^{285, 290} and absorption cross sections.²⁹¹ The photolysis mechanism of carbonyls proceeds through the well-known Norrish reactions.²⁷³⁻²⁷⁵ The production of CO and an alkyl radical, Norrish type I, is the predominant path for small aldehydes and ketones such as acetaldehyde and acetone. The Norrish type II processes tend to

dominate in aldehydes and ketones that have accessible hydrogen atoms in the γ -position relative to the carbonyl group. Photolysis products resulting from the Norrish type II channel are typically olefins and smaller aldehydes or ketones.²⁶⁹ Photoisomerization of ketones into cyclic alcohols has also been reported from photolysis.^{269, 292}

The photochemistry of carbonyls in solution has also been studied, though less extensively. The $n \rightarrow \pi^*$ bands in carbonyls tend to experience hypsochromic (blue) shifts in solutions. The quantum yields for CO production via Norrish type-I splitting is known to decrease greatly in the liquid phase, and as the size of the aldehyde or ketone increases.^{268, 269} The total carbonyl photolysis quantum yield is also reduced in solution relative to the gas-phase.^{278, 293, 294} The photochemistry of condensed phase carbonyls has not been studied extensively.

Current techniques for studying the photochemistry of condensed phase carbonyls employ thin films of an analyte containing a carbonyl and a method to detect the gas-phase photoproducts. Infrared cavity ring-down spectroscopy (IR-CRDS) has been employed to study the condensed phase photochemistry of biogenic SOA^{18, 20} and of thin films of analytes.^{295, 296} Chemical ionization mass spectrometry (CIMS) has also been used to monitor the production of gas-phase species from photolysis of biogenic SOA.²¹ These studies were largely qualitative and only observed the photolysis products without quantifying the efficiency of the process.^{18, 20, 21, 296}

In a previous work we monitored the production of CO from photolysis of carbonyl species found in SOA.²⁰ This chapter is a continuation of our previous work, but simplifies the complexity of SOA by using a single model carbonyl compound embedded into an “SOA-like” organic matrix. Furthermore, the IR-CRDS methodology was adapted in this work to yield

absolute measurements of carbon monoxide and a chemical actinometer was used to measure the absolute photon flux. Using these two measurements the quantum yields were measured as a function of photolysis wavelength for the photoproduction of carbon monoxide from condensed phase photolysis of carbonyls. With this knowledge the potential for long-chain carbonyls in SOA to be a source of small VOCs and greenhouse gases can be predicted, as well as the timescales of photolysis.

7.2 Experimental

IR-CRDS and Photolysis Setup

A modified IR-CRDS system was used to measure the photoproduction of gas-phase species from photolysis of solid thin films. The system has been described in detail previously.²⁹⁶ Briefly, the system involves a two-axis quartz tube, one axis contains the UV photolysis beam and sample thin film, while the other axis is centered around the IR beam and cavity mirrors. High reflectance ($R = 99.98\%$) CRDS mirrors (Los Gatos Research) optimized in the $4.5\ \mu\text{m}$ wavelength range were used for cavity mirrors. The tunable IR light was generated from a pulsed Nd:YAG (Continuum Powerlite 8000) laser pumping an optical parametric oscillator (OPO) laser (LaserVision). This produced wavelengths in the fundamental carbon monoxide vibrational band ($2100\ \text{cm}^{-1}$). A characteristic CRDS ro-vibrational spectrum of CO is plotted in Figure 7.1, as well as the theoretical CO spectrum from the HITRAN database.²⁹⁷ The database was used to match the experimental origin (band gap) with the absolute wavenumber (cm^{-1}) value and ensure the OPO output was at the correct wavelength.

All experiments used the R(5) line in the $\nu=1\leftarrow 0$ band of CO for measurements of CO concentrations in the cavity as will be exemplified later.

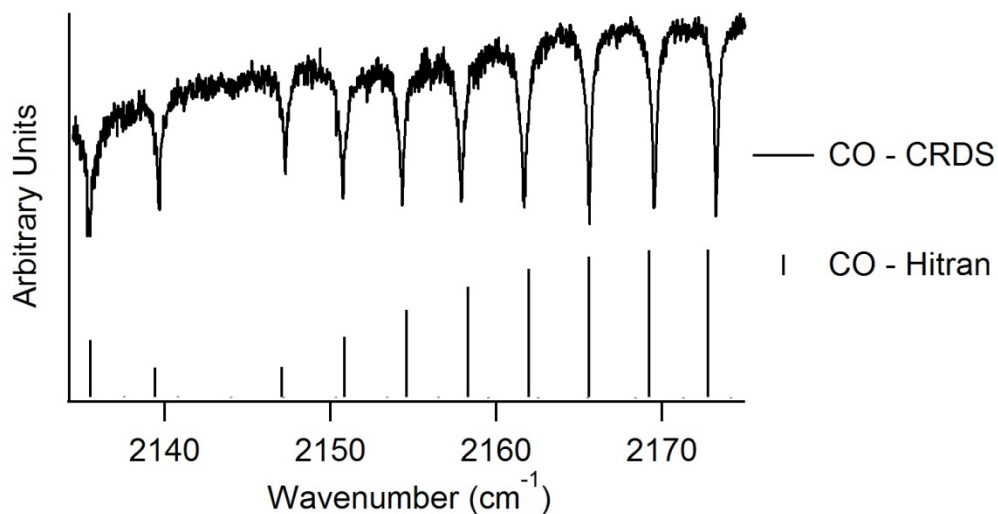


Figure 7.1. A portion of the rotationally resolved IR spectrum of $\nu=1\leftarrow 0$ band of carbon monoxide obtained with IR-CRDS. The known spectrum, obtained from HITRAN database, is also plotted. The weak lines in the simulated HITRAN spectrum are due to the ^{13}CO .

The UV-photolysis beam was produced from a 100W Xenon lamp (Newport PhotoMax) reflected by a dichroic mirror (330 nm) into a monochromator (Spectra Physics Cornerstone 1/8 m) with slits wide open, resulting in 20 nm full-width at half maximum (FWHM) bandwidth light. The emerging light was focused onto the sample using a converging lens. The total power ranged from 0.5 to 15 mW for wavelengths ranging from 260 to 360 nm, respectively. The thin film samples were generated on 1.5 in. diameter CaF_2 windows. The photolysis beam passed through one of the windows before hitting the film. Photolysis experiments were conducted under vacuum at ~ 100 torr. A small flow of He (UHP, 99.999%) was used to flush contaminants

from the high reflectance cavity mirrors. The pressure in the cell was monitored throughout the experiments using a capacitance manometer (Baratron).

Absolute Calibration of CO concentrations

A standard of 9.70 ppmv CO with nitrogen make-up gas (Scott-Marrin, Inc) was used for calibrations. The CO standard was further diluted with He (UHP, 99.999%) using calibrated flow meters (SEC-4400MC, STEC, Inc) controlled using a 4-channel readout (MKS Type 247) to produce known concentrations of CO in the CRDS cell. The concentration of CO in the CRDS cell was measured from the change in the cavity ring-down time constant, τ , with and without varying amounts of CO present in the cell. Figure 7.2a displays representative data on the measured changes in τ from increasing amounts of CO (~0.07 – 5 ppm).

To calculate the absolute concentration of CO in the cell, the change in ring-down time (τ) is related to the absorption coefficient (α) as follows:

$$\alpha(\text{cm}^{-1}) = \frac{1}{c} \left(\frac{1}{\tau} - \frac{1}{\tau_0} \right) \quad (7.1)$$

and the absorption coefficient is related to the CO concentration by the following relationship:

$$[\text{CO}] = \frac{\int \alpha d\bar{\nu}}{S} \quad (7.2)$$

where c is the speed of light, τ is the ring-down time with absorber (CO), τ_0 is the ring-down time of the empty cell, α is the absorption coefficient measured in (cm^{-1}), $\bar{\nu}$ is the wavenumber in (cm^{-1}) and S is the band strength in (cm molecule^{-1}). Therefore the absolute concentration can be calculated from a specific rovibrational line by integrating the measured absorption coefficient over the peak width in wavenumbers and dividing by the band strength. The known band strengths of CO were obtained from the HITRAN database.²⁹⁷ In practice, however, the

time requirement to scan over a typical CO peak is inconvenient for measurements of gases emitted during photolysis, due to possible photobleaching. Therefore, the peak height is substituted for the integrated peak area and the CO concentration can be measured continuously during both photolysis and calibration experiments.

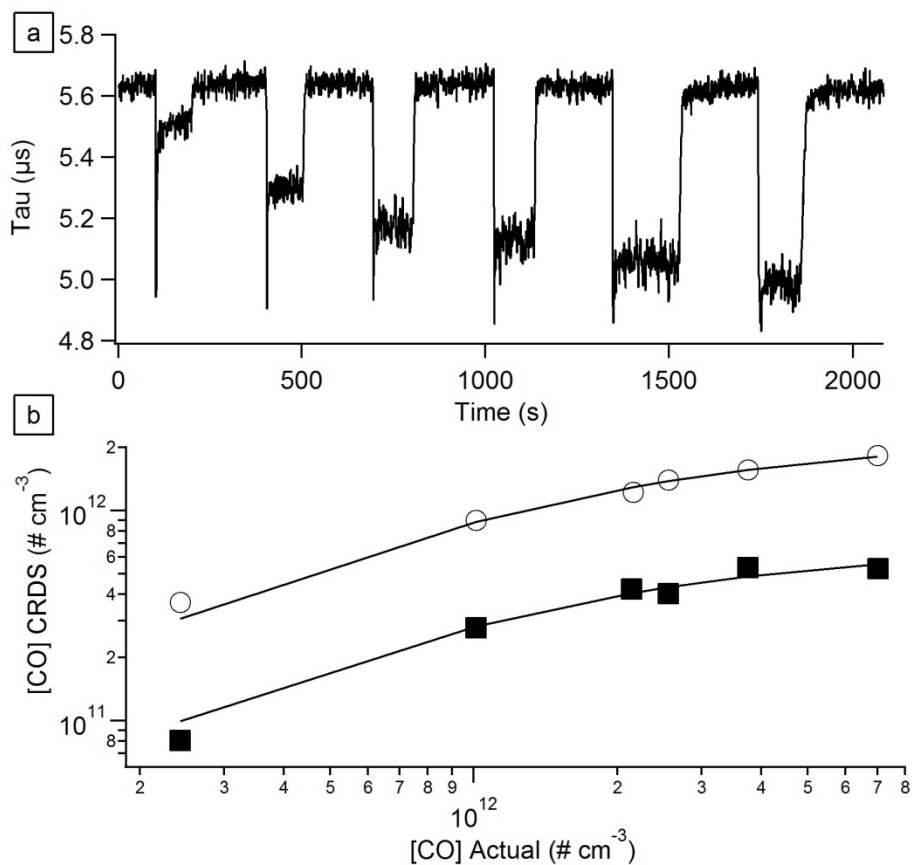


Figure 7.2. (a) IR-CRDS response from increasing concentrations of CO in the CRDS cell. (b) Representative calibration curves obtained from known concentrations of CO versus the IR-CRDS response. The plotted curves are a fit to a saturation function, Equation 7.3.

The measured calibration curves were generated from known concentrations ranging from $\sim 0.07 - 5$ ppm and plotted in Figure 7.2b. The concentrations from the known calibration standard are plotted on the x-axis versus the measured concentration from CRDS on the y-axis.

The calibration curves would typically saturate at the higher concentrations (1 ppm and above) and were therefore fit to an empirical saturation-type formula:

$$y = \frac{ax}{b+x} \quad (7.3)$$

The value of the coefficients a and b varied between experiments as exemplified in Figure 7.2b, thus requiring calibrations before every experiment. The calculated fits are included as solid lines. The differences in generated calibration curves (Figure 7.2b) were attributed to day-to-day fluctuations in laser bandwidth, which depends on laser alignment, and τ_0 , the empty cavity ring-down time constant. The cavity ring-down time constant can be affected by compounds adsorbing to the mirror surfaces and the alignment of the IR laser with the cavity mirrors. An empirical relationship between the measured empty cavity ring-down time constant and the calibration curve was established, as lower ring-down time constants produced a smaller peak height and therefore calibration curves would saturate at lower values. While an experimental inconvenience, the daily calibrations were necessary to convert the CRDS measurements to absolute concentrations from the generated calibration curve.

Thin Film Samples

Thin films were produced from solvent evaporation of either undecanal (Acros Organics, 97%) or 2-nitrobenzaldehyde (Fluka, 99%) mixed with poly(methyl)methacrylate (PMMA) (Aldrich, $M_w = 15000$) and methylene chloride (Fisher, HPLC grade). A 50 % solution of undecanal was made by mixing 0.7 g of analyte with 1.4 g PMMA into a 100 mL of methylene chloride in a volumetric flask. A single aliquot of 250 μL of each solution was pipetted using a gas-tight syringe onto a 1" diameter circle and the solvent was allowed to dry for a period of a few hours, resulting in an opaque uniform film of undecanal/PMMA. A 10%

solution of 2-nitrobenzaldehyde (2-NB) was made by mixing 1.5 g of PMMA and 0.15 g of 2NB with 100 mL methylene chloride in a volumetric flask. Aliquots of 150 μL of this solution were used to prepare films in order to measure the photon flux from the UV-vis photolysis beam. All films were placed under vacuum (~ 100 torr) in the CRDS system for 1 – 2 hours before photolysis measurements were conducted. A blank solution containing only PMMA (1.4 g) dissolved in 100 mL methylene chloride was used to prepare a pure PMMA film to test for the photoproduction of gas-phase products from photolysis of the polymer matrix.

Actinometry

Actinometry measurements were conducted using a thin-film actinometer as described above and in the literature.²⁹⁸⁻³⁰⁰ All work with 2-NB was done in the dark or under red light. 2-NB is converted to 2-nitrosobenzoic acid during photolysis. The concentration of 2-NB in the film was measured using the area of the 1530 cm^{-1} (nitro group asymmetrical stretch) absorbance peak via FTIR spectroscopy.³⁰⁰ Figure 7.3 displays a typical FTIR spectra obtained before and after photolysis. The disappearance of the 1530 cm^{-1} absorbance peaks is evident, as well as the formation of carboxylic acid hydrogen bonds between 3000 and 3400 cm^{-1} . The absolute concentrations of 2-NB measured were calibrated using thin films prepared from $50\text{ }\mu\text{L}$ aliquots of the 2-NB solution.

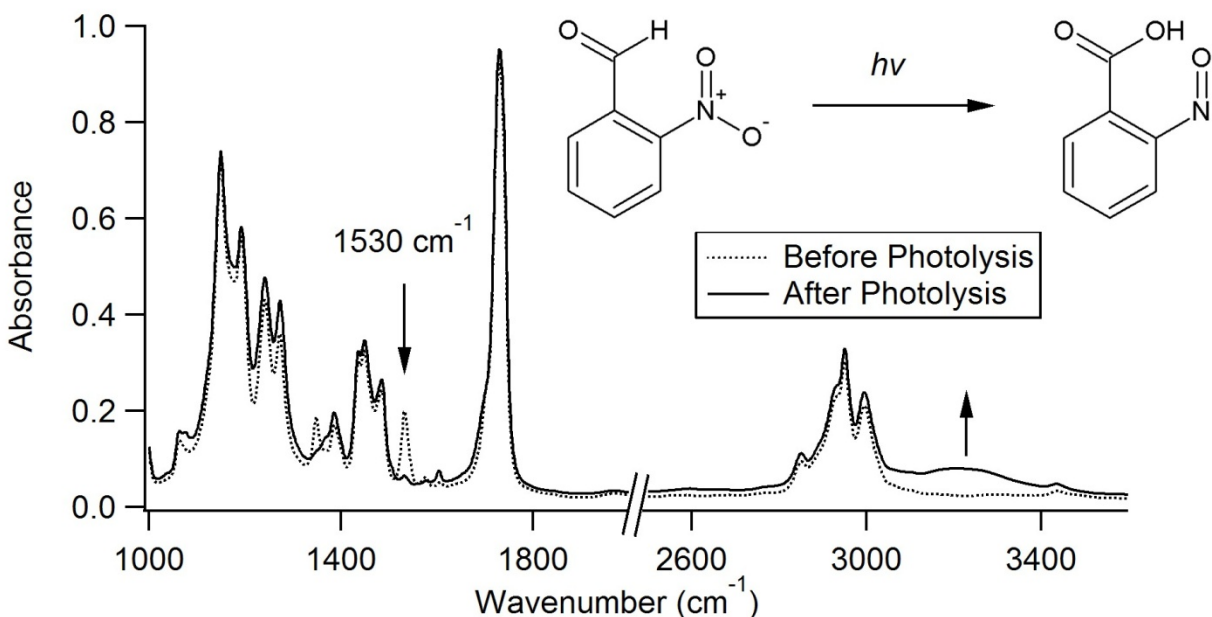


Figure 7.3. Representative FTIR spectra of a 2-NB/PMMA film before photolysis (dotted trace) and after photolysis (solid trace). The photolysis was followed through the 1530 cm^{-1} peak, corresponding to the nitro group, which is lost upon photolysis.

The conversion of 2-NB to 2-nitrosobenzoic acid can also be measured via high performance liquid chromatography (HPLC) with UV detection.³⁰¹ This technique requires 2-NB to be dissolved in aqueous solution or solvent. The quantitative transfer of 2-NB films into solutions was not convenient in our experimental setup. In addition, photolysis of 2-NB in aqueous solution does not reflect the same experimental system as used in the photolysis of thin films. Therefore calibration using films of 2-NB/PMMA was preferred.

During photolysis experiments, FTIR spectra were taken after thirty seconds of irradiation. Representative data collected during photolysis from four different wavelengths are displayed in Figure 7.4, along with the corresponding calculated rate constants. From the

photolysis rate constant, the absolute number of photons s^{-1} , $I(\lambda)$, can be calculated using the following equation, for the full absorbance limit:

$$I(\lambda) = \frac{k(\lambda) \cdot [C] \cdot A \cdot l}{\Phi(\lambda)} \quad (7.4)$$

where $k(\lambda)$ is the rate constant measured from photolysis in units of s^{-1} , A is the beam area measured in cm^2 , l is the path length in cm , $\sigma(\lambda)$ is the absorption cross section in $cm^2 \text{ molecule}^{-1}$, and $\Phi(\lambda)$ is the quantum yield. The suggested literature value of 0.5 for the quantum yield of solid 2-NB was used.^{299, 300}

The total radiation power incident on the sample was also measured using a power meter (Coherent FieldMate PS19Q). The absolute number of photons s^{-1} was estimated from the measured power using the energy per photon calculated as follows:

$$I(\lambda) = \frac{P_{Tot}}{E_{\text{photon}, \lambda}} = \frac{P_{Tot}}{\frac{hc}{\lambda_{\text{avg}}}} \quad (7.5)$$

where P_{Tot} is the total power measured ($W \text{ cm}^{-2}$), $E_{\text{photon}, \lambda}$ is the energy of a single photon with wavelength λ , h is the Planck constant ($J \text{ s}^{-1}$), c is the speed of light ($m \text{ s}^{-1}$) and λ_{avg} is the average photolysis wavelength (m^{-1}). Figure 7.4b plots the total number of photons s^{-1} calculated from the power meter versus total number of photons s^{-1} measured using actinometry. As observed, the # of photons s^{-1} calculated is a function of the wavelength at UV colors, due to the dichroic turning mirror in the lamp housing. The regression line generated from this plot was used to convert power meter measurements to the absolute # of photons s^{-1} incident on the sample (for experiments in which explicit calibration was not performed).

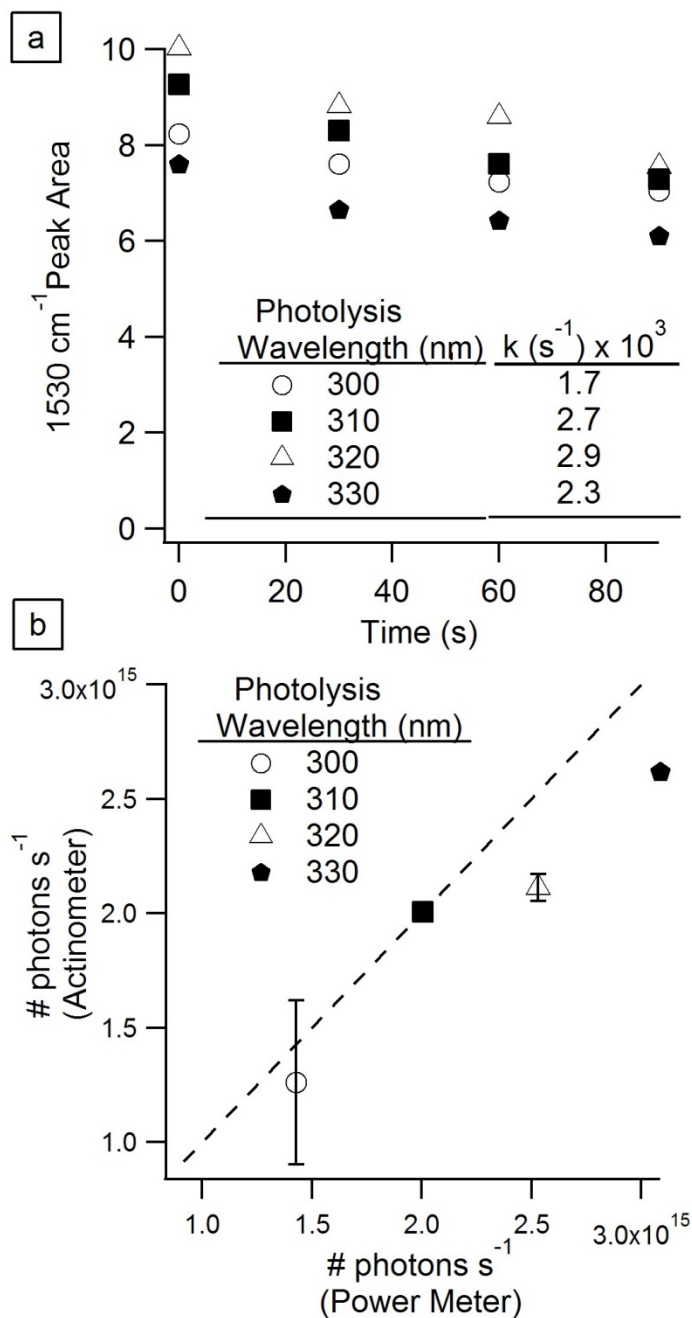


Figure 7.4. (a) Representative data from photolysis of films of 2-NB/PMMA at various wavelengths. The 1530 cm^{-1} peak is integrated and plotted versus photolysis time. The rate constants obtained from fitting the data are also listed. (b) Using the rates determined above, the absolute fluxes ($\# \text{ photons s}^{-1}$) can be determined from Equation 7.4. The absolute $\# \text{ photons s}^{-1}$ measured by the actinometer is plotted versus the $\# \text{ photons s}^{-1}$ as determined from the measured power and Equation 7.5. Error bars represent one standard deviation.

Quantum Yields

The quantum yield of CO production from photolysis of thin films can be calculated according to the following formula:

$$\frac{d[CO]}{dt} = \Phi(\lambda) \cdot I_0 \cdot A_{abs} / V_{CRDS} \quad (7.6)$$

where $d[CO]/dt$ is the observed rate of photoproduction in the CRDS cell, $\Phi(\lambda)$ is the quantum yield, I_0 is the total flux of photons incident on the sample, A_{abs} is the sample absorbance and V_{CRDS} is the volume of the CRDS cell (assuming uniform mixing). The absorbance of the sample can be estimated from the following equation:

$$A_{abs} = \sigma(\lambda) \cdot \ell \cdot [C] \quad (7.7)$$

where, $\sigma(\lambda)$ is the absorption cross section ($\text{cm}^2 \text{ molecule}^{-1}$), ℓ is the path length in cm and $[C]$ is the concentration in molecules cm^3 . The absorption cross sections of undecanal have not been reported in the literature. The cross sections of heptanal are used instead from 280 – 330 nm. The absorption cross sections for wavelengths outside this range are inferred from trends in similar aldehydes.^{291, 302} The literature value molar base-10 extinction coefficients were then converted to absorption cross sections using the following formula:

$$\sigma(\lambda) = \frac{\varepsilon_{10}(\lambda) \cdot \ln(10) \cdot 1000}{N_a} \quad (7.8)$$

where $\sigma(\lambda)$ is the absorption cross section ($\text{cm}^2 \text{ molecule}^{-1}$), $\varepsilon_{10}(\lambda)$ is the base-10 molar extinction coefficient ($\text{L mol}^{-1} \text{ cm}^{-1}$), and N_a is the Avogadro constant (molecule mol^{-1}). As the monochromator employed in this work had a resolution of 20 nm FWHM, the average wavelength was used as measured by a portable UV/vis spectrometer (Ocean Optics

USB4000). The quantum yield for the photoproduction of CO from undecanal thin films can then be calculated.

7.3 Results

The experimental detection limit for CO concentrations was determined from numerous calibrations to be $\sim 10^{10}$ molecules cm^{-3} in the CRDS cell (~ 10 ppb at atmospheric pressure). As evidenced in Figure 7.4, the photons counts calculated from the power meter measurements and actinometry measurements did not always yield the same values. The discrepancies likely arise from unaccounted scattering from the thin films and/or errors associated with using broad monochromatic light with 20nm FWHM. However, as the two measurements are proportional to each other, the actinometry experiments were used as a calibration for the power meter. After this re-calibration, the power meter was used in all experiments. The linear regression fit from the actinometry calibration was then used to give the absolute photon counts. Therefore, the actinometry experiments did not need to be conducted daily.

As the PMMA chains contain carbonyl groups in the ester functionalities, the photolysis of the polymer matrix (without undecyl aldehyde added) could also be a source of CO. Photolysis of thin films of PMMA have been studied previously.³⁰³⁻³⁰⁶ In general experiments were conducted at photolysis wavelengths of higher energy (250 – 260 nm) and at elevated temperatures (~ 200 °C), while such studies have indicated the production of CO, no yields were reported.³⁰⁴ However, the quantum yields for total production of radical species have been measured at room temperature and wavelengths relevant to this study, 260 – 340 nm. The maximum quantum yield observed was $\sim 10^{-4}$ at 280 nm and decreased to zero around 320

nm.³⁰⁶ Therefore the production of carbon monoxide from photolysis of PMMA would be negligible compared to the production of CO from undecanal (assuming that undecanal yield is >0.01). Photooxidative degradation of polymer films from simulated solar radiation have been observed but on much longer timescales (~ 100 h) than experiments performed here.³⁰³ Nevertheless, photolysis experiments were conducted using pure PMMA films with no added analyte. The photoproduction of carbon monoxide from the PMMA films was below the detection limit (~10 ppb) for any of the photolysis wavelengths used in this experiment.

The absolute measurements of photons and CO concentration allowed the calculation of the quantum yields for formation of CO. The calculated quantum yields are plotted as a function of photolysis wavelength, as in Figure 7.5. The quantum yields remain relatively constant with the exception of 270 nm and 280 nm points where S/N was the lowest. The determined yields were on the order of a five percent. Multiple quantum yield measurements have not been conducted and therefore absolute errors were not calculated. The estimated error of this data set, based on errors in CO concentration measurements and actinometry measurements, was 40%. Therefore, the measured quantum yields from 290 nm – 340 nm can be thought of as wavelength independent within our error values. Some of the production of CO from photolysis at the lower energy wavelengths (330 -340 nm) could be due to the 20nm FWHM monochromatic light with 20 nm FWHM and presence of a small portion of higher energy light (290 – 300 nm) with better overlap for the absorption cross section of undecanal.

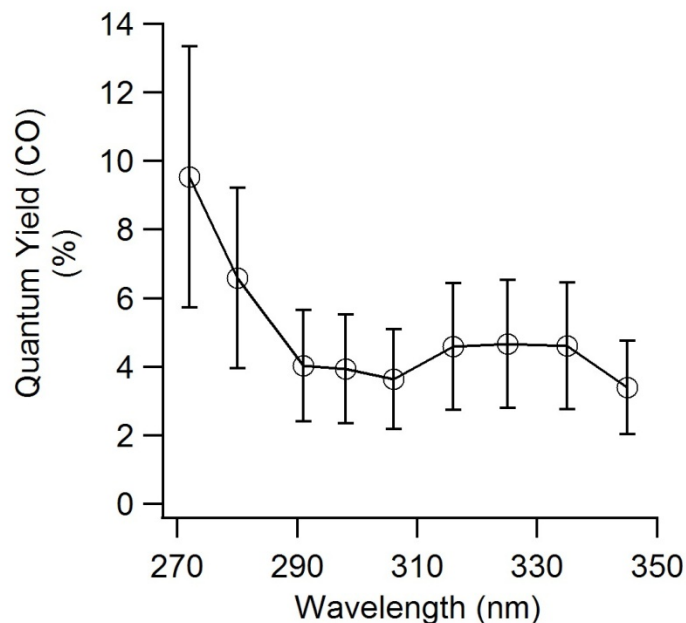


Figure 7.5. Quantum yields for the production of CO from photolysis of undecanal/PMMA thin films as a function of photolysis wavelength. Error bars are the estimated uncertainty of 40%.

7.4 Discussion

The use of IR-CRDS has been examined to determine the quantum yields for evolution of gas-phase products from condensed phase photolysis of a long chain aliphatic aldehyde. The technique has been developed using undecanal/PMMA thin films. The determination of quantum yields from condensed phase photolysis is an important step toward understanding the relative importance of atmospheric processes of SOA. Using absolute concentration and actinometry calibrations the quantum yields for production of CO from undecanal photolysis were measured. CO yields of ~ 4% were measured for wavelengths relevant to the atmosphere ($\lambda > 295$ nm). The overall photolysis quantum yields, i.e. for all photolysis products, are likely higher. In addition, the poor overlap between pure carbonyls absorption band and actinic

radiation result in long estimated lifetimes from actinic photolysis (~ 100 hr). The absorption band for pure carbonyls barely reaches the UV-A region. This creates a poor overlap between pure carbonyls absorption band and actinic radiation resulting in long estimated lifetimes.

In order to better understand the photolysis of long chain carbonyl species, several experimental artifacts need to be addressed. The following paragraphs describe possible experimental changes to address measurement errors and artifacts. The error associated with the individual measurements necessary for quantum yield calculations were $\sim 20\%$. Several experimental changes can be made to determine these measurements with less error. The actinometry measurements must be conducted for all wavelengths with multiple repetitions. These changes should decrease the measured error substantially, as at most two measurements have been made at the same wavelength. Variances from the IR-CRDS measurements were due mainly to minute changes in the film thickness and therefore the surface concentration. More uniform films can be created on the CaF_2 windows using a smaller film area.

The accuracy of the yields obtained was possibly influenced by gas-phase photolysis of undecanal. The vapor pressure of undecanal is ~ 0.43 Torr, which would result in a concentration of ~ 500 ppm under static condition (the PMMA film should help reduce the vapor pressure). As there is a continuous flow throughout the photolysis measurements, the actual concentration of gas-phase undecanal present in the photolysis beam will be reduced by a large factor (~ 500). The quantum yields for production of gas-phase carbon monoxide from photolysis of gas-phase undecanal are also unknown. Assuming a similar value as obtained in the condensed phase ($\sim 2\%$), we could generate on the order of 20 ppb CO from gas-phase photolysis. In order to more accurately calculate quantum yields from condensed phase photolysis, less volatile species should be used in further studies. Tridecanal (C-13 aldehyde)

and tridecanone (C-13 ketone) have vapor pressures of ~ 0.00947 torr and ~ 0.0030 torr, respectively, a difference of almost two orders of magnitude compared with undecanal. This will greatly reduce the possibility of measuring CO from gas-phase photolysis, as the amounts will be well below our detection limit.

Carbon monoxide has been demonstrated to be a marker for the photolysis of carbonyls.²⁰ It has been previously observed that the quantum yield of Norrish type I photolysis of ketones in liquid hydrocarbon solvents was reduced as the carbon chain length was increased, from ~ 0.02 to 0.015 for chain lengths of 10 to 15 carbon atoms, respectively.²⁶⁸ These values are quite similar to the values obtained in this work. However, quantum yields for Norrish Type II processes for similar chain length carbons are on the order of ~ 0.1 .²⁶⁸ Therefore, the total quantum yield for photolysis of undecanal/PMMA thin films is likely much greater than the quantum yield of CO production, which only monitors one potential photolysis channel. Due to these factors, calculating the estimated lifetime of such long-chain carbonyls in the atmosphere will under predict the actual lifetime using the quantum yield values obtained in this study. The experimental technique can be modified to include GC-MS analysis of gas-phase photoproducts to yield the total quantum yield from photolysis of thin films, or the photolysis of the thin film could be monitored separately using ATR-FTIR spectroscopy, to track the concentration of the analyte in the thin film. GC-MS of the condensed phase products could be hampered by the large polymers of PMMA.

Chapter 8

ESI Sensitivity

8.1 Introduction

The utility of high-resolution electrospray ionization mass spectrometry (HR ESI-MS) has been established for the elemental composition analysis of complex environmental mixtures,³⁰⁷ such-as atmospheric organic aerosol samples,³⁰⁸⁻³¹⁰ atmospheric waters,^{220, 228} dissolved organic matter (DOM) samples,^{145, 247, 248, 311-318} biomass burning aerosol samples,^{213, 319, 320} and laboratory generated organic aerosols^{14, 17, 89, 90, 100, 133, 135, 259, 321} are all being studied with HR ESI-MS techniques. At the heart of the technique is the ESI process, which promotes rapid ionization of analytes (either directly or through adducts), with minimal fragmentation, but with greatly varying efficiency.¹⁴⁹

As not all analytes are ionized equally, the ESI response can vary significantly among differing analytes, even with identical solution concentrations.^{139, 322} In addition, the ESI response can be altered by competing analytes and their concentrations, known as the matrix effect.^{139, 149, 150, 323} These complications are inherent to the ESI process, and without previous knowledge of the compounds present and calibration standards, direct quantitative analysis of unknown analytes is not possible.

There have been recent attempts into tabulation of ESI sensitivities for various analytes, with the majority of studies being focused on metabolites and molecules found in biological systems.³²²⁻³²⁷ The most extensive efficiency scale focuses on relative ionization efficiencies (RIE) calculated from interpolation of the ESI response from numerous binary solutions.³²² In

addition, there have been a number of studies on molecular properties and the ability to predict the ESI response from a variety of parameters, including: molecular weight, molecular volume, molecular structure, pKa, gas phase proton affinity, gas-phase basicity, non-polar surface area, surface activity, and octanol-water solubility (log D).^{321-323, 325-334} The findings indicate that molecules containing non-polar character, as well as a polar group capable of ionization produce the greatest ESI response. Therefore, octanol-water partitioning, surface activity and non-polar surface areas are the most useful metrics to predict a compounds ESI response.^{139, 326, 327}

ESI analysis is also limited to liquid samples and analytes must be dissolved in a solvent convenient to the ESI process. Small polar solvents such as methanol or acetonitrile are ideal and are often added to aqueous samples before ESI analysis.¹³⁹ DOM and atmospheric water samples, are already in the liquid state, aerosol samples must be collected and dissolved in a suitable solvent. Variation in electrolyte / analyte concentrations due to sampling and work-up, may affect the ESI response and further hamper quantitative ESI analysis.¹⁴⁹

A popular new technique for elemental composition analysis of organic aerosols is the high-resolution time-of-flight aerosol mass spectrometer (HR-ToF-AMS). The technique involves a series of aerosol lens followed by electron impact ionization to fragment and ionize the organic constituents which are then detected with a HR-ToF detector. Several studies have calibrated the technique for the measurement of atomic ratios using a variety of organic standards.^{146, 335} Such calibrations have not been performed using aerosol relevant mixtures and the ESI technique.

In this chapter, the investigation of model compounds with similar structures and chemical activity as those found in organic aerosol samples was conducted. Solutions of known

constituents in varying concentrations were analyzed and the ESI response was investigated. In addition, AMS and ESI-MS response were investigated, on the basis of accurately recording the solution oxygen to carbon ratios.

8.2 Experimental

Standard solutions were prepared in acetonitrile solvent (HPLC grade) for the 10 organic compounds used in this study. Compounds included DL-malic acid, succinic acid, 6-methyl-2,4-heptanedione, 7-oxooctanoic acid, azelaic acid, 5-oxoazelaic acid, cis-pinic acid, cis-pinonic acid, citric acid, and camphoric acid. Stock solutions were prepared for all standards, with concentrations ranging from 10^{-5} to 10^{-3} M. Aliquots between 5 – 500 μ L of each standard were mixed and diluted with acetonitrile in a 25 mL volumetric flask. Six mixtures with varying concentrations of each analyte were created. Table 1 lists the compounds and their concentrations in each mixture. The standard mixtures were made with total organics on the order of 10^{-4} M, each standard mixture was further diluted with acetonitrile to create two more standards with total organics of $\sim 10^{-6}$ M and $\sim 10^{-8}$ M.

Table 8.1 Compounds and their mixtures used for ESI sensitivity study for measuring the O/C ratio for a complex solution of organics. The concentration of each compound for all six mixtures created in this study are listed, along with the solution O/C ratio.

Standard Compound	Molecular Weight	O/C ratio	Concentration in standard mixture ($\times 10^{-5}$ M)					
			Mix 1	Mix 2	Mix 3	Mix 4	Mix 5	Mix 6
Succinic Acid	118.09	1.00	0.2	0.02	2	X	X	X
DL-Malic Acid	134.09	1.25	0.4	0.06	4	X	X	X
6-methyl-2,4-heptanedione	142.2	0.25	3	10	1	3	10	1
7-oxooctanoic acid	158.19	0.38	5	3	3	5	4	1
cis-Pinonic Acid	184.23	0.30	2	2	1	2	10	1
cis-Pinic Acid	186.21	0.44	1	1	1	1	1	0.7
Azelaic Acid	188.22	0.44	1	0.4	0.4	7	2	2
citric acid	192.12	1.17	X	X	X	0.1	0.1	1
Camphoric Acid	200.23	0.40	X	X	X	0.8	0.2	8
5-oxoazelaic acid	202.2	0.56	2	0.4	2	4	1	5
Average Molar O/C Ratio			0.41	0.30	0.71	0.41	0.32	0.51

HR ESI-MS analysis was performed on all mixtures and dilutions. Data analysis proceeded as outlined in the methods section. Following peak identification, average properties were calculated from both the known molar fractions x_i and the ESI MS intensities from equations 2.4 and 2.8 respectively, using the assumption of equation 2.7.

$$\langle O:C \rangle_{exact} = \frac{\sum_i x_i o_i}{\sum_i x_i c_i} \quad (2.4)$$

$$Intensity_i = Sensitivity_i \times x_i \quad (2.7)$$

$$\langle O : C \rangle = \frac{\sum_i Intensity_i \cdot \frac{O_i}{C_i}}{\sum_i Intensity_i} \quad (2.8)$$

An important metric in the analysis of complex organic mixtures is the average oxygen to carbon ratio, or O/C ratio. The mixtures were created with engineered O:C ratios, i.e. two solutions were created with O/C ratios of ~ 0.3, two solutions with O/C ratio of ~ 0.4, one solution with O/C ratio of ~ 0.5, and one solution with O/C ratio of ~ 0.7 (Table 8.1). The assumption presented in Equation 2.7 is that, for a sufficiently dilute solution, the ESI-MS instrument response should be directly proportional to the molar fractions of the analyte molecules, and can therefore be used in place of molar fraction to form Equation 2.8.

The relevance of this assumption for organic aerosol is a major question addressed in this work.

New techniques have been introduced that also allow a direct measure of an aerosols O/C ratio, namely an Aerodyne aerosol mass spectrometer (AMS). The AMS has been calibrated using a variety of organics to establish a calibration factor for the measured atomic ratios to the true solution atomic ratio from nebulized organic solutions. In order to compare AMS and ESI, AMS measurements were performed using the 3 of the standard mixtures shown in Table 1. The standard mixtures were nebulized into a clean 300 L Teflon chamber. The generated aerosols passed through a series of four diffusion dryers before entering the collection devices operated in parallel: an SMPS, consisting of a differential mobility analyzer (DMA) platform (TSI Model 3080), DMA column (TSI Model 3081) and condensation particle counter (TSI Model 3775), and an AMS instrument (Aerodyne).

Octanol – water partitioning constant (log P) is a ratio of the non-ionized compounds concentrations between the two solutions and thus a measure of a compounds hydrophobic/hydrophilic character. Prediction of log P was performed using ACD/ChemSketch Freeware version 12.01 (Advanced Chemical Development Inc., Toronto, Canada). It is closely

related to the distribution coefficient ($\log D$), which is a ratio of both ionized and non-ionized forms in each of the two phases and is therefore pH dependent. pH was not measured for any of our standard mixtures and therefore, no corrections have been made to our concentrations measured to adjust for ionized/non-ionized forms.

8.3 Results and Discussion

The measured O/C was calculated from Equation 2.8, while the actual solution O/C ratio was calculated from Equation 2.6. Figure 8.1 plots the measured defect (measured O/C – known O/C) versus the solutions known O/C ratio for (a) the exact mixtures in Table 8.1 and (b) similar mixtures as in Table 8.1 but missing citric acid (Mixes 4-6), succinic acid and malic acid (Mixes 1-3). Notice, this reduces the spread of solution O/C ratios and thus a smaller axis range. Measured solution O/C ratios were calculated from (+) mode ESI, (-) mode ESI, average of (+) and (-) mode ESI, and AMS operated in the positive ion mode.

The calculated O/C ratio from the AMS data is within ~ 0.2 units of the known O/C ratio at all solution O/C. Both positive and negative defects are found from AMS experiments with no correlation to the compounds present or solution O/C. The O/C ratios calculated from the (+) ESI mode and (-) ESI mode spectra show a wide range of deviation up to 0.3 units especially at the higher O/C solutions. Mixtures with O/C ratios of ~ 0.4 were always the most accurate with deviations of less than 0.1 units. Deviations for the high O/C mixtures are largest, up to ~ 0.3 units. In general, the positive ESI mode under predicts the solution O/C, while the negative ESI mode calculates a higher O/C ratio. This is understandable as (-) mode ESI tends to ionize

species with higher O/C values more efficiently than (+) ESI mode. Taking the average of the two modes gives a value much closer to the actual solution O/C.

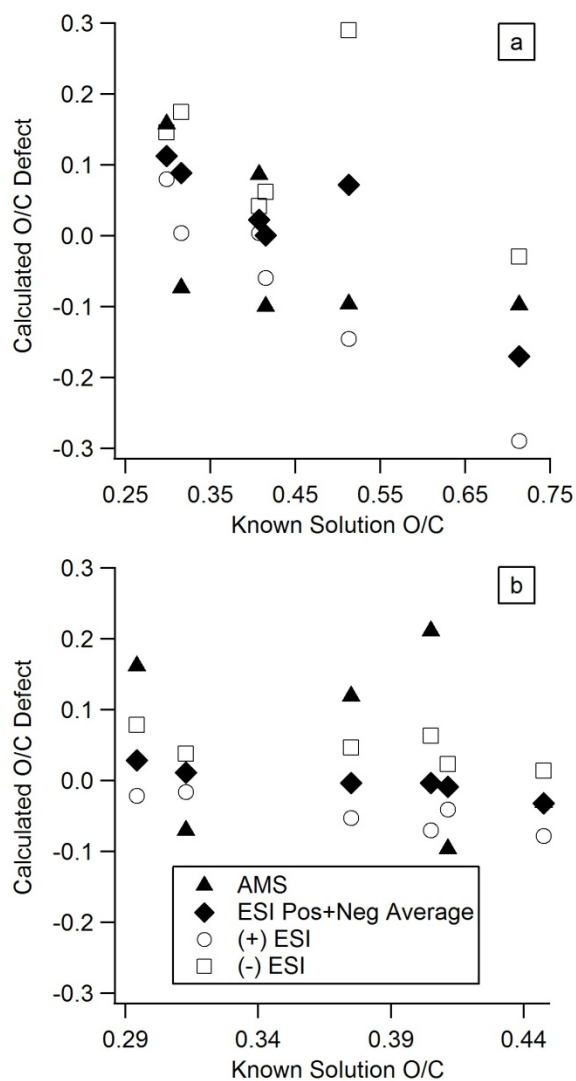


Figure 8.1. (a) The O/C defect (measured O/C – known O/C) is plotted against each solutions known O/C ratio for the mixtures listed in Table 1. (b) The O/C defect (measured O/C – known O/C) is plotted against each solutions known O/C ratio for the mixtures listed in Table 1 without citric acid, succinic acid and malic acid. Data from AMS, (+) mode ESI, (-) mode ESI and the average calculated from ESI (+) and (-) mode.

To investigate this behavior more closely and as a function of molecular composition the ESI sensitivity factor can be calculated for each compound in all mixtures and dilutions. The

sensitivity factors, calculated using Equation 2.7 for each mixture and dilution, are averaged and tabulated in Table 8.2 for each compound. The negative mode ESI sensitivities are of similar magnitude for all but 6-methyl-2,4-heptanedione, which contains two ketone groups and no carboxylic acids, the remaining molecules all contain at least one carboxylic acids and thus similar sensitivities. The largest positive ESI mode deviations arise from the small carbon number high oxygen number compounds, succinic acid (C₄H₆O₄), malic acid (C₄H₆O₅), and citric acid (C₆H₈O₇). The other compounds sensitivities are within two orders of magnitude of each other.

Table 8.2. The ESI sensitivity of each standard compound is averaged across all the mixtures for each ionization mode. The compounds O/C ratio and ratio of (+) mode sensitivity to (-) mode sensitivity is also listed.

Standard Compound	Molecular Weight	O/C ratio	Neg Mode Sensitivity	Pos Mode Sensitivity	Ratio Pos:Neg Sensitivity
Succinic Acid	118.09	1.00	4.56×10^{-1}	1.10×10^{-2}	0.024
DL-Malic Acid	134.09	1.25	1.59×10^{-1}	3.79×10^{-3}	0.024
6-methyl-2,4-heptanedione	142.2	0.25	1.19×10^{-3}	7.30×10^{-3}	6.1
7-oxooctanoic acid	158.19	0.38	1.40×10^{-1}	2.28×10^{-1}	1.6
cis-Pinonic Acid	184.23	0.30	4.19×10^{-1}	9.07×10^{-2}	0.22
cis-Pinic Acid	186.21	0.44	1.38×10^{-1}	4.56×10^{-3}	0.033
Azelaic Acid	188.22	0.44	1.13×10^{-1}	1.49×10^{-1}	1.3
citric acid	192.12	1.17	1.00	9.65×10^{-5}	0.00010
Camphoric Acid	200.23	0.40	4.31×10^{-1}	2.29×10^{-2}	0.053
5-oxoazelaic acid	202.2	0.56	3.97×10^{-1}	2.54×10^{-1}	0.64

As the ESI sensitivity factors have a clear correlation with a compounds structure, each compounds sensitivity in the (+) and (-) ESI mode is plotted in Figure 8.2 (a) against the compounds log P value. Compounds with low log P values have very low (+) mode ESI sensitivities. The ratio of positive ESI sensitivity to negative ESI sensitivity was used to decipher the response of known compounds using ESI-MS. The ratios are tabulated in Table 8.2 and Figure 8.2 (b) plots the each compounds ratio of positive ESI mode sensitivity to negative ESI mode sensitivity versus the compounds log P value. Ratios above one indicate increased sensitivity in the positive mode and ratios below one indicate increased sensitivity in the negative mode. The largest deviations from one (equal sensitivities) are, the diketone compound (MW 142), with the largest ratio and citric acid (MW 192), with the lowest ratio. Also notable are the low-molecular weight carboxylic acids which have fairly low positive to negative sensitivity ratios. A strong correlation between a compounds log P value and the compounds O/C ratio was found from the plot in Figure 8.2 (c). This explains the correlation between low carbon number high oxygen number having low sensitivities and low log P value compounds having low sensitivities. While, the compounds structure must be known to calculate log P values, the O/C ratio can be calculated from the compounds molecular formula, which can be obtained using HR ESI-MS.

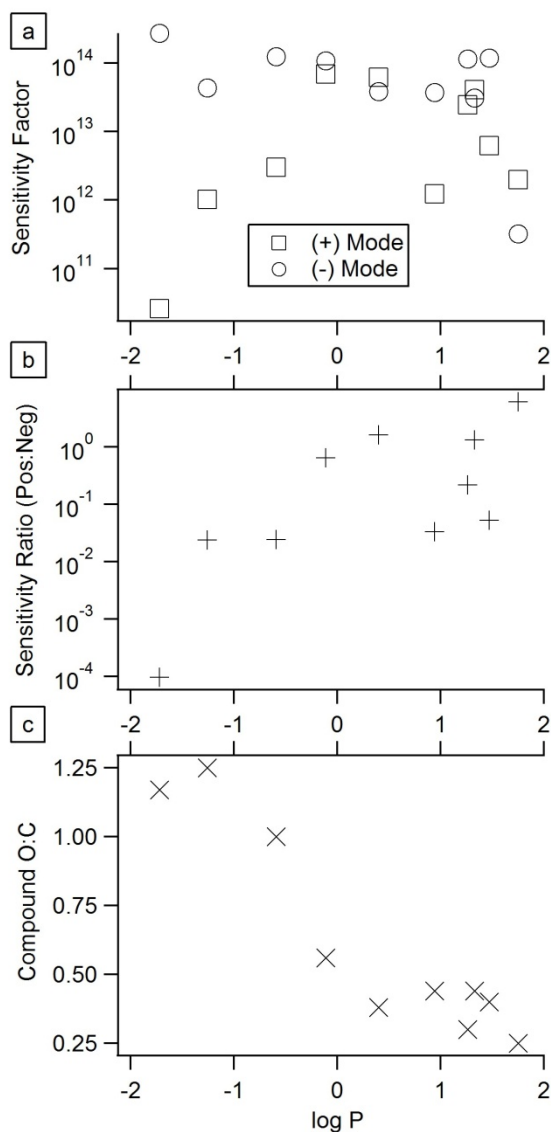


Figure 8.2. The log P values are calculated for each standard compound and plotted against (a) the average sensitivity factor for both ESI modes, (b) the ratio of (+) mode sensitivity to (-) mode sensitivity, and (c) the compounds O/C ratio. The sensitivity factor and the sensitivity ratio is plotted on a log scale.

Therefore, the ratio of positive ESI mode sensitivity to negative ESI mode sensitivity was plotted against the compounds O/C ratio, in Figure 8.3. The sensitivity in the negative ESI mode increases with increasing O/C ratio. Figure 8.3 emphasizes the fact that high O/C compounds are easier to detect in ESI (-) mode relative to low O/C compounds. This trend can

be useful in the analysis of unknown mixtures such as, limonene SOA. As the positive ESI mode abundance, negative ESI mode abundance, and compound O/C ratio can all be measured, an adjustment can be made to the compounds sensitivity to provide equal weighting. The deviations seen in the calculated O/C ratios of Figure 8.1 (a) can be explained from the sensitivities (high or low) for each compound present. For instance, succinic, malic, and citric acid were barely over the instrument detection limit and often not detected in the positive ESI mode, resulting in a lower calculated O/C ratio from the ESI mass spectra. This explains the smaller O/C defects found from electrosprayed solutions missing these compounds (Figure 8.2 (b)). In addition, the sensitivity ratios could be used to predict structural or functional group information, as the presence or absence of a carboxylic acid is fairly apparent from these experimental compounds. Applications of these results to calibrate the sensitivities and calculate more accurate solution O/C ratios are still underway. This work is ongoing and will form the basis for a future publication.

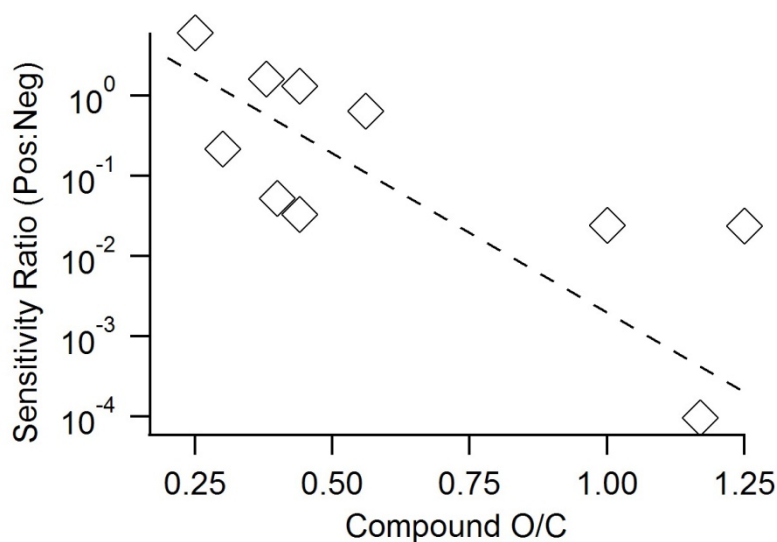


Figure 8.3. The ratio of (+) mode sensitivity to (-) mode sensitivity for each compound is plotted versus the compounds O/C ratio. The sensitivity ratio is plotted on a log scale.

References

1. Finlayson-Pitts, B. J.; Pitts, J. N., *Chemistry of the Upper and Lower Atmosphere: Theory, Experiments, and Applications*. Academic Press: San Diego, 2000; p 1040.
2. Hidy, G. M., Surface-Level Fine Particle Mass Concentrations: From Hemispheric Distributions to Megacity Sources. *J. Air Waste Manage. Assoc.* **2009**, *59* (7), 770-789.
3. Kanakidou, M.; Seinfeld, J. H.; Pandis, S. N.; Barnes, I.; Dentener, F. J.; Facchini, M. C.; Van Dingenen, R.; Ervens, B.; Nenes, A.; Nielsen, C. J.; Swietlicki, E.; Putaud, J. P.; Balkanski, Y.; Fuzzi, S.; Horth, J.; Moortgat, G. K.; Winterhalter, R.; Myhre, C. E. L.; Tsigaridis, K.; Vignati, E.; Stephanou, E. G.; Wilson, J., Organic Aerosol and Global Climate Modelling: A Review. *Atmospheric Chemistry and Physics* **2005**, *5*, 1053-1123.
4. Sun, J. M.; Ariya, P. A., Atmospheric Organic and Bio-Aerosols as Cloud Condensation Nuclei (Ccn): A Review. *Atmospheric Environment* **2006**, *40* (5), 795-820.
5. Mochida, M.; Kitamori, Y.; Kawamura, K.; Nojiri, Y.; Suzuki, K., Fatty Acids in the Marine Atmosphere: Factors Governing Their Concentrations and Evaluation of Organic Films on Sea-Salt Particles. *J. Geophys. Res.-Atmos.* **2002**, *107* (D17), 4325, doi: 10.1029/2001jd001278.
6. Tervahattu, H.; Hartonen, K.; Kerminen, V. M.; Kupiainen, K.; Aarnio, P.; Koskentalo, T.; Tuck, A. F.; Vaida, V., New Evidence of an Organic Layer on Marine Aerosols. *J. Geophys. Res.-Atmos.* **2002**, *107* (D7-8), 4053, doi: 10.1029/2000jd000282.
7. Tervahattu, H.; Juhanaja, J.; Vaida, V.; Tuck, A. F.; Niemi, J. V.; Kupiainen, K.; Kulmala, M.; Vehkamäki, H., Fatty Acids on Continental Sulfate Aerosol Particles. *J. Geophys. Res.-Atmos.* **2005**, *110* (D6), D06207, doi: 10.1029/2004jd005400.
8. Penner, J. E.; Andreae, M. O.; Annegarn, H.; Barrie, L.; Feichter, J.; Hegg, D. A.; Jayaraman, A.; Leaitch, R.; Murphy, D. M.; Nganga, J.; Pitari, G., Aerosols, Their Direct and Indirect Effects. In *Climate Change 2001: The Scientific Basis. Contribution of Working Group I to the Third Assessment Report of the Intergovernmental Panel on Climate Change.*, Houghton, J. T.; Ding, Y.; Griggs, D. J.; Noguer, M.; van der Linden, P. J.; Dai, X.; Maskell, K.; Johnson, C. A., Eds. Cambridge University Press: New York, USA, 2001; p 881.
9. Solomon, S.; Qin, D.; Manning, M.; Chen, Z.; Marquis, M.; Averyt, K. B.; Tignor, M.; Miller, H. L., *Climate Change 2007: The Physical Science Basis. Contribution of Working Group I to the Fourth Assessment Report of the Intergovernmental Panel on Climate Change. IPCC:2007* **2007**.
10. Twomey, S., Aerosols, Clouds and Radiation. *Atmospheric Environment Part a-General Topics* **1991**, *25* (11), 2435-2442.
11. Kroll, J. H.; Seinfeld, J. H., Chemistry of Secondary Organic Aerosol: Formation and Evolution of Low-Volatility Organics in the Atmosphere. *Atmospheric Environment* **2008**, *42* (16), 3593-3624.
12. Rudich, Y.; Donahue, N. M.; Mentel, T. F., Aging of Organic Aerosol: Bridging the Gap between Laboratory and Field Studies. *Annu. Rev. Phys. Chem.* **2007**, *58*, 321-352.
13. Robinson, A. L.; Donahue, N. M.; Shrivastava, M. K.; Weitkamp, E. A.; Sage, A. M.; Grieshop, A. P.; Lane, T. E.; Pierce, J. R.; Pandis, S. N., Rethinking Organic Aerosols: Semivolatile Emissions and Photochemical Aging. *Science* **2007**, *315* (5816), 1259-1262.

14. Bones, D. L.; Henricksen, D. K.; Mang, S. A.; Gonsior, M.; Bateman, A. P.; Nguyen, T. B.; Cooper, W. J.; Nizkorodov, S. A., Appearance of Strong Absorbers and Fluorophores in Limonene-O-3 Secondary Organic Aerosol Due to NH_4^+ -Mediated Chemical Aging over Long Time Scales. *J. Geophys. Res.-Atmos.* **2010**, *115*, D05203, doi: 10.1029/2009JD012864
15. De Haan, D. O.; Hawkins, L. N.; Kononenko, J. A.; Turley, J. J.; Corrigan, A. L.; Tolbert, M. A.; Jimenez, J. L., Formation of Nitrogen-Containing Oligomers by Methylglyoxal and Amines in Simulated Evaporating Cloud Droplets. *Environ. Sci. Technol.* **2011**, *45* (3), 984-991.
16. Laskin, J.; Laskin, A.; Roach, P. J.; Slysz, G. W.; Anderson, G. A.; Nizkorodov, S. A.; Bones, D. L.; Nguyen, L. Q., High-Resolution Desorption Electrospray Ionization Mass Spectrometry for Chemical Characterization of Organic Aerosols. *Analytical Chemistry* **2010**, *82* (5), 2048-2058.
17. Bateman, A. P.; Nizkorodov, S. A.; Laskin, J.; Laskin, A., Photolytic Processing of Secondary Organic Aerosols Dissolved in Cloud Droplets. *Physical Chemistry Chemical Physics* **2011**, In Press.
18. Walser, M. L.; Park, J.; Gomez, A. L.; Russell, A. R.; Nizkorodov, S. A., Photochemical Aging of Secondary Organic Aerosol Particles Generated from the Oxidation of D-Limonene. *J. Phys. Chem. A* **2007**, *111* (10), 1907-1913.
19. Hawkins, L. N.; Russell, L. M., Oxidation of Ketone Groups in Transported Biomass Burning Aerosol from the 2008 Northern California Lightning Series Fires. *Atmospheric Environment* **2010**, *44* (34), 4142-4154.
20. Mang, S. A.; Henricksen, D. K.; Bateman, A. P.; Andersen, M. P. S.; Blake, D. R.; Nizkorodov, S. A., Contribution of Carbonyl Photochemistry to Aging of Atmospheric Secondary Organic Aerosol. *J. Phys. Chem. A* **2008**, *112* (36), 8337-8344.
21. Pan, X.; Underwood, J. S.; Xing, J. H.; Mang, S. A.; Nizkorodov, S. A., Photodegradation of Secondary Organic Aerosol Generated from Limonene Oxidation by Ozone Studied with Chemical Ionization Mass Spectrometry. *Atmospheric Chemistry and Physics* **2009**, *9* (12), 3851-3865.
22. Kalberer, M.; Paulsen, D.; Sax, M.; Steinbacher, M.; Dommen, J.; Prevot, A. S. H.; Fisseha, R.; Weingartner, E.; Frankevich, V.; Zenobi, R.; Baltensperger, U., Identification of Polymers as Major Components of Atmospheric Organic Aerosols. *Science* **2004**, *303* (5664), 1659-1662.
23. Jang, M. S.; Czoschke, N. M.; Lee, S.; Kamens, R. M., Heterogeneous Atmospheric Aerosol Production by Acid-Catalyzed Particle-Phase Reactions. *Science* **2002**, *298* (5594), 814-817.
24. Sax, M.; Zenobi, R.; Baltensperger, U.; Kalberer, M., Time Resolved Infrared Spectroscopic Analysis of Aerosol Formed by Photo-Oxidation of 1,3,5-Trimethylbenzene and Alpha-Pinene. *Aerosol Science and Technology* **2005**, *39* (9), 822-830.
25. Baltensperger, U.; Kalberer, M.; Dommen, J.; Paulsen, D.; Alfarra, M. R.; Coe, H.; Fisseha, R.; Gascho, A.; Gysel, M.; Nyeki, S.; Sax, M.; Steinbacher, M.; Prevot, A. S. H.; Sjogren, S.; Weingartner, E.; Zenobi, R., Secondary Organic Aerosols from Anthropogenic and Biogenic Precursors. *Faraday Discuss.* **2005**, *130*, 265-278.
26. Surratt, J. D.; Murphy, S. M.; Kroll, J. H.; Ng, N. L.; Hildebrandt, L.; Sorooshian, A.; Szmigielski, R.; Vermeylen, R.; Maenhaut, W.; Claeys, M.; Flagan, R. C.; Seinfeld, J.

- H., Chemical Composition of Secondary Organic Aerosol Formed from the Photooxidation of Isoprene. *J. Phys. Chem. A* **2006**, *110* (31), 9665-9690.
27. Petters, M. D.; Prenni, A. J.; Kreidenweis, S. M.; DeMott, P. J.; Matsunaga, A.; Lim, Y. B.; Ziemann, P. J., Chemical Aging and the Hydrophobic-to-Hydrophilic Conversion of Carbonaceous Aerosol. *Geophysical Research Letters* **2006**, *33* (24), L24806, doi: 10.1029/2006gl027249.
 28. Hecobian, A.; Zhang, X.; Zheng, M.; Frank, N.; Edgerton, E. S.; Weber, R. J., Water-Soluble Organic Aerosol Material and the Light-Absorption Characteristics of Aqueous Extracts Measured over the Southeastern United States. *Atmospheric Chemistry and Physics* **2010**, *10* (13), 5965-5977.
 29. Barnard, J. C.; Volkamer, R.; Kassianov, E. I., Estimation of the Mass Absorption Cross Section of the Organic Carbon Component of Aerosols in the Mexico City Metropolitan Area. *Atmospheric Chemistry and Physics* **2008**, *8* (22), 6665-6679.
 30. Ramanathan, V.; Ramana, M. V.; Roberts, G.; Kim, D.; Corrigan, C.; Chung, C.; Winker, D., Warming Trends in Asia Amplified by Brown Cloud Solar Absorption. *Nature* **2007**, *448* (7153), 575-U5.
 31. Li, Z. Q.; Lee, K. H.; Wang, Y. S.; Xin, J. Y.; Hao, W. M., First Observation-Based Estimates of Cloud-Free Aerosol Radiative Forcing across China. *J. Geophys. Res.-Atmos.* **2011**, *115*, D00K18, doi: 10.1029/2009jd013306.
 32. Dockery, D. W., Health Effects of Particulate Air Pollution. *Ann. Epidemiol.* **2009**, *19* (4), 257-263.
 33. Gauderman, W. J.; Gilliland, G. F.; Vora, H.; Avol, E.; Stram, D.; McConnell, R.; Thomas, D.; Lurmann, F.; Margolis, H. G.; Rappaport, E. B.; Berhane, K.; Peters, J. M., Association between Air Pollution and Lung Function Growth in Southern California Children - Results from a Second Cohort. *Am. J. Respir. Crit. Care Med.* **2002**, *166* (1), 76-84.
 34. Pope, C. A., Review: Epidemiological Basis for Particulate Air Pollution Health Standards. *Aerosol Science and Technology* **2000**, *32* (1), 4-14.
 35. Delfino, R. J.; Zeiger, R. S.; Seltzer, J. M.; Street, D. H.; McLaren, C. E., Association of Asthma Symptoms with Peak Particulate Air Pollution and Effect Modification by Anti-Inflammatory Medication Use. *Environ. Health Perspect.* **2002**, *110* (10), A607-A617.
 36. von Klot, S.; Wolke, G.; Tuch, T.; Heinrich, J.; Dockery, D. W.; Schwartz, J.; Kreyling, W. G.; Wichmann, H. E.; Peters, A., Increased Asthma Medication Use in Association with Ambient Fine and Ultrafine Particles. *Eur. Resp. J.* **2002**, *20* (3), 691-702.
 37. Schulz, H.; Harder, V.; Ibaldo-Mulli, A.; Khandoga, A.; Koenig, W.; Krombach, F.; Radykewicz, R.; Stampfl, A.; Thorand, B.; Peters, A., Cardiovascular Effects of Fine and Ultrafine Particles. *J. Aerosol Med.-Depos. Clear. Eff. Lung* **2005**, *18* (1), 1-22.
 38. von Klot, S.; Peters, A.; Aalto, P.; Bellander, T.; Berglind, N.; D'Ippoliti, D.; Elosua, R.; Hormann, A.; Kulmala, M.; Lanki, T.; Lowel, H.; Pekkanen, J.; Picciotto, S.; Sunyer, J.; Forastiere, F.; Grp, H. S., Ambient Air Pollution Is Associated with Increased Risk of Hospital Cardiac Readmissions of Myocardial Infarction Survivors in Five European Cities. *Circulation* **2005**, *112* (20), 3073-3079.
 39. Cohen, A. J.; Pope, C. A., Lung Cancer and Air Pollution. *Environ. Health Perspect.* **1995**, *103*, 219-224.
 40. Krewski, D.; Burnett, R.; Jerrett, M.; Pope, C. A.; Rainham, D.; Calle, E.; Thurston, G.; Thun, M., Mortality and Long-Term Exposure to Ambient Air Pollution: Ongoing

- Analyses Based on the American Cancer Society Cohort. *J. Toxicol. Env. Health Part A* **2005**, *68* (13-14), 1093-1109.
41. Dockery, D. W.; Pope, C. A.; Xu, X. P.; Spengler, J. D.; Ware, J. H.; Fay, M. E.; Ferris, B. G.; Speizer, F. E., An Association between Air-Pollution and Mortality in 6 United-States Cities. *N. Engl. J. Med.* **1993**, *329* (24), 1753-1759.
 42. Laden, F.; Schwartz, J.; Speizer, F. E.; Dockery, D. W., Reduction in Fine Particulate Air Pollution and Mortality - Extended Follow-up of the Harvard Six Cities Study. *Am. J. Respir. Crit. Care Med.* **2006**, *173* (6), 667-672.
 43. Pope, C. A.; Burnett, R. T.; Thun, M. J.; Calle, E. E.; Krewski, D.; Ito, K.; Thurston, G. D., Lung Cancer, Cardiopulmonary Mortality, and Long-Term Exposure to Fine Particulate Air Pollution. *JAMA-J. Am. Med. Assoc.* **2002**, *287* (9), 1132-1141.
 44. Oberdorster, G.; Sharp, Z.; Atudorei, V.; Elder, A.; Gelein, R.; Kreyling, W.; Cox, C., Translocation of Inhaled Ultrafine Particles to the Brain. *Inhal. Toxicol.* **2004**, *16* (6-7), 437-445.
 45. Guenther, A.; Hewitt, C. N.; Erickson, D.; Fall, R.; Geron, C.; Graedel, T.; Harley, P.; Klinger, L.; Lerdau, M.; McKay, W. A.; Pierce, T.; Scholes, B.; Steinbrecher, R.; Tallamraju, R.; Taylor, J.; Zimmerman, P., A Global-Model of Natural Volatile Organic-Compound Emissions. *J. Geophys. Res.-Atmos.* **1995**, *100* (D5), 8873-8892.
 46. Pio, C. A.; Valente, A. A., Atmospheric Fluxes and Concentrations of Monoterpenes in Resin-Tapped Pine Forests. *Atmospheric Environment* **1998**, *32* (4), 683-691.
 47. Geron, C.; Rasmussen, R.; Arnts, R. R.; Guenther, A., A Review and Synthesis of Monoterpene Speciation from Forests in the United States. *Atmospheric Environment* **2000**, *34* (11), 1761-1781.
 48. Janson, R., Monoterpene Concentrations in and above a Forest of Scots Pine. *Journal of Atmospheric Chemistry* **1992**, *14* (1-4), 385-394.
 49. Janson, R.; Kristensson, J. *Sampling and Analysis of Atmospheric Monoterpenes*; Report CM-79; Stockholm University: Stockholm, Sweden, 1991; p 91.
 50. Warneke, C.; De Gouw, J. A.; Kuster, W. C.; Goldan, P. D.; Fall, R., Validation of Atmospheric Voc Measurements by Proton-Transfer-Reaction Mass Spectrometry Using a Gas-Chromatographic Preseparation Method. *Environ. Sci. Technol.* **2003**, *37* (11), 2494-2501.
 51. Warneke, C.; de Gouw, J. A.; Del Negro, L.; Brioude, J.; McKeen, S.; Stark, H.; Kuster, W. C.; Goldan, P. D.; Trainer, M.; Fehsenfeld, F. C.; Wiedinmyer, C.; Guenther, A. B.; Hansel, A.; Wisthaler, A.; Atlas, E.; Holloway, J. S.; Ryerson, T. B.; Peischl, J.; Huey, L. G.; Hanks, A. T. C., Biogenic Emission Measurement and Inventories Determination of Biogenic Emissions in the Eastern United States and Texas and Comparison with Biogenic Emission Inventories. *J. Geophys. Res.-Atmos.* **2010**, *115*, D00F18, doi: 10.1029/2009jd012445.
 52. Businger, J. A.; Oncley, S. P., Flux Measurement with Conditional Sampling. *J. Atmos. Ocean. Technol.* **1990**, *7* (2), 349-352.
 53. Christensen, C. S.; Hummelshoj, P.; Jensen, N. O.; Larsen, B.; Lohse, C.; Pilegaard, K.; Skov, H., Determination of the Terpene Flux from Orange Species and Norway Spruce by Relaxed Eddy Accumulation. *Atmospheric Environment* **2000**, *34* (19), 3057-3067.
 54. Ciccioli, P.; Brancaleoni, E.; Frattoni, M.; Di Palo, V.; Valentini, R.; Tirone, G.; Seufert, G.; Bertin, N.; Hansen, U.; Csiky, O.; Lenz, R.; Sharma, M., Emission of Reactive

- Terpene Compounds from Orange Orchards and Their Removal by within-Canopy Processes. *J. Geophys. Res.-Atmos.* **1999**, *104* (D7), 8077-8094.
55. Aurela, M.; Tuovinen, J. P.; Laurila, T., Carbon Dioxide Exchange in a Subarctic Peatland Ecosystem in Northern Europe Measured by the Eddy Covariance Technique. *J. Geophys. Res.-Atmos.* **1998**, *103* (D10), 11289-11301.
 56. Tani, A.; Nozoe, S.; Aoki, M.; Hewitt, C. N., Monoterpene Fluxes Measured above a Japanese Red Pine Forest at Oshiba Plateau, Japan. *Atmospheric Environment* **2002**, *36* (21), 3391-3402.
 57. Rinne, J.; Hakola, H.; Laurila, T.; Rannik, U., Canopy Scale Monoterpene Emissions of Pinus Sylvestris Dominated Forests. *Atmospheric Environment* **2000**, *34* (7), 1099-1107.
 58. Spirig, C.; Guenther, A.; Greenberg, J. P.; Calanca, P.; Tarvainen, V., Tethered Balloon Measurements of Biogenic Volatile Organic Compounds at a Boreal Forest Site. *Atmospheric Chemistry and Physics* **2004**, *4*, 215-229.
 59. Centritto, M.; Di Bella, C. M.; Baraldi, R.; Beget, M. E.; Kemerer, A.; Rapparini, F.; Oricchio, P.; Rebella, C.; Loreto, F., Monoterpene Emissions from Three Nothofagus Species in Patagonia, Argentina. *J. Plant Interact.* **2008**, *3* (2), 119-125.
 60. Hakola, H.; Tarvainen, V.; Laurila, T.; Hiltunen, V.; Hellen, H.; Keronen, P., Seasonal Variation of Voc Concentrations above a Boreal Coniferous Forest. *Atmospheric Environment* **2003**, *37* (12), 1623-1634.
 61. Harrison, D.; Hunter, M. C.; Lewis, A. C.; Seakins, P. W.; Nunes, T. V.; Pio, C. A., Isoprene and Monoterpene Emission from the Coniferous Species Abies Borisii-Regis - Implications for Regional Air Chemistry in Greece. *Atmospheric Environment* **2001**, *35* (27), 4687-4698.
 62. Hayward, S.; Muncey, R. J.; James, A. E.; Halsall, C. J.; Hewitt, C. N., Monoterpene Emissions from Soil in a Sitka Spruce Forest. *Atmospheric Environment* **2001**, *35* (24), 4081-4087.
 63. Kainulainen, P.; Holopainen, T.; Holopainen, J. K., Decomposition of Secondary Compounds from Needle Litter of Scots Pine Grown under Elevated Co₂ and O₃. *Glob. Change Biol.* **2003**, *9* (2), 295-304.
 64. Rapparini, F.; Baraldi, R.; Facini, O., Seasonal Variation of Monoterpene Emission from Malus Domestica and Prunus Avium. *Phytochemistry* **2001**, *57* (5), 681-687.
 65. Staudt, M.; Mir, C.; Joffre, R.; Rambal, S.; Bonin, A.; Landais, D.; Lumaret, R., Isoprenoid Emissions of Quercus Spp. (Q-Suber and Q-Ilex) in Mixed Stands Contrasting in Interspecific Genetic Introgression. *New Phytol.* **2004**, *163* (3), 573-584.
 66. Hakola, H.; Laurila, T.; Rinne, J.; Puhto, K., The Ambient Concentrations of Biogenic Hydrocarbons at a Northern European, Boreal Site. *Atmospheric Environment* **2000**, *34* (29-30), 4971-4982.
 67. Zhang, J. Y.; Hartz, K. E. H.; Pandis, S. N.; Donahue, N. M., Secondary Organic Aerosol Formation from Limonene Ozonolysis: Homogeneous and Heterogeneous Influences as a Function of Nox. *J. Phys. Chem. A* **2006**, *110* (38), 11053-11063.
 68. Went, F. W., Blue Hazes in the Atmosphere. *Nature* **1960**, *187* (4738), 641-643.
 69. Hildemann, L. M.; Markowski, G. R.; Cass, G. R., Chemical-Composition of Emissions from Urban Sources of Fine Organic Aerosol. *Environ. Sci. Technol.* **1991**, *25* (4), 744-759.
 70. Rogge, W. F.; Mazurek, M. A.; Hildemann, L. M.; Cass, G. R.; Simoneit, B. R. T., Quantification of Urban Organic Aerosols at a Molecular-Level - Identification,

- Abundance and Seasonal-Variation. *Atmospheric Environment Part a-General Topics* **1993**, 27 (8), 1309-1330.
71. Nolte, C. G.; Schauer, J. J.; Cass, G. R.; Simoneit, B. R. T., Highly Polar Organic Compounds Present in Meat Smoke. *Environ. Sci. Technol.* **1999**, 33 (19), 3313-3316.
 72. Tolocka, M. P.; Jang, M.; Ginter, J. M.; Cox, F. J.; Kamens, R. M.; Johnston, M. V., Formation of Oligomers in Secondary Organic Aerosol. *Environ. Sci. Technol.* **2004**, 38 (5), 1428-1434.
 73. Surratt, J. D.; Kroll, J. H.; Kleindienst, T. E.; Edney, E. O.; Claeys, M.; Sorooshian, A.; Ng, N. L.; Offenberg, J. H.; Lewandowski, M.; Jaoui, M.; Flagan, R. C.; Seinfeld, J. H., Evidence for Organosulfates in Secondary Organic Aerosol. *Environ. Sci. Technol.* **2007**, 41 (2), 517-527.
 74. Inuma, Y.; Muller, C.; Boge, O.; Gnauk, T.; Herrmann, H., The Formation of Organic Sulfate Esters in the Limonene Ozonolysis Secondary Organic Aerosol (Soa) under Acidic Conditions. *Atmospheric Environment* **2007**, 41 (27), 5571-5583.
 75. Claeys, M.; Szmigielski, R.; Kourtchev, I.; Van der Veken, P.; Vermeylen, R.; Maenhaut, W.; Jaoui, M.; Kleindienst, T. E.; Lewandowski, M.; Offenberg, J. H.; Edney, E. O., Hydroxydicarboxylic Acids: Markers for Secondary Organic Aerosol from the Photooxidation of Alpha-Pinene. *Environ. Sci. Technol.* **2007**, 41 (5), 1628-1634.
 76. Presto, A. A.; Hartz, K. E. H.; Donahue, N. M., Secondary Organic Aerosol Production from Terpene Ozonolysis. 2. Effect of Nox Concentration. *Environ. Sci. Technol.* **2005**, 39 (18), 7046-7054.
 77. Gao, S.; Ng, N. L.; Keywood, M.; Varutbangkul, V.; Bahreini, R.; Nenes, A.; He, J. W.; Yoo, K. Y.; Beauchamp, J. L.; Hodyss, R. P.; Flagan, R. C.; Seinfeld, J. H., Particle Phase Acidity and Oligomer Formation in Secondary Organic Aerosol. *Environ. Sci. Technol.* **2004**, 38 (24), 6582-6589.
 78. Jaoui, M.; Kleindienst, T. E.; Lewandowski, M.; Offenberg, J. H.; Edney, E. O., Identification and Quantification of Aerosol Polar Oxygenated Compounds Bearing Carboxylic or Hydroxyl Groups. 2. Organic Tracer Compounds from Monoterpenes. *Environ. Sci. Technol.* **2005**, 39 (15), 5661-5673.
 79. Sipin, M. F.; Guazzotti, S. A.; Prather, K. A., Recent Advances and Some Remaining Challenges in Analytical Chemistry of the Atmosphere. *Analytical Chemistry* **2003**, 75 (12), 2929-2940.
 80. Glasius, M.; Duane, M.; Larsen, B. R., Determination of Polar Terpene Oxidation Products in Aerosols by Liquid Chromatography-Ion Trap Mass Spectrometry. *Journal of Chromatography A* **1999**, 833 (2), 121-135.
 81. Jang, M.; Kamens, R. M., Newly Characterized Products and Composition of Secondary Aerosols from the Reaction of Alpha-Pinene with Ozone. *Atmospheric Environment* **1999**, 33 (3), 459-474.
 82. Szmigielski, R.; Surratt, J. D.; Vermeylen, R.; Szmigielska, K.; Kroll, J. H.; Ng, N. L.; Murphy, S. M.; Sorooshian, A.; Seinfeld, J. H.; Claeys, M., Characterization of 2-Methylglyceric Acid Oligomers in Secondary Organic Aerosol Formed from the Photooxidation of Isoprene Using Trimethylsilylation and Gas Chromatography/Ion Trap Mass Spectrometry. *Journal of Mass Spectrometry* **2007**, 42 (1), 101-116.
 83. Leungsakul, S.; Jaoui, M.; Kamens, R. M., Kinetic Mechanism for Predicting Secondary Organic Aerosol Formation from the Reaction of D-Limonene with Ozone. *Environ. Sci. Technol.* **2005**, 39 (24), 9583-9594.

84. Hakola, H.; Arey, J.; Aschmann, S. M.; Atkinson, R., Product Formation from the Gas-Phase Reactions of Oh Radicals and O₃ with a Series of Monoterpenes. *Journal of Atmospheric Chemistry* **1994**, *18* (1), 75-102.
85. Jaoui, M.; Corse, E.; Kleindienst, T. E.; Offenberg, J. H.; Lewandowski, M.; Edney, E. O., Analysis of Secondary Organic Aerosol Compounds from the Photooxidation of D-Limonene in the Presence of Nox and Their Detection in Ambient Pm_{2.5}. *Environ. Sci. Technol.* **2006**, *40* (12), 3819-3828.
86. Larsen, B. R.; Lahaniati, M.; Calogirou, A.; Kotzias, D., Atmospheric Oxidation Products of Terpenes: A New Nomenclature. *Chemosphere* **1998**, *37* (6), 1207-1220.
87. Glasius, M.; Lahaniati, M.; Calogirou, A.; Di Bella, D.; Jensen, N. R.; Hjorth, J.; Kotzias, D.; Larsen, B. R., Carboxylic Acids in Secondary Aerosols from Oxidation of Cyclic Monoterpenes by Ozone. *Environ. Sci. Technol.* **2000**, *34* (6), 1001-1010.
88. Warscheid, B.; Hoffmann, T., Structural Elucidation of Monoterpene Oxidation Products by Ion Trap Fragmentation Using on-Line Atmospheric Pressure Chemical Ionisation Mass Spectrometry in the Negative Ion Mode. *Rapid Commun. Mass Spectrom.* **2001**, *15* (23), 2259-2272.
89. Reinhardt, A.; Emmenegger, C.; Gerrits, B.; Panse, C.; Dommen, J.; Baltensperger, U.; Zenobi, R.; Kalberer, M., Ultrahigh Mass Resolution and Accurate Mass Measurements as a Tool to Characterize Oligomers in Secondary Organic Aerosols. *Analytical Chemistry* **2007**, *79* (11), 4074-4082.
90. Walser, M. L.; Desyaterik, Y.; Laskin, J.; Laskin, A.; Nizkorodov, S. A., High-Resolution Mass Spectrometric Analysis of Secondary Organic Aerosol Produced by Ozonation of Limonene. *Physical Chemistry Chemical Physics* **2008**, *10* (7), 1009-1022.
91. Hamilton, J. F.; Lewis, A. C.; Carey, T. J.; Wenger, J. C., Characterization of Polar Compounds and Oligomers in Secondary Organic Aerosol Using Liquid Chromatography Coupled to Mass Spectrometry. *Analytical Chemistry* **2008**, *80* (2), 474-480.
92. Warscheid, B.; Hoffmann, T., Direct Analysis of Highly Oxidised Organic Aerosol Constituents by on-Line Ion Trap Mass Spectrometry in the Negative-Ion Mode. *Rapid Commun. Mass Spectrom.* **2002**, *16* (6), 496-504.
93. Grannas, A. M.; Hockaday, W. C.; Hatcher, P. G.; Thompson, L. G.; Mosley-Thompson, E., New Revelations on the Nature of Organic Matter in Ice Cores. *J. Geophys. Res.-Atmos.* **2006**, *111* (D4), D04304, doi: 10.1029/2005jd006251.
94. Hughey, C. A.; Hendrickson, C. L.; Rodgers, R. P.; Marshall, A. G.; Qian, K. N., Kendrick Mass Defect Spectrum: A Compact Visual Analysis for Ultrahigh-Resolution Broadband Mass Spectra. *Analytical Chemistry* **2001**, *73* (19), 4676-4681.
95. Wu, Z. G.; Rodgers, R. P.; Marshall, A. G., Two- and Three-Dimensional Van Krevelen Diagrams: A Graphical Analysis Complementary to the Kendrick Mass Plot for Sorting Elemental Compositions of Complex Organic Mixtures Based on Ultrahigh-Resolution Broadband Fourier Transform Ion Cyclotron Resonance Mass Measurements. *Analytical Chemistry* **2004**, *76* (9), 2511-2516.
96. Hughey, C. A.; Rodgers, R. P.; Marshall, A. G., Resolution of 11 000 Compositionally Distinct Components in a Single Electrospray Ionization Fourier Transform Ion Cyclotron Resonance Mass Spectrum of Crude Oil. *Analytical Chemistry* **2002**, *74* (16), 4145-4149.

97. Kim, S.; Kramer, R. W.; Hatcher, P. G., Graphical Method for Analysis of Ultrahigh-Resolution Broadband Mass Spectra of Natural Organic Matter, the Van Krevelen Diagram. *Analytical Chemistry* **2003**, *75* (20), 5336-5344.
98. Leungsakul, S.; Jeffries, H. E.; Kamens, R. M., A Kinetic Mechanism for Predicting Secondary Aerosol Formation from the Reactions of D-Limonene in the Presence of Oxides of Nitrogen and Natural Sunlight. *Atmospheric Environment* **2005**, *39* (37), 7063-7082.
99. Heaton, K. J.; Dreyfus, M. A.; Wang, S.; Johnston, M. V., Oligomers in the Early Stage of Biogenic Secondary Organic Aerosol Formation and Growth. *Environ. Sci. Technol.* **2007**, *41* (17), 6129-6136.
100. Bateman, A. P.; Nizkorodov, S. A.; Laskin, J.; Laskin, A., Time-Resolved Molecular Characterization of Limonene/Ozone Aerosol Using High-Resolution Electrospray Ionization Mass Spectrometry. *Physical Chemistry Chemical Physics* **2009**, *11* (36), 7931-7942.
101. Donahue, N. M.; Tischuk, J. E.; Marquis, B. J.; Hartz, K. E. H., Secondary Organic Aerosol from Limona Ketone: Insights into Terpene Ozonolysis Via Synthesis of Key Intermediates. *Physical Chemistry Chemical Physics* **2007**, *9* (23), 2991-2998.
102. Geddes, S.; Nichols, B.; Flemer, S.; Eisenhauer, J.; Zahardis, J.; Petrucci, G. A., Near-Infrared Laser Desorption/Ionization Aerosol Mass Spectrometry for Investigating Primary and Secondary Organic Aerosols under Low Loading Conditions. *Analytical Chemistry* **2010**, *82* (19), 7915-7923.
103. Maksymiuk, C. S.; Gayahtri, C.; Gil, R. R.; Donahue, N. M., Secondary Organic Aerosol Formation from Multiphase Oxidation of Limonene by Ozone: Mechanistic Constraints Via Two-Dimensional Heteronuclear Nmr Spectroscopy. *Physical Chemistry Chemical Physics* **2009**, *11* (36), 7810-7818.
104. Hoffmann, T.; Odum, J. R.; Bowman, F.; Collins, D.; Klockow, D.; Flagan, R. C.; Seinfeld, J. H., Formation of Organic Aerosols from the Oxidation of Biogenic Hydrocarbons. *Journal of Atmospheric Chemistry* **1997**, *26* (2), 189-222.
105. Jonsson, A. M.; Hallquist, M.; Ljungstrom, E., Impact of Humidity on the Ozone Initiated Oxidation of Limonene, Delta(3)-Carene, and Alpha-Pinene. *Environ. Sci. Technol.* **2006**, *40* (1), 188-194.
106. Rohr, A. C.; Weschler, C. J.; Koutrakis, P.; Spengler, J. D., Generation and Quantification of Ultrafine Particles through Terpene/Ozone Reaction in a Chamber Setting. *Aerosol Science and Technology* **2003**, *37* (1), 65-78.
107. Odum, J. R.; Hoffmann, T.; Bowman, F.; Collins, D.; Flagan, R. C.; Seinfeld, J. H., Gas/Particle Partitioning and Secondary Organic Aerosol Yields. *Environ. Sci. Technol.* **1996**, *30* (8), 2580-2585.
108. Pankow, J. F., An Absorption-Model of Gas-Particle Partitioning of Organic-Compounds in the Atmosphere. *Atmospheric Environment* **1994**, *28* (2), 185-188.
109. Pankow, J. F., An Absorption-Model of the Gas Aerosol Partitioning Involved in the Formation of Secondary Organic Aerosol. *Atmospheric Environment* **1994**, *28* (2), 189-193.
110. Kondo, Y.; Miyazaki, Y.; Takegawa, N.; Miyakawa, T.; Weber, R. J.; Jimenez, J. L.; Zhang, Q.; Worsnop, D. R., Oxygenated and Water-Soluble Organic Aerosols in Tokyo. *J. Geophys. Res.-Atmos.* **2007**, *112* (D1), D01203, doi: 10.1029/2006jd007056.

111. Saathoff, H.; Naumann, K. H.; Mohler, O.; Jonsson, A. M.; Hallquist, M.; Kiendler-Scharr, A.; Mentel, T. F.; Tillmann, R.; Schurath, U., Temperature Dependence of Yields of Secondary Organic Aerosols from the Ozonolysis of Alpha-Pinene and Limonene. *Atmospheric Chemistry and Physics* **2009**, *9* (5), 1551-1577.
112. Northcross, A. L.; Jang, M., Heterogeneous Soa Yield from Ozonolysis of Monoterpenes in the Presence of Inorganic Acid. *Atmospheric Environment* **2007**, *41* (7), 1483-1493.
113. Chen, X.; Hopke, P. K., A Chamber Study of Secondary Organic Aerosol Formation by Limonene Ozonolysis. *Indoor Air-Int. J. Indoor Air Qual. Clim.* **2010**, *20* (4), 320-328.
114. Hellen, H.; Hakola, H.; Reissell, A.; Ruuskanen, T. M., Carbonyl Compounds in Boreal Coniferous Forest Air in Hyytiala, Southern Finland. *Atmospheric Chemistry and Physics* **2004**, *4*, 1771-1780.
115. Kourtchev, I.; Copolovici, L.; Claeys, M.; Maenhaut, W., Characterization of Atmospheric Aerosols at a Forested Site in Central Europe. *Environ. Sci. Technol.* **2009**, *43* (13), 4665-4671.
116. Hoyle, C. R.; Berntsen, T.; Myhre, G.; Isaksen, I. S. A., Secondary Organic Aerosol in the Global Aerosol - Chemical Transport Model Oslo Ctm2. *Atmospheric Chemistry and Physics* **2007**, *7* (21), 5675-5694.
117. Heald, C. L.; Henze, D. K.; Horowitz, L. W.; Feddema, J.; Lamarque, J. F.; Guenther, A.; Hess, P. G.; Vitt, F.; Seinfeld, J. H.; Goldstein, A. H.; Fung, I., Predicted Change in Global Secondary Organic Aerosol Concentrations in Response to Future Climate, Emissions, and Land Use Change. *J. Geophys. Res.-Atmos.* **2008**, *113* (D5), D05211, doi: 10.1029/2007jd009092.
118. Sarwar, G.; Olson, D. A.; Corsi, R. L.; Weschler, C. J., Indoor Fine Particles: The Role of Terpene Emissions from Consumer Products. *J. Air Waste Manage. Assoc.* **2004**, *54* (3), 367-377.
119. Weschler, C. J., Ozone in Indoor Environments: Concentration and Chemistry. *Indoor Air-Int. J. Indoor Air Qual. Clim.* **2000**, *10* (4), 269-288.
120. Wainman, T.; Zhang, J. F.; Weschler, C. J.; Liroy, P. J., Ozone and Limonene in Indoor Air: A Source of Submicron Particle Exposure. *Environ. Health Perspect.* **2000**, *108* (12), 1139-1145.
121. Destailats, H.; Lunden, M. M.; Singer, B. C.; Coleman, B. K.; Hodgson, A. T.; Weschler, C. J.; Nazaroff, W. W., Indoor Secondary Pollutants from Household Product Emissions in the Presence of Ozone: A Bench-Scale Chamber Study. *Environ. Sci. Technol.* **2006**, *40* (14), 4421-4428.
122. Liu, X. Y.; Mason, M.; Krebs, K.; Sparks, L., Full-Scale Chamber Investigation and Simulation of Air Freshener Emissions in the Presence of Ozone. *Environ. Sci. Technol.* **2004**, *38* (10), 2802-2812.
123. Sunil, V. R.; Laumbach, R. J.; Patel, K. J.; Turpin, B. J.; Lim, H. J.; Kipen, H. M.; Laskin, J. D.; Laskin, D. L., Pulmonary Effects of Inhaled Limonene Ozone Reaction Products in Elderly Rats. *Toxicology and Applied Pharmacology* **2007**, *222* (2), 211-220.
124. Wolkoff, P.; Clausen, P. A.; Wilkins, C. K.; Nielsen, G. D., Formation of Strong Airway Irritants in Terpene/Ozone Mixtures. *Indoor Air-Int. J. Indoor Air Qual. Clim.* **2000**, *10* (2), 82-91.

125. Nojgaard, J. K.; Christensen, K. B.; Wolkoff, P., The Effect on Human Eye Blink Frequency of Exposure to Limonene Oxidation Products and Methacrolein. *Toxicol. Lett.* **2005**, *156* (2), 241-251.
126. Kaiser, J., Mounting Evidence Indicts Fine-Particle Pollution. *Science* **2005**, *307* (5717), 1858-1861.
127. Calogirou, A.; Larsen, B. R.; Kotzias, D., Gas-Phase Terpene Oxidation Products: A Review. *Atmospheric Environment* **1999**, *33* (9), 1423-1439.
128. Criegee, R., Mechanism of Ozonolysis. *Angew. Chem.-Int. Edit. Engl.* **1975**, *14* (11), 745-752.
129. Johnson, D.; Marston, G., The Gas-Phase Ozonolysis of Unsaturated Volatile Organic Compounds in the Troposphere. *Chem. Soc. Rev.* **2008**, *37* (4), 699-716.
130. Lee, A.; Goldstein, A. H.; Keywood, M. D.; Gao, S.; Varutbangkul, V.; Bahreini, R.; Ng, N. L.; Flagan, R. C.; Seinfeld, J. H., Gas-Phase Products and Secondary Aerosol Yields from the Ozonolysis of Ten Different Terpenes. *J. Geophys. Res.-Atmos.* **2006**, *111* (D7), D07302, doi: 10.1029/2005jd006437.
131. Keywood, M. D.; Kroll, J. H.; Varutbangkul, V.; Bahreini, R.; Flagan, R. C.; Seinfeld, J. H., Secondary Organic Aerosol Formation from Cyclohexene Ozonolysis: Effect of Oh Scavenger and the Role of Radical Chemistry. *Environ. Sci. Technol.* **2004**, *38* (12), 3343-3350.
132. Henry, K. M.; Donahue, N. M., Effect of the Oh Radical Scavenger Hydrogen Peroxide on Secondary Organic Aerosol Formation from Alpha-Pinene Ozonolysis. *Aerosol Science and Technology* **2011**, *45* (6), 686-690.
133. Nguyen, T. B.; Bateman, A. P.; Bones, D. L.; Nizkorodov, S. A.; Laskin, J.; Laskin, A., High-Resolution Mass Spectrometry Analysis of Secondary Organic Aerosol Generated by Ozonolysis of Isoprene. *Atmospheric Environment* **2010**, *44* (8), 1032-1042.
134. Hart, K. M.; Pankow, J. F., High-Volume Air Sampler for Particle and Gas Sampling .2. Use of Backup Filters to Correct for the Adsorption of Gas-Phase Polycyclic Aromatic-Hydrocarbons to the Front Filter. *Environ. Sci. Technol.* **1994**, *28* (4), 655-661.
135. Bateman, A. P.; Walser, M. L.; Desyaterik, Y.; Laskin, J.; Laskin, A.; Nizkorodov, S. A., The Effect of Solvent on the Analysis of Secondary Organic Aerosol Using Electrospray Ionization Mass Spectrometry. *Environ. Sci. Technol.* **2008**, *42* (19), 7341-7346.
136. Cahill, T. A.; Wakabayashi, P., Compositional Analysis of Size-Segregated Aerosol Samples. *Adv. Chem. Ser.* **1993**, (232), 211-228.
137. Laskin, A.; Cowin, J. P.; Iedema, M. J., Analysis of Individual Environmental Particles Using Modern Methods of Electron Microscopy and X-Ray Microanalysis. *J. Electron Spectrosc. Relat. Phenom.* **2006**, *150* (2-3), 260-274.
138. Weber, R. J.; Orsini, D.; Daun, Y.; Lee, Y. N.; Klotz, P. J.; Brechtel, F., A Particle-into-Liquid Collector for Rapid Measurement of Aerosol Bulk Chemical Composition. *Aerosol Science and Technology* **2001**, *35* (3), 718-727.
139. Cech, N. B.; Enke, C. G., Practical Implications of Some Recent Studies in Electrospray Ionization Fundamentals. *Mass Spectrom. Rev.* **2001**, *20* (6), 362-387.
140. Makarov, A.; Denisov, E.; Kholomeev, A.; Baischun, W.; Lange, O.; Strupat, K.; Horning, S., Performance Evaluation of a Hybrid Linear Ion Trap/Orbitrap Mass Spectrometer. *Analytical Chemistry* **2006**, *78* (7), 2113-2120.

141. Makarov, A.; Denisov, E.; Lange, O.; Horning, S., Dynamic Range of Mass Accuracy in Lq Orbitrap Hybrid Mass Spectrometer. *J. Am. Soc. Mass Spectrom.* **2006**, *17* (7), 977-982.
142. Makarov, A., Electrostatic Axially Harmonic Orbital Trapping: A High-Performance Technique of Mass Analysis. *Analytical Chemistry* **2000**, *72* (6), 1156-1162.
143. Hu, Q. Z.; Noll, R. J.; Li, H. Y.; Makarov, A.; Hardman, M.; Cooks, R. G., The Orbitrap: A New Mass Spectrometer. *Journal of Mass Spectrometry* **2005**, *40* (4), 430-443.
144. Meija, J., Mathematical Tools in Analytical Mass Spectrometry. *Anal. Bioanal. Chem.* **2006**, *385* (3), 486-499.
145. Koch, B. P.; Dittmar, T., From Mass to Structure: An Aromaticity Index for High-Resolution Mass Data of Natural Organic Matter. *Rapid Commun. Mass Spectrom.* **2006**, *20* (5), 926-932.
146. Aiken, A. C.; Decarlo, P. F.; Kroll, J. H.; Worsnop, D. R.; Huffman, J. A.; Docherty, K. S.; Ulbrich, I. M.; Mohr, C.; Kimmel, J. R.; Sueper, D.; Sun, Y.; Zhang, Q.; Trimborn, A.; Northway, M.; Ziemann, P. J.; Canagaratna, M. R.; Onasch, T. B.; Alfarra, M. R.; Prevot, A. S. H.; Dommen, J.; Duplissy, J.; Metzger, A.; Baltensperger, U.; Jimenez, J. L., O/C and Om/Oc Ratios of Primary, Secondary, and Ambient Organic Aerosols with High-Resolution Time-of-Flight Aerosol Mass Spectrometry. *Environ. Sci. Technol.* **2008**, *42* (12), 4478-4485.
147. Altieri, K. E.; Seitzinger, S. P.; Carlton, A. G.; Turpin, B. J.; Klein, G. C.; Marshall, A. G., Oligomers Formed through in-Cloud Methylglyoxal Reactions: Chemical Composition, Properties, and Mechanisms Investigated by Ultra-High Resolution Ft-Icr Mass Spectrometry. *Atmospheric Environment* **2008**, *42* (7), 1476-1490.
148. Perri, M. J.; Seitzinger, S.; Turpin, B. J., Secondary Organic Aerosol Production from Aqueous Photooxidation of Glycolaldehyde: Laboratory Experiments. *Atmospheric Environment* **2009**, *43* (8), 1487-1497.
149. Kebarle, P., A Brief Overview of the Present Status of the Mechanisms Involved in Electrospray Mass Spectrometry. *Journal of Mass Spectrometry* **2000**, *35* (7), 804-817.
150. Enke, C. G., A Predictive Model for Matrix and Analyte Effects in Electrospray Ionization of Singly-Charged Ionic Analytes. *Analytical Chemistry* **1997**, *69* (23), 4885-4893.
151. Solomons, T. W. G.; Fryhle, C. B., *Organic Chemistry*. 7th ed.; John Wiley & Sons: New York, 2002.
152. McIntyre, C.; McRae, C., Proposed Guidelines for Sample Preparation and Esi-MS Analysis of Humic Substances to Avoid Self-Esterification. *Organic Geochemistry* **2005**, *36* (4), 543-553.
153. Graber, E. R.; Rudich, Y., Atmospheric Hulis: How Humic-Like Are They? A Comprehensive and Critical Review. *Atmospheric Chemistry and Physics* **2006**, *6*, 729-753.
154. Grujic, S.; Vasiljevic, T.; Lausevic, M.; Ast, T., Study on the Formation of an Amoxicillin Adduct with Methanol Using Electrospray Ion Trap Tandem Mass Spectrometry. *Rapid Commun. Mass Spectrom.* **2008**, *22* (1), 67-74.
155. Parris, C. L.; Christenson, R. M., N-Alkylation of Nitriles with Benzyl Alcohol, Related Alcohols, and Glycols. *Journal of Organic Chemistry* **1960**, *25* (3), 331-334.

156. Dibise, S. A.; Lipisko, B. A.; Haag, A.; Wolak, R. A.; Gokel, G. W., Direct Synthesis of Alpha,Beta-Unsaturated Nitriles from Acetonitrile and Carbonyl-Compounds - Survey, Crown Effects, and Experimental Conditions. *Journal of Organic Chemistry* **1979**, *44* (25), 4640-4649.
157. Roger, R.; Neilson, D. G., The Chemistry of Imidates. *Chemical Reviews* **1961**, *61* (2), 179-211.
158. Gao, S.; Surratt, J. D.; Knipping, E. M.; Edgerton, E. S.; Shahgholi, M.; Seinfeld, J. H., Characterization of Polar Organic Components in Fine Aerosols in the Southeastern United States: Identity, Origin, and Evolution. *J. Geophys. Res.-Atmos.* **2006**, *111* (D14), D14314, doi: 10.1029/2005JD006601.
159. Roberts, J. D.; Caserio, M. C., *Basic Principles of Organic Chemistry.-2nd Edition*. 2nd ed.; W.A. Benjamin, Inc.: Menlo Park, CA, 1977; p 1596.
160. Turpin, B. J.; Lim, H. J., Species Contributions to Pm2.5 Mass Concentrations: Revisiting Common Assumptions for Estimating Organic Mass. *Aerosol Science and Technology* **2001**, *35* (1), 602-610.
161. Pang, Y.; Turpin, B. J.; Gundel, L. A., On the Importance of Organic Oxygen for Understanding Organic Aerosol Particles. *Aerosol Science and Technology* **2006**, *40* (2), 128-133.
162. Gross, D. S.; Galli, M. E.; Kalberer, M.; Prevot, A. S. H.; Dommen, J.; Alfarra, M. R.; Duplissy, J.; Gaeggeler, K.; Gascho, A.; Metzger, A.; Baltensperger, U., Real-Time Measurement of Oligomeric Species in Secondary Organic Aerosol with the Aerosol Time-of-Flight Mass Spectrometer. *Analytical Chemistry* **2006**, *78* (7), 2130-2137.
163. Liu, Y.; Cain, J. P.; Wang, H.; Laskin, A., Kinetic Study of Heterogeneous Reaction of Deliquesced Nacl Particles with Gaseous Hno3 Using Particle-on-Substrate Stagnation Flow Reactor Approach. *J. Phys. Chem. A* **2007**, *111* (40), 10026-10043.
164. Liu, Y.; Gibson, E. R.; Cain, J. P.; Wang, H.; Grassian, V. H.; Laskin, A., Kinetics of Heterogeneous Reaction of Caco3 Particles with Gaseous Hno3 over a Wide Range of Humidity. *J. Phys. Chem. A* **2008**, *112* (7), 1561-1571.
165. Inuma, Y.; Boge, O.; Gnauk, T.; Herrmann, H., Aerosol-Chamber Study of the Alpha-Pinene/O-3 Reaction: Influence of Particle Acidity on Aerosol Yields and Products. *Atmospheric Environment* **2004**, *38* (5), 761-773.
166. Kane, S. M.; Timonen, R. S.; Leu, M. T., Heterogeneous Chemistry of Acetone in Sulfuric, Acid Solutions: Implications for the Upper Troposphere. *J. Phys. Chem. A* **1999**, *103* (46), 9259-9265.
167. Li, Y. J.; Lee, A. K. Y.; Lau, A. P. S.; Chan, C. K., Accretion Reactions of Octanal Catalyzed by Sulfuric Acid: Product Identification, Reaction Pathways, and Atmospheric Implications. *Environ. Sci. Technol.* **2008**, *42* (19), 7138-7145.
168. Gratien, A.; Johnson, S. N.; Ezell, M. J.; Dawson, M. L.; Bennett, R.; Finlayson-Pitts, B. J., Surprising Formation of P-Cymene in the Oxidation of Alpha-Pinene in Air by the Atmospheric Oxidants Oh, O-3, and No3. *Environ. Sci. Technol.* **2011**, *45* (7), 2755-2760.
169. Shilling, J. E.; King, S. M.; Mochida, M.; Martin, S. T., Mass Spectral Evidence That Small Changes in Composition Caused by Oxidative Aging Processes Alter Aerosol Ccn Properties. *J. Phys. Chem. A* **2007**, *111* (17), 3358-3368.
170. Battino, R.; Editor, *Solubility Data Series, Vol. 7: Oxygen and Ozone*. 1981; p 519 pp.

171. Hoigne, J.; Bader, H., Rate Constants of Reactions of Ozone with Organic and Inorganic-Compounds in Water .1. Non-Dissociating Organic-Compounds. *Water Res.* **1983**, *17* (2), 173-183.
172. Tolocka, M. P.; Heaton, K. J.; Dreyfus, M. A.; Wang, S. Y.; Zordan, C. A.; Saul, T. D.; Johnston, M. V., Chemistry of Particle Inception and Growth During Alpha-Pinene Ozonolysis. *Environ. Sci. Technol.* **2006**, *40* (6), 1843-1848.
173. Ng, N. L.; Kroll, J. H.; Keywood, M. D.; Bahreini, R.; Varutbangkul, V.; Flagan, R. C.; Seinfeld, J. H.; Lee, A.; Goldstein, A. H., Contribution of First- Versus Second-Generation Products to Secondary Organic Aerosols Formed in the Oxidation of Biogenic Hydrocarbons. *Environ. Sci. Technol.* **2006**, *40* (7), 2283-2297.
174. Sullivan, A. P.; Weber, R. J., Chemical Characterization of the Ambient Organic Aerosol Soluble in Water: 1. Isolation of Hydrophobic and Hydrophilic Fractions with a Xad-8 Resin. *J. Geophys. Res.-Atmos.* **2006**, *111* (D5), D05314, doi: 10.1029/2005jd006485.
175. Zappoli, S.; Andracchio, A.; Fuzzi, S.; Facchini, M. C.; Gelencser, A.; Kiss, G.; Krivacsy, Z.; Molnar, A.; Meszaros, E.; Hansson, H. C.; Rosman, K.; Zebuhr, Y., Inorganic, Organic and Macromolecular Components of Fine Aerosol in Different Areas of Europe in Relation to Their Water Solubility. *Atmospheric Environment* **1999**, *33* (17), 2733-2743.
176. Decesari, S.; Mircea, M.; Cavalli, F.; Fuzzi, S.; Moretti, F.; Tagliavini, E.; Facchini, M. C., Source Attribution of Water-Soluble Organic Aerosol by Nuclear Magnetic Resonance Spectroscopy. *Environ. Sci. Technol.* **2007**, *41* (7), 2479-2484.
177. Sullivan, A. P.; Weber, R. J.; Clements, A. L.; Turner, J. R.; Bae, M. S.; Schauer, J. J., A Method for on-Line Measurement of Water-Soluble Organic Carbon in Ambient Aerosol Particles: Results from an Urban Site. *Geophysical Research Letters* **2004**, *31* (13), L13105, doi: 10.1029/2004GL019681.
178. Jurado, E.; Dachs, J.; Duarte, C. M.; Simo, R., Atmospheric Deposition of Organic and Black Carbon to the Global Oceans. *Atmospheric Environment* **2008**, *42* (34), 7931-7939.
179. Orsini, D. A.; Ma, Y. L.; Sullivan, A.; Sierau, B.; Baumann, K.; Weber, R. J., Refinements to the Particle-into-Liquid Sampler (Pils) for Ground and Airborne Measurements of Water Soluble Aerosol Composition. *Atmospheric Environment* **2003**, *37* (9-10), 1243-1259.
180. Zhang, J.; Chameides, W. L.; Weber, R.; Cass, G.; Orsini, D.; Edgerton, E.; Jongejan, P.; Slanina, J., An Evaluation of the Thermodynamic Equilibrium Assumption for Fine Particulate Composition: Nitrate and Ammonium During the 1999 Atlanta Supersite Experiment. *J. Geophys. Res.-Atmos.* **2002**, *108* (D7), D78414, doi: 10.1029/2001jd001592.
181. Lee, Y. N.; Weber, R.; Ma, Y.; Orsini, D.; Maxwell-Meier, K.; Blake, D.; Meinardi, S.; Sachse, G.; Harward, C.; Chen, T. Y.; Thornton, D.; Tu, F. H.; Bandy, A., Airborne Measurement of Inorganic Ionic Components of Fine Aerosol Particles Using the Particle-into-Liquid Sampler Coupled to Ion Chromatography Technique During Ace-Asia and Trace-P. *J. Geophys. Res.-Atmos.* **2003**, *108* (D23), D238646, doi: 10.1029/2002JD003265.
182. Hogrefe, O.; Schwab, J. J.; Drewnick, F.; Lala, G. G.; Peters, S.; Demerjian, K. L.; Rhoads, K.; Felton, H. D.; Rattigan, O. V.; Husain, L.; Dutkiewicz, V. A.,

- Semicontinuous Pm2.5 Sulfate and Nitrate Measurements at an Urban and a Rural Location in New York: Pmtacs-Ny Summer 2001 and 2002 Campaigns. *J. Air Waste Manage. Assoc.* **2004**, *54* (9), 1040-1060.
183. Li, Z.; Hopke, P. K.; Husain, L.; Qureshi, S.; Dutkiewicz, V. A.; Schwab, J. J.; Drewnick, F.; Demerjian, K. L., Sources of Fine Particle Composition in New York City. *Atmospheric Environment* **2004**, *38* (38), 6521-6529.
184. Ma, Y.; Weber, R. J.; Maxwell-Meier, K.; Orsini, D. A.; Lee, Y. N.; Huebert, B. J.; Howell, S. G.; Bertram, T.; Talbot, R. W.; Dibb, J. E.; Scheuer, E., Intercomparisons of Airborne Measurements of Aerosol Ionic Chemical Composition During Trace-P and Ace-Asia. *J. Geophys. Res.-Atmos.* **2004**, *109* (D15), D15S06, doi: 10.1029/2003jd003673.
185. Malm, W. C.; Day, D. E.; Carrico, C.; Kreidenweis, S. M.; Collett, J. L.; McMeeking, G.; Lee, T.; Carrillo, J.; Schichtel, B., Intercomparison and Closure Calculations Using Measurements of Aerosol Species and Optical Properties During the Yosemite Aerosol Characterization Study. *J. Geophys. Res.-Atmos.* **2005**, *110* (D14), D14302, doi: 10.1029/2004jd005494.
186. Miyazaki, Y.; Kondo, Y.; Takegawa, N.; Weber, R. J.; Koike, M.; Kita, K.; Fukuda, M.; Ma, Y.; Clarke, A. D.; Kapustin, V. N.; Flocke, F.; Weinheimer, A. J.; Zondlo, M.; Eisele, F. L.; Blake, D. R.; Liley, B., Contribution of Particulate Nitrate to Airborne Measurements of Total Reactive Nitrogen. *J. Geophys. Res.-Atmos.* **2005**, *110* (D15), D15304, doi: 10.1029/2004jd005502.
187. Song, C. H.; Ma, Y.; Orsini, D.; Kim, Y. P.; Weber, R. J., An Investigation into the Ionic Chemical Composition and Mixing State of Biomass Burning Particles Recorded During Trace-P P3b Flight#10. *Journal of Atmospheric Chemistry* **2005**, *51* (1), 43-64.
188. Weimer, S.; Drewnick, F.; Hogrefe, O.; Schwab, J. J.; Rhoads, K.; Orsini, D.; Canagaratna, M.; Worsnop, D. R.; Demerjian, K. L., Size-Selective Nonrefractory Ambient Aerosol Measurements During the Particulate Matter Technology Assessment and Characterization Study - New York 2004 Winter Intensive in New York City. *J. Geophys. Res.-Atmos.* **2006**, *111* (D18), D18305, doi: 10.1029/2006jd007215.
189. Bae, M. S.; Schwab, J. J.; Zhang, Q.; Hogrefe, O.; Demerjian, K. L.; Weimer, S.; Rhoads, K.; Orsini, D.; Venkatachari, P.; Hopke, P. K., Interference of Organic Signals in Highly Time Resolved Nitrate Measurements by Low Mass Resolution Aerosol Mass Spectrometry. *J. Geophys. Res.-Atmos.* **2007**, *112* (D22), D22305, doi: 10.1029/2007jd008614.
190. Lee, T.; Yu, X. Y.; Kreidenweis, S. M.; Malm, W. C.; Collett, J. L., Semi-Continuous Measurement of Pm2.5 Ionic Composition at Several Rural Locations in the United States. *Atmospheric Environment* **2008**, *42* (27), 6655-6669.
191. Lee, T.; Yu, X. Y.; Ayres, B.; Kreidenweis, S. M.; Malm, W. C.; Collett, J. L., Observations of Fine and Coarse Particle Nitrate at Several Rural Locations in the United States. *Atmospheric Environment* **2008**, *42* (11), 2720-2732.
192. Sorooshian, A.; Murphy, S. N.; Hersey, S.; Gates, H.; Padro, L. T.; Nenes, A.; Brechtel, F. J.; Jonsson, H.; Flagan, R. C.; Seinfeld, J. H., Comprehensive Airborne Characterization of Aerosol from a Major Bovine Source. *Atmospheric Chemistry and Physics* **2008**, *8* (17), 5489-5520.

193. Yao, X. H.; Shairsingh, K.; Lam, P. H.; Evans, G. J., Underestimation of Sulfate Concentration in Pm2.5 Using a Semi-Continuous Particle Instrument Based on Ion Chromatography. *J. Environ. Monit.* **2009**, *11* (6), 1292-1297.
194. Sorooshian, A.; Lu, M. L.; Brechtel, F. J.; Jonsson, H.; Feingold, G.; Flagan, R. C.; Seinfeld, J. H., On the Source of Organic Acid Aerosol Layers above Clouds. *Environ. Sci. Technol.* **2007**, *41* (13), 4647-4654.
195. Sorooshian, A.; Ng, N. L.; Chan, A. W. H.; Feingold, G.; Flagan, R. C.; Seinfeld, J. H., Particulate Organic Acids and Overall Water-Soluble Aerosol Composition Measurements from the 2006 Gulf of Mexico Atmospheric Composition and Climate Study (Gomaccs). *J. Geophys. Res.-Atmos.* **2007**, *112* (D13), D13201, doi: 10.1029/2007jd008537.
196. Sorooshian, A.; Varutbangkul, V.; Brechtel, F. J.; Ervens, B.; Feingold, G.; Bahreini, R.; Murphy, S. M.; Holloway, J. S.; Atlas, E. L.; Buzorius, G.; Jonsson, H.; Flagan, R. C.; Seinfeld, J. H., Oxalic Acid in Clear and Cloudy Atmospheres: Analysis of Data from International Consortium for Atmospheric Research on Transport and Transformation 2004. *J. Geophys. Res.-Atmos.* **2006**, *111* (D23), D23S45, doi: 10.1029/2005jd006880.
197. Takegawa, N.; Miyakawa, T.; Watanabe, M.; Kondo, Y.; Miyazaki, Y.; Han, S.; Zhao, Y.; van Pinxteren, D.; Brüggemann, E.; Gnauk, T.; Herrmann, H.; Xiao, R.; Deng, Z.; Hu, M.; Zhu, T.; Zhang, Y., Performance of an Aerodyne Aerosol Mass Spectrometer (Ams) During Intensive Campaigns in China in the Summer of 2006. *Aerosol Science and Technology* **2009**, *43* (3), 189-204.
198. Bae, M. S.; Demerjian, K. L.; Schwab, J. J.; Weimer, S.; Hou, J.; Zhou, X. L.; Rhoads, K.; Orsini, D., Intercomparison of Real Time Ammonium Measurements at Urban and Rural Locations in New York. *Aerosol Science and Technology* **2007**, *41* (3), 329-341.
199. Hennigan, C. J.; Sandholm, S.; Kim, S.; Stickel, R. E.; Huey, L. G.; Weber, R. J., Influence of Ohio River Valley Emissions on Fine Particle Sulfate Measured from Aircraft over Large Regions of the Eastern United States and Canada During Intex-Na. *J. Geophys. Res.-Atmos.* **2006**, *111* (D24), D24S04, doi: 10.1029/2006/jd007282.
200. Sorooshian, A.; Brechtel, F. J.; Ma, Y. L.; Weber, R. J.; Corless, A.; Flagan, R. C.; Seinfeld, J. H., Modeling and Characterization of a Particle-into-Liquid Sampler (Pils). *Aerosol Science and Technology* **2006**, *40* (6), 396-409.
201. Takegawa, N.; Miyazaki, Y.; Kondo, Y.; Komazaki, Y.; Miyakawa, T.; Jimenez, J. L.; Jayne, J. T.; Worsnop, D. R.; Allan, J. D.; Weber, R. J., Characterization of an Aerodyne Aerosol Mass Spectrometer (Ams): Intercomparison with Other Aerosol Instruments. *Aerosol Science and Technology* **2005**, *39* (8), 760-770.
202. Hogrefe, O.; Drewnick, F.; Lala, G. G.; Schwab, J. J.; Demerjian, K. L., Development, Operation and Applications of an Aerosol Generation, Calibration and Research Facility. *Aerosol Science and Technology* **2004**, *38*, 196-214.
203. Malm, W. C.; McMeeking, G. R.; Kreidenweis, S. M.; Levin, E.; Carrico, C. M.; Day, D. E.; Collett, J. L.; Lee, T.; Sullivan, A. P.; Raja, S., Using High Time Resolution Aerosol and Number Size Distribution Measurements to Estimate Atmospheric Extinction. *J. Air Waste Manage. Assoc.* **2009**, *59* (9), 1049-1060.
204. Miyazaki, Y.; Kondo, Y.; Shiraiwa, M.; Takegawa, N.; Miyakawa, T.; Han, S.; Kita, K.; Hu, M.; Deng, Z. Q.; Zhao, Y.; Sugimoto, N.; Blake, D. R.; Weber, R. J., Chemical Characterization of Water-Soluble Organic Carbon Aerosols at a Rural Site in the Pearl

- River Delta, China, in the Summer of 2006. *J. Geophys. Res.-Atmos.* **2009**, *114*, D14208, doi: 10.1029/2009jd011736.
205. Sullivan, A. P.; Peltier, R. E.; Brock, C. A.; de Gouw, J. A.; Holloway, J. S.; Warneke, C.; Wollny, A. G.; Weber, R. J., Airborne Measurements of Carbonaceous Aerosol Soluble in Water over Northeastern United States: Method Development and an Investigation into Water-Soluble Organic Carbon Sources. *J. Geophys. Res.-Atmos.* **2006**, *111* (D23), D23S46, doi: 10.1029/2006jd007072.
206. Russell, L. M.; Takahama, S.; Liu, S.; Hawkins, L. N.; Covert, D. S.; Quinn, P. K.; Bates, T. S., Oxygenated Fraction and Mass of Organic Aerosol from Direct Emission and Atmospheric Processing Measured on the R/V Ronald Brown During Texaqs/Gomaccs 2006. *J. Geophys. Res.-Atmos.* **2009**, *114*, D00f05, doi: 10.1029/2008jd011275.
207. Peltier, R. E.; Sullivan, A. P.; Weber, R. J.; Wollny, A. G.; Holloway, J. S.; Brock, C. A.; de Gouw, J. A.; Atlas, E. L., No Evidence for Acid-Catalyzed Secondary Organic Aerosol Formation in Power Plant Plumes over Metropolitan Atlanta, Georgia. *Geophysical Research Letters* **2007**, *34* (6), L06801, doi: 10.1029/2006gl028780.
208. Miyazaki, Y.; Kondo, Y.; Takegawa, N.; Komazaki, Y.; Fukuda, M.; Kawamura, K.; Mochida, M.; Okuzawa, K.; Weber, R. J., Time-Resolved Measurements of Water-Soluble Organic Carbon in Tokyo. *J. Geophys. Res.-Atmos.* **2006**, *111* (D23), D23206, doi: 10.1029/2006jd007125.
209. Peltier, R. E.; Weber, R. J.; Sullivan, A. P., Investigating a Liquid-Based Method for Online Organic Carbon Detection in Atmospheric Particles. *Aerosol Science and Technology* **2007**, *41* (12), 1117-1127.
210. Rastogi, N.; Oakes, M. M.; Schauer, J. J.; Shafer, M. M.; Majestic, B. J.; Weber, R. J., New Technique for Online Measurement of Water-Soluble Fe(II) in Atmospheric Aerosols. *Environ. Sci. Technol.* **2009**, *43* (7), 2425-2430.
211. Parshintsev, J.; Rasanen, R.; Hartonen, K.; Kulmala, M.; Riekkola, M. L., Analysis of Organic Compounds in Ambient Aerosols Collected with the Particle-into-Liquid Sampler. *Boreal Environ. Res.* **2009**, *14* (4), 630-640.
212. Parshintsev, J.; Hyotylainen, T.; Hartonen, K.; Kulmala, M.; Riekkola, M. L., Solid-Phase Extraction of Organic Compounds in Atmospheric Aerosol Particles Collected with the Particle-into-Liquid Sampler and Analysis by Liquid Chromatography-Mass Spectrometry. *Talanta* **2010**, *80* (3), 1170-1176.
213. Laskin, A.; Smith, J. S.; Laskin, J., Molecular Characterization of Nitrogen-Containing Organic Compounds in Biomass Burning Aerosols Using High-Resolution Mass Spectrometry. *Environ. Sci. Technol.* **2009**, *43* (10), 3764-3771.
214. Saxena, P.; Hildemann, L. M., Water-Soluble Organics in Atmospheric Particles: A Critical Review of the Literature and Application of Thermodynamics to Identify Candidate Compounds. *Journal of Atmospheric Chemistry* **1996**, *24* (1), 57-109.
215. Varutbangkul, V.; Brechtel, F. J.; Bahreini, R.; Ng, N. L.; Keywood, M. D.; Kroll, J. H.; Flagan, R. C.; Seinfeld, J. H.; Lee, A.; Goldstein, A. H., Hygroscopicity of Secondary Organic Aerosols Formed by Oxidation of Cycloalkenes, Monoterpenes, Sesquiterpenes, and Related Compounds. *Atmospheric Chemistry and Physics* **2006**, *6*, 2367-2388.
216. Duplissy, J.; Gysel, M.; Alfarra, M. R.; Dommen, J.; Metzger, A.; Prevot, A. S. H.; Weingartner, E.; Laaksonen, A.; Raatikainen, T.; Good, N.; Turner, S. F.; McFiggans, G.; Baltensperger, U., Cloud Forming Potential of Secondary Organic Aerosol under

- near Atmospheric Conditions. *Geophysical Research Letters* **2008**, *35* (3), L03818, doi: 10.1029/2007GL031075.
217. Hartz, K. E. H.; Rosenoern, T.; Ferchak, S. R.; Raymond, T. M.; Bilde, M.; Donahue, N. M.; Pandis, S. N., Cloud Condensation Nuclei Activation of Monoterpene and Sesquiterpene Secondary Organic Aerosol. *J. Geophys. Res., D, Atmos.* **2005**, *110* (D14), D14208, doi: 10.1029/2004JD005754.
218. Dinar, E.; Taraniuk, I.; Graber, E. R.; Anttila, T.; Mentel, T. F.; Rudich, Y., Hygroscopic Growth of Atmospheric and Model Humic-Like Substances. *J. Geophys. Res.-Atmos.* **2007**, *112* (D5), D05211, doi: 10.1029/2006jd007442.
219. VanReken, T. M.; Ng, N. L.; Flagan, R. C.; Seinfeld, J. H., Cloud Condensation Nucleus Activation Properties of Biogenic Secondary Organic Aerosol. *J. Geophys. Res.-Atmos.* **2005**, *110* (D7), D07206, doi: 10.1029/2004JD005465.
220. Altieri, K. E.; Turpin, B. J.; Seitzinger, S. P., Oligomers, Organosulfates, and Nitrooxy Organosulfates in Rainwater Identified by Ultra-High Resolution Electrospray Ionization Ft-Icr Mass Spectrometry. *Atmospheric Chemistry and Physics* **2009**, *9* (7), 2533-2542.
221. Willey, J. D.; Kieber, R. J.; Eyman, M. S.; Avery, G. B., Rainwater Dissolved Organic Carbon: Concentrations and Global Flux. *Glob. Biogeochem. Cycle* **2000**, *14* (1), 139-148.
222. Raymond, P. A., The Composition and Transport of Organic Carbon in Rainfall: Insights from the Natural (C-13 and C-14) Isotopes of Carbon. *Geophysical Research Letters* **2005**, *32* (14), L14402, doi: 10.1029/2005gl022879.
223. Kawamura, K.; Steinberg, S.; Kaplan, I. R., Concentrations of Monocarboxylic and Dicarboxylic Acids and Aldehydes in Southern California Wet Precipitations: Comparison of Urban and Nonurban Samples and Compositional Changes During Scavenging. *Atmospheric Environment* **1996**, *30* (7), 1035-1052.
224. Avery, G. B.; Kieber, R. J.; Witt, M.; Willey, J. D., Rainwater Monocarboxylic and Dicarboxylic Acid Concentrations in Southeastern North Carolina, USA, as a Function of Air-Mass Back-Trajectory. *Atmospheric Environment* **2006**, *40* (9), 1683-1693.
225. Pena, R. M.; Garcia, S.; Herrero, C.; Losada, M.; Vazquez, A.; Lucas, T., Organic Acids and Aldehydes in Rainwater in a Northwest Region of Spain. *Atmospheric Environment* **2002**, *36* (34), 5277-5288.
226. Andreae, M. O.; Talbot, R. W.; Andreae, T. W.; Harriss, R. C., Formic and Acetic-Acid over the Central Amazon Region, Brazil .1. Dry Season. *J. Geophys. Res.-Atmos.* **1988**, *93* (D2), 1616-1624, doi: 10.1029/JD093iD02p01616.
227. Birdwell, J. E.; Valsaraj, K. T., Characterization of Dissolved Organic Matter in Fogwater by Excitation-Emission Matrix Fluorescence Spectroscopy. *Atmospheric Environment* **2010**, *44* (27), 3246-3253.
228. Mazzoleni, L. R.; Ehrmann, B. M.; Shen, X. H.; Marshall, A. G.; Collett, J. L., Water-Soluble Atmospheric Organic Matter in Fog: Exact Masses and Chemical Formula Identification by Ultrahigh-Resolution Fourier Transform Ion Cyclotron Resonance Mass Spectrometry. *Environ. Sci. Technol.* **2010**, *44* (10), 3690-3697.
229. Raja, S.; Raghunathan, R.; Kommalapati, R. R.; Shen, X. H.; Collett, J. L.; Valsaraj, K. T., Organic Composition of Fogwater in the Texas-Louisiana Gulf Coast Corridor. *Atmospheric Environment* **2009**, *43* (27), 4214-4222.

230. Collett, J. L.; Herckes, P.; Youngster, S.; Lee, T., Processing of Atmospheric Organic Matter by California Radiation Fogs. *Atmos. Res.* **2008**, *87* (3-4), 232-241.
231. Gelencser, A.; Sallai, M.; Krivacsy, Z.; Kiss, G.; Meszaros, E., Voltammetric Evidence for the Presence of Humic-Like Substances in Fog Water. *Atmos. Res.* **2000**, *54* (2-3), 157-165.
232. Herckes, P.; Hannigan, M. P.; Trenary, L.; Lee, T.; Collett, J. L., Organic Compounds in Radiation Fogs in Davis (California). *Atmos. Res.* **2002**, *64* (1-4), 99-108.
233. Herckes, P.; Leenheer, J. A.; Collett, J. L., Comprehensive Characterization of Atmospheric Organic Matter in Fresno, California Fog Water. *Environ. Sci. Technol.* **2007**, *41* (2), 393-399.
234. Zhang, Q.; Anastasio, C., Chemistry of Fog Waters in California's Central Valley - Part 3: Concentrations and Speciation of Organic and Inorganic Nitrogen. *Atmospheric Environment* **2001**, *35* (32), 5629-5643.
235. Facchini, M. C.; Decesari, S.; Mircea, M.; Fuzzi, S.; Loglio, G., Surface Tension of Atmospheric Wet Aerosol and Cloud/Fog Droplets in Relation to Their Organic Carbon Content and Chemical Composition. *Atmospheric Environment* **2000**, *34* (28), 4853-4857.
236. Decesari, S.; Facchini, M. C.; Fuzzi, S.; Tagliavini, E., Characterization of Water-Soluble Organic Compounds in Atmospheric Aerosol: A New Approach. *J. Geophys. Res.-Atmos.* **2000**, *105* (D1), 1481-1489, doi: 10.1029/1999JD900950.
237. Kiss, G.; Varga, B.; Gelencser, A.; Krivacsy, Z.; Molnar, A.; Alsberg, T.; Persson, L.; Hansson, H. C.; Facchini, M. C., Characterisation of Polar Organic Compounds in Fog Water. *Atmospheric Environment* **2001**, *35* (12), 2193-2200.
238. Fuzzi, S.; Facchini, M. C.; Decesari, S.; Matta, E.; Mircea, M., Soluble Organic Compounds in Fog and Cloud Droplets: What Have We Learned over the Past Few Years? *Atmos. Res.* **2002**, *64* (1-4), 89-98.
239. Hitzenberger, R.; Berner, A.; Kasper-Giebl, A.; Loflund, M.; Puxbaum, H., Surface Tension of Rax Cloud Water and Its Relation to the Concentration of Organic Material. *J. Geophys. Res.-Atmos.* **2002**, *107* (D24), 4752, doi: 10.1029/2002JD002506.
240. Cappiello, A.; De Simoni, E.; Fiorucci, C.; Mangani, F.; Palma, P.; Trufelli, H.; Decesari, S.; Facchini, M. C.; Fuzzi, S., Molecular Characterization of the Water-Soluble Organic Compounds in Fogwater by Esims/Ms. *Environ. Sci. Technol.* **2003**, *37* (7), 1229-1240.
241. Anastasio, C.; Faust, B. C.; Allen, J. M., Aqueous-Phase Photochemical Formation of Hydrogen-Peroxide in Authentic Cloud Waters. *J. Geophys. Res.-Atmos.* **1994**, *99* (D4), 8231-8248, doi: 10.1029/94JD00085.
242. Rincon, A. G.; Guzman, M. I.; Hoffmann, M. R.; Colussi, A. J., Optical Absorptivity Versus Molecular Composition of Model Organic Aerosol Matter. *J. Phys. Chem. A* **2009**, *113* (39), 10512-10520.
243. Rincon, A. G.; Guzman, M. I.; Hoffmann, M. R.; Colussi, A. J., Thermochromism of Model Organic Aerosol Matter. *J. Phys. Chem. Lett.* **2010**, *1* (1), 368-373.
244. Schmitt-Kopplin, P.; Hertkorn, N.; Schulten, H. R.; Kettrup, A., Structural Changes in a Dissolved Soil Humic Acid During Photochemical Degradation Processes under O-2 and N-2 Atmosphere. *Environ. Sci. Technol.* **1998**, *32* (17), 2531-2541.
245. Del Vecchio, R.; Blough, N. V., Photobleaching of Chromophoric Dissolved Organic Matter in Natural Waters: Kinetics and Modeling. *Mar. Chem.* **2002**, *78* (4), 231-253.

246. Brinkmann, T.; Horsch, P.; Sartorius, D.; Frimmel, F. H., Photoformation of Low-Molecular-Weight Organic Acids from Brown Water Dissolved Organic Matter. *Environ. Sci. Technol.* **2003**, *37* (18), 4190-4198.
247. Kujawinski, E. B.; Del Vecchio, R.; Blough, N. V.; Klein, G. C.; Marshall, A. G., Probing Molecular-Level Transformations of Dissolved Organic Matter: Insights on Photochemical Degradation and Protozoan Modification of Dom from Electrospray Ionization Fourier Transform Ion Cyclotron Resonance Mass Spectrometry. *Mar. Chem.* **2004**, *92* (1-4), 23-37.
248. Gonsior, M.; Peake, B. M.; Cooper, W. T.; Podgorski, D.; D'Andrilli, J.; Cooper, W. J., Photochemically Induced Changes in Dissolved Organic Matter Identified by Ultrahigh Resolution Fourier Transform Ion Cyclotron Resonance Mass Spectrometry. *Environ. Sci. Technol.* **2009**, *43* (3), 698-703.
249. Dalrymple, R. M.; Carfagno, A. K.; Sharpless, C. M., Correlations between Dissolved Organic Matter Optical Properties and Quantum Yields of Singlet Oxygen and Hydrogen Peroxide. *Environ. Sci. Technol.* **2010**, *44* (15), 5824-5829.
250. Guzman, M. I.; Colussi, A. J.; Hoffmann, M. R., Photoinduced Oligomerization of Aqueous Pyruvic Acid. *J. Phys. Chem. A* **2006**, *110* (10), 3619-3626.
251. Faust, B. C.; Powell, K.; Rao, C. J.; Anastasio, C., Aqueous-Phase Photolysis of Biacetyl (an Alpha-Dicarbonyl Compound): A Sink for Biacetyl, and a Source of Acetic Acid, Peroxyacetic Acid, Hydrogen Peroxide, and the Highly Oxidizing Acetylperoxyl Radical in Aqueous Aerosols, Fogs, and Clouds. *Atmospheric Environment* **1997**, *31* (3), 497-510.
252. Lim, Y. B.; Tan, Y.; Perri, M. J.; Seitzinger, S. P.; Turpin, B. J., Aqueous Chemistry and Its Role in Secondary Organic Aerosol (Soa) Formation. *Atmospheric Chemistry and Physics* **2010**, *10* (21), 10521-10539.
253. Altieri, K. E.; Carlton, A. G.; Lim, H. J.; Turpin, B. J.; Seitzinger, S. P., Evidence for Oligomer Formation in Clouds: Reactions of Isoprene Oxidation Products. *Environ. Sci. Technol.* **2006**, *40* (16), 4956-4960.
254. Carlton, A. G.; Turpin, B. J.; Altieri, K. E.; Seitzinger, S.; Reff, A.; Lim, H. J.; Ervens, B., Atmospheric Oxalic Acid and Soa Production from Glyoxal: Results of Aqueous Photooxidation Experiments. *Atmospheric Environment* **2007**, *41* (35), 7588-7602.
255. Arakaki, T.; Anastasio, C.; Shu, P. G.; Faust, B. C., Aqueous-Phase Photoproduction of Hydrogen-Peroxide in Authentic Cloud Waters - Wavelength Dependence, and the Effects of Filtration and Freeze-Thaw Cycles. *Atmospheric Environment* **1995**, *29* (14), 1697-1703.
256. Faust, B. C.; Anastasio, C.; Allen, J. M.; Arakaki, T., Aqueous-Phase Photochemical Formation of Peroxides in Authentic Cloud and Fog Waters. *Science* **1993**, *260* (5104), 73-75.
257. Nojgaard, J. K.; Norgaard, A. W.; Wolkoff, P., On-Line Analysis of Secondary Ozonides from Cyclohexene and D-Limonene Ozonolysis Using Atmospheric Sampling Townsend Discharge Ionization Mass Spectrometry. *Atmospheric Environment* **2007**, *41* (37), 8345-8354.
258. Hearn, J. D.; Smith, G. D., Reactions and Mass Spectra of Complex Particles Using Aerosol Cims. *Int. J. Mass Spectrom.* **2006**, *258* (1-3), 95-103.

259. Bateman, A. P.; Nizkorodov, S. A.; Laskin, J.; Laskin, A., High-Resolution Electrospray Ionization Mass Spectrometry Analysis of Water-Soluble Organic Aerosols Collected with a Particle into Liquid Sampler. *Analytical Chemistry* **2010**, *82* (19), 8010-8016.
260. Docherty, K. S.; Wu, W.; Lim, Y. B.; Ziemann, P. J., Contributions of Organic Peroxides to Secondary Aerosol Formed from Reactions of Monoterpenes with O-3. *Environ. Sci. Technol.* **2005**, *39* (11), 4049-4059.
261. Zelenyuk, A.; Ezell, M. J.; Perraud, V.; Johnson, S. N.; Bruns, E. A.; Yu, Y.; Imre, D.; Alexander, M. L.; Finlayson-Pitts, B. J., Characterization of Organic Coatings on Hygroscopic Salt Particles and Their Atmospheric Impacts. *Atmospheric Environment* **2010**, *44* (9), 1209-1218.
262. Matsumoto, K.; Kawai, S.; Igawa, M., Dominant Factors Controlling Concentrations of Aldehydes in Rain, Fog, Dew Water, and in the Gas Phase. *Atmospheric Environment* **2005**, *39* (38), 7321-7329.
263. Munger, J. W.; Collett, J.; Daube, B.; Hoffmann, M. R., Fogwater Chemistry at Riverside, California. *Atmospheric Environment Part B-Urban Atmosphere* **1990**, *24* (2), 185-205.
264. Volkamer, R.; Ziemann, P. J.; Molina, M. J., Secondary Organic Aerosol Formation from Acetylene (C₂H₂): Seed Effect on Soa Yields Due to Organic Photochemistry in the Aerosol Aqueous Phase. *Atmospheric Chemistry and Physics* **2009**, *9* (6), 1907-1928.
265. Gao, Y. Q.; Hall, W. A.; Johnston, M. V., Molecular Composition of Monoterpene Secondary Organic Aerosol at Low Mass Loading. *Environ. Sci. Technol.* **2010**, *44* (20), 7897-7902.
266. Shilling, J. E.; Chen, Q.; King, S. M.; Rosenoern, T.; Kroll, J. H.; Worsnop, D. R.; DeCarlo, P. F.; Aiken, A. C.; Sueper, D.; Jimenez, J. L.; Martin, S. T., Loading-Dependent Elemental Composition of Alpha-Pinene Soa Particles. *Atmospheric Chemistry and Physics* **2009**, *9* (3), 771-782.
267. Mang, S. A.; Walser, M. L.; Pan, X.; Xing, J. H.; Bateman, A. P.; Underwood, J. S.; Gomez, A. L.; Park, J.; Nizkorodov, S. A., Photochemistry of Secondary Organic Aerosol Formed from Oxidation of Monoterpenes. In *Atmospheric Aerosols: Characterization, Chemistry and Modeling*, Valsaraj, K. T.; Kommalapati, R. R., Eds. American Chemical Society: 2009; Vol. 1005, pp 91-109.
268. Harlley, G. H.; Guillet, J. E., Photochemistry of Ketone Polymers. Ii. Studies of Model Compounds. *Macromolecules* **1968**, *1*, 413-417.
269. Pitts, J. N.; Wan, J. K. S., Photochemistry of Ketones and Aldehydes. In *The Chemistry of the Carbonyl Group*, Patai, S., Ed. Interscience: Chichester, 1966; p 823.
270. Chen, X.; Hopke, P. K.; Carter, W. P. L., Secondary Organic Aerosol from Ozonolysis of Biogenic Volatile Organic Compounds: Chamber Studies of Particle and Reactive Oxygen Species Formation. *Environ. Sci. Technol.* **2011**, *45* (1), 276-282.
271. Chu, L.; Anastasio, C., Formation of Hydroxyl Radical from the Photolysis of Frozen Hydrogen Peroxide. *J. Phys. Chem. A* **2005**, *109* (28), 6264-6271.
272. Monod, A.; Chevallier, E.; Jolibois, R. D.; Doussin, J. F.; Picquet-Varrault, B.; Carlier, P., Photooxidation of Methylhydroperoxide and Ethylhydroperoxide in the Aqueous Phase under Simulated Cloud Droplet Conditions. *Atmospheric Environment* **2007**, *41* (11), 2412-2426.

273. Norrish, R. G. W., Free Radicals of Short Life: Chemical Aspects. A. General and Inorganic. The Primary Photochemical Production of Some Free Radicals. *Trans. Faraday Soc.* **1934**, *30*, 0103-0113.
274. Noyes, W. A., The Contribution to R G W Norrish to Photochemistry. In *Photochemistry and Reaction Kinetics*, Ashmore, P. G.; Dainton, F. S.; Sugden, T. M., Eds. Cambridge University Press: Cambridge, 1967; pp 1-21.
275. Pitts, J. N.; Wan, J. K. S.; Schuck, E. A., Photochemical Studies in Alkali Haliide Matrix .I. O-Nitrobenzaldehyde Actinometer + Its Application to Kinetic Study of Photoreduction of Benzophenone by Benzhydrol in Pressed Potassium Bormide Disk. *Journal of the American Chemical Society* **1964**, *86* (18), 3606-&.
276. Cox, R. A.; Patrick, K. F.; Chant, S. A., Mechanism of Atmospheric Photo-Oxidation of Organic-Compounds - Reactions of Alkoxy Radicals in Oxidation of Normal-Butane and Simple Ketones. *Environ. Sci. Technol.* **1981**, *15* (5), 587-592.
277. McElroy, W. J.; Waygood, S. J., Oxidation of Formaldehyde by the Hydroxyl Radical in Aqueous-Solution. *J. Chem. Soc.-Faraday Trans.* **1991**, *87* (10), 1513-1521.
278. Xu, H.; Wentworth, P. J.; Howell, N. W.; Joens, J. A., Temperature-Dependent near-Uv Molar Absorptivities of Aliphatic-Aldehydes and Ketones in Aqueous-Solution. *Spectroc. Acta Pt. A-Molec. Biomolec. Spectr.* **1993**, *49* (8), 1171-1178.
279. Faust, B. C.; Allen, J. M., Aqueous-Phase Photochemical Sources of Peroxyl Radicals and Singlet Molecular-Oxygen in Clouds and Fog. *J. Geophys. Res.-Atmos.* **1992**, *97* (D12), 12913-12926, doi: 10.1029/92JD00843.
280. Monod, A.; Chebbi, A.; Durand-Jolibois, R.; Carlier, P., Oxidation of Methanol by Hydroxyl Radicals in Aqueous Solution under Simulated Cloud Droplet Conditions. *Atmospheric Environment* **2000**, *34* (29-30), 5283-5294.
281. DeCarlo, P. F.; Dunlea, E. J.; Kimmel, J. R.; Aiken, A. C.; Sueper, D.; Crouse, J.; Wennberg, P. O.; Emmons, L.; Shinozuka, Y.; Clarke, A.; Zhou, J.; Tomlinson, J.; Collins, D. R.; Knapp, D.; Weinheimer, A. J.; Montzka, D. D.; Campos, T.; Jimenez, J. L., Fast Airborne Aerosol Size and Chemistry Measurements above Mexico City and Central Mexico During the Milagro Campaign. *Atmospheric Chemistry and Physics* **2008**, *8* (14), 4027-4048.
282. Jimenez, J. L.; Canagaratna, M. R.; Donahue, N. M.; Prevot, A. S. H.; Zhang, Q.; Kroll, J. H.; DeCarlo, P. F.; Allan, J. D.; Coe, H.; Ng, N. L.; Aiken, A. C.; Docherty, K. S.; Ulbrich, I. M.; Grieshop, A. P.; Robinson, A. L.; Duplissy, J.; Smith, J. D.; Wilson, K. R.; Lanz, V. A.; Hueglin, C.; Sun, Y. L.; Tian, J.; Laaksonen, A.; Raatikainen, T.; Rautiainen, J.; Vaattovaara, P.; Ehn, M.; Kulmala, M.; Tomlinson, J. M.; Collins, D. R.; Cubison, M. J.; Dunlea, E. J.; Huffman, J. A.; Onasch, T. B.; Alfarra, M. R.; Williams, P. I.; Bower, K.; Kondo, Y.; Schneider, J.; Drewnick, F.; Borrmann, S.; Weimer, S.; Demerjian, K.; Salcedo, D.; Cottrell, L.; Griffin, R.; Takami, A.; Miyoshi, T.; Hatakeyama, S.; Shimono, A.; Sun, J. Y.; Zhang, Y. M.; Dzepina, K.; Kimmel, J. R.; Sueper, D.; Jayne, J. T.; Herndon, S. C.; Trimborn, A. M.; Williams, L. R.; Wood, E. C.; Middlebrook, A. M.; Kolb, C. E.; Baltensperger, U.; Worsnop, D. R., Evolution of Organic Aerosols in the Atmosphere. *Science* **2009**, *326* (5959), 1525-1529.
283. Ng, N. L.; Canagaratna, M. R.; Zhang, Q.; Jimenez, J. L.; Tian, J.; Ulbrich, I. M.; Kroll, J. H.; Docherty, K. S.; Chhabra, P. S.; Bahreini, R.; Murphy, S. M.; Seinfeld, J. H.; Hildebrandt, L.; Donahue, N. M.; DeCarlo, P. F.; Lanz, V. A.; Prevot, A. S. H.; Dinar, E.; Rudich, Y.; Worsnop, D. R., Organic Aerosol Components Observed in Northern

- Hemispheric Datasets from Aerosol Mass Spectrometry. *Atmospheric Chemistry and Physics* **2010**, *10* (10), 4625-4641.
284. Hallquist, M.; Wenger, J. C.; Baltensperger, U.; Rudich, Y.; Simpson, D.; Claeys, M.; Dommen, J.; Donahue, N. M.; George, C.; Goldstein, A. H.; Hamilton, J. F.; Herrmann, H.; Hoffmann, T.; Iinuma, Y.; Jang, M.; Jenkin, M. E.; Jimenez, J. L.; Kiendler-Scharr, A.; Maenhaut, W.; McFiggans, G.; Mentel, T. F.; Monod, A.; Prevot, A. S. H.; Seinfeld, J. H.; Surratt, J. D.; Szmigielski, R.; Wildt, J., The Formation, Properties and Impact of Secondary Organic Aerosol: Current and Emerging Issues. *Atmospheric Chemistry and Physics* **2009**, *9* (14), 5155-5236.
285. Carlier, P.; Hannachi, H.; Mouvier, G., The Chemistry of Carbonyl-Compounds in the Atmosphere - a Review. *Atmospheric Environment* **1986**, *20* (11), 2079-2099.
286. Ciccioli, P.; Brancaleoni, E.; Frattoni, M.; Cecinato, A.; Brachetti, A., Ubiquitous Occurrence of Semivolatile Carbonyl-Compounds in Tropospheric Samples and Their Possible Sources. *Atmospheric Environment Part a-General Topics* **1993**, *27* (12), 1891-1901.
287. Grosjean, D.; Williams, E. L.; Seinfeld, J. H., Atmospheric Oxidation of Selected Terpenes and Related Carbonyls - Gas-Phase Carbonyl Products. *Environ. Sci. Technol.* **1992**, *26* (8), 1526-1533.
288. Grosjean, D.; Williams, E. L.; Grosjean, E., Atmospheric Chemistry of Isoprene and of Its Carbonyl Products. *Environ. Sci. Technol.* **1993**, *27* (5), 830-840.
289. Lee, A.; Goldstein, A. H.; Kroll, J. H.; Ng, N. L.; Varutbangkul, V.; Flagan, R. C.; Seinfeld, J. H., Gas-Phase Products and Secondary Aerosol Yields from the Photooxidation of 16 Different Terpenes. *J. Geophys. Res.-Atmos.* **2006**, *111* (D17), D17305, doi: 10.1029/2006jd007050.
290. Nadasdi, R.; Zugner, G. L.; Farkas, M.; Dobe, S.; Maeda, S.; Morokuma, K., Photochemistry of Methyl Ethyl Ketone: Quantum Yields and S-1/S-0-Diradical Mechanism of Photodissociation. *ChemPhysChem* **2010**, *11* (18), 3883-3895.
291. Martinez, R. D.; Buitrago, A. A.; Howell, N. W.; Hearn, C. H.; Joens, J. A., The near Uv Absorption-Spectra of Several Aliphatic-Aldehydes and Ketones at 300-K. *Atmospheric Environment Part a-General Topics* **1992**, *26* (5), 785-792.
292. Schulteelte, K. H.; Ohloff, G., Intramolecular Ene-Synthesis of Photoactivated Carbonyl Compounds. *Tetrahedron Lett.* **1964**, (19-2), 1143-1146.
293. Anpo, M.; Kubokawa, Y., Reactivity of Excited Triplet Alkyl Ketones in Solution .1. Quenching and Hydrogen Abstraction of Triplet Acetone. *Bull. Chem. Soc. Jpn.* **1977**, *50* (8), 1913-1916.
294. Volman, D. H.; Swanson, L. W., The Photochemical Decomposition of Acetone in Aqueous Solutions of Allyl Alcohol at 2537-A. *Journal of the American Chemical Society* **1960**, *82* (16), 4141-4144.
295. Tang, Y. X.; Zhu, L.; Chu, L. T.; Xiang, B., Cavity Ring-Down Spectroscopic Study of Acetaldehyde Photolysis in the Gas Phase, on Aluminum Surfaces, and on Ice Films. *Chem. Phys.* **2006**, *330* (1-2), 155-165.
296. Gomez, A. L.; Park, J.; Walser, M. L.; Lin, A.; Nizkorodov, S. A., Uv Photodissociation Spectroscopy of Oxidized Undecylenic Acid Films. *J. Phys. Chem. A* **2006**, *110* (10), 3584-3592.
297. Rothman, L. S.; Gordon, I. E.; Barbe, A.; Benner, D. C.; Bernath, P. E.; Birk, M.; Boudon, V.; Brown, L. R.; Campargue, A.; Champion, J. P.; Chance, K.; Coudert, L. H.;

- Dana, V.; Devi, V. M.; Fally, S.; Flaud, J. M.; Gamache, R. R.; Goldman, A.; Jacquemart, D.; Kleiner, I.; Lacombe, N.; Lafferty, W. J.; Mandin, J. Y.; Massie, S. T.; Mikhailenko, S. N.; Miller, C. E.; Moazzen-Ahmadi, N.; Naumenko, O. V.; Nikitin, A. V.; Orphal, J.; Perevalov, V. I.; Perrin, A.; Predoi-Cross, A.; Rinsland, C. P.; Rotger, M.; Simeckova, M.; Smith, M. A. H.; Sung, K.; Tashkun, S. A.; Tennyson, J.; Toth, R. A.; Vandaele, A. C.; Vander Auwera, J., The Hitran 2008 Molecular Spectroscopic Database. *J. Quant. Spectrosc. Radiat. Transf.* **2009**, *110* (9-10), 533-572.
298. Cowell, G. W.; Pitts, J. N., Photochemical Studies in Rigid Matrices .2. A Study of Photochemical Reactivity of Anthracene in Polystyrene and Development of an O-Nitrobenzaldehyde Actinometer in Poly(Methyl Methacrylate). *Journal of the American Chemical Society* **1968**, *90* (5), 1106-&.
299. Fleischmann, E. M., The Measurement and Penetration of Ultraviolet-Radiation into Tropical Marine Water. *Limnology and Oceanography* **1989**, *34* (8), 1623-1629.
300. Pitts, J. N.; Cowell, G. W.; Burley, D. R., Film Actinometer for Measurement of Solar Ultraviolet Radiation Intensities in Urban Atmospheres. *Environ. Sci. Technol.* **1968**, *2* (6), 435-437.
301. Galbavy, E. S.; Ram, K.; Anastasio, C., 2-Nitrobenzaldehyde as a Chemical Actinometer for Solution and Ice Photochemistry. *J. Photochem. Photobiol. A-Chem.* **2010**, *209* (2-3), 186-192.
302. Tang, Y. X.; Zhu, L., Wavelength-Dependent Photolysis of N-Hexanal and N-Heptanal in the 280-330-Nm Region. *J. Phys. Chem. A* **2004**, *108* (40), 8307-8316.
303. Chiantore, O.; Trossarelli, L.; Lazzari, M., Photooxidative Degradation of Acrylic and Methacrylic Polymers. *Polymer* **2000**, *41* (5), 1657-1668.
304. Fox, R. B.; Kagarise, R. E.; Stokes, S.; Isaacs, L. G., Photodegradation of Poly(Methyl Acrylate). *Journal of Polymer Science Part a-General Papers* **1964**, *2* (5PA), 2085-&.
305. Gupta, A.; Liang, R.; Tsay, F. D.; Moacanin, J., Characterization of a Dissociative Excited-State in the Solid-State - Photochemistry of Poly(Methyl Methacrylate) - Photochemical Processes in Polymeric Systems .5. *Macromolecules* **1980**, *13* (6), 1696-1700.
306. Torikai, A.; Ohno, M.; Fueki, K., Photodegradation of Poly(Methyl Methacrylate) by Monochromatic Light - Quantum Yield, Effect of Wavelengths, and Light-Intensity. *J. Appl. Polym. Sci.* **1990**, *41* (5-6), 1023-1032.
307. Nizkorodov, S. A.; Laskin, J.; Laskin, A., Molecular Chemistry of Organic Aerosols through the Application of High Resolution Mass Spectrometry. *Physical Chemistry Chemical Physics* **2011**, *13* (9), 3612-3629.
308. Heaton, K. J.; Sleighter, R. L.; Hatcher, P. G.; Hall, W. A.; Johnston, M. V., Composition Domains in Monoterpene Secondary Organic Aerosol. *Environ. Sci. Technol.* **2009**, *43* (20), 7797-7802.
309. Schmitt-Kopplin, P.; Gelencser, A.; Dabek-Zlotorzynska, E.; Kiss, G.; Hertkorn, N.; Harir, M.; Hong, Y.; Gebefugi, I., Analysis of the Unresolved Organic Fraction in Atmospheric Aerosols with Ultrahigh-Resolution Mass Spectrometry and Nuclear Magnetic Resonance Spectroscopy: Organosulfates as Photochemical Smog Constituents. *Analytical Chemistry* **2010**, *82* (19), 8017-8026.
310. Wozniak, A. S.; Bauer, J. E.; Sleighter, R. L.; Dickhut, R. M.; Hatcher, P. G., Technical Note: Molecular Characterization of Aerosol-Derived Water Soluble Organic Carbon Using Ultrahigh Resolution Electrospray Ionization Fourier Transform Ion Cyclotron

- Resonance Mass Spectrometry. *Atmospheric Chemistry and Physics* **2008**, *8* (17), 5099-5111.
311. Hockaday, W. C.; Grannas, A. M.; Kim, S.; Hatcher, P. G., Direct Molecular Evidence for the Degradation and Mobility of Black Carbon in Soils from Ultrahigh-Resolution Mass Spectral Analysis of Dissolved Organic Matter from a Fire-Impacted Forest Soil. *Organic Geochemistry* **2006**, *37* (4), 501-510.
312. Koch, B. P.; Dittmar, T.; Witt, M.; Kattner, G., Fundamentals of Molecular Formula Assignment to Ultrahigh Resolution Mass Data of Natural Organic Matter. *Analytical Chemistry* **2007**, *79* (4), 1758-1763.
313. Koch, B. P.; Witt, M. R.; Engbrodt, R.; Dittmar, T.; Kattner, G., Molecular Formulae of Marine and Terrestrial Dissolved Organic Matter Detected by Electrospray Ionization Fourier Transform Ion Cyclotron Resonance Mass Spectrometry. *Geochim. Cosmochim. Acta* **2005**, *69* (13), 3299-3308.
314. Kujawinski, E. B.; Behn, M. D., Automated Analysis of Electrospray Ionization Fourier Transform Ion Cyclotron Resonance Mass Spectra of Natural Organic Matter. *Analytical Chemistry* **2006**, *78* (13), 4363-4373.
315. Kujawinski, E. B.; Longnecker, K.; Blough, N. V.; Del Vecchio, R.; Finlay, L.; Kitner, J. B.; Giovannoni, S. J., Identification of Possible Source Markers in Marine Dissolved Organic Matter Using Ultrahigh Resolution Mass Spectrometry. *Geochim. Cosmochim. Acta* **2009**, *73* (15), 4384-4399.
316. Sleighter, R. L.; Hatcher, P. G., Molecular Characterization of Dissolved Organic Matter (Dom) Along a River to Ocean Transect of the Lower Chesapeake Bay by Ultrahigh Resolution Electrospray Ionization Fourier Transform Ion Cyclotron Resonance Mass Spectrometry. *Mar. Chem.* **2008**, *110* (3-4), 140-152.
317. Sleighter, R. L.; Lie, Z. F.; Xue, J. H.; Hatcher, P. G., Multivariate Statistical Approaches for the Characterization of Dissolved Organic Matter Analyzed by Ultrahigh Resolution Mass Spectrometry. *Environ. Sci. Technol.* **2010**, *44* (19), 7576-7582.
318. Sleighter, R. L.; McKee, G. A.; Hatcher, P. G., Direct Fourier Transform Mass Spectral Analysis of Natural Waters with Low Dissolved Organic Matter. *Organic Geochemistry* **2009**, *40* (1), 119-125.
319. Smith, J. S.; Laskin, A.; Laskin, J., Molecular Characterization of Biomass Burning Aerosols Using High-Resolution Mass Spectrometry. *Analytical Chemistry* **2009**, *81* (4), 1512-1521.
320. Chang-Graham, A. L.; Profeta, L. T. M.; Johnson, T. J.; Yokelson, R. J.; Laskin, A.; Laskin, J., Case Study of Water-Soluble Metal Containing Organic Constituents of Biomass Burning Aerosol. *Environ. Sci. Technol.* **2011**, *45* (4), 1257-1263.
321. Schug, K.; McNair, H. M., Adduct Formation in Electrospray Ionization Mass Spectrometry II. Benzoic Acid Derivatives. *Journal of Chromatography A* **2003**, *985* (1-2), 531-539.
322. Oss, M.; Krueve, A.; Herodes, K.; Leito, I., Electrospray Ionization Efficiency Scale of Organic Compounds. *Analytical Chemistry* **2010**, *82* (7), 2865-2872.
323. Tang, L.; Kebarle, P., Dependence of Ion Intensity in Electrospray Mass-Spectrometry on the Concentration of the Analytes in the Electrosprayed Solution. *Analytical Chemistry* **1993**, *65* (24), 3654-3668.

324. Leito, I.; Herodes, K.; Huopola, M.; Virro, K.; Kunnapas, A.; Krueve, A.; Tanner, R., Towards the Electrospray Ionization Mass Spectrometry Ionization Efficiency Scale of Organic Compounds. *Rapid Commun. Mass Spectrom.* **2008**, *22* (3), 379-384.
325. Ehrmann, B. M.; Henriksen, T.; Cech, N. B., Relative Importance of Basicity in the Gas Phase and in Solution for Determining Selectivity in Electrospray Ionization Mass Spectrometry. *J. Am. Soc. Mass Spectrom.* **2008**, *19* (5), 719-728.
326. Chalcraft, K. R.; Lee, R.; Mills, C.; Britz-McKibbin, P., Virtual Quantification of Metabolites by Capillary Electrophoresis-Electrospray Ionization-Mass Spectrometry: Predicting Ionization Efficiency without Chemical Standards. *Analytical Chemistry* **2009**, *81* (7), 2506-2515.
327. Cech, N. B.; Enke, C. G., Relating Electrospray Ionization Response to Nonpolar Character of Small Peptides. *Analytical Chemistry* **2000**, *72* (13), 2717-2723.
328. Koster, S.; Mulder, B.; Duursma, M. C.; Boon, J. J.; Philipsen, H. J. A.; von Velde, J. W.; Nielen, M. W. F.; de Koster, C. G.; Heeren, R. M. A., Quantitative Analysis of Copolymers: Influence of the Structure of the Monomer on the Ionization Efficiency in Electrospray Ionization Ftms. *Macromolecules* **2002**, *35* (13), 4919-4928.
329. Mohamed, S.; Charles, L., Selectivity of Electrospray Response in Small Polymer Analysis by Mass Spectrometry. *Rapid Commun. Mass Spectrom.* **2006**, *20* (21), 3188-3192.
330. Amad, M. H.; Cech, N. B.; Jackson, G. S.; Enke, C. G., Importance of Gas-Phase Proton Affinities in Determining the Electrospray Ionization Response for Analytes and Solvents. *Journal of Mass Spectrometry* **2000**, *35* (7), 784-789.
331. Henriksen, T.; Juhler, R. K.; Svensmark, B.; Cech, N. B., The Relative Influences of Acidity and Polarity on Responsiveness of Small Organic Molecules to Analysis with Negative Ion Electrospray Ionization Mass Spectrometry (Esi-MS). *J. Am. Soc. Mass Spectrom.* **2005**, *16* (4), 446-455.
332. Kippenberger, M.; Winterhalter, R.; Moortgat, G. K., Determination of Higher Carboxylic Acids in Snow Samples Using Solid-Phase Extraction and Lc/Ms-Tof. *Anal. Bioanal. Chem.* **2008**, *392* (7-8), 1459-1470.
333. Rostad, C. E.; Leenheer, J. A., Factors That Affect Molecular Weight Distribution of Suwannee River Fulvic Acid as Determined by Electrospray Ionization/Mass Spectrometry. *Analytica Chimica Acta* **2004**, *523* (2), 269-278.
334. Schug, K.; McNair, H. M., Adduct Formation in Electrospray Ionization. Part 1: Common Acidic Pharmaceuticals. *Journal of Separation Science* **2002**, *25* (12), 760-766.
335. Aiken, A. C.; DeCarlo, P. F.; Jimenez, J. L., Elemental Analysis of Organic Species with Electron Ionization High-Resolution Mass Spectrometry. *Analytical Chemistry* **2007**, *79* (21), 8350-8358.